DOCKET: EPA-HQ-OAR-2014-0609

FINAL

TECHNICAL SUPPORT DOCUMENT FOR SECTION 194.24

EVALUATION OF THE COMPLIANCE RECERTIFICATION ACTINIDE SOURCE TERM, GAS GENERATION, BACKFILL EFFICACY, WATER BALANCE AND CULEBRA DOLOMITE DISTRIBUTION COEFFICIENT VALUES

U. S. Environmental Protection Agency
Office of Radiation and Indoor Air
Center for Waste Management and Regulations
1301 Constitution Ave., N.W.
Washington, DC 20004

June 2017

TABLE OF CONTENTS

LIST OF TABLES

LIST OF FIGURES

ACRONYM AND ABBREVIATION LIST

A_d	Surface area of steel associated with a waste disposal drum
AMWTF	Advanced Mixed Waste Treatment Facility
Brine A	Simulated Salado brine formulation
CAPMIC	Maximum Actinide Concentration Associated with Microbes
CCA	Compliance Certification Application
CCDF	Complementary cumulative distribution function
CDF	Cumulative distribution function
CEMRC	Carlsbad Environmental Monitoring and Research Center
CFR	*Code of Federal Regulations*
CH	Contact handled
Ci	Curie
CPR	Cellulosics, plastics, and rubber
CRA	Compliance Recertification Application
CRA-2004	First Compliance Recertification Application, March 2004
CRA-2009	Second Compliance Recertification Application, March 2009
CRA-2014	Third Compliance Recertification Application, March 2014
CRA14_SEN4 PA	Sensitivity study of CRA-2014 PA
D	Difference value, $\log_{10}$(measured solubility) – $\log_{10}$(predicted solubility)
DATA0.FM1	EQ3/6 thermodynamic database used for the CRA-2014 PA
DATA0.FM2	Revised EQ3/6 thermodynamic database
DBR	Direct brine release
DL	Direct load
DOE	U.S. Department of Energy
DRSPALL	Spallings released to accessible environment from a future drilling event
DRZ	Disturbed rock zone
D_S	Steel surface area per unit disposal volume
EDTA	Ethylenediaminetetraacetic acid
EEF	Effective Excess Factor
EF	Excess Factor
EEG	Environmental Evaluation Group
Eh	Oxidation/reduction potential
EPA	U.S. Environmental Protection Agency
EQ3/6	Geochemical modeling code used for CRA-2014 PA
ERDA-6	Simulated Castile brine formulation
EXAFS	Extended x-ray absorption fine structure

FMT	Fracture Matrix Transport geochemical modeling code
FEP	Feature, event and process
FMT_021120.CHEMDAT	FMT Thermodynamic database used for the CRA-2004 PA
FMT_050405.CHEMDAT	FMT Thermodynamic database used for the PABC04 and PABC09
FMT_970407.CHEMDAT	FMT Thermodynamic database used for the PAVT
GWB	Generic Weep Brine, simulated Salado brine formulation
K_d	Distribution coefficient
kPa	kilopascal
K_{sp}^0	Solubility product at zero ionic strength
LANL	Los Alamos National Laboratory
LIBD	Laser-induced breakdown detection
LOI	loss on ignition
m	meter
M	molar, moles/liter
MB	Marker bed
meq	milliequivalent
M_{H2}	Molecular weight of H_2 [kg H_2 per mole H_2, 2.02×10^{-3}, parameter REFCON:MW_H2].
MPa	megapascal
μ^0/RT	Standard chemical potential (dimensionless)
n_d	Number of waste drums that can be close-packed into a single room in the repository
OP	Overpack
Pa	Pascal
PA	Performance assessment
PABC04	CRA-2004 Performance Assessment Baseline Calculations
PABC09	CRA-2009 Performance Assessment Baseline Calculations
PAVT	Performance Assessment Verification Testing
PCR	Planned change request
ρ_{Fe}	Themolar density of steel (1.41×10^5 moles/m[3)]
pH	Negative log of the hydrogen ion activity
pcH	Negative log of the hydrogen ion concentration, molar units
pmH	Negative log of the hydrogen ion concentration, molal units
PVC	Polyvinylchloride

$q_{r\,gc}$	Rate of gas production per unit volume of waste due to anoxic corrosion of iron-based metals ($kg/m^3/sec$)
R_{ci}	Corrosion rate under inundated conditions, STEEL:CORRMCO2 (m/s)
R_{ch}	Corrosion rate under humid conditions, STEEL:HUMCORR (m/s)
REFCON:ASDRUM	A performance assessment parameter name used to represent the surface area of a waste drum
REFCON:DRROOM	A performance assessment parameter name used to represent the number of drums emplaced in a waste panel
REFCON:MW_H2	A performance assessment parameter name used to represent the molecular weight of hydrogen gas
REFCON:VROOM	A performance assessment parameter name used to represent the volume of a waste drum
RH	Remote handled
RSI	Institute for Regulatory Science
$S_{b,eff}$	Effective brine saturation due to capillary action in the waste materials
S_g*	Equals 1- $S_{b,eff}$ if $S_{b,eff} > 0$, or equals 0 if $S_{b,eff} = 0$
S_m	Measured solubility
SNL	Sandia National Laboratories
S_p	Solubility predicted by FMT or EQ3/6 calculations
STEEL:CORMCO2	Represents inundated steel corrosion rate (m/s)
STEEL:HUMCORR	Represents the humid steel corrosion rate (m/s)
STEEL:STOIFX	Represent the stoichiometric coefficients for gas generation from steel corrosion (m/m)
STTP	Actinide Source-Term Waste Test Program
TRLFS	Time-resolved laser fluorescence spectroscopy
TRU	Transuranic waste
V_R	Initial volume of a single room in the repository
WAS_AREA:BIOGENFC	A performance assessment parameter name used to represent the gas generation from microbes in the waste panels
WAS_AREA:GRATMICI	A performance assessment parameter name used to represent biodegradation of cellulose plastics and rubber under anaerobic and brine inundated conditions
WAS_AREA:GRATMICH	A performance assessment parameter name used to represent biodegradation of cellulose plastics and rubber under anaerobic and humid conditions

WAS_AREA:PROBDEG	A performance assessment property used to estimate the probability of biodegradation of organic materials in a waste panel
WDS	WIPP Waste Data System
WIPP	Waste Isolation Pilot Plant
XAFS	X-ray absorption fine structure
XANES	X-ray absorption near-edge spectroscopy
X_C (H_2 | Fe)	Stoichiometric coefficient for gas generation due to the corrosion of steel [1 mole H_2 per mole Fe, parameter (Kicker and Herrick 2013)]
XRD	X-ray diffraction

PREFACE

The U.S. Department of Energy (DOE) is required to submit a Compliance Recertification Application (CRA) to the U.S. Environmental Protection Agency (EPA) for the Waste Isolation Pilot Plant (WIPP) facility every five years including an updated assessment of future WIPP performance. During EPA's review of DOE's CRA-2014 performance assessment (PA), events associated with the February 2014 repository fire and radionuclide release have closed portions of the underground facility. This temporary closure has created a situation where certain parts of the underground facility could not be accessed for ground control. Panel 9 may be abandoned along with plans to modify the design change used for panel closures in panels 3, 4, 5 and 6.

Because the CRA PAs are predictions of post-closure repository performance and the EPA knows there will be modifications to the current repository design, modifying the CRA-2014 PA at this time to incorporate alternative parameter values would not add more reality to predictions of repository post-closure performance. Consequently, the EPA adopted the CRA-2014 PA as originally submitted by DOE as the baseline, rather than have DOE conduct a revised PA baseline calculation (PABC). In lieu of requesting a PABC-2014, the EPA requested that DOE conduct a set of sensitivity studies to address some of the significant technical concerns arising from the EPA's CRA-2014 review. The inputs to these sensitivity studies broadly address many of the EPA's technical concerns that could potentially impact long-term repository performance. The Agency has reviewed the results of these studies and determined that there exists an adequate level of confidence—that is, a reasonable expectation—that the repository will continue to comply with EPA regulations. These results are described and evaluated in this report, but are addressed in more detail in a companion Technical Support Document, "Review of EPA Sensitivity Studies of DOE CRA-2014 WIPP Compliance Recertification Performance Assessment."

Additionally, the EPA recommends further work that can be conducted to evaluate many of the technical concerns identified in the EPA's review of the CRA-2014 PA, as well as incorporate future repository design changes. The EPA will work with DOE to determine the best path forward for resolution of EPA's concerns, which could include additional data reviews, independent technical reviews, and possibly additional sensitivity analyses to reach a consensus for the next CRA. It is anticipated that the results of these efforts will be incorporated into the CRA-2019 PA or otherwise be made available during EPA's review of the CRA-2019 PA.

EXECUTIVE SUMMARY AND REPORT OUTLINE

The Waste Isolation Pilot Plant (WIPP) in southeastern New Mexico is an underground facility designed for the permanent disposal of defense-related transuranic (TRU) waste. The U.S. Department of Energy (DOE) operates the WIPP repository under the regulatory oversight of the U.S. Environmental Protection Agency (EPA). DOE submitted the Compliance Certification Application (CCA) to the EPA in 1996. After extensive review of the CCA and supplemental information provided by DOE, including additional performance assessment (PA) calculations referred to as Performance Assessment Verification Testing (PAVT), EPA certified that DOE had met the regulatory requirements and WIPP began accepting waste in March 1999.

DOE is required to submit a Compliance Recertification Application (CRA) every 5 years after the initial receipt of waste at WIPP, and the first CRA (CRA-2004) was submitted to EPA in March 2004 (DOE 2004). EPA reviewed the CRA-2004 and supplemental information provided by DOE, including PA calculations referred to as the CRA-2004 Performance Assessment Baseline Calculations (PABC04), and certified that DOE continued to meet WIPP regulatory requirements (EPA 2006a). DOE submitted the second CRA (CRA-2009) to EPA in March 2009 (DOE 2009). The CRA-2009 PA included the actinide solubility calculations incorporated in the PABC04. The EPA performed a completeness review of the CRA-2009 and instructed DOE to perform a new PA to capture changes since the 2004 recertification (Cotsworth 2009a). This PA, the CRA-2009 Performance Assessment Baseline Calculations (PABC09), was performed by DOE and reviewed by EPA. Based on their review of the CRA-2009 and PABC09, EPA certified that DOE continued to meet WIPP regulatory requirements (EPA 2010b). At the time of the recertification decision, however, EPA (2010b) noted a number of uncertainties related to WIPP chemistry and also identified issues related to WIPP repository chemical processes for additional investigation prior to the CRA-2014.

DOE submitted the third CRA (CRA-2014) to EPA in March 2014 (DOE 2014b). This Technical Support Document summarizes EPA's review of chemistry-related issues important to PA, including actinide source term modeling, gas generation, backfill efficacy, water balance calculations and actinide transport in the Culebra Dolomite above the repository for the WIPP CRA-2014.

Section 1.0 provides a summary of WIPP certification and recertification activities since the CCA. It also summarizes the regulatory requirements and important waste chemical characteristics and repository chemical processes considered during certification and recertification. WIPP waste characteristics and components that have been identified as potentially affecting the chemistry of the system and repository releases include actinide solubilities and oxidation state distributions; formation of colloidal suspensions containing radionuclides; production of gas from steel corrosion and waste degradation; ferrous metals inventory; cellulosics, plastics and rubber (CPR) inventory; chelating agents (organic ligands) and oxyanions; and the activity of each isotope of the radionuclides present in the waste [40 CFR 194.24(b), EPA 1997b].

A summary of the geologic setting, mineralogy of the Salado Formation surrounding the repository and WIPP brine chemistry is provided in Section 2.0. The WIPP repository is excavated within the Salado Formation, a relatively thick bedded salt, composed mainly of layers

of impure halite [NaCl], with interbedded layers of anhydrite [$CaSO_4$(s)], polyhalite [$K_2MgCa_2(SO_4)_4 \cdot 2H_2O$(s)] and mudstone. The Salado Formation is underlain by the Castile Formation. The Castile Formation is mainly composed of thick beds of high-purity halite, alternating with thick beds of interlaminated carbonate and anhydrite. Pressurized brines are associated with the deformed areas of this formation. The Salado Formation is overlain by the Rustler Formation, of which the Culebra Dolomite is the most significant to WIPP PA. The Culebra Dolomite, which is mostly composed of dolomite [$CaMg(CO_3)_2$(s)] with small amounts of anhydrite or gypsum [$CaSO_4 \cdot 2H_2O$(s)], is the most transmissive continuously saturated unit above the WIPP facility. It therefore provides the most direct pathway from the repository to the accessible environment, apart from releases directly to the surface.

PA calculations have used representations of both Salado and Castile brines. Small quantities of intergranular and intragranular Salado brines are associated with the salt at the repository horizon. These brines are highly concentrated (ionic strengths up to 8 M), with a composition of mostly sodium, magnesium, potassium, chloride and sulfate, and with smaller amounts of calcium, carbonate and borate. The brine formulation used to represent Salado brine in WIPP laboratory experiments and PA calculations is denoted as Generic Weep Brine (GWB). Since the CRA-2004 PA calculations to the present CRA-2014 PA, it is the only brine formulation used to represent that of the Salado (Snider 2003b). Castile brine may enter the repository if a borehole penetrates a waste panel and also penetrates an area of pressurized brine in the underlying Castile Formation. The brine composition used to represent that of the Castile is withdrawn from the ERDA-6 well and used to represent all Castile brines in WIPP related laboratory experiments as well as WIPP PA calculations. Brine taken from the ERDA-6 borehole has lower magnesium and chloride concentrations and a lower ionic strength than GWB—the Salado brine analog.

Section 3.0 provides a review and discussion of the Gas Generation conceptual model and its implementation for WIPP PA. The Gas Generation conceptual model includes the assumptions that significant gas generation will occur in the repository through corrosion of ferrous metals and through microbial degradation of CPR. The model also assumes that essentially all carbon dioxide [CO_2] will be removed from the gas phase by reaction with the magnesium oxide (MgO) backfill.

The PA uses two anoxic steel corrosion rates depending on brine saturation: humid and inundated. These rates cannot occur unless brine is present and are proportional to the estimated surface area of iron-based waste and steel waste containers. Anoxic corrosion of iron-based metals in the waste and waste containers produces hydrogen and the reaction products are two solids, $Fe(OH)_2 \cdot xH_2O$(s) and FeS(s). New project-specific data was used in the CRA-2014 PA to modify and lower the inundated corrosion rates from those used in prior PAs. Upon EPA's review of the updated experimental data and DOE revisions to the 2014-CRA PA, the EPA concluded that DOE's corrosion rate updates as most likely being underestimated. Consequently, the EPA recommends that the inundated and humid corrosion rates used in the CRA-2014 PA be reassessed by DOE for the CRA-2019 PA such that corrosion rates are aligned with current theoretical and experimental data. EPA's evaluation of the steel surface area calculations demonstrated that the steel surface area per unit volume used in the CRA-2014 PA is a reasonable value for WIPP waste that has been emplaced through December 31, 2014. EPA recommends that DOE continue to update the steel surface area per unit volume using future

inventories and waste emplacement data to demonstrate that the value used in PA continues to be representative for the CRA-2019.

DOE assumed that all $H_2S(g)$ generated by CPR degradation would instantaneously react with Fe(s) and $Fe(OH)_2(s)$. This assumption resulted in lower gas pressures and higher brine volumes. EPA's assessment of the available experimental data concludes this assumption is inconsistent with that data and indicates H_2S could passivate iron surfaces. Therefore, EPA concludes it would not be appropriate for DOE to assume $H_2S(g)$ would instantaneously react with Fe(s) and $Fe(OH)_2(s)$ in the CRA-2019 PA.

For the PABC04 and all later PA calculations, significant microbial degradation of cellulosics was assumed for 100% of the PA realizations, with significant microbial degradation of plastics and rubber assumed for 25% of the PA realizations. For the PABC04 and all later PA calculations, an initial gas pressure was used to account for rapid initial microbial gas generation rates, with lower rates used to account for slower long-term microbial gas generation through CPR degradation. Based on the available data that include WIPP-specific long-term degradation experiments, the current approach for modeling microbial gas generation rates is appropriate for PA.

Based on information available at the time of the CCA, lead and aluminum corrosion are assumed to be insignificant to PA because of the small amount of gas production that is likely to result relative to anoxic corrosion of iron-based metals. Evaluation of the CRA-2014 PA aluminum inventory shows that aluminum corrosion is unlikely to have significant effects on gas generation. The CRA-2014 PA lead inventory is also relatively small, indicating that lead corrosion is unlikely to affect gas generation rates. However, WIPP has emplaced some remote-handled (RH) shielded containers that contain significant amounts of lead and may use more shielded containers in the future. The CRA-2014 PA inventory does not include the large future increase in lead inventory that may occur as shielded containers are placed in the repository. Bounding calculations of the effects of shielded containers on lead inventory using information from Crawford and Taggart (2007) indicate that the amounts of lead associated with the shielded containers might significantly increase gas generation rates. EPA believes bounding calculations for the CRA-2019 PA would be appropriate to assess the possible effects of additional lead from shielded containers on gas generation rates and repository performance.

The Gas Generation Conceptual model includes the assumption that radiolysis of water in the waste and brine, and irradiation of plastics and rubber in the waste will not significantly affect the amounts of gas generated. However, lower microbial and anoxic corrosion gas generation rates were used in the CRA-2014 PA compared to those used in the CCA PA or PAVT, consequently, it is no longer certain that radiolytic gas generation will be relatively insignificant. Based on these modifications to the microbial and anoxic contributions to gas generation, gas generation from radiolysis may now be more significant than assumed in the past. Therefore, the EPA believes that it would be appropriate to include an assessment of the potential importance of radiolytic gas generation in the 2019 PA.

Section 4.0 describes the MgO backfill included in the WIPP repository to control repository chemical conditions and minimize actinide solubilities in the postclosure repository. EPA determined that the MgO backfill met the requirements for an engineered barrier to control CO_2

fugacities and buffer brine. MgO reacts with water in the repository to create brucite [$Mg(OH)_2(s)$], and brucite dissolution prevents low brine pH values that could increase actinide solubilities. Brucite also reacts with CO_2 produced by microbial degradation of CPR to form hydromagnesite [$Mg_5(CO_3)_4(OH)_2 \cdot 4H_2O(s)$], controlling CO_2 fugacities at low levels that minimize actinide solubilities in repository brines. Hydromagnesite may convert over long time periods to magnesite [$MgCO_3(s)$], which is the more stable phase and which will control CO_2 fugacities at even lower levels.

Evaluation of the available data indicates that the MgO backfill will control CO_2 fugacities under inundated conditions and maintain chemical conditions in WIPP brines that limit actinide solubilities. The current emplacement plan ensures adequate amounts of MgO will be present in the repository, because the quantities of CPR and MgO are monitored in each room of the repository during emplacement and additional MgO is emplaced if necessary. Because of uncertainties in the rate at which hydromagnesite will convert to magnesite in the repository environment, it is assumed for PA that the brucite-hydromagnesite reaction will buffer CO_2 fugacity at levels consistent with relatively low actinide solubilities under inundated conditions. Current data suggests the backfill material will adequately control chemical conditions in the repository.

Section 5.0 provides a review of the expected actinide oxidation states that will dissolve in brines that enter the repository. The actinide oxidation states assumed for PA have remained unchanged since the CCA. Am(III), Cm(III) and Th(IV) are assumed to be the only stable oxidation states for these radionuclides. However, U, Np, and Pu may be present in different oxidation states. It is assumed for PA that U may exist in either the +IV or +VI oxidation state and Np may exist in either the +IV or +V oxidation states. These assumptions remain valid, based on the available data. U(IV) and Np(IV) are likely to be the most stable oxidation states under the reducing conditions in the WIPP repository. However, U(VI) may persist because of the effects of complexation on uranium reduction. The assumption that Np may be present in the +V oxidation state in the WIPP repository brines is conservative, because of the greater solubility of Np(V) solid phases.

Available data continue to support the assumption that Pu will be present in the +III and +IV oxidation states, rather than the +V and +VI states. DOE has assumed that Pu concentrations in the PA realizations with reducing conditions is controlled by equilibrium between Pu(III) solid and Pu(III) aqueous species. For the PA realizations with more oxidizing conditions, DOE has assumed the Pu solubility is controlled by equilibrium between Pu(IV) solid and Pu(IV) aqueous species. However, EPA's evaluation of recent experimental data has indicated that reductive dissolution of Pu(IV) solid to form Pu(III) aqueous species may be more realistic for the more oxidizing realizations, which would result in a higher range of Pu concentrations in the more oxidizing realizations. DOE disagrees with EPA's assessment of likely Pu oxidation states. Based on EPA's evaluation of the available experimental data, the Agency is recommending that DOE conduct an independent technical review to establish the appropriate Pu oxidation states. Additionally, the EPA would like to see the recommendations from this review be implemented as soon as possible, and ideally implemented in the CRA-2019 PA.

Section 6.0 addresses the calculation of Am, Cm, Np, Pu, Th, and U solubilities used in PA. Representative Salado or Castile brines are equilibrated with Salado minerals and MgO

hydration and carbonation products. The CRA-2014 PA solubilities of Am(III), Th(IV) and Np(V) are calculated for WIPP repository conditions using the EQ3/6 code and database, replacing the FMT code and database used for previous WIPP PAs. The Dissolved Actinide Source Term conceptual model includes the assumption that actinides in the same oxidation state will exhibit the same solubilities and aqueous speciation. Accordingly, the solubilities of Cm(III) and Pu(III) are assumed equal to the solubility calculated for Am(III) and the solubilities of U(IV), Np(IV) and Pu(IV) are assumed equal to the calculated Th(IV) concentration. Calculated Np(V) solubilities are used only for neptunium, because it is the only actinide predicted to be present in WIPP brines in the +V oxidation state. Because DOE has not developed an aqueous speciation and solubility model for U(VI), an upper-limit concentration of 10^{-3} M is assumed for PA.

The organic ligands acetate, citrate, ethylenediaminetetraacetic acid (EDTA) and oxalate could affect actinide solubilities in the repository because these ligands are water soluble and present in significant quantities in the WIPP inventory. The effects of organic ligands on actinide solubilities were not included in the CCA PAVT actinide solubility calculations because it was assumed that other constituents, including transition metals in the waste and magnesium from the MgO backfill, would compete with the actinides for binding sites on the organic ligands. The effects of organic ligands on actinide solubilities have been included in subsequent PAs, showing that EDTA and other ligands may affect +III actinide concentrations.

EPA's review of DOE's thermodynamic database indicates actinide solubilities and aqueous speciation in the WIPP thermodynamic database have not been updated since 2005. The Agency had informed the DOE that a thorough review and update of the thermodynamic database of available and relevant actinide solubility and speciation experimental data be considered in the 2014-CRA. At the time, the EPA recommended DOE evaluate data presented by Altmaier et al. (2005, 2006) to be considered in a revision of thorium-carbonate speciation. Additionally, EPA recommended the results of the Neck et al. (2009) $Nd(OH)_3(s)$ solubility studies be evaluated and considered in a database update as they relate to the solubility of $Am(OH)_3(s)$ (EPA 2010b). During EPA's evaluation of DOE's 2014-CRA thermodynamic database it was discovered no revisions related to the actinide solubility and aqueous speciation had been incorporated as recommend during our PABC09 review. This omission was communicated to DOE as part of the Agency's CRA-2014 completeness review. In response, DOE revised the WIPP thermodynamic database that included changes to the solubility of hydromagnesite; changes to borate, EDTA and citrate chemistry; addition of the $MgSO_4(aq)$ dissociation constant; and addition of lead aqueous speciation and solubility data.

EPA's preliminary review of the DOE's revised database indicates that DOE's modified hydromagnesite solubility is not well-supported. The Agency recommends this solubility be revised back to its previous value. Additionally, DOE did not revise the aqueous speciation and solubility data for Am(III) and Th(IV) based on data that have become available since the PABC04. EPA expects DOE to revise the Th(IV)-carbonate aqueous species and the $Am(OH)_3(s)$ solubility data in the WIPP database that is aligned and consistent with updated and relevant experimental data prior to the CRA-2019 PA. EPA also expects DOE to continue updating the database for CRA-2019 such that it is aligned and consistent with recent information. If data is to be excluded from any updates, EPA expects a defensible argument for that exclusion.

The calculated solubilities for the +III, +IV, and +V actinides are constant values, with associated uncertainties to bound the upper and lower solubility values. They are developed by comparing the measured solubility of actinides in peer-reviewed studies to their modeled solubility. The studies used for this uncertainty distribution are chosen using a predetermined set of selection criteria. For the CRA-2014 PA DOE evaluated the +III and +IV actinide solubility uncertainty distributions using revised data selection criteria and sampled these revised distributions in order to represent the uncertainty in modeling. EPA found DOE's use of the selection criteria for this study to be inconsistent and amended the data criteria for a sensitivity analysis PA (CRA14_SEN4 PA). The revised criteria included studies previously omitted by DOE as well as some expanded criteria such as the inclusion of studies that emphasize the presence of borate and carbonate.

The mean and median of the +IV actinide solubility uncertainty distribution decreased between the PABC04 and PABC09, then increased for the CRA-2014 PA. For the CRA14_SEN4 PA, the amended uncertainty distribution resulted in a decrease of the mean and median +IV actinide solubility when compared to the CRA-2014 PA values, with many close to zero. These results indicate DOE predicted higher +IV actinide solubilities for the CRA-2014 PA given the data used in the EPA directed analysis.

The mean and median values of the +III actinide solubility uncertainty distribution decreased significantly between the PABC09 and CRA-2014 PA. Using the EPA-amended data selection criteria, the mean and median +III actinide solubility distribution for the CRA14_SEN4 PA increased compared to the CRA-2014 PA values. The combined effect of the modified +IV and +III uncertainty distributions was to increase overall releases because more emphasis was placed on the more soluble +III actinides. EPA recommends that DOE use the amended data selection criteria included in the SEN4 PA as the starting point for calculations of the +III and +IV actinide solubility uncertainty distributions for the CRA-2019 PA.

The WIPP colloidal actinide source term is summarized in Section 7.0. Four types of colloids can form in WIPP repository brines, including microbial, humic, intrinsic and mineral fragment colloids. Actinide concentrations associated with microbial and humic colloids are based on proportionality constants with maximum values. The concentrations of actinide intrinsic colloids and mineral fragment colloids used in PA are constant values based on the results of experimental investigations. No new data have been identified for actinide-humic colloids, so the humic colloid parameters remain unchanged for the CRA-2014 PA.

Experimental data have been reported indicating that mineral fragment colloids may form from MgO hydration and carbonation products and mobilize Th(IV) in $MgCl_2$ brines. EPA's assessment of DOE's mineral-fragment colloid parameter used in PA calculations indicate this parameter is not aligned with the empirical data. The EPA concludes that it would be appropriate for DOE to evaluate the potential formation of mineral-fragment colloids from MgO hydration and carbonation under WIPP-relevant conditions as soon as possible, and ideally for use in the CRA-2019 PA.

In the absence of evidence of the formation of actinide intrinsic colloids for radionuclides other than plutonium, previous PAs have set the concentrations of Th, U, Np, and Am intrinsic

colloids to zero. More recent Th(IV) solubility investigations, however, identified the existence of intrinsic Th(IV) colloids in dilute solution and in brines. DOE performed experiments to evaluate the formation of intrinsic colloids using a narrow pcH range and used data from these experiments to increase the intrinsic colloid parameters used in the CRA-2014 PA. Review of the data used to develop these parameters indicates that the Th(IV) intrinsic colloid parameter for the CRA-2019 PA would be more appropriately based on data collected over a wider pcH range than the range used by DOE, and would increase Th(IV) intrinsic colloid concentrations. EPA's assessment indicates DOE's concentration range for intrinsic colloid is not aligned with intrinsic colloid formation in predicted pcH conditions in the repository. Therefore, EPA concludes that it would be appropriate for DOE to develop a Pu(III) intrinsic colloid parameter range, aligned with this data, that includes and an upper bounding value.

DOE conducted a series of experiments to determine revised parameters for actinides associated with microbial colloids. DOE reduced the maximum concentrations for the microbially associated actinides based on a revised conceptual model assumption. In previous PAs it was assumed that the maximum for the microbially associated actinide concentration is the concentration at which no growth was observed, but DOE changed this upper limit for the CRA-2014 PA to the concentration calculated from an assumed maximum cell concentration multiplied by the moles of actinides per cell. Experiments also used short reaction times, the result of which is increased uncertainty because important actinide-cell interactions (e.g., bioaccumulation and biomineralization) have been ignored and could result in a colloid underestimation. These approaches deviate from the conceptual model and as a result, the Agency does not accept this change. Until DOE can provide a more acceptable change to this parameter, EPA will accept the maximum concentrations used in previous CRAs for the CRA-2019 PA. The Agency also finds that further uncertainty was introduced in the experimental procedures due to the improper use of filters, resulting in added intrinsic colloids to solutions and a non-representative calculation of microbial colloid formation. In future experiments, the Agency expects DOE to provide the appropriate controls to demonstrate intrinsic colloids have been removed from their post-test solutions. Because of the uncertainty introduced by the effects of intrinsic colloids, it would also be appropriate for DOE to compare the CCA PAVT proportionality constants to the constants calculated from the recent investigations and use the higher values for the CRA-2019 PA.

Section 8.0 provides a comparison of the mean calculated total mobilized actinides for the PABC09, CRA-2014 PA and the CRA14_SEN4 PA. Evaluation of the total mobilized actinide concentrations calculated for these PAs demonstrates that mineral fragment colloids and intrinsic colloids make only minor contributions to mean total mobilized concentrations. Mean total Am(III) and Pu(III) mobilized concentrations for the CRA-2014 PA were significantly lower than their respective concentrations for the PABC09 and CRA14_SEN4 PA because of the negative mean +III actinide solubility uncertainty parameter and decreases in microbially associated colloids used for the CRA-2014 PA. In addition, mean and median total mobilized concentrations in all cases were higher for Pu(IV) than for Pu(III), despite the higher baseline Pu(III) solubility. These results show the importance of the microbial colloid parameters in PA.

Section 9.0 summarizes the actinide elements and isotopes included in WIPP PA calculations. Not all radionuclides in the WIPP inventory are included in PA calculations because of computational and time constraints. Consequently, the number of radionuclides included in PA

has been reduced according to an algorithm initially developed for the CCA. The results of PA calculations indicate that radionuclide releases are dominated by Pu and Am. These assumptions have not changed since the CRA-2009.

Distribution coefficient (K_d) values used to calculate radionuclide transport through the Culebra are described in Section 10.0. These distribution coefficients are based on the results of WIPP-specific sorption studies carried out on Culebra rock samples and pure dolomite. The PABC09 K_d distributions were also used for the CRA-2014 PA and continue to be appropriate.

Section 11.0 examines the likely effects of assuming homogeneous waste emplacement for WIPP PA on chemical processes in the repository. This assumption is potentially significant because of heterogeneous waste loading that has occurred in the WIPP repository. Furthermore, the empirical and theoretical data of excavated openings in salt indicate each waste panel will be isolated from one-another for the majority of the regulatory period due to the creep-closure process. Therefore, it is highly unlikely that brine in contact with waste in one panel of the repository will contact brine in another panel. Because chemical equilibrium is assumed between brine and actinide solubility-controlling solids, heterogeneous distribution of the radionuclide inventory between the panels will not affect the calculated actinide solubilities. DOE has adequately accounted for the effects of possible heterogeneous distribution of organic ligands between panels in the actinide solubility calculations. Panels filled with waste following the approval of shielded RH containers may have significantly higher lead contents from the container shielding.

Section 12.0 addresses the effects of chemical processes on the repository water balance. Anoxic corrosion was the only chemical process included in calculations of the quantity of brine in the repository for the CCA PAVT, PABC04 and PABC09. The revised CRA-2014 PA water balance added the effects of iron sulfidation, microbial degradation of CPR, MgO hydration, MgO and brucite carbonation and the hydromagnesite conversion reaction. DOE has updated corrosion rates without considering steel passivation. MgO hydration rates included in the water balance were based on data from Premier MgO, which is present in the repository in smaller quantities than Martin Marietta MgO. Premier MgO hydrates more slowly than Martin Marietta MgO. EPA's assessment of DOE's MgO hydration rates used in the 2014-CRA PA indicate this parameter is not aligned with the experimental data for Martin Marietta MgO hydration, the predominate supplier of MgO. Therefore, EPA recommends that DOE develop hydration rates using Martin Marietta MgO and use these rates in combination with Premier MgO hydration rates in the CRA-2019 PA. A 'composite' hydration rate will likely decrease brine volumes in the repository. Updates to the CRA-2014 PA water balance are a significant improvement over the water balance calculations used for previous WIPP PAs. The available information indicates that the effects of the CRA-2014 PA water balance issues identified by EPA are likely to be reasonably minor, but DOE should address these issues for the CRA-2019 PA water balance.

Section 13.0 summarizes the results of an additional PA (CRA14_SEN4) that incorporated some changes to the CRA-2014 PA and assesses the effects of these changes on repository releases. Chemistry parameter changes included revised distributions for the +III and +IV actinide solubility uncertainties based on criteria amended by EPA and changes to the stoichiometric parameters for reaction of H_2S with Fe(s) and $Fe(OH)_2$(s) to reflect surface passivation. Total releases calculated for the CRA14_SEN4 PA were minimally changed at high probabilities

relative to total releases for the CRA-2014 PA. However, direct brine releases (DBRs) were noticeably increased in the CRA14_SEN4 PA compared to the CRA-2014 PA because of higher total mobilized Pu(III) and Am(III) concentrations resulting from the increased +III actinide solubility in the revised uncertainty distribution, an increased probability of encountering pressured brine during a drilling intrusion and increased repository pressure because of the removal of the iron sulfidation reactions from the repository water balance.

Section 14.0 summarizes EPA's conclusions regarding chemistry issues related to the CRA-2014. Review of the CRA-2014 and supporting information, including the results of the CRA-2014 PA and CRA14_SEN4 PA, demonstrates that because of their importance to releases from the repository, issues related to the plutonium oxidation states in WIPP repository brines and solids and DOE's proposed changes to the microbial colloid conceptual model are particularly important to resolve as soon as possible. In addition, EPA recommends that DOE take the following actions for performance assessment, ideally for inclusion in the CRA-2019:

- Use the revised, higher humid and inundated anoxic corrosion rate ranges identified by EPA that account for the effects of CO_2 and high pressure
- Confirm that the steel surface area per unit disposal volume is representative of WIPP waste using updated inventory data, the sheet metal surrogate and 55-gallon drum surrogate assumptions and updated waste emplacement data
- Develop a reasonable upper-bound estimate for the lead inventory and lead surface area per unit disposal volume that accounts for the potential future inventory of lead associated with shielded containers; it would be appropriate for DOE to use available project-specific lead corrosion data to assess the effects of lead corrosion on gas generation and brine consumption in the WIPP repository
- Use the available radiolytic $H_2(g)$ generation data from monitoring of sealed WIPP panels to evaluate whether radiolytic gas generation rate is significant relative to the rates of gas generation by microbial degradation and anoxic corrosion
- Remove the assumption that all $H_2S(g)$ generated by CPR degradation will instantaneously react with Fe(s) and $Fe(OH)_2(s)$ from the gas generation rate calculations by revising the relevant stoichiometric coefficients
- Because of their importance to releases from the repository, perform an independent technical review of likely plutonium oxidation states in solids and aqueous species in the repository
- Use the solubility of hydromagnesite established by Robie and Hemingway (1973) in the EQ3/6 database
- Review the results of investigations published after the CRA-2014 cutoff date related to complexation of +III actinides by borate species and precipitation of borate solid phases, and if appropriate, revise the EQ3/6 thermodynamic database to incorporate the data
- Use the data provided by Altmaier et al. (2005, 2006) to develop revised aqueous speciation and Pitzer parameters for the Th(IV)-carbonate aqueous species and incorporate the results in the EQ3/6 database

- Use the results of the Neck et al. (2009) $Nd(OH)_3(s)$ solubility study to update the solubility of $Am(OH)_3(s)$ in the EQ3/6 database
- Provide supporting information for the revised data in the EQ3/6 database DATA0.FM2 to demonstrate agreement with acceptance criteria; EPA would like to see this supporting information sufficiently in advance of the CRA-2019 to enable EPA review and acceptance before its use to calculate dissolved actinide concentrations for the CRA-2019 PA
- Modify the criteria to select solubility data for the +III and +IV actinide solubility uncertainty distributions
- Experimentally evaluate formation of mineral fragment colloids from MgO hydration and carbonation products and their effects on total mobilized actinides
- Revise the Th(IV) intrinsic colloid parameter to be consistent with upper bounding values for samples collected within the pcH range of 8.5 – 10.5
- Provide documentation for the data used to determine the Pu(III) and Am(III) intrinsic colloid parameters and develop a Pu(III) intrinsic colloid parameter that is an upper bounding value
- Incorporate the effects of bioaccumulation and biomineralization in addition to biosorption in the development of revised microbial colloid parameters; until the effects of bioaccumulation and biomineralization have been included in the revised parameters, the Agency will only accept the higher proportionality constants (either from the CCA PA or CRA-2014 PA) for the CRA-2019 PA
- Use the higher CAPMIC parameters developed for the CCA based on the conceptual model assumption that these parameters represent the concentrations at which no growth of microbial colloids occurs
- Use 2 nm filtration to remove intrinsic colloids from post-test solutions in future microbial colloid experiments to establish the dissolved concentration for calculating proportionality constants for microbial colloids
- Develop MgO hydration rates that adequately account for the more rapid hydration rates of Martin Marietta MgO relative to Premier MgO for use in the CRA-2019 PA water balance
- Use the lower rate range established by EPA for the hydromagnesite conversion rate for the CRA-2019 PA water balance

1.0 INTRODUCTION

The Waste Isolation Pilot Plant (WIPP) in southeastern New Mexico is an underground facility designed for the permanent disposal of transuranic (TRU) defense-related waste. The U.S. Department of Energy (DOE) operates the WIPP repository under the regulatory oversight of the U.S. Environmental Protection Agency (EPA). DOE submitted the Compliance Certification Application (CCA) to the EPA in 1996. After extensive review of the CCA and supplemental information provided by DOE, including an additional performance assessment (PA) calculation referred to as the Performance Assessment Verification Testing (PAVT), EPA certified that DOE had met the regulatory requirements and WIPP began accepting waste in March 1999.

Waste characteristics and waste components must be analyzed and the results must be included in any certification application [40 CFR 194.24(b)]. Those waste characteristics and components that could affect releases must be incorporated into PA [40 CFR 194.32(a)]. All additional data collected since the most recent CCA or Compliance Recertification Application (CRA) must be included in the CRA [40 CFR 194.15(a)], including any geochemical information, analyses, or results of laboratory experiments that are relevant to the performance of the repository. WIPP waste characteristics and components that have been identified as potentially affecting the chemistry of the system and releases include actinide solubilities and oxidation state distributions; formation of colloidal suspensions containing radionuclides; production of gas from the waste; ferrous metals inventory; cellulosics, plastics, and rubber (CPR) inventory; chelating agents (organic ligands) and oxyanions; and the activity of each isotope of the radionuclides present in the waste [40 CFR 194.24(b), EPA 1997b].

DOE is required to submit a CRA every 5 years after the initial acceptance of waste at WIPP and the first CRA (CRA-2004) was submitted to EPA in March 2004 (DOE 2004). EPA reviewed the CRA-2004 and supplemental information provided by DOE, including PA calculations referred to as the CRA-2004 Performance Assessment Baseline Calculations (PABC04), and certified that DOE continued to meet WIPP regulatory requirements (EPA 2006a).

DOE submitted the second CRA (CRA-2009) to EPA in March 2009 (DOE 2009). The CRA-2009 PA included the actinide solubility and colloidal actinide source term calculations from the PABC04. EPA performed a completeness review of the CRA-2009 and instructed DOE to perform a new PA to capture changes since the 2004 recertification (Cotsworth 2009a). DOE performed this revised PA, the CRA-2009 Performance Assessment Baseline Calculations (PABC09). Based on their review of the CRA-2009 and PABC09, EPA certified that DOE continued to meet WIPP regulatory requirements (EPA 2010a). At the time of the recertification decision, EPA (2010b) noted some uncertainties related to WIPP chemistry and also identified issues related to WIPP repository chemical processes for additional investigation by DOE prior to the CRA-2014.

DOE submitted the third CRA (CRA-2014) in March 2014 (DOE 2014b) that included the CRA-2014 PA. Because of uncertainties associated with some of the parameters used in the PA, EPA requested a sensitivity study of the CRA-2014 PA (CRA14_SEN4 PA), which included changes to the probability of encountering a Castile brine reservoir, changes to the uncertainty distributions for the +III and +IV actinide solubilities, a change to the shear strength of degraded waste, changes to the stoichiometric parameters for the iron sulfidation reactions, use of a

corrected version of the DRSPALL code for calculating spallings[1] releases, and use of a corrected panel closure length.

This Technical Support Document summarizes EPA's review of chemistry-related issues important to PA, including actinide source term modeling, gas generation, backfill efficacy and actinide transport in the Culebra Dolomite above the repository for the WIPP CRA-2014 and CRA14_SEN4. The principal portions of CRA-2014 (DOE 2014b) addressed during this review are Appendix SOTERM and its supporting references, portions of §194.44 and Appendix MgO and their supporting references, portions of Appendix PA and its supporting references and portions of Appendix MASS and its supporting references. Information has also been obtained from DOE's responses to EPA's requests for additional information and from the results of reviews of chemistry-related issues carried out by EPA since the CCA.

Chemistry-related topics addressed in this report include Salado Formation mineralogy surrounding the repository and the chemistry of Salado and Castile brines (Section 2.0); gas generation caused by microbial degradation of CPR and anoxic corrosion of metals in the repository (Section 3.0); the ability of the magnesium oxide (MgO) backfill to control chemical conditions (Section 4.0); actinide oxidation states assumed in source term modeling (Section 5.0); dissolved actinide source term modeling (Section 6.0); colloidal actinide source term modeling (Section 7.0); PA calculations of total mobilized actinides (Section 8.0); an assessment of the actinides included in PA (Section 9.0); distribution coefficients (K_ds) used in PA to model the release of actinides by transport through the Culebra member of the Rustler Formation (Section 10.0); the effects of heterogeneous waste loading (Section 11.0); the effects of chemical processes on repository water balance (Section 12.0); and the sensitivity of repository releases to parameter changes made in the CRA14_SEN4 (Section 13.0).

The results of this review indicate that DOE has modified its assessment of repository chemical processes as additional information has become available since the CCA PAVT, PABC04 and PABC09. EPA has identified additional modifications to incorporate in DOE's assessment of repository chemical processes for the CRA-2019 PA.

[1] Spallings are solids that are forced into the borehole by pressurized gas when a hole is drilled into the repository.

2.0 GEOLOGIC SETTING, SALADO FORMATION MINERALOGY, AND BRINE CHEMISTRY

WIPP repository chemical processes are influenced by the chemistry of the waste and by interaction of the waste with brines that may contact the waste and with the minerals in the Salado Formation that surrounds the repository. As a result, the geologic setting, Salado Formation mineralogy and the chemistry of brines that could contact the waste can affect actinide releases from the repository and subsequent transport. The Salado mineralogy and the chemistry of brines that may contact WIPP waste are described in the CRA-2014 (DOE 2014b, Appendix SOTERM, Section 2.0).

2.1 GEOLOGIC SETTING

The WIPP repository is excavated within the Salado Formation. The low permeability of the Salado Formation surrounding the WIPP repository provides a significant hydrologic barrier between the repository and other, more transmissive water-bearing strata. A more permeable, transitory region forms within the Salado around the repository in response to the stress field caused by repository excavation; this region is called the Disturbed Rock Zone (DRZ). The DRZ is relatively thin compared to the thickness of the Salado Formation surrounding the repository (DOE 2014b, Appendix PA, Section 2.2.1).

The Salado Formation is underlain by the Castile Formation. The Castile Formation is mainly composed of thick beds of high-purity halite, alternating with thick beds of interlaminated carbonate and anhydrite [$CaSO_4$(s)] (DOE 2014b, Appendix SOTERM, Section 2.1). The Castile Formation has been significantly deformed in some areas near the WIPP repository and pressurized brines are associated with the deformed areas.

The Salado Formation is overlain by the Rustler Formation (DOE 2014b, Appendix SOTERM, Section 2.1). This formation is composed of evaporite layers called, from bottom to top, the Los Medaños Member, the Culebra Dolomite Member, the Tamarisk Member, the Magenta Dolomite Member, and the Forty-Niner Member. The Culebra Dolomite is mostly composed of dolomite [$CaMg(CO_3)_2$(s)], with small amounts of anhydrite or gypsum [$CaSO_4 \cdot 2H_2O$(s)] (Lambert 1992). The Culebra Dolomite is the most transmissive continuously saturated unit above the WIPP facility. It therefore provides the most direct pathway from the repository to the accessible environment, apart from releases directly to the surface (DOE 2004, Section 2.0). As a consequence, this aquifer has been studied more extensively than other portions of the Rustler Formation (Lambert 1992; DOE 2004, Section 2.0). The Magenta Dolomite has lower transmissivity than the Culebra Dolomite, and is unfractured at the WIPP site (DOE 2004, Section 2.0).

2.2 SALADO MINERALOGY

In the area around WIPP, the Salado Formation is a thick bedded salt, composed mainly of layers of impure halite [NaCl], with interbedded layers of anhydrite, polyhalite [$K_2MgCa_2(SO_4)_4 \cdot 2H_2O$(s)] and mudstone (Lambert 1992). These sulfate-bearing interbeds are called Marker Beds (MB). Within the Salado Formation, these beds are labeled using numbers

that range from MB 100 near the top of the formation to MB 144 near the bottom (DOE 2004, Section 2.0).

Stein (1985) provided mineralogical analyses of drill core from the Salado Formation above and below the repository horizon. Based on x-ray diffraction (XRD) data, Stein (1985) identified quartz [SiO_2(s)], magnesite [$MgCO_3$(s)], anhydrite, gypsum, halite, polyhalite, bassanite [$CaSO_4 \bullet 0.5H_2O$(s)], alkali feldspar [$(NaK)AlSi_3O_8$(s)], and clay minerals in the Salado Formation. Brush (1990) used these data to calculate the average mineralogical composition of the Salado to use for geochemical modeling of the effects of different backfill additives. Because this XRD evaluation of the mineralogical composition was only semiquantitative, Brush (1990) assumed that halite constituted 93.2 wt% of the Salado Formation, with the remaining fraction composed of equal parts magnesite, anhydrite, gypsum and polyhalite (1.7 wt% each). Brush (1990) did not include clay minerals, feldspar and quartz in the assumed mineralogy because Pitzer data for aqueous silica species were not available at that time for use in geochemical modeling. Bassanite was not included in the assumed mineralogy, because it was identified in only one sample.

3.0 GAS GENERATION

The Gas Generation conceptual model includes the assumption that significant gas generation will occur in the repository from corrosion of ferrous metals and from microbial degradation of CPR. The Gas Generation conceptual model also includes the assumptions that essentially all carbon dioxide [CO_2] will be removed from the gas phase by reaction with the MgO backfill and that radiolysis of water in the waste and brine and radiation of plastics and rubber in the waste will not have significant effects on the amounts of gas generated (Wilson et al. 1996a and 1996b). The model assumes that corrosion of other metals in the WIPP inventory, such as aluminum and lead, will not contribute significantly to gas generation rates because of low inventories.

The Gas Generation conceptual model implemented in WIPP PA is called the average stoichiometry model, to differentiate it from alternative gas generation conceptual models considered for the CCA (Wilson et al. 1996a). The current Gas Generation conceptual model is described in detail by SC&A (2008b, Section 2.0 and Appendix A.1).

3.1 SALADO FORMATION AND CASTILE FORMATION BRINE CHEMISTRY

Small quantities of intergranular and intragranular Salado brines are associated with the salt at the repository horizon. These brines are highly concentrated (ionic strengths up to 8 molar), with a composition of mostly sodium, magnesium, potassium, chloride and sulfate, and with smaller amounts of calcium, carbonate and borate. Two formulations of these Salado brines have been used in WIPP laboratory experiments and PA calculations—Brine A and Generic Weep Brine (GWB) (Snider 2003b). In the CCA PAVT, the Brine A formulation was used to simulate intergranular Salado brines. However, the GWB Salado brine formulation has been used in the CRA-2004 PA and all subsequent WIPP PA calculations. A detailed discussion of GWB brine and a comparison of this brine to Brine A were provided by Snider (2003b).

GWB was developed based on chemical analyses of intergranular fluids that seep into the WIPP excavations from the DRZ (Snider 2003b). DOE developed the GWB formulation because of the potential effects of magnesium concentrations in the brine on the modeled and experimental chemical behavior of the MgO backfill; the concentration of magnesium in GWB is lower than in Brine A (Table 2-1). Snider (2003b) verified the calculations supporting the formulation of GWB and compared the concentrations of major cations and anions in several WIPP brines. The comparison between GWB and Brine A indicated that GWB has higher boron, sodium, bromide, chloride and sulfate concentrations, and lower calcium, potassium and magnesium than Brine A. Brine A has a relatively low reported inorganic carbon concentration, whereas none was reported for GWB (Table 2-1). The ionic strength[2] of GWB is approximately 6.5 compared to approximately 5.9 for Brine A.

EPA (2006c) reviewed DOE's proposed use of the GWB brine formulation to model actinide solubilities for the CRA-2004 PA and concluded that the GWB formulation was adequately

[2] Ionic strength (I) is defined by the equation $I = \frac{1}{2} \Sigma_I c_i Z_i^2$. This summation is carried out for all cations and anions in the solution, and c_i and Z_i are the concentrations and charges, respectively, of all ions in solution.

documented. EPA concurred with DOE that the GWB brine formulation more closely matches the composition of Salado intergranular brines than Brine A, and that use of the GWB formulation in place of Brine A for the CRA-2004 PA and future actinide solubility calculations is appropriate. Only minor differences were observed in actinide solubility calculations carried out with GWB and Brine A.

Table 3-1. Brine A, GWB and ERDA-6 Compositions

Component	Brine A	GWB	ERDA-6
Boron	0.020	0.155	0.063
Calcium	0.020	0.014	0.012
Potassium	0.770	0.458	0.097
Magnesium	1.44	1.00	0.019
Sodium	1.83	3.48	4.87
Bromide	0.010	0.026	0.011
Chloride	5.35	5.51	4.8
Sulfate	0.040	0.175	0.170
Total Inorganic Carbon	0.010	Not reported	0.016
pH	6.5	Not reported	6.17
Specific Gravity (kg/L)	1.2	1.2	1.216
Total Dissolved Solids (mg/L)	306,000	Not reported	330,000

All units are moles/L solution, unless otherwise specified.
Source: Brush and Xiong (2003a)

Castile brine may enter the repository if a borehole that penetrates the repository also penetrates an area of pressurized brine in the underlying Castile Formation. Borehole ERDA-6 encountered pressurized brine in the Castile Formation. The composition of this ERDA-6 brine has been used to represent the likely composition of Castile brine in laboratory experiments and all WIPP PA calculations (Table 2-1).

3.2 IRON CORROSION

Relatively large quantities of reduced iron will be present in the repository in the form of steel waste containers and as iron-based alloys in the waste. The most recent inventory estimates of the masses of iron-based waste material and packaging materials in contact-handled (CH) and remote-handled (RH) waste are provided by Van Soest (2012, Table 5-5). This estimate is based on the annual inventory report as of December 31, 2011 (DOE 2012) and includes emplaced, stored and projected WIPP waste, scaled to a full repository. These estimates indicate that over 49,000 metric tons of iron-based materials will be present in the repository at closure (Table 3-1). CH and RH waste constitutes 25% of the iron-based metals and alloys inventory, and packaging materials make up 75% of this inventory (Table 3-1).

Table 3-2. CRA-2014 PA Inventories of Iron-Based Metals and Alloys in Waste and Steel Packaging Materials

Parameter	Mass (kg)	Mass (%)
CH Waste Iron-Based Metal and Alloys	10,900,000	22
CH Steel Packaging Materials	30,000,000	61
RH Waste Iron-Based Metal and Alloys	1,350,000	3
RH Steel Packaging Materials	6,860,000	14
Repository Total	49,110,000	100

Source: Van Soest (2012)

The Gas Generation conceptual model includes assumptions related to iron corrosion (Wilson et al. 1996a and 1996b, SC&A 2008b):

- The small amounts of oxygen trapped in the repository immediately after closure will be consumed by oxic corrosion or aerobic microbial degradation, and these processes will not generate a significant amount of gas
- Anoxic corrosion can occur in the repository as soon as the shafts are sealed
- Anoxic corrosion of steel in the repository cannot occur unless brine is present and in contact with the steel, and the corrosion rate is assumed to be a function of both brine saturation and steel surface area
- Carbon dioxide generated by microbial degradation of CPR will not passivate steel, because CO_2 will be consumed by reaction with the MgO backfill
- Hydrogen sulfide (H_2S) might passivate steel by forming FeS(s) on the steel surfaces if H_2S is produced in sufficient quantities; however, reducing chemical conditions would continue to be maintained by the FeS(s).
- Fe will be represented by Fe(s) and/or $Fe(OH)_2$[3]

3.2.1 Corrosion Reaction Products and Stoichiometry

Anoxic corrosion of steel in the waste and waste containers produces hydrogen (H_2). The chemical reactions that represent the stoichiometry of anoxic corrosion of steel in the WIPP repository for CRA-2014 are:

$$Fe(s) + (x+2)\ H_2O \leftrightarrow Fe(OH)_2 \bullet xH_2O(s) + H_2 \quad \textbf{(1)}$$

$$Fe(s) + H_2S \leftrightarrow FeS(s) + H_2 \quad \textbf{(2)}$$

[3] The product of iron metal corrosion is most accurately represented as $Fe(OH)_2 \bullet xH_2O(s)$. However, because the waters of hydration in this reaction product are indeterminate, $Fe(OH)_2(s)$ is used for stoichiometric calculations

In the CRA-2004 (DOE 2004, Appendix PA, Attachment SOTERM-2.2.3) and CRA-2009 (DOE 2009, Appendix SOTERM-2.3.4), DOE listed additional iron corrosion reactions based on WIPP-specific experiments (Telander and Westerman 1993 and 1997):

$$3\ Fe(s) + 4\ H_2O \leftrightarrow Fe_3O_4(s) + 4\ H_2 \quad \textbf{(3)}$$

$$Fe(s) + H_2O + CO_2 \leftrightarrow FeCO_3(s) + H_2 \quad \textbf{(4)}$$

Reactions (3) and (4) indicate that iron corrosion could produce magnetite [$Fe_3O_4(s)$] or siderite [$FeCO_3(s)$]. The possible occurrence of reaction (3) is important, because reaction (3) produces 1.33 moles of gas per mole of iron, whereas reactions (1) and (2) produce only one mole of gas per mole of iron. EPA previously considered whether inclusion of reactions (3) and (4) in the Gas Generation conceptual model is appropriate (SC&A 2008b). The available experimental data indicate that magnetite formation will not occur at the low temperatures expected in the WIPP repository. Siderite formation is not expected to be a significant process in the repository, because of the presence of the MgO backfill, which will control CO_2 fugacities at low levels. Consequently, reactions (1) and (2) describe the expected anoxic corrosion reactions in the WIPP repository (SC&A 2008b).

DOE (2014b, Appendix SOTERM, Section 2.3.4) stated that based on new iron corrosion experiments, Roselle (2013) had identified green rust [idealized formula $Fe(III)_2Fe(II)_4(OH)_{12}CO_3{\cdot}2H_2O$] as the "most likely corrosion product in experiments with low atmospheric CO_2 concentrations (<350 ppm)." The corrosion reaction to form green rust was given as:

$$6\ Fe(s) + CO_2 + 15\ H_2O \rightarrow Fe(III)_2Fe(II)_4(OH)_{12}CO_3{\cdot}2H_2O(s) + 7\ H_2 \quad \textbf{(5)}$$

However, EPA noted that Roselle (2013) did not identify green rust as an iron corrosion product and that green rust formation could affect the moles of gas produced per mole of iron consumed (Edwards 2015a, Completeness Comment 4-C-6). In response, DOE reviewed the available data regarding likely iron corrosion products (Shrader 2016), including WIPP-specific data from Telander and Westerman (1993, 1997), Roselle (2009, 2010, 2011a, 2011b, 2013) and Nemer et al. (2011) as well as data related to corrosion of iron archaeological artifacts in chloride-rich environments (Neff et al. 2005, Réguer et al. 2007, Bellot-Gurlet et al. 2009, Rémazeilles et al. 2009, Saheb et al. 2009). The available data indicate that the most likely corrosion product is $Fe(OH)_2{\bullet}xH_2O(s)$, as observed by Telander and Westerman (1993), or possibly $Fe_2(OH)_3Cl(cr)$. Consequently, EPA believes the molar ratio of hydrogen gas produced per mole of iron should remain equal to 1 for anoxic corrosion of iron in the WIPP environment.

3.2.2 Corrosion Rates

Two parameters are used in PA to represent iron corrosion rates, STEEL:CORRMCO2, representing the inundated steel corrosion rate (m/s) and STEEL:HUMCORR, representing the humid steel corrosion rate (m/s). The same values and distributions for these parameters were

used for the CCA PAVT, PABC04 and PABC09. In these PAs, the humid corrosion rate for steel was assumed equal to 0.0 m/s (Wang and Brush 1996).

For the CCA PA, DOE estimated the inundated corrosion rate would range from 0.0 to 1.59×10^{-14} m/s, with a uniform distribution over this range (Wang and Brush 1996). However, EPA requested that DOE double the upper bound of the inundated corrosion rate because of the rate increase observed at pressures from 70 to 127 atm by Telander and Westerman (1997), which are comparable to WIPP repository gas pressures (Camphouse 2013a). MFG (2000) confirmed these corrosion rates and established iron corrosion would also maintain repository reducing conditions. Consequently, the sampled range for the inundated steel corrosion rate was from 0 to 3.17×10^{-14} m/s, with a uniform distribution for the CCA PAVT, PABC04 and PABC09 (Fox 2008).

DOE (2014b, Appendix PA) established a revised range and distribution for the inundated steel corrosion rate for the CRA-2014 PA (Table 3-2) based on WIPP-specific experiments (Roselle 2009, 2010, 2011a, 2011b, 2013). The humid corrosion rate remained unchanged for the CRA-2014 PA at zero, based on a recommendation by Roselle (2013).

Table 3-3. WIPP PA Inundated Steel Corrosion Rates (STEEL:CORRMCO2) and Humid Steel Corrosion Rates (STEEL:HUMCORR)

	Distribution	Maximum	Mean	Minimum
Inundated Steel Corrosion Rates (m/s)				
CCA PA	Uniform	1.59×10^{-14}	7.95×10^{-15}	0.0
CCA PAVT, PABC04, PABC09	Uniform	3.17×10^{-14}	1.585×10^{-14}	0.0
CRA-2014	Student	1.84×10^{-14}	6.06×10^{-15}	3.29×10^{-16}
Revised (Zeitler and Hansen 2015a)	CDF	3.96×10^{-14}	6.76×10^{-15}	0.0
EPA-Revised (increased pressure)	CDF	7.92×10^{-14}	1.35×10^{-14}	0.0
Humid Steel Corrosion Rates (m/s)				
CCA PA, CCA PAVT, PABC04, PABC09, CRA 2014 PA	--	0.0	0.0	0.0
Revised (Zeitler and Hansen 2015b)	CDF	1.03×10^{-15}	2.71×10^{-16}	0.0

EPA requested that DOE provide copies of the spreadsheets containing the iron and lead corrosion rate data (Edwards 2015b, Comment 2-C-8) and received the data from DOE (Franco 2015a).

EPA requested justification for the revised inundated steel corrosion rate because Roselle (2013) used only data obtained at a CO_2 atmospheric concentration of 0 ppm to determine the revised rates (Edwards 2015a, Comment 4-C-2). EPA observed that CO_2 atmospheric concentrations in equilibrium with repository brines, while low, are nonzero and corrosion experiments conducted at higher CO_2 appeared to have higher maximum corrosion rates. EPA stated that the minimum sampled range should remain at zero because of the possibility of passivation of the steel surface

by H_2S reported by Telander and Westerman (1993, 1997). EPA also requested that DOE provide justification for the distribution selected for the inundated steel corrosion rate parameter. DOE responded with a revised assessment of the corrosion rate data (Shrader 2016, Zeitler and Hansen 2015a).

DOE (Zeitler and Hansen 2015a) acknowledged that it was appropriate to include corrosion experiments conducted with nonzero CO_2 concentrations because CRA-2014 calculations (Brush and Domski 2013b) predicted a gas-phase CO_2 concentration of 3.14 ppm in equilibrium with WIPP brines. Zeitler and Hansen (2015a) recalculated the inundated steel corrosion rate by including data collected at CO_2 concentrations of 0 and 350 ppm and 1 atm total pressure (Table 3-2). The data set included 64 samples tested at 0 ppm CO_2 and 64 samples tested at 350 ppm CO_2. Four of the 350 ppm CO_2 samples were excluded because of negative measured reaction rates, and an additional data point was added to represent the lower-bound zero reaction rate, resulting in a final data set of 125 observations. Zeitler and Hansen (2015a) accumulated these rates into a cumulative distribution function (CDF) that could be used in PA because it represents the range of variability in the inundated corrosion rate data. This data analysis and distribution is reasonable, but does not account for the previously noted effects of higher repository pressure on the inundated corrosion rate. Consequently, EPA recommends the inundated corrosion rates measured by Roselle (2013) and accumulated into the CDF for PA be increased by a factor of two, as previously directed by EPA for the CCA PAVT (Table 3-2).

Humid steel corrosion rates previously used in PA have been zero based on assessments of data available from Telander and Westerman (1993, 1997). EPA observed that the Roselle (2013) data appeared to be non-zero and requested that DOE assess the humid steel corrosion rate using data obtained with gas-phase CO_2 concentrations of 0 and 350 ppm, which bracket anticipated repository conditions (Edwards 2015a, Comment 4-C-3). DOE responded with a revised assessment of the humid corrosion rate data (Shrader 2016, Zeitler and Hansen 2015b).

DOE (Zeitler and Hansen 2015b) considered 16 data points from Roselle (2013), eight each for samples tested at 0 ppm and 350 ppm CO_2. After constructing separate CDFs for 0 ppm and 350 ppm CO_2 data, Zeitler and Hansen (2015b) developed a common set of percentiles by linearly interpolating between the CDFs using a CO_2 concentration of 3.14 ppm, consistent with predicted WIPP repository conditions from Brush and Domski (2013b). The resulting CDF ranges from 0 m/s to 1.03×10^{-15} m/s with a mean value of 2.71×10^{-16} m/s (Zeitler and Hansen 2015b). Because of the limited number of data points, any selected distribution would be debatable. The upper bound for the humid corrosion rate is reasonable, because only a single data point obtained at 350 ppm CO_2 significantly exceeds this rate and a lower bound of zero is appropriate considering the possibility of surface passivation by H_2S and low to slightly negative rates observed in some of the experiments (Figure 3-1). The mean value also appears adequately descriptive of the data. Because this CDF is reasonable, we believe the CRA-2019 PA will be strengthend if DOE used the distribution developed by Zeitler and Hansen (2015b) for the humid steel corrosion rate. A nonzero humid corrosion rate represents a revision to the Gas Generation conceptual model, but this change is adequately supported by new experimental data.

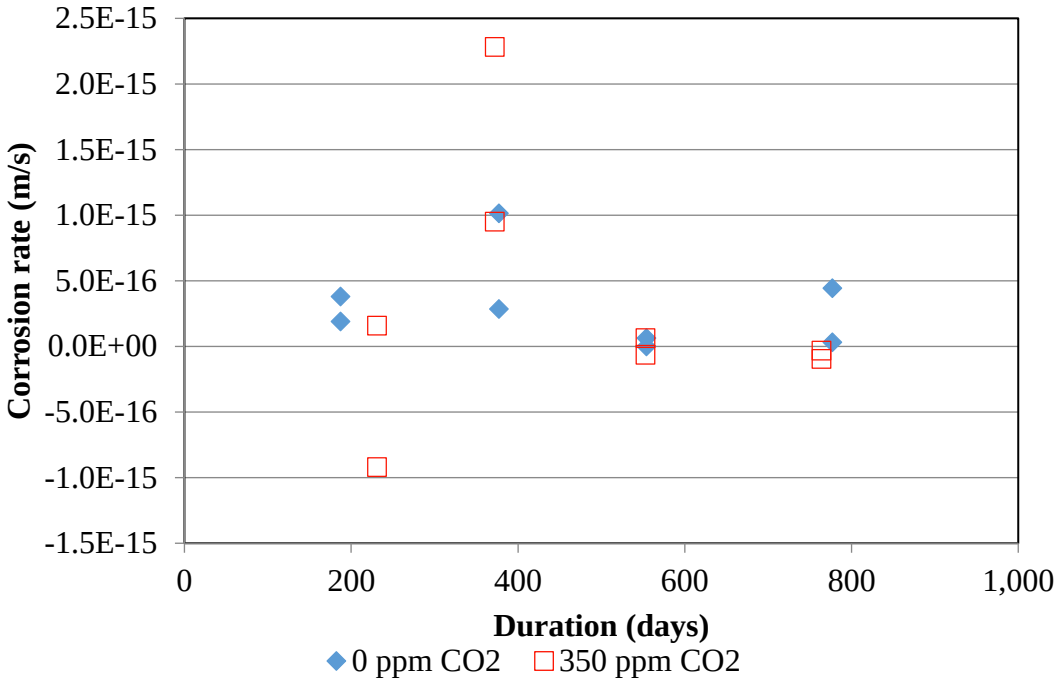

Figure 3-1. Humid Steel Corrosion Rate Data (Roselle 2013)

3.2.3 Passivation of Iron Surfaces by H_2S

EPA requested that DOE provide the basis for the PA assumption that all H_2S produced by microbial degradation of cellulose will instantaneously react to produce iron sulfide (Edwards 2015a, Comment 4-C-5), noting that WIPP-specific corrosion experiments had indicated H_2S passivated steel (Telander and Westerman 1997). In their response, DOE cited Wang and Brush (1996), who opined that steel passivation is unlikely based on the length of time necessary for repository H_2S concentrations to increase to the levels used in the WIPP-specific experiments (Shrader 2015). In addition, Wang and Brush (1996) stated that the lack of total steel passivation in the WIPP repository is consistent with other studies, citing Ikeda et al. (1983) and Schmitt (1983). Wang and Brush (1996) noted that although total passivation of iron corrosion by H_2S has not been observed, varying degrees of corrosion inhibition (i.e., a significant decrease in corrosion rates) has been observed in the presence of H_2S.

DOE did not provide the Ikeda et al. (1983) and Schmitt (1983) articles, but their titles indicate that they address the effects of CO_2 on steel corrosion. The effects of CO_2 on steel corrosion rates are minimally significant to the WIPP repository environment because of the low CO_2 concentrations that will be maintained by the MgO backfill. Although complete passivation of steel in the repository by H_2S is uncertain, DOE's response includes the observation that corrosion may be inhibited by H_2S. Consequently, DOE has not adequately justified the assumption of instantaneous reaction of H_2S with iron and iron hydroxide in the repository.

The iron metal sulfidation and ferrous hydroxide sulfidation reactions are reaction (2) and:

$$Fe(OH)_2(s) + H_2S(g) \rightarrow FeS(s) + 2\ H_2O(l) \quad \textbf{(6)}$$

Reaction (2) has no net effect on the amount of gas or brine in the repository. However, reaction (6) reduces the amount of gas and increases the brine volume.

The available data (e.g., Nešić et al. 2008) indicate that $H_2S(g)$ in the repository will initially rapidly react with iron and form a thin layer of FeS(s) on iron surfaces. This time period is consistent with DOE's assumption of instantaneous reaction of H_2S. However, after this initial period of rapid reaction, reaction rates decline significantly as iron sulfidation rates are controlled by diffusion through this adherent inner FeS(s) layer and a porous outer layer of FeS(s) reaction product. The assumption of instantaneous iron sulfidation reactions is inconsistent with this later period of slower reaction. Because H_2S presumably preferentially reacts with iron hydroxide versus metallic iron (DOE 2014b, CRA-2014 Appendix MASS, page MASS-57), overestimation of the iron sulfidation rate would result in an underestimation of the gas pressure and overestimation of the brine volume in the repository (reaction 6). The effects of underestimating the repository gas pressure appear likely to be non-conservative, because implementation of revised (lower) iron corrosion rates and water balance refinements in the CRA-2014 PA decreased the number of vectors with direct brine releases, which affects overall mean releases (Zeitler 2013, Figures 3-26 and 3-46; DOE 2014b, CRA-2014 Appendix PA, page PA-241). Because the assumption of instantaneous iron sulfidation may have non-conservative effects on repository releases, DOE should assume no reaction of H_2S with iron in the repository will occur, consistent with the WIPP-specific data from the experiments reported by Telander and Westerman (1997). EPA communicated with DOE regarding the validity of the iron sulfidation assumptions (Economy 2016). DOE agreed that there are insufficient data to support the assumption of instantaneous iron sulfidation reactions and stated that the stoichiometric coefficients for equations PA.89 and PA.90 (DOE 2014b, Appendix PA) should be set equal to zero, removing these reactions from PA (Patterson 2016b).

The stoichiometric coefficients for reactions (2) and (6) were set equal to zero for the CRA14_SEN4 PA (Zeitler and Day 2016). The effects of this change and other changes made for the CRA14_SEN4 PA are discussed in Section 13.0.

3.2.4 Steel Surface Area

The gas generation rate caused by anoxic corrosion of iron-based metal in the repository is proportional to the steel surface area per unit volume, D_S (DOE 2014b Appendix PA Equation PA.67). The value of D_S is calculated from (Appendix PA equation PA.75):

$$D_S = \frac{A_d n_d}{V_R} \quad \textbf{(7)}$$

Where:

A_d is the surface area of steel associated with a waste disposal drum (parameter REFCON:ASDRUM, m^2/drum)

V_R is the initial volume of a single room in the repository (parameter REFCON:VROOM, m^3), and

n_d is the ideal number of waste drums that can be close-packed into a single room (parameter REFCON:DRROOM).

Based on information developed prior to the CCA PA, the surface area of steel associated with a 55-gallon waste disposal drum (A_d) is approximately 6 m^2/drum (Brush 1990). This estimated surface area included both the surface area of the steel drum and the iron-based waste contents. A generic room size was assumed to be 33 ft by 300 ft by 13 ft (V_R, 3,640 m^3) allowing for 6,800 (n_d) 55-gallon drums. These parameters result in D_S = 11.2 m^2/m^3, which was used in the CRA-2014 PA and all previous WIPP PA calculations. EPA requested that DOE evaluate the potential effects of waste inventory and emplacement data collected since the CCA PAVT on the calculation of D_S (Edwards 2015a, Comment 4-C-4).

3.2.4.1 Technical Exchanges Over CRA-2014 Steel Surface Area

DOE responded with an evaluation of the PA parameters associated with the steel surface area (Shrader 2015, Day 2015). The results of these calculations show that the current value of D_S adequately represents current waste inventory, container types and waste emplacement in the repository. Because the waste inventory, relative numbers of different containers and emplacement practices may evolve over time, we expect future WIPP PAs to include recalculations of appropriate D_S values. A detail of this calculation is discussed below.

DOE (Day 2015) identified the different waste containers in the repository based on a WIPP Waste Data System (WDS) query as of December 31, 2014 refining surface area calculations and iron inventory. The inner plus outer surface areas for all authorized waste containers were calculated from the container dimensions (DOE 2014b, Appendix DATA, Attachment B). For authorized payload container types that were overpacked, the overpacked containers were not included in the average iron-based metal waste weight, but were instead used to directly calculate the steel surface areas based on their known geometry (Day 2015). For the 100-gallon drums containing compressed Advanced Mixed Waste Treatment Facility (AMWTF) waste, the mass of iron in the compressed drums was included with the iron-based waste in the surface area calculations (Patterson 2016b).

Because only the masses and not surface areas of iron-based waste are known from the inventory (Table 3-1), Day (2015) developed surrogate assumptions relating the surface area of the iron-based waste to its mass: a spherical assumption and a sheet metal assumption. For the spherical surrogate assumption, the surface area of the iron-based waste was assumed to be equivalent to the surface area of the same mass of 1-cm diameter steel spheres. For the sheet metal surrogate assumption, the surface area to mass ratio of the waste was assumed to be equivalent to the surface area to tare weight ratio of its container. Day (2015) did not provide evidence demonstrating that these assumptions are representative of WIPP waste or that these two surrogate assumptions are bounding of the possible range of surface area to mass ratios for WIPP waste.

In response to an EPA request for additional information (Economy 2016), DOE indicated that the spherical surrogate assumption is justified because 1 cm is a reasonable lower limit for identifying metal waste during radiographic examination of the waste drums (Patterson 2016b). Because the assumed spherical shape provides a minimum surface area to volume ratio, the surface area associated with the inventory of iron waste (6.5×10^5 m^2) is 27% of the total iron-based waste and container surface area (2.38×10^6 m^2, Patterson 2016b).

3.2.4.2 Recalculation of Steel Surface Area per Unit Volume

The sheet metal surrogate assumption used by Day (2015) does not provide a consistent upper bound for the range of the iron-based waste surface area to mass ratio because its results differ from the spherical surrogate assumption results by varying amounts, depending on container type (Day 2015, Table 2). For example, the sheet-metal surrogate provides an estimated iron-based waste surface area to mass ratio that is approximately twice the surface area to mass ratio for the spherical surrogate for 55-gallon drums. However, the estimated iron-based waste surface area values are approximately equal for the direct-load standard waste boxes.

The tare weights and surface areas reported by Day (2015, Table 1 and Appendix A) were used to calculate the surface area to tare weight ratios of the WIPP waste containers (Table 3-3). The ratios in Table 3-3 range over more than an order of magnitude, from 0.01 m^2/kg for the shielded container overpack of one drum up to 0.30 m^2/kg for the 85 gallon overpack of one drum. DOE justified the sheet metal surrogate assumption by stating that larger pieces of iron-based waste with lower surface area to mass ratios would be placed in more robust containers with lower surface-area to tare weight ratios. The sheet metal surrogate assumption results in an iron-based waste surface area that is 35% of the total iron-based waste plus container surface area (Patterson 2016b).

Most of the iron-based waste in the AMWTF containers (100-gallon drums) likely has a surface area to mass ratio consistent with 55-gallon drums, because the AMWTF drums are expected to contain an average of four compacted 55-gallon drums (Hansen et al. 2003b). Based on the tare weight for 55-gallon drums (28.6 kg), the mass of four 55-gallon drums represents 67% of the average iron-based waste weight in these containers (170.59 kg, Table 3-4). The two surrogate assumptions used by Day (2015) likely underestimate the steel surface areas in the AMWTF iron-based waste because the surface area to mass ratio for the AMWTF waste using the spherical assumption is 0.076 m^2/kg and the ratio used for the sheet metal surrogate assumption is 0.12 m^2/kg, both of which are lower than the 0.16 m^2/kg ratio for a 55-gallon drum.

The potential effect on D_S of a higher surface area to mass ratio for iron-based waste was assessed by assuming all iron-based waste had a surface area to mass ratio consistent with the ratio for a 55-gallon drum (55-gallon drum surrogate). This assumption is a reasonable approach for evaluating the possible maximum effects of the relatively large amount of iron-based metal waste in the AMWTF drums that is composed of compacted 55-gallon drums.

Table 3-4. WIPP Container Surface Areas, Tare Weights and Surface Area to Tare Weight Ratios

Container Type	Tare weight (kg)	Surface area of outer and overpacked containers (m^2)	Container surface area/tare weight (m^2/kg)
55-gallon drum (DL)[1]	28.6	4.58	0.16
12-in. standard pipe overpack (DL)	110.3	6.34	0.06
S100 pipe overpack (DL)	70.5	6.34	0.09
S300 pipe overpack (DL)	109.8	6.34	0.06
85-gallon drum (OP[2] one drum)	37	10.92	0.30
100-gallon drum (DL of compacted pucks)[3]	56.7	6.62	0.12
Standard waste box (DL)	290.3	21.93	0.08
Standard waste box (OP four drums)	290.3	40.23	0.14
Standard large box 2 (DL)	1,224.49	52.58	0.04
Ten drum overpack (DL)	770.98	31.42	0.04
Ten drum overpack (OP ten drums)	770.98	77.19	0.10
Shielded container (OP one drum)	782.77	8.98	0.01
RH FL waste canister (DL)	799.09	14.06	0.02
RH RL waste canister (DL)	517.01	14.06	0.03
RH RL waste canister (OP 3 drums)	517.01	27.79	0.05
Shield Plug	n.r.	10.18	n.c.

[1] DL = direct load
[2] OP = overpack
[3] AMWTF waste

The results of the steel surface area per drum equivalent calculations using the three surrogate assumptions are summarized in Table 3-4. RH waste that is not placed on the disposal room floor was not included in these calculations. The results show that there is a wide variation in the calculated steel surface area per drum equivalent depending on the container type and the average iron-based metal waste per container. Because a single A_d value is used for the entire repository, a representative steel surface area per drum equivalent must be calculated from an average that is weighted for the volumes occupied by each container type. Seven-packs of 55-gallon drums can be stacked in three layers within a disposal room. Consequently, there are 21 containers (7 drums stacked in three layers) present in each stack of 55-gallon drums. Day (2015, Appendix A) calculated for the other container types the number of containers that would occupy the same space as a stack of 55-gallon drums and the equivalent number of stacks that would be occupied by the number of each container (Table 3-5). The contribution of each waste container type to the steel surface area per drum equivalent was calculated by multiplying the surface area per drum equivalent (Table 3-4) by the number of equivalent stacks and dividing by the total number of stack equivalents. The results of this calculation for the three surrogate waste assumptions are provided in Table 3-5.

Table 3-5. Container plus Iron Waste Surface Areas Calculated per 55-Gallon Drum Equivalent Using Different Surrogate Assumptions

Container Type	Number of containers	Average iron-based metal waste per container type (kg)	Containers per stack	Spherical surrogate, surface area/drum equivalent (m^2/drum)	Sheet metal surrogate, surface area/ drum equivalent (m^2/drum)	55-gallon drum surrogate, surface area/drum equivalent (m^2/drum)
55-gallon drum (DL)	96,494	6.41	21	5.07	5.61	5.61
12-in. standard pipe overpack (DL)	25,626	2	21	6.49	6.45	6.66
S100 pipe overpack (DL)	814	0	21	6.34	6.34	6.34
S300 pipe overpack (DL)	45	0	21	6.34	6.34	6.34
85-gallon drum (OP one drum)	5	27.76	12	7.45	10.92	8.78
100-gallon drum (DL of compacted pucks)	34,255	170.59	9	8.41	11.37	14.54
Standard waste box (DL)	6,807	234.36	3	5.69	5.66	8.49
Standard waste box (OP four drums)	6,054	17.9	3	5.94	6.10	6.16
Standard large box 2 (DL)	228	492.13	0.678	2.91	2.38	4.24
Ten drum overpack (DL)	24	928.91	1.5	7.30	4.95	12.87
Ten drum overpack (OP ten drums)	6,023	22.87	1.5	5.64	5.68	5.78
Shielded container (OP one drum)	9	16.4	9	4.38	3.93	4.97

Table 3-6. Surface Area per Drum Equivalent, Weighted by Waste Container Volume and Number

Container Type	Number of containers	Containers per stack	Number of equivalent stacks	Spherical surrogate assumption, contribution to surface area per drum equivalent, (m^2/drum)	Sheet metal surrogate assumption, contribution to surface area per drum equivalent (m^2/drum)	55-gallon drum surrogate assumption, contribution to surface area per drum equivalent (m^2/drum)
55-gallon drum (DL)	96,494	21	4,595	1.27	1.41	1.41
12-in. standard pipe overpack (DL)	25,626	21	1,220	0.43	0.43	0.44
S100 pipe overpack (DL)	814	21	39	0.01	0.01	0.01
S300 pipe overpack (DL)	45	21	2	7×10^{-4}	7×10^{-4}	7×10^{-4}
85-gallon drum (OP one drum)	5	12	0	2×10^{-4}	2×10^{-4}	2×10^{-4}
100-gallon drum (DL of compacted pucks)	34,255	9	3,806	1.75	2.36	3.02
Standard waste box (DL)	6,807	3	2,269	0.70	0.70	1.05
Standard waste box (OP four drums)	6,054	3	2,018	0.65	0.67	0.68
Standard large box 2 (DL)	228	0.678	336	0.05	0.04	0.08
Ten drum overpack (DL)	24	1.5	16	0.01	4E-03	0.01
Ten drum overpack (OP ten drums)	6,023	1.5	4,015	1.24	1.24	1.27
Shielded container (OP one drum)	9	9	1	2×10^{-4}	2×10^{-4}	3×10^{-4}
Total			18,318	6.12	6.88	7.97

The largest contributions to the average weighted surface area per drum come from the 100-gallon drum containers with AMWTF waste, the 55-gallon drums and ten-drum overpacks (OP ten drums) because these container types comprise the largest numbers of equivalent stacks (Table 3-5). Significant contributions to the average weighted surface area per drum also come from the standard waste boxes (DL and OP four drums) and the 12-in. standard pipe overpacks, which also represent relatively large numbers of equivalent stacks. The total surface area per drum ranges from 6.12 m^2/drum for the spherical surrogate up to 7.97 m^2/drum for the 55-gallon drum surrogate. The most significant increase in the surface area per drum when using the 55-gallon drum surrogate instead of the spherical surrogate assumption comes from the 100-gallon drums containing compressed AMWTF waste. Because a large fraction (~67%) of the iron-based metal waste inside these 100-gallon drums will be compressed 55-gallon drums, this result shows that the spherical surrogate assumption likely underestimates a significant contribution to the steel surface area in WIPP waste. The representativeness of the different surrogate assumptions cannot be assessed given the available data, because there is no information regarding the physical dimension of the iron-based waste (Patterson 2016b). However, the spherical surrogate appears to provide an unrealistic and non-conservative result, so the most reasonable value for A_d likely falls within the range from the sheet metal surrogate value (6.88 m^2/drum) through the 55-gallon drum surrogate value (7.97 m^2/drum). Based on a panel volume of 46,097.6 m^3 (Schreiber 1991) and seven rooms per panel, Day (2015) calculated an idealized waste room volume of 6,585 m^3. Day (2015) used the CH-TRU waste emplacement information in the CRA-2014 (DOE 2014b, Appendix DATA Attachment B, Figure DATA-B-11) to establish that there are an idealized 10,908 55-gallon drum equivalent container positions per room. Both the room volume and number of drums per room increased relative to the values used in the CRA-2014 PA, but as noted by Day (2015), the revised n_d/V_R value (10,908 drums/room ÷ 6,585 m^3/room = 1.66 drums/m^3) is smaller than the n_d/V_R value used in the CRA-2014 PA (6,804 drums/room ÷ 3,644 m^3/room = 1.87 drums/m^3), which would reduce the steel surface area per unit volume (D_S). Using the idealized emplacement number of drums, both the sheet metal surrogate and 55-gallon drum surrogate assumptions result in average steel surface area to unit volume values greater than the value used in the CRA-2014 PA (Table 3-6).

Day (2015) reported that the waste emplaced through December 31, 2014 occupies a total of 40 rooms. Based on the total number of stacks (Table 3-5) and 21 55-gallon drums per stack, the emplaced waste represents a total of 384,678 drum equivalents, yielding 9,616 drums/room. This number of drums per room represents a fill factor of 88%. If the steel surface area is recalculated using the more realistic number of drums per room, the sheet metal surrogate and 55-gallon drum surrogate assumptions result in average steel surface area to unit volume values of 10.0 m^2/m^3 and 11.6 m^2/m^3, which range from slightly below to slightly above the 11.2 m^2/m^3 value used in the CRA-2014 PA (Table 3-6). These results indicate that the current value of D_S is a reasonable approximation of the steel surface area for WIPP waste that has been emplaced through December 31, 2014.

Table 3-7. Steel Surface Area per Unit Volume (D_S) from the CRA-2014 PA and Calculated Using Different Waste Surface Area to Mass Surrogate Assumptions for Idealized and Reported Waste Emplacement

Calculation	Surface Area Per Drum (m^2/drum, A_d)	Number of Drums per Room (n_d)	Disposal Room Volume (m^3/room, V_R)	Steel Surface Area per Unit Volume (D_s, m^2/m^3)
Idealized Waste Emplacement				
CRA-2014 PA	6	6,804	3,644	11.2
Spherical surrogate	6.12	10,908	6,585	10.1
Sheet metal surrogate	6.88	10,908	6,585	11.4
55-gallon drum surrogate	7.97	10,908	6,585	13.2
Reported Waste Emplacement				
Spherical surrogate	6.12	9,616	6,585	8.9
Sheet metal surrogate	6.88	9,616	6,585	10.0
55-gallon drum surrogate	7.97	9,616	6,585	11.6

These calculations of average D_S depend on both the proportions of different wastes and waste containers and the fill factor achieved during waste emplacement. If the proportions of different wastes in the repository change over time, e.g., a higher proportion of AMWTF waste is emplaced, or if higher fill factors are achieved in the future, the average D_S value could be significantly affected. Accordingly, future WIPP PAs should include recalculation of the appropriate D_S values. Because of the potential effects of D_S on brine releases (DOE 2014b, Appendix PA), EPA also expects DOE to assess the panel-by-panel variation of D_S to determine whether the average D_S adequately represents the possible range of this parameter calculated for the different panels.

The current value of D_S (11.2 m^2/m^3) combined with the reported waste emplacement n_d and V_R values (9,616 drums/room and 6,585 m^3, respectively) results in an A_d value of 7.67 m^2. Because the parameters REFCON:DRROOM, REFCON:VROOM and REFCON:ASDRUM are used only to calculate D_S, revising these parameter values to be more consistent with available data will have no practical effect on PA. EPA asked in an August 2016 teleconference with DOE whether REFCON:VROOM is used in any other PA calculations, because equations in the CRA-2014 indicate that V_R is used to calculation D_c, the estimated cellulosics and rubber density, and D_m, the MgO mass concentration (DOE 2014b, Appendix PA, Equations PA.76 and PA.93). DOE responded that REFCON:DRROOM, REFCON:VROOM and REFCON:ASDRUM are used only to calculate D_S, and the cited equations contained typographical errors (Patterson 2016b).

3.2.5 PA Implementation

In the CCA PAVT, CRA-2004 PABC and CRA-2009 PA, the inundated corrosion rate was a sampled parameter (STEEL:CORRMCO2) uniformly distributed from zero to 3.17×10^{-14} m/sec

(Table 3-2). For the CRA-2014 PA, DOE (2014b) used a revised range and distribution (Table 3-2) based on the experimental results of Roselle (2013). Zeitler and Hansen (2015a) revised this range and distribution to include corrosion data obtained at low CO_2 concentrations, and an additional revision to this range and distribution should be used for the CRA-2019 PA to account for the effects of increased pressure on the inundated corrosion rate (EPA-revised rate, Table 3-2).

Gas generation by anoxic corrosion of steel has been implemented for all WIPP PA calculations by assuming the humid corrosion rate parameter (STEEL:HUMCORR) is equal to zero. However, Zeitler and Hansen (2015b) developed a CDF for the humid corrosion rate parameter that ranges from 0 m/s to 1.03×10^{-15} m/s with a mean value of 2.71×10^{-16} m/s. EPA recommends DOE incorporate this parameter range to represent the humid steel corrosion rate in the CRA-2019 PA calculations.

The equation used to calculate the anoxic steel corrosion gas generation rate is (DOE 2014b, CRA-2014 Appendix PA-4.2.5):

$$q_{r\,gc} = (R_{ci}\, S_{b,eff} + R_{ch}\, S_g^*)\, D_s\, \rho_{Fe}\, X_C\, (H_2 \mid Fe)\, M_{H2} \qquad \textbf{(8)}$$

Where:

$q_{r\,gc}$ is the rate of gas production per unit volume of waste due to anoxic corrosion of iron-based metals ($kg/m^3/sec$)

R_{ci} is the corrosion rate under inundated conditions, STEEL:CORRMCO2 (m/s)

$S_{b,eff}$ is the effective brine saturation due to capillary action in the waste materials

R_{ch} is the corrosion rate under humid conditions, STEEL:HUMCORR (m/s)

S_g^* equals 1- $S_{b,eff}$ if $S_{b,eff} > 0$, or

equals 0 if $S_{b,eff} = 0$

D_s is the steel surface area per unit volume in the repository (11.2 m^2/m^3), calculated from the parameters REFCON:ASDRUM (6 m^2/drum), REFCON:DRROOM (6,800 drums/room), and REFCON:VROOM (3,640 m^3/room) (Kicker and Herrick 2013)

ρ_{Fe} is themolar density of steel (1.41×10^5 moles/m^3, Telander and Westerman 1993)

X_C ($H_2 \mid Fe$) is the stoichiometric coefficient for gas generation due to the corrosion of steel [1 mole H_2 per mole Fe, parameter STEEL:STOIFX (Kicker and Herrick 2013)]

M_{H2} is the molecular weight of H_2 [kg H_2 per mole H_2, 2.02×10^{-3}, parameter REFCON:MW_H2 (Kicker and Herrick 2013)].

For each realization, the sampled anoxic inundated and humid corrosion rates are used to calculate anoxic corrosion gas generation per unit volume of waste as a function of the effective brine saturation.

In Appendix PA Section 4.2.5 (page PA-71), the gas and brine production rates in Equation PA.65 and PA.66 are described in terms of unit waste volume. However, the individual components of these gas and brine production rates are calculated per unit disposal volume rather than per unit waste volume (Equations PA.67 through PA.74). EPA will expect DOE to resolve this apparent inconsistency.

3.2.6 Effects of Anoxic Corrosion Gas Generation Rates on Repository Releases

DOE (Triay 2002) requested EPA approval for the disposal of compressed waste from the AMWTF. During review of the AMWTF planned change request (PCR), EPA questioned whether higher iron surface areas expected in compressed waste would affect modeled releases from the repository because of increased anoxic corrosion and repository pressures (TEA 2004). DOE assessed the sensitivity of the PA results to changes in the assumed iron surface area and found that increased iron surface area and anoxic corrosion resulted in decreased overall gas production, with increased gas pressures during the first 2,500 years, followed by decreased gas pressures during later time periods (Stein and Zielinski 2004). Decreased overall gas production was predicted because higher initial gas pressures forced brine from the repository and decreased microbial gas production. DOE concluded that increased iron surface areas would not have significant effects on total repository releases, and EPA concurred with this conclusion (TEA 2004).

The inundated steel corrosion rates used in the CRA-2014 PA were lower than the rates used in the CRA-2009 PABC (Table 3-2). The lower corrosion rates resulted in reduced spallings releases and fewer vectors with the conditions necessary for DBR in the CRA-2014 PA than the CRA-2009 PABC, leading to lower mean total releases (DOE 2014b, Appendix PA page PA-241). Further evaluation of the inundated and humid corrosion rate data shows that higher rates should have been used in the CRA-2014 PA (Zeitler and Hansen 2015a, 2015b). The revised inundated corrosion rate adjusted for increased pressure has a similar mean to the CRA-2009 PABC mean inundated corrosion rate (Table 3-2). The revised humid corrosion rate (Zeitler and Hansen 2015b) is also higher than the CRA-2009 PABC humid corrosion rate. The higher mean inundated and humid corrosion rates would be expected to lead to higher mean total releases. However, because these higher rates have not been incorporated in a new PA, the magnitude of the effects of these increased rates on repository releases cannot be quantified. The effects of the nonzero humid corrosion rate are particularly difficult to assess, even qualitatively, because previous WIPP PAs have not included humid anoxic corrosion.

3.3 CORROSION OF ALUMINUM, LEAD AND OTHER METALS

DOE (2014b, Appendix SOTERM-2.3.5) addressed the potential effects of lead corrosion on repository chemical conditions, but did not address the effects on gas generation of the corrosion of metals other than iron in the WIPP inventory, such as lead and aluminum. Peer review of the Gas Generation conceptual model determined that the quantities of aluminum in the repository will be too small to cause significant gas generation (Wilson et al. 1996a, 1996b, 1997a, 1997b).

Whether this assumption continues to be true can be assessed by comparing the relative masses of iron and aluminum in the CRA-2014 PA inventory (Table 3-7). The aluminum inventory is less than 1% of the iron-based metals inventory, so aluminum corrosion is unlikely to significantly affect gas generation rates.

Table 3-8. CRA-2014 PA Inventories of Aluminum, Lead and Other Metals and Alloys in Waste and Packaging Materials

Waste or Packaging Material	Mass (kg)
CH Waste Aluminum-Based Metal and Alloys	437,000
RH Waste Aluminum-Based Metal and Alloys	20,100
CH Waste Other Metals and Alloys	762,000
RH Waste Other Metals and Alloys	471,000
CH Lead Packaging Materials	--
RH Lead Packaging Materials	8,280
Total Waste Other Metals and Alloys and Lead Packaging Materials	1,241,280
Total Waste Aluminum-Based Metals and Alloys, Waste Other Metals and Alloys and Lead Packaging Materials	1,698,380
Total Iron-Based Waste and Packaging Materials	49,110,000

Source: Van Soest 2012

Anoxic corrosion of lead can be expected to consume brine and generate H_2, based its reaction stoichiometry:

$$Pb(s) + H_2O \leftrightarrow PbO(s) + H_2 \quad \textbf{(9)}$$

The WIPP lead inventory from packaging materials is reported, but the lead inventory associated with CH and RH waste is only included as "other metals and alloys" (Van Soest 2012). The total inventory of lead will be less than the sum of the "other metals and alloys" plus the lead packaging materials (Table 3-7). The 1,241,280 kg upper limit on lead inventory reported for the CRA-2014 is less than 3% of the iron inventory, so if the data in Table 3-7 adequately represent the final lead inventory at closure, lead corrosion would not be expected to significantly affect gas generation rates.

DOE submitted a PCR to allow use of shielded containers for disposal of RH waste (Moody 2007) and EPA approved this request (Edwards 2011, 2013). Because lead is used in the container shielding, disposal of RH waste in these containers will increase the amounts of lead in the repository. EPA requested information from DOE regarding how lead shielding in RH shielded containers is included in the PA (Edwards 2014, Comment 1-24-1). DOE responded that only one shielded container had been placed in the repository as of the CRA-2014 PA inventory cut-off date of December 31, 2011 (Franco 2015b). Its contribution to the volume, radionuclide inventory, waste inventory and packaging inventory was included under RH waste. DOE stated that the mass of lead contributed by this single container was 431 kg out of the total lead packaging inventory of 8,280 kg reported by Van Soest (2012).

EPA requested information from DOE regarding the volume of RH waste that has been and will be placed in the shielded containers on the waste panel floors (Edwards 2014, Comment 1-24-2). DOE responded that since the CRA-2014 PA inventory cut-off date of December 31, 2011, nine shielded containers have been emplaced in WIPP (Franco 2015b). DOE further stated that "As of

12/31/2013, no other lead-shielded containers had been identified by the sites to be shipped to WIPP."

Because DOE's response to comments 1-24-1 and 1-24-2 only addressed shielded containers identified as of the end of 2013 and did not adequately address the possible future volume of RH waste that could be placed in shielded containers, EPA requested that DOE provide the total lead that will be in the WIPP repository and the basis for that estimate by taking into account the expected increased lead from shielded containers, as well as an assessment of the effects of lead corrosion on gas generation and repository water balance (Edwards 2015c, Comment 3-C-7). DOE stated in their response that as of 12/31/2013 (the cut-off date for ATWIR-2014, DOE 2014a), 27 shielded containers are anticipated to be emplaced in WIPP in addition to the 9 shielded containers emplaced between 12/31/2011 and 12/31/2013 (Bryson 2015b). Combining the lead in the additional shielded containers with the "other waste metals" and RH packaging lead inventory (Table 3-7) yields an upper limit for the total lead inventory of 1,256,796 kg. This upper bound for the lead inventory is less than 3% of the iron inventory. However, this evaluation only includes RH waste identified for packaging in shielded containers as of 12/31/2013. It is likely that more than 37 shielded containers (10 emplaced as of 12/31/2013 and 27 anticipated) will ultimately be placed in the repository as additional RH wastes are identified for disposal in shielded containers.

DOE (Crawford and Taggart 2007) provided an upper estimate of an additional 27,000,000 kg of lead packaging material if the entire RH capacity of 7,080 m^3 was to be placed in shielded containers on the panel floor rather than in RH canisters placed into boreholes in the panel walls (Table 3-8). This mass of lead is equal to 55% of the CRA-2014 inventory of iron-based waste and packaging material mass (49,110,000 kg). Only RH waste that can be adequately shielded to less than 200 mrem/hour can be placed in shielded containers. Consequently, the 27,000,000 kg estimate by Crawford and Taggart (2007) for lead mass associated with shielded containers is an unrealistically high value for the additional lead that may be included in the repository. Crawford and Taggart (2007) estimated that the volume of RH waste streams that were candidates for placement in shielded containers based on their concentrations of maximum gamma emitters was 1,922 m^3 (Table 3-8). This volume of RH waste would occupy 17,006 shielded containers and would add 7,329,441 kg of lead to the WIPP inventory. This mass of lead added to the CRA-2014 PA CH waste and RH waste "other metals and alloys" inventory (Table 3-7) equals 8,562,441 kg, which is 17% of the mass of iron-based waste and packaging materials in the CRA-2014 inventory. Because it is likely that some of the candidate waste streams will not be placed in shielded containers and some of the "other metals and alloys" are metals other than lead, the 8,562,441 kg of lead represents an upper limit.

The results of this calculation of the potential effects of shielded containers on lead inventory based on candidate waste streams indicate that the current method of estimating lead inventory for the CRA-2014 PA did not adequately account for the future effects of adding shielded RH containers to the repository. Estimating the effects of shielded container lead based on candidate waste streams identified by Crawford and Taggart (2007) yields a total mass of lead that may affect gas generation rates. However, the mass of lead determined in these calculations is based on inventory data that have subsequently been updated.

Table 3-9. Possible Effects of Shielded Containers on WIPP Lead Inventory

RH Waste	Total RH Volume	Candidate RH Waste Streams[1]
Volume of RH waste in shielded containers (m^3)	7,080	1,921.64
Volume of RH waste per shielded container (m^3)	0.113	0.113
Number of shielded containers	62,655	17,006
Lead mass per shielded container (kg)	431	431
Lead mass from shielded containers (kg)	27,004,248	7,329,441
Repository total iron waste plus packaging materials	49,110,000	49,110,000
Ratio lead mass from shielded containers/repository total iron mass	0.55	0.15

[1] Crawford and Taggart (2007) Table 10

Lead corrosion rates in WIPP brine have been investigated by Roselle (2009, 2010, 2011a, 2011b, 2013). EPA requested that DOE provide copies of the spreadsheets containing the lead corrosion rate data (Edwards 2015b, Comment 2-C-8) and DOE provided these data (Franco 2015a). The results of the lead corrosion studies showed that the inundated and humid corrosion rates declined over time (Roselle 2013). However, the longer-term rates (24 months) reported by Roselle (2013, Table 9) were positive, so surface passivation was not demonstrated. These lead corrosion rates combined with potentially significant masses of lead from shielded containers indicate that DOE currently underestimates the possible effects of inundated and humid anoxic corrosion of lead on gas generation.

The calculations using the data from Crawford and Taggart (2007) indicate that the WIPP lead inventory could be large enough to warrant inclusion of lead corrosion rates in WIPP gas generation calculations. Accordingly, the CRA-2019 PA will benefit from an assessment of the possible mass of lead from shielded containers by: 1) determining the volume of waste streams that are candidates for disposal in shielded containers based on their concentrations of maximum gamma emitters, 2) calculating the number of shielded containers needed to dispose of this waste volume, and 3) calculating the mass of lead associated with this number of shielded containers. If the mass of lead from shielded containers, other packaging materials and waste "other metals and alloys" is a significant fraction of the mass of iron-based waste and packing materials, then gas generation and brine consumption from lead corrosion should be included in the CRA-2019 PA.

3.4 MICROBIAL GAS GENERATION

Cellulosics, plastics and rubber are present in WIPP waste and in waste emplacement and packaging materials. Microbial gas generation in the WIPP repository can occur because microbes are likely to be naturally present at the repository horizon or introduced with the waste. As these microbes utilize CPR materials as a carbon source, production of CO_2 could acidify repository brines or increase the solubility of actinides by carbonate complexation. To control chemical conditions and limit the possible effects of acidic conditions and carbonate complexation on actinide solubilities, MgO backfill is included in the repository to react with

CO_2 and maintain mildly alkaline conditions with low CO_2 fugacity consistent with relatively low actinide solubilities (Section 4.0).

3.4.1 CCA PA, PAVT, and CRA-2004 PA Microbial Gas Generation

The CCA-PA, PAVT and CRA-2004 PA conceptual model for gas generation all assume that microbial degradation of CPR may occur in the repository and produce methane [CH_4] and CO_2. The major pathways for microbial degradation of CPR are predicted to include the following reactions:

$$C_6H_{10}O_5 + 4.8\ H^+ + 4.8\ NO_3^- \rightarrow 7.4\ H_2O + 6\ CO_2 + 2.4\ N_2 \quad \textbf{(10)}$$

$$C_6H_{10}O_5 + 6\ H^+ + 3\ SO_4^{2-} \rightarrow 5\ H_2O + 6\ CO_2 + 3\ H_2S \quad \textbf{(11)}$$

$$C_6H_{10}O_5 + H_2O \rightarrow 3\ CH_4 + 3\ CO_2 \quad \textbf{(12)}$$

where $C_6H_{10}O_5$ is the chemical formula for cellulose monomer. In reactions (10) and (11), one mole of CO_2 is produced for each mole of organic carbon consumed. However, reaction (12) produces only 0.5 moles of CO_2 per mole of organic carbon consumed. Reactions (10) to (12) are predicted to proceed sequentially according to the energy yield of the reactions (Wang and Brush 1996). As the denitrification and sulfate-reduction reactions [reactions (10) and (11), respectively] proceed, DOE predicted that they would consume the limited amounts of nitrate [NO_3^-] and sulfate [SO_4^{2-}] in the WIPP waste inventory and produce limited quantities of nitrogen [N_2] and hydrogen sulfide [H_2S]. In both the CCA and the CRA-2004, DOE predicted that the methanogenesis reaction (12) would be the dominant reaction pathway and, consequently, that approximately half of the CPR carbon consumed would be converted to CO_2 and the other half converting to CH_4 (DOE 1996, Appendix SOTERM, Section 8.2.2; DOE 2004, Appendix PA, Attachment SOTERM, Section 2.2.2).

DOE assumed that microbial consumption of CPR could be limited by the long-term viability of microbes in the repository, and uncertainty associated with whether microbes would consume plastics and rubbers was also considered important in development of the conceptual model. DOE's conceptual model also assumed that the rate of microbial gas generation was dependent on brine saturation (DOE 2004, Appendix PA, Attachment MASS). DOE assumed that MgO backfill will remove CO_2 from the repository brines and gas phase, so CO_2 generated from CPR degradation will not significantly affect repository gas pressures. The effects of CPR degradation on the amount of brine in the repository were considered uncertain, so these effects were not accounted for in PA. It was also assumed that gas generation would take place homogeneously throughout the repository, because of the assumed homogeneous distribution of waste.

Microbial gas production was assumed to occur at a rate dependent on the availability of brine. Significant microbial gas production was assumed to occur in only 50% of the realizations for the CCA PA, CCA PAVT and CRA-2004 PA because of uncertainties associated with microbial processes. In half of these realizations in which significant microbial consumption of CPR occurred (25% of all realizations), microbial activity consumed only cellulosics. In the remaining half of the realizations, microbial activity consumed (25% of all realizations), all CPR materials,

including plastics and rubber, were assumed to be consumed by microbial activity (DOE 2004, Section 6.4.3.3).

The ranges of microbial gas generation rates used for the CCA PA, the CCA PAVT and the CRA-2004 PA were determined using initial results from inundated and humid condition microbial degradation experiments with cellulose (Francis and Gillow 1994; Wang and Brush 1996; DOE 2004, Appendix PA, Attachment PAR). The rates were determined from experiments that did not contain bentonite.[4] A gas-generation rate was calculated in BRAGFLO from the humid and inundated rates based on the effective liquid saturation (DOE 2004, Section 6.4.3.3). Gas-generation rates for plastics and rubber are assumed equal to the rate for cellulose; the larger average carbon content by weight for plastics is accounted for by multiplying the mass of plastics by a factor of 1.7 for calculation of the gas generation rate (Wang and Brush 1996).

EPA (1998d) reviewed microbial gas generation during their evaluation of the CCA. In their review, EPA noted the uncertainties associated with whether microbial communities capable of degrading CPR would be present in the hypersaline WIPP environment, and numerous factors that may limit microbial gas generation, including the concentrations of nutrient and toxic compounds and limitations imposed by temperature, salinity, Eh, pH and the availability of electron acceptors. EPA observed that it is generally difficult to estimate the rate and extent of slow processes, such as CPR degradation, over long periods by extrapolating the results of short-term studies. Based on the available evidence, EPA concluded that DOE's approach to addressing the probability of significant microbial gas generation was an adequately conservative overestimate, and that addition of MgO backfill to the WIPP repository made CO_2 production unlikely to be of significant concern (EPA 1998d).

Table 3-10. Inundated Microbial Gas Generation Rates (WAS_AREA:GRATMICI) Used in PA

(moles CO_2/kg cellulose/sec)

Performance Assessment	Minimum	Maximum	Reference
CCA/PAVT and CRA-2004 PA	3.17100×10^{-10}	9.51290×10^{-9}	DOE (1996), DOE (2004)
PABC04, CRA-2009 PA, PABC09 and CRA-2014 PA	3.08269×10^{-11}	5.56921×10^{-10}	Nemer et al. (2005), Fox (2008), Kicker and Herrick (2013)

Table 3-11. Humid Microbial Gas Generation Rates (WAS_AREA:GRATMICH) Used in PA

(moles CO_2/kg cellulose/sec)

Performance Assessment	Minimum	Maximum	Reference
CCA/PAVT and CRA-2004 PA	0.00	1.26840×10^{-9}	DOE (1996), DOE (2004)
PABC04, CRA-2009 PA, PABC09 and CRA-2014 PA	0.00	1.02717×10^{-9}	Nemer et al. (2005), Fox (2008), Kicker and Herrick (2013)

[4] At the time the experiments began, bentonite was being considered for use as backfill material and was included in some experiments. Because the backfill does not contain bentonite, these experiments were not used in the determination of the microbial gas generation rates.

3.4.2 Microbial Gas Generation Evaluation during AMWTF Review

At the time of the CCA PA, DOE assumed that all carbon in CPR could potentially be converted to CO_2 and used this assumption to calculate the amount of MgO required in the backfill. By the time of the AMWTF review, Gillow and Francis (2003) observed methanogenesis in some of the microbial degradation experiments. DOE stated that methane generation in the experiments demonstrated that methanogenesis will occur in the WIPP repository environment, if microbial degradation of CPR occurs. DOE also assumed that only limited amounts of CPR degradation will take place through denitrification and sulfate reduction [reactions (10) and (11)] because of the relatively small amounts of nitrate and sulfate in the waste (Hansen et al. 2003 and 2003b). DOE stated that after sulfate and nitrate inventories in the waste are consumed, CPR degradation will either cease or will proceed through methanogenesis [reaction (12)]. Because methanogenesis produces only 0.5 moles of CO_2 for each mole of CPR carbon, CPR degradation through methanogenesis would significantly reduce the amount of CO_2 that could be produced and the amount of MgO needed to maintain the required chemical conditions in the repository.

TEA (2004) reviewed the information DOE provided (Hansen et al. 2003 and 2003b; Kanney et al. 2004), and concluded that DOE's consideration of the sulfate available for CPR degradation by sulfate reduction did not adequately account for sulfate in the brine and sulfate-bearing minerals in the Salado Formation. EPA considered the available information and the uncertainty associated with possible microbial processes in the repository, and directed DOE to continue calculating required quantities of MgO backfill by assuming all CPR carbon could be converted to CO_2 unless new and convincing evidence became available demonstrating that methanogenesis would occur in the WIPP repository (Cotsworth 2004a, Marcinowski 2004).

3.4.3 PABC04 Microbial Gas Generation

For the CRA-2004 PA, DOE did not change the CCA PA and PAVT microbial gas generation conceptual model assumptions or the sampled humid or inundated microbial gas generation rates (DOE 2004, Appendix PA, Attachment SOTERM). EPA's review of the CRA-2004 PA included an evaluation of additional experimental data related to microbial gas generation rates and reaction products (EPA 2006c). These data included results from WIPP-specific experiments that continued after approval of the CCA (Francis et al. 1997; Francis and Gillow 2000; Gillow and Francis 2001a, 2001b, 2002a, 2002b, and 2003), as well as additional experiments carried out under WIPP-relevant conditions (Felicione et al. 2001). The data review assessed both microbial degradation probabilities and gas generation rates.

3.4.3.1 Microbial Degradation Probabilities

EPA requested additional information from DOE regarding microbial degradation probabilities (Cotsworth 2004b). The response to this request (Detwiler 2004b) was based on an analysis by Brush (2004) of uncertainties originally considered by Brush (1995) for the CCA. The uncertainties considered in the evaluation of the probability included whether: (1) microorganisms will be present in the repository when it is filled and sealed, (2) sterilization of the waste and other contents of the repository will prevent microbial activity, (3) microbes will survive for a significant fraction of the 10,000 years of repository performance, (4) sufficient water will be present, (5) sufficient quantities of biodegradable substances will be present, (6)

sufficient electron acceptors will be present and available and (7) enough nutrients, especially nitrogen and phosphorous, will be present and available. EPA (2006c) determined that information developed since the CCA indicated an increased probability that microorganisms will be present in the repository when it is filled and sealed, that there is insufficient evidence that MgO will prevent microbial activity in the WIPP environment, that some new evidence was available making long-term viability of microbes appear more probable than at the time of the CCA and that the amount of nutrients, specifically phosphate, in the inventory had increased, making the microbial degradation of cellulosics in the repository appear more likely.

DOE evaluated the potential effects of a higher probability of significant degradation of CPR on microbial gas generation rates by comparing gas volumes and repository pressures for realizations with and without significant microbial activity using BRAGFLO simulation results from the CRA-2004 PA (Detwiler 2004b). The gas generation rate and repository pressure at early times was larger for realizations with significant microbial activity, as was the maximum cumulative gas generation and repository pressure over the 10,000-year regulatory period. The maximum cumulative gas generation and the range in the amount of gas generated for the realizations with significant microbial activity was approximately 1.4 to 1.5 times the values observed for realizations without significant microbial activity (Detwiler 2004b).

The effects of the increased assumed probability of microbial degradation of CPR were assessed by comparing total radionuclide mobilization for microbial and non-microbial realizations, based on PANEL output for Scenarios S1 (undisturbed- no drilling intrusions, Salado brine) and S3 (single drilling intrusion at 1,000 years into excavated area, pressurized brine is penetrated, Castile brine) (Detwiler 2004b). For Scenario S1, the range of mobilized radionuclides was similar for the microbial and non-microbial realizations. For Scenario S3, the range of mobilized concentrations for the microbial realizations were higher than for non-microbial realizations. These higher mobilized concentrations for Scenario S3 could influence releases through the Culebra and direct brine releases (DBRs), because these release modes are associated with intrusions (Detwiler 2004b).

For microbial and non-microbial realizations, DOE compared releases through the Culebra, DBRs, spallings releases, and total releases to assess the possible effects of microbial activity (Detwiler 2004b). The comparison indicated that releases through the Culebra were minimally affected, most likely because the probability of such releases is low and not sensitive to microbial activity. Higher releases were observed in microbial realizations for DBRs and for spallings releases. However, total releases were only slightly higher for microbial realizations than non-microbial realizations, because of the importance of cuttings and cavings[5] to total releases, and cuttings and cavings should not be significantly affected by microbial activity (Detwiler 2004b).

EPA (2006c) concluded that the overall balance of information developed since the CCA indicated that microbial degradation of cellulosic materials may be more likely than previously assumed and that this higher probability would be likely to increase calculated releases from the

[5] Cuttings are solids that are cut from the borehole by the drill and brought to the surface; cavings are solids that fall from the wall of the borehole

repository. Results from DOE's experiments indicated that rubber materials may be microbially degraded in the WIPP repository environment. On the other hand, no evidence was found in the DOE experiments of microbial degradation of polyethylene or PVC performed for up to 8.4 years (Gillow and Francis 2003). Based on this information, EPA (2006c) concluded that the probability of significant microbial degradation of cellulosic materials should be higher than assumed for the CCA PA, PAVT, and the CRA-2004 PA, and directed DOE to assume that microbial degradation of cellulosics would occur in all realizations (Cotsworth 2005). Because only limited degradation of rubber materials was observed and no degradation of plastics was observed, there was no evidence that the probabilities of plastics or rubber degradation assumed for the CCA PA and PAVT should be revised.

The parameter WAS_AREA:PROBDEG is sampled within BRAGFLO to indicate whether microbial gas generation occurs and what type of material degrades (Nemer 2005). DOE updated this parameter for the PABC04 to reflect the increased probability (0.75) of microbial degradation of only cellulosics materials, and the unchanged probability (0.25) of microbial degradation of all CPR materials. EPA (2006b) found that these changes to WAS_AREA:PROBDEG are consistent with the available data and were an adequate response to EPA's request that significant microbial degradation should be assumed to occur in all PABC04 realizations.

3.4.3.2 Microbial Gas Generation Rates

Wang et al. (2003) recalculated inundated and humid microbial gas generation rates using lower, longer-term CO_2 generation rates from the WIPP-specific experiments that continued after the CCA PA and PAVT. Although Wang et al. (2003) stated that these lower rates were more representative of rates likely to occur in the WIPP repository, the higher CCA PA and PAVT microbial gas generation rates were used in the CRA-2004 PA.

Because of the higher probability assumed for microbial degradation in the PABC04, DOE revised the microbial gas generation rates to account for rate data that had become available since the CCA PA and PAVT (Nemer et al. 2005). DOE used a two-step process to simulate microbial gas production rates in the WIPP repository for the PABC04 (Nemer et al. 2005). The initially rapid rates of microbial gas production were simulated by increasing the initial pressure in the BRAGFLO input file. This "precharging" of the repository gas pressure was combined with the use of lower gas generation rates determined from long-term experimental data.

Nemer et al. (2005) described the derivation of the microbial gas generation rates used in the PABC04. The microbial gas generation data were obtained from experiments summarized by Francis et al. (1997) and Gillow and Francis (2002a, 2003). The microbial production of CO_2 as a function of time in these experiments took place at relatively high rates at the beginning of the experiments, but CO_2 production typically slowed after about 1.5 years. The causes of these slowing rates are unknown. However, this type of bacterial growth curve is commonly encountered because of limitations on resources, such as nutrients or readily-degradable substrate, or because of increasing concentrations of metabolites. The microbial gas generation rates were modeled by obtaining a least-squares fit of two linear functions to the reported mean values for the CO_2 gas generation data. In this manner, both a short-term and a long-term rate were determined for each experimental dataset. A minimum of three data points was included in

each short-term or long-term fit to the data. The best fit was determined by choosing the result with the smallest residual between the observed and fitted values of CO_2 produced as a function of time (Nemer et al. 2005).

None of the data considered by Nemer et al. (2005) were from experiments that included bentonite, which is consistent with DOE's previous determination of microbial gas generation rates (Section 3.3.1). Samples from initially aerobic experiments were also not considered; Wang and Brush (1996) justified the use of data only from initially anaerobic experiments by noting that the WIPP repository was expected to become anoxic shortly after closure. Nemer et al. (2005) used the 95% upper confidence limit and 95% lower confidence limit about the mean slope values to determine the maximum and minimum possible rates for inundated and humid conditions (Tables 3-3 and 3-4). EPA (2006b) reviewed the derivation of the humid and inundated microbial gas generation rates and found that they were reasonable and adequately supported by the available experimental data.

3.4.3.3 PABC04 Implementation of Microbial Gas Generation Rates

Nemer and Stein (2005) described the implementation of the revised microbial gas generation rates in BRAGFLO for the PABC04. The two zero-order microbial gas generation rates for humid (WAS_AREA:GRATMICH) and inundated (WAS_AREA:GRATMICI) conditions were determined as described by Nemer et al. (2005), with units converted to those used by BRAGFLO (moles C/kg cellulose/sec) and accounting for the dissolution of CO_2 in water for the inundated rates. The rates used in the different PAs are compared in Tables 3-9 and 3-10. The revised inundated long-term microbial gas generation rate used in the PABC04 and subsequent PA calculations is more than an order of magnitude lower than the previous rate. The revised humid long-term microbial gas generation rate is only slightly lower than the previous humid rate.

Because DOE believed the humid rate should be lower than the inundated rate, the sampled humid and inundated rates were compared within BRAGFLO for the PABC04. If the sampled humid rate exceeded the sampled inundated rate, the humid rate was set equal to the inundated rate. Stein and Nemer (2005) did not provide information on the likely effects of assuming that the humid rate would always be lower than the inundated rate. However, because the maximum inundated and humid rates differ by only about a factor of two (Tables 3-9 and 3-10), it is likely that the humid rates used in BRAGFLO were not significantly reduced by this assumption.

The revised microbial gas generation rates were based on long-term experimental data. Therefore, gas generation during the early stages of the repository was accounted for in BRAGFLO for the PABC04 by assuming a fixed amount of gas was present in the repository at the beginning of the calculations (Nemer et al. 2005, Appendix B). The amount of gas in the repository was assumed to be equivalent to the amount of gas generated per gram of cellulose at the point where the relatively rapid short-term rate changed to the slower long-term rate in the nutrient and nitrate-amended inundated experiments; these experiments were used to evaluate the maximum long-term inundated rate.

The amount of gas initially present in the repository because of rapid early microbial gas generation rates equaled 181 μmole/g cellulose (Nemer et al. 2005). This value was converted to

the total moles of gas in the repository, based on the equivalent amounts of cellulose in the CRA-2004 PA inventory (Nemer et al. 2005, Appendix B) and the microbial gas generation model of Wang and Brush (1996). The amount of gas was then converted to a pressure value of 26.714 kPa, using the ideal gas equation and the volume and temperature of the repository. This additional pressure was assumed to be generated immediately upon closure, resulting in an initial total repository pressure of 128.039 kPa (Nemer et al. 2005, Stein and Nemer 2005). Use of the CRA-2004 PA inventory to calculate the initial pressure generated by microbial gas generation for the PABC04 resulted in a slightly smaller initial pressure than would have been calculated using the PABC04 inventory. The differences in the CPR inventory between the CRA-2004 inventory (Nemer et al. 2005) and the PABC04 inventory (Leigh et al. 2005b) were relatively small so the difference between the calculated initial pressures using the two inventories is also small.

At EPA's direction, DOE changed the probability of microbial degradation to account for new evidence regarding the presence and viability of microbes capable of degrading CPR in the WIPP repository. The revised probability parameters resulted in microbial gas generation in all realizations for the PABC04 (Section 3.3.3.1). However, DOE asserted that uncertainties remained regarding the viability of microbes in the repository, because of different conditions in the repository compared to the conditions in the experiments (Nemer et al. 2005). DOE therefore introduced an additional sampled parameter, WAS_AREA:BIOGENFC. This parameter, which has a uniform distribution from 0 to 1, was multiplied by the sampled humid and inundated microbial gas generation rates to reduce the rates from the experimentally determined long-term rates. The uncertainties listed by DOE as justification for this rate reduction are stated in Section 3.3.3.

EPA (2006b) noted that these factors had already been considered and, in fact, assessment of many of these uncertainties had resulted in a decision to increase the probability of significant microbial degradation for WIPP PA (Cotsworth 2005). However, EPA (2006b) concluded that because of the inherent uncertainties associated with extrapolating experimentally measured microbial gas generation rates to repository conditions, it was reasonable to add an uncertainty factor to these rates.

DOE reported that implementation of lower long-term microbial gas generation rates reduced both the rate of pressurization and the pressure in the undisturbed repository (Nemer et al. 2005, Leigh et al. 2005a). This implementation also resulted in slightly higher brine saturation for the undisturbed repository. For the disturbed repository, pressures are relatively unchanged by the different microbial gas generation rates, but the brine saturation is higher using the lower long-term rates. Higher brine saturation may lead to increased flow up the borehole and DBR of radionuclides. Therefore, lower microbial gas generation rates may have had some previously unanticipated effects, in that the likelihood of DBR of radionuclides was increased. However, the frequency and volume of spallings releases were decreased in the PABC04 compared to the CRA-2004 PA because of lower gas pressures (Leigh et al. 2005a).

DOE's implementation of an initially rapid microbial gas generation rate, followed by slower long-term rates, is more likely to be representative of future repository conditions. Assuming a rapid initial rate followed by slower long-term rates is more consistent with the experimental data and with general patterns of microbial processes. A consequence of this change is likely to

be longer persistence of microbial gas-generating processes and higher brine saturations in both the disturbed and undisturbed repository scenarios.

3.4.4 Microbial Gas Generation Review for MgO Planned Change Request

At DOE's request, an expert panel was convened by the Institute for Regulatory Science (RSI) to consider issues associated with the MgO backfill and microbial degradation of CPR in the WIPP repository (RSI 2006). The expert panel recommended that an expert elicitation panel be formed to determine the likely extent of degradation of CPR materials and to determine if the amounts of MgO currently placed in the repository could be safely reduced. To address the potential need for an expert elicitation panel related to gas generation from CPR, EPA carried out a review to identify technical questions and uncertainties related to gas generation from CPR degradation (SC&A 2006). This review included the potential CO_2-generating microbial degradation reactions that could occur within the repository and the extent to which these reactions could occur.

SC&A (2006) performed a review of WIPP-specific data and a survey of the scientific literature regarding gas generation from CPR degradation under WIPP repository conditions. SC&A (2006) concluded that uncertainties in CPR inventories in the WIPP should be addressed before changes in the MgO backfill engineered barrier were made. SC&A (2006) evaluated the potential effects of radiolysis, and found that additional information should be obtained related to the radiolytic degradation of CPR, along with the potential interactions of radiolytic and microbial processes. SC&A (2006) concluded that cellulosics could potentially be completely degraded in the repository environment over the 10,000-year regulatory period, but that more investigation of radiolytic and microbial degradation of plastics and rubber would be required to assess likely extents of degradation of these materials.

EPA regulations require that expert judgment should not be substituted for available experimental data or data that could be obtained from a reasonable set of experiments (40 CFR 194.26). The results of the review by SC&A (2006) indicated that literature data are available that might reduce the uncertainties associated with the extent of CPR degradation in the WIPP repository and improve understanding of WIPP's future performance. SC&A (2006) concluded that the use of expert judgment to assess the likely extent of CPR degradation in the WIPP repository would require further justification from DOE that included an in-depth analysis of the available data.

3.4.5 Microbial Gas Generation for the CRA-2009 PA and PABC09

Implementation of microbial gas generation for the CRA-2009 and PABC09 was essentially the same as for the PABC04. The initial gas pressure in the repository resulting from the short-term, rapid microbial degradation of CPR was assumed to be equal to the pressure of 128.039 kPa calculated by Nemer et al. (2005) for the PABC04 using the CRA-2004 PA inventory (Nemer and Clayton 2008). The long-term rates used in the CRA-2009 PA were the same as the rates used in the PABC04 (Tables 3-9 and 3-10).

The sampled humid and inundated rates were compared within BRAGFLO for the PABC04. If the sampled humid rate exceeded the sampled inundated rate, the humid rate was set equal to the

inundated rate. For the CRA-2009 PA, DOE determined that changing the higher sampled humid rate to equal the inundated rate introduced a small error into the sensitivity analysis, because the regression analysis was based on the sampled values rather than the lower conditional values for the humid rate. Consequently, DOE applied a conditional relationship for the CRA-2009, so that the sampled inundated rate is used as the maximum value for humid rate sampling (DOE 2009, Section 23.11.5; Kirchner 2008). The effects of this change on predicted repository performance are small.

DOE (2009 CRA, Appendix PA-2009, Section 7.1.1) attributed slower changes in repository pressure after 2,000 years to cessation of room closure, slowing of brine inflow and consumption of CPR. To understand whether complete consumption of CPR contributes to slower changes in repository pressure after 2,000 years, EPA requested that DOE provide information regarding whether the slower rates of microbial degradation assumed for the CRA-2009 resulted in the persistence of CPR in the PA realizations (Cotsworth 2009a, Comment 1-C-3). Moody (2009a) provided a graph of the fraction of initial CPR remaining in the repository over time for the undisturbed scenario. This graph demonstrated that for most realizations, 70% or more of the initial CPR remained in the undisturbed repository at the end of the 10,000-year period of performance. Nemer and Clayton (2008, Figures 6-65 and 6-66) illustrated the fraction of cellulosics remaining versus time for all realizations in Replicate R1, Scenarios S2 and S4, which are disturbed repository scenarios. These figures show that, in the vast majority of disturbed realizations, undegraded CPR also remained at the end of the 10,000-year period of performance. The persistence of CPR in the repository under most conditions is a reasonable result, because of the likely resistance to rapid microbial degradation of plastics and rubber and potential limitations on the amounts of brine in the repository.

During review of the CRA-2009 PA, EPA requested additional information from DOE regarding whether it was reasonable to assume that plastic and rubber degradation, in the 25% of realizations where it occurred, will take place at the same rate as cellulose degradation when normalized to the assumed carbon content of the CPR (Cotsworth 2009a, Comment 1-C-4). EPA noted that this assumption may no longer be appropriate, based on WIPP-specific experimental results showing essentially no plastic degradation and limited degradation of rubber over periods of up to 8.4 years (Gillow and Francis 2003), evaluations of literature data regarding plastics and rubber degradation process that have become available since the PABC04 (SC&A 2006), and evidence from the PABC04 that lower microbial gas generation rates resulted in a slight increase in releases. EPA accordingly requested that DOE consider the possible effects on PA of lower microbial gas generation rates from plastics and rubber degradation.

DOE noted in their response that there is a high level of uncertainty regarding the rates of degradation of plastics and rubber over the 10,000-year repository period of performance (Moody 2009a). DOE explained that this uncertainty is addressed in PA by only modeling significant degradation of plastics and rubber in 25% of the realizations, and by using a lower bound of zero for the sampled microbial degradation rate range. DOE stated that the effects on releases for lower microbial degradation rates implemented for the PABC04 were not calculated, and that Nemer and Stein (2005) showed very little difference between the CRA-2004 PA and PABC04 intermediate results. DOE further stated that they do not believe that reduction in gas generation rates increases releases. DOE also noted that reducing the rates of plastic and rubber degradation would likely have only minor effects on the gas volumes generated, because on

average, gas generation rates from iron corrosion are three times greater than from CPR degradation, and plastics and rubber degradation is modeled to occur in only 25% of the realizations.

DOE's conclusions regarding the lack of effect of lower microbial gas generation rates differ from the conclusions drawn by EPA (2006b) during review of the PABC04. Higher releases were calculated at low probability for the PABC04 than for the CCA PAVT, which EPA (2006b) found were caused by increased DBRs. EPA (2006b) believed these higher DBRs were primarily due to higher brine saturations resulting from lower microbial gas generation rates, and to changes in the PABC04 that increased actinide solubilities. Although DOE and EPA appear to have reached different conclusions regarding potential effects on releases of lower gas generation rates from microbial degradation of plastic and rubber in the WIPP inventory, comparison of the results of the CCA PAVT and PABC04 shows that large decreases in microbial gas generation rates had relatively small effects on repository releases and only at low probabilities. Consequently, although the relatively high microbial gas generation rates used for plastic and rubber in the CRA-2009 PA may not be consistent with the available data, it is likely that reducing these rates would have insignificant effects on repository releases. Consequently, the assumption that microbial gas generation from plastic and rubber degradation will occur at the same rate as from cellulosics degradation remains adequate for the purposes of PA.

No changes were made to the implementation of microbial gas generation or to microbial gas generation rate parameters for the PABC09. The initial gas pressure in the repository resulting from the short-term, rapid microbial degradation of CPR was assumed equal to the pressure of 128.039 kPa calculated by Nemer et al. (2005) using the CRA-2004 PA inventory (Nemer and Clayton 2008). Based on the inventory used for the PABC09 (Crawford et al. 2009), the total amount of CPR carbon in the repository was estimated to be 1.063×10^9 moles, which is essentially unchanged from the value of 1.069×10^9 moles used by Nemer et al. (2005). Consequently, the initial pressure used in the PABC09 remained appropriate. The long-term gas generation rates used in the PABC09 were the same as the rates used in the PABC04 (Tables 3-9 and 3-10), because no additional data were identified that would justify modifying these rates.

3.4.6 Microbial Gas Generation for the CRA-2014 PA

Implementation of microbial gas generation and microbial gas generation rate parameters remained unchanged for the CRA-2014 PA. The initial gas pressure was 128.039 kPa, which was calculated by Nemer et al. (2005) using the CRA-2004 PA inventory. The total amount of CPR carbon in the CRA-2014 PA inventory was 8.169×10^8 moles, which is 76% of the total CPR carbon value used by Nemer et al. (2005) to calculate the initial gas pressure. Using the CRA-2014 PA total CPR carbon value results in a lower initial pressure of 122.09 kPA. DOE has not analyzed the sensitivity of the PA results to the initial gas pressure in the repository, but because the pressure difference is relatively small, it is reasonable to assume that its effects on releases will be minor.

The microbial gas generation rate is calculated using the following equation (DOE 2014b, Appendix PA-4.2.5):

$$q_{r\,gm} = (R_{mi}\, S_{b,eff} + R_{mh} S^{*}_{g})\, D_c\, X_m\, (H_2 \mid C)\, M_{H2}\, B_{fc} \quad \textbf{(13)}$$

Where:

$q_{r\,gm}$ is the rate of microbial gas production per unit volume of waste ($kg/m^3/sec$)

R_{mi} is the rate of CO_2 production from cellulose biodegradation under inundated conditions (WAS_AREA:GRATMICI, moles C consumed/kg $C_6H_{10}O_5$/sec)

R_{mh} is the rate of CO_2 production from biodegradation under humid conditions (WAS_AREA:GRATMICH, moles C consumed/kg $C_6H_{10}O_5$/sec)

$S_{b,eff}$ is the effective brine saturation due to capillary action in the waste materials

S^{*}_{g} equals 1 - $S_{b,eff}$ if $S_{b,eff} > 0$

equals 0 if $S_{b,eff} = 0$

D_c is the mass concentration of cellulosics in the repository (kg biodegradable material/m^3 disposal volume)

$X_m(H_2 \mid C)$ is the average stoichiometric factor for microbial gas generation of cellulose, i.e., moles of H_2 generated per mole of carbon consumed by microbial action (moles H_2/mole C)

M_{H2} is the molecular weight of H_2 (REFCON:MW_H2, kg H_2 per mole H_2)

B_{fc} is the variable representing uncertainty related to long-term microbial degradation of CPR (WAS_AREA:BIOGENFC).

The variable D_c is the initial CPR inventory, with the mass of plastics increased by a factor of 1.7 to account for the higher average carbon concentration per kg of plastic (Wang and Brush 1996). The modeled microbial gas generation rate is zero-order with respect to the mass of CPR, meaning that the rate does not change as CPR is degraded. Because the inventory of cellulosics is smaller in the CRA-2014 PA than in previous PAs, lower overall rates of microbial gas generation would be expected.

3.5 EFFECTS OF CHEMICALLY INCOMPATIBLE MATERIALS ON GAS GENERATION FOR THE CRA-2014 PA

On February 14, 2014, an incident occurred in the WIPP underground that caused the release of radioactive material into the environment that exposed 21 people to low-level contamination (Wilson et al. 2015). This release was caused by incompatibility of chemicals within a waste drum (Drum 68660) that lead to a thermal runaway reaction, buildup of gases within the drum, displacment of the drum lid and venting of radioactive materials. The incompatible materials in the waste drum were identified as an absorbent (Swheat Scoop®, a wheat-based kitty litter) and an acid- neutralizing agent (Kolorsafe®, which contains triethanolamine, or TEA, and an

indicator dye). This drum was part of waste stream LA-MIN02-V.001, a solidified inorganic waste that was packaged at LANL.

Because the wheat-based absorbent was inconsistent with the previously expected CPR materials in WIPP waste, EPA requested additional information about this absorbent, including its composition, mass emplaced in WIPP, the number of drums that contained this material, the type of waste emplaced in these drums and whether the organic absorbent material had been used in other waste streams (Edwards 2014, Comment 1-C-1). In addition, EPA requested that DOE assess the effects of this absorbent on the CPR inventory and microbial gas generation.

DOE responded with the Swheat Scoop® MSDS sheet indicating that the absorbent is mainly composed of wheat-based materials and a small amount of soybean oil (Franco 2015c). The WDS data indicates that waste stream LA-MIN02-V.001was emplaced in Panels 6 and 7, with a total emplaced waste mass of 30,723.70 kg. The amount of Swheat Scoop® in waste stream LA-MIN02-V.001 is unknown, but the total amount used in all TRU waste remediation activities at LANL, where Drum 68660 originated, is approximately 18,600 kg. At the time of DOE's response, LANL had reported that three additional waste streams contained nitrate salt waste: LA-CIN01.001, LA-MHD01.001 and LA-MIN04-S.001. Franco (2015c) stated that the number of containers and the amount of Swheat Scoop® in these three waste streams were unknown. Franco (2015c) observed that the total amount of Swheat Scoop® used by LANL represents 0.4% of the total mass of cellulose predicted for the CRA-2014 PA and 0.1% of the total CPR (Van Soest 2012). This small amount of cellulosic material should not significantly influence the total CPR inventory or consequent gas generation.

EPA noted that screening of gas generation FEPs (CRA-2014, Appendix SCR Section SCR-6.5.1) did not consider gas generation caused by chemical incompatibility such as occurred in Drum 68660 (Edwards 2015a, Comment 4-C-1). EPA requested that DOE assess whether other drums from waste stream LA-MIN02-V.001 could have similar chemical incompatibilities that may cause gas generation sufficient to affect performance assessment. EPA also requested information regarding the use of Swheat Scoop® kitty litter in any other waste streams that have been emplaced in the WIPP, and the potential effects on performance assessment of possible gas generation from these waste streams.

DOE (Shrader 2015) responded that as part of a then-ongoing process, four waste streams had been identified as containing nitrate salt wastes and SwheatScoop® kitty litter or other CPR that might cause incompatibility: LA-MIN02-V.001 (349 drums including Drum 68660), LA-CIN01.001, (82 drums), LA-MHD01.001 (73 drums) and LA-MIN04-S.001 (3 drums). These 507 drums were emplaced in WIPP. DOE performed bounding calculations using the assumption that all 507 drums generated gas in a runaway thermal reaction, transforming 3.4 kg per drum of waste, which was based on an analysis of the amount of waste transformed during reaction of Drum 68660. Based on a model of the reaction stoichiometry and consumption of H_2O and CO_2 generated by the reaction by the MgO backfill, DOE calculated that the amount of gas (CH_4, N_2 and H_2) generated by the reaction would represent less than 0.0056% of the gas generated by CPR degradation and anoxic corrosion in the CRA-2014 PA in a single panel (Shrader 2015). Even if a small number of drums containing chemically incompatible waste remain unidentified or a slightly higher mass of waste than assumed for this calculation is transformed by runaway

thermal reaction, the results of this calculation reasonably indicate that gas generation by chemical incompatibilities in these waste streams are unlikely to significantly affect PA results.

3.6 RADIOLYSIS

The Gas Generation Conceptual model includes the assumption that radiolysis of water in the waste and brine and radiation of plastics and rubber in the waste will not have significant effects on the amounts of gas generated (SC&A 2008b). In their initial evaluation of the Gas Generation conceptual model, the CCA Peer Review Panel found that possible radiolytic hydrogen and oxygen gas generation from wetted and dissolved actinides and gas generation from radiolysis of cellulosics and plastics had not been adequately evaluated (Wilson et al. 1996a). DOE supplied additional information about radiolytic gas generation in the CCA (DOE 1996). DOE's reasoning for assuming negligible radiolytic gas generation was based on their determination that radiolysis of brine, cellulosics and plastics would result in a maximum two-fold to three-fold increase in total gas generation. Because gas pressures above 12.7 MPa would be vented into the interbeds, maximum gas pressures that had been calculated without radiolysis would not be increased. The Peer Review Panel accepted DOE's conclusion that radiolysis would not be an important source of gas generation in WIPP (Wilson et al. 1996b).

This assumption that radiolytic processes will not significantly influence overall rates of gas generation has remained unchanged since the CCA. However, because lower microbial and anoxic corrosion gas generation rates were used in the CRA-2014 PA, it is no longer certain that radiolytic gas generation will be insignificant. Radiolysis effects on WIPP chemistry are addressed in CRA-2014 (DOE 2014b, Appendix SOTERM-2.4.2). However, this discussion did not provide information on potential rates of gas generation through radiolysis of water or CPR in WIPP. SC&A (2006) carried out a preliminary review of WIPP-specific data, as well as literature data regarding radiolytic gas generation from CPR. SC&A (2006) concluded that there is some evidence indicating that radiolytic gas production may occur in the WIPP repository, but whether radiolytic gas generation would affect repository performance was not determined. Nelson (2011) describes the results of hydrogen gas monitoring in WIPP Panels 3 and 4 and concluded that radiolytic hydrogen generation was occurring. However, DOE (2014b) did not calculate possible bounds on radiolytic hydrogen gas generation rates using the available hydrogen monitoring data.

The CCA PA, PAVT and CRA-2004 PA assumed that higher gas generation rates would result in the overestimation of repository releases because of increased spallings releases. However, EPA (2006b) observed that evidence found during review of the CRA-2004 PA and PABC04 indicates that lower gas generation rates may slightly increase repository releases from DBR at low probabilities because of higher brine saturation. This evidence was developed during implementation of lower microbial gas generation rates, as described in Section 3.3.3.3 (Nemer et al. 2005, Leigh et al. 2005a). Leigh et al. (2005a) reported that mean spallings releases were lower and DBRs were higher in the PABC04 than in the CRA-2004 PA. Leigh et al. (2005a) also reported higher mean total releases at low probabilities for the PABC04 than for the CRA-2004 PA. The lower spallings releases were attributed to lower microbial gas generation rates. EPA (2006b) found that higher releases through DBRs were due partly to higher brine saturation, because of lower microbial gas generation rates, but also to increased actinide solubilities used in the PABC04.

With the lower gas generation caused by lower microbial degradation rates and lower anoxic steel corrosion rates used in the CRA-2014 PA, it is no longer certain that radiolytic gas generation of brine and CPR will be insignificant. DOE (2014b, Appendix PA, page PA-241) observed that lower gas generation rates and the revised water balance in the CRA-2014 PA compared to the CRA-2009 PABC resulted in fewer vectors that met conditions necessary for a DBR and lower DBR releases. Accordingly, the Agency would like DOE to use available hydrogen gas monitoring data from sealed WIPP panels to assess the potential magnitude of radiolytic hydrogen gas generation in future recertifications. If this assessment shows that radiolytic hydrogen gas generation rates are sufficiently large to affect total gas generation rates, it would be appropriate for DOE to include the derived radiolytic gas generation rates in the CRA-2019 PA.

3.7 CONCLUSIONS REGARDING WIPP GAS GENERATION

The conceptual model assumptions and DOE's implementation of gas generation by anoxic corrosion of iron-based metals and alloys have remained unchanged since the CCA PAVT. The available data continue to support the conceptual model and overall approach for gas generation by anoxic corrosion of iron-based metals and alloys. Review of the available data regarding reaction products of anoxic corrosion of iron-based metals and alloys indicates that the reaction stoichiometry used in the CRA-2014 PA remains appropriate. Based on new project-specific iron corrosion data, DOE reduced the sampled range for the inundated iron-based metal corrosion rate. After evaluation of the project-specific data for both inundated and humid corrosion rates, EPA recommends that DOE use revised, higher values for these parameters in the CRA-2019 PA.

Review of the steel surface area per unit disposal volume demonstrated that the current PA value of 11.2 m^2/m^3 is reasonable for WIPP waste that has been emplaced through December 31, 2014. Because the D_S value could change in the future as different wastes are emplaced or if a different fill factor is achieved, the Agency expects DOE to recalculate the steel surface area per unit disposal volume for the CRA-2019 PA using updated inventory data.

Review of the potential effects of increased lead inventory and lead surface areas resulting from emplacement of shielded RH containers indicates that the current method of accounting for container lead does not adequately predict the probable lead inventory at closure for the WIPP repository. DOE should develop a reasonable upper-bound estimate for the lead inventory and lead surface area per unit disposal volume for the CRA-2019 PA and combine this with available project-specific lead corrosion data to assess the potential effects of lead corrosion on gas generation in the WIPP repository. If these effects are potentially significant, DOE should use the project-specific lead corrosion rates and likely lead inventory and surface areas to include gas generation from anoxic corrosion of lead in the CRA-2019 PA.

The microbial gas generation rates used for the CRA-2014 PA were the same rates used for the PABC04, CRA-2009 PA and PABC09. These rates were based on WIPP-specific microbial gas generation experiments carried out with cellulose. Consequently, these rates are appropriate for modeling gas generation rates from degradation of cellulosic materials, but may overestimate gas generation rates from the degradation of plastics and rubber. DOE accounted for uncertainties regarding the rates of plastic and rubber degradation in the WIPP repository environment by

assuming it occurs in only 25% of the realizations. Based on the available data, the current approach for modeling microbial gas generation rates is appropriate for PA.

Gas generation from radiolysis of water in the waste and brine and of plastics and rubber in the waste and emplacement materials has been assumed to be insignificant since the CCA PA. Lower microbial gas generation rates used since the PABC04 may invalidate this assumption, and there are monitoring data showing that radiolytic hydrogen gas generation is occurring in filled WIPP waste panels. EPA would like DOE to use the available radiolytic gas generation data to evaluate whether the gas generation rate is significant relative to the rates of gas generation by microbial degradation and anoxic corrosion for the CRA-2019 PA.

The gas generation rates used in the CRA-2014 PA and CRA14_SEN4 PA were likely underestimated:

- Development of the inundated and humid iron corrosion rates did not adequately account for the presence of low concentrations of CO_2 in the repository gas phase and brines (Edwards 2015a). DOE recalculated higher inundated and humid corrosion rates that included data collected in the presence of CO_2 (Shrader 2016, Zeitler 2015a, Zeitler 2015b), but these higher rates were not used in the CRA14_SEN4 PA. DOE also did not account for the increased inundated corrosion rate that would be likely at high pressure. The higher inundated and humid corrosion rates would result in higher anoxic corrosion gas generation than was modeled for the CRA-2014 PA or CRA14_SEN4 PA.

- DOE assumed that all $H_2S(g)$ generated by CPR degradation would instantaneously react with Fe(s) and $Fe(OH)_2(s)$, but this assumption is inconsistent with data showing that H_2S could passivate iron surfaces (Edwards 2015a). DOE agreed with this assessment (Patterson 2016b), and revised the reaction stoichiometry in the CRA14_SEN4 PA to remove this assumption.

- Based on the relatively high lead inventory calculated using data from the 2007 shielded container PCR (Crawford and Taggart 2007), and project-specific lead corrosion rate data (Roselle 2013), lead corrosion may significantly contribute to gas generation in the repository. Omission of lead corrosion from the CRA-2014 PA and CRA14_SEN4 PA gas generation calculations may have underestimated gas generation rates.

- Radiolytic gas generation was not included even though monitoring data from sealed WIPP panels shows that hydrogen is generated from WIPP waste.

Underestimation of gas generation rates may have had nonconservative effects on releases based on a likelihood of fewer PA vectors with DBRs at lower gas pressure. The level of significance of the underestimation of the gas generation rates in the CRA-2014 PA and CRA14_SEN4 PA is unknown, because the sensitivity of the PA results to higher inundated and humid steel corrosion rates, anoxic corrosion of lead or radiolytic gas generation has not been evaluated.

4.0 BACKFILL EFFICACY

Magnesium oxide backfill was included in the WIPP repository design to control repository chemical conditions and thereby minimize actinide solubilities in the postclosure repository (DOE 1996, Appendix BACK, Section 1). DOE selected MgO as an engineered barrier based on an analysis described in the CCA (DOE 1996, Appendix EBS), and EPA determined that MgO met the engineered barrier requirements (40 CFR Part 194.44).

4.1 CCA PA CONCEPTUAL MODEL AND IMPLEMENTATION

The CCA described the expected performance of the MgO backfill (DOE 1996, Appendices BACK and SOTERM). DOE provided additional information during the EPA's review of the CCA (EPA 1997c). The MgO chemical reactions and their ability to control chemical conditions in WIPP brines were addressed in the Chemical Conditions conceptual model, which was peer reviewed and accepted for the CCA (Wilson et al. 1996a, 1996b, 1997a, 1997b).

4.1.1 MgO Reactions in the Repository

The magnesium oxide backfill consumes CO_2 produced by microbial degradation of CPR and buffers brine pH to moderately alkaline values (approximately 8 to 10). Both actions control actinide solubilities in brine within the post-closure repository. MgO will initially react with brine to form brucite [$Mg(OH)_2(s)$]:

$$MgO(s) + H_2O \leftrightarrow Mg(OH)_2(s) \quad \textbf{(14)}$$

and brucite dissolution is expected to buffer brine pH in the repository by consuming acidity:

$$Mg(OH)_2(s) + 2\ H^+ \leftrightarrow Mg^{2+} + 2\ H_2O \quad \textbf{(15)}$$

Microbial degradation of CPR will produce CO_2, which can react with brucite to form magnesium-carbonate phases such as magnesite ($MgCO_3$):

$$Mg(OH)_2(s) + CO_2(g) \leftrightarrow MgCO_3(s) + H_2O \quad \textbf{(16)}$$

Brucite can also consume carbon dioxide and form hydromagnesite[6] (reactions 17 and 18) and nesquehonite (reaction 19):

$$5\ Mg(OH)_2(s) + 4\ CO_2(g) \leftrightarrow Mg_5(CO_3)_4(OH)_2{\bullet}4H_2O(s) \quad \textbf{(17)}$$

[6] DOE has reported two compositions for hydromagnesite: hydromagnesite$_{5424}$ [$Mg_5(CO_3)_4(OH)_2{\bullet}4H_2O(s)$] and hydromagnesite$_{4323}$ [$Mg_4(CO_3)_3(OH)_2{\bullet}3H_2O(s)$] (DOE 2009, Appendix MgO, Section 4.2.1). Only the hydromagnesite$_{5424}$ composition has been observed to form in WIPP-specific experiments and hydromagnesite$_{5424}$ is the composition recognized by the International Mineralogical Association (http://pubsites.uws.edu.au/ima-cnmnc/IMA2009-01%20UPDATE%20160309.pdf). Consequently, all references to hydromagnesite in this document refer to the hydromagnesite$_{5424}$ composition.

$$4\ Mg(OH)_2(s) + 3\ CO_2(g) \leftrightarrow Mg_4(CO_3)_3(OH)_2 \cdot 3H_2O(s) \quad \textbf{(18)}$$

$$Mg(OH)_2(s) + CO_2(g) + 2\ H_2O \leftrightarrow MgCO_3 \cdot 3H_2O(s) \quad \textbf{(19)}$$

Because of the magnesium ion's high energy of hydrolysis, magnesite does not precipitate directly from low-temperature solutions. Instead, metastable formation of hydrated magnesium-carbonate phases, such as hydromagnesite and nesquehonite, are more likely to occur. Because these phases are not thermodynamically stable under repository conditions, they are expected to eventually dehydrate to form magnesite, for example:

$$Mg_5(CO_3)_4(OH)_2 \cdot 4H_2O(s) + CO_2(g) \leftrightarrow 5\ MgCO_3(s) + 5\ H_2O \quad \textbf{(20)}$$

At equilibrium in the repository, magnesite is expected to be the most stable magnesium-carbonate phase (EPA 1998d). However, the rate at which metastable hydrated magnesium-carbonate phases will convert to stable magnesite is uncertain.

The reaction of brucite to form magnesium-carbonate solids in the repository will control the CO_2 partial pressure. In the CCA PA, DOE assumed that the brucite-magnesite reaction (16) would control CO_2 partial pressure (DOE 1996, Appendix SOTERM). EPA (1998d) reviewed experimental data on magnesium-carbonate solids formation in WIPP brines (SNL 1997) and found that nesquehonite formed initially in the experiments, but nesquehonite converted within a few days to a solid phase with a composition similar to proto-hydromagnesite [$(MgCO_3)_4 \cdot Mg(OH)_2 \cdot 4H_2O(s)$]. Hydromagnesite formation was observed in other scoping experiments (SNL 1997). There was no evidence of hydromagnesite conversion to magnesite in the experiments EPA (1998d) reviewed.

Based on a review of the literature, EPA (1998d) developed a conceptualization of the sequence and time scales of reactions between infiltrating brine and MgO backfill in the WIPP repository:

1. Rapid reaction of MgO with brine to produce brucite (hours to days)
2. Rapid carbonation of brucite to produce nesquehonite and possibly hydromagnesite (hours to days)
3. Rapid conversion of nesquehonite to hydromagnesite (days to weeks)
4. Slow conversion of hydromagnesite to magnesite (hundreds to thousands of years)

EPA (1998d) found that brucite in combination with the different magnesium carbonates buffered CO_2 fugacities at different values, with the highest value observed for nesquehonite, intermediate values for the two different forms of hydromagnesite and the lowest fugacities for magnesite. Higher CO_2 fugacities generally increase actinide solid solubilities, because of the formation of aqueous actinide-carbonate complexes. Verification calculations indicated that predicted actinide concentrations did not significantly change when the different reported compositions of hydromagnesite [either $Mg_5(CO_3)_4(OH)_2 \cdot 4H_2O(s)$ or $Mg_4(CO_3)_3(OH)_2 \cdot 3H_2O(s)$] were assumed to form (EPA 1998d). Errors in the thermodynamic database used for the CCA PA were corrected for the CCA PAVT (EPA 1998d). Because of the database errors, the actinide solubilities predicted for the CCA PA using the brucite-magnesite buffer were higher than the

actinide solubilities calculated for the CCA PAVT using the brucite-hydromagnesite buffer (EPA 1998d).

4.1.2 Placement of MgO Backfill

Magnesium oxide (MgO) emplaced in the repository is obtained from the supplier in a dry granular form (WTS 2003). This form was selected to minimize dusting in case of a premature bag rupture, ensure sufficient permeability for access of brine for reaction, reduce possible entrainment of MgO in brine flow and provide sufficient density so adequate amounts can be placed in the repository (DOE 1996, Appendix BACK, Section 2; DOE 2004, Appendix BARRIERS, Section 2.2). Adequate reactivity of supplied MgO has been tested using a laboratory procedure (Krumhansl et al. 1997; WTS 2003).

Initially, MgO was placed in the repository in 4,200-pound supersacks and 25-pound minisacks. The supersacks were placed on top of various combinations of waste containers (Standard Waste Boxes, 7-packs of 55-gallon drums, ten-drum overpacks, 4-packs of 85-gallon overpack drums, and 3-packs of 100 gallon drums), whereas the minisacks were placed among the waste containers and between the waste containers and the sides of the disposal rooms. The MgO supersacks are constructed of woven polypropylene material and are designed to provide a barrier to atmospheric moisture and CO_2 (WTS 2003). The supersacks are provided with a plastic support sheet, which remains under the supersacks after placement on the waste containers (WTS 2003).

At the time of the CCA, DOE calculated the required amount of MgO by assuming that all CPR carbon in the repository could be converted to CO_2; DOE determined that the amount of MgO required to react with this amount of CO_2 would be 43,700 tons (EPA 1997c). The MgO Excess Factor[7] (EF) is defined as:

$$EF = \frac{M_{MgO}}{M_{CO2}} \quad \textbf{(21)}$$

Where:

M_{MgO} = total moles of emplaced MgO
M_{CO2} = the maximum possible number of moles of CO_2 that could be generated by microbial consumption of all carbon in the CPR

An appropriate EF was included in the engineered barrier design by setting the amount of MgO at 85,000 tons. This quantity was based on the density of the MgO, the volume of the backfill packages, and the amount of space available in the repository for the backfill. The amount of MgO backfill in the CCA provided an EF of 1.95 (EPA 1997c).

[7] The MgO Excess Factor was originally called the MgO Safety Factor by EPA.

4.2 REVIEWS OF MgO EFFICACY AND IMPLEMENTATION CHANGES PRIOR TO THE CRA-2004 PA

The Actinide Source-Term Waste Test Program (STTP) experiments were designed to provide data on the concentrations of actinides, actinide-containing colloids, complexing agents, and other chemical reactants in simulated WIPP brine in contact with candidate backfill materials and actual TRU wastes (Villareal 1996, Villareal et al. 2001). MgO slurry was added to one experiment carried out at a CO_2 partial pressure of 60 bars to test the ability of the MgO to control chemical conditions. However, the MgO did not buffer the pH of this experiment in the slightly alkaline range predicted by the Chemical Conditions conceptual model. EPA reviewed the results of the STTP experiments and concerns regarding the efficacy of the MgO engineered barrier expressed by the Environmental Evaluation Group (EEG), and determined that the STTP experiment with MgO was not relevant to repository conditions because of the high CO_2 partial pressure (SC&A 2000). EPA also reviewed the uncertainty regarding the persistence of nesquehonite in the repository and concluded that no new evidence had been developed since the CCA to demonstrate that the MgO backfill would not behave as previously predicted. (TEA 2000, TEA 2001).

DOE requested EPA's approval to eliminate the MgO minisacks to enhance worker safety; EPA approved this change in January 2001 (DOE 2004, Appendix BARRIERS; EPA 2001a and 2001b). Elimination of the MgO minisacks decreased the EF to 1.67 (EPA 2001a).

EPA addressed the MgO EF during their review of DOE's request for AMWTF waste disposal at WIPP (Marcinowski 2004). This review was required because of the higher CPR densities in AMWTF waste and the potential effects on the amounts of MgO required to maintain an adequate EF (see Section 3.3.2) (TEA 2004). Because of the potential availability of sulfate in brines and in Salado minerals such as anhydrite, it is possible that all CPR degradation could take place by denitrification and sulfate reduction [reactions (10) and (11)]. EPA approved DOE's request to dispose of AMWTF compressed waste at WIPP, subject to the conditions that DOE maintain the MgO EF of 1.67 by adding extra MgO backfill with the compressed waste and that the MgO EF would be calculated on a room-by-room basis assuming that all CPR carbon in the waste could be converted to CO_2 (Marcinowski 2004).

4.3 CRA-2004 PA AND PABC04 REVIEW OF MgO BACKFILL EFFICACY

EPA (2006c) evaluated additional information related to MgO backfill efficacy during their review of the CRA-2004 PA and PABC04. This information included characteristics of the MgO used in the repository at that time, results from ongoing experiments related to MgO hydration and carbonation reactions, and calculations of the excess quantities of MgO in the repository.

4.3.1 Characterization of Premier MgO

At the time of the CRA-2004, WIPP MgO backfill was obtained from Premier Chemicals. Premier MgO was generated using a different process, had a different texture, and contained higher percentages of potentially reactive impurities than the MgO from National Magnesia Chemicals initially used as WIPP backfill (Bryan and Snider 2001b). Premier MgO was manufactured from mined sedimentary magnesite that was calcined to expel all CO_2 (DOE 2004,

Appendix BARRIERS-2.3.1). This material was characterized by XRD and found to contain primarily periclase [MgO], along with minor phases, such as forsterite [Mg_2SiO_4(s)], lime [CaO(s)], monticellite [$CaMgSiO_4$(s)], spinel [$MgAl_2O_4$(s)] and ulvospinel [$FeTi_2O_4$(s)]. Periclase and lime, which are expected to be reactive, made up approximately 90 wt% of the Premier MgO, with the unreactive constituents forming the remaining 10 wt% (Snider 2003a). Particle-size analysis was carried out for two batches of Premier MgO (Bryan and Snider 2001a; DOE 2004, Appendix BARRIERS, Section 2.3.1). The particle-size distribution of these two batches varied considerably; one batch had a bimodal distribution, with most MgO falling into the higher or lower size ranges (31% less than 0.15 mm and 37% greater than 2 mm), whereas the other batch had a single distribution of particle sizes centered at the middle of the range (59% between 0.30 and 0.71 mm).

4.3.2 MgO Hydration and Carbonation Experiments

DOE reported the results of MgO hydration and carbonation experiments (Bryan and Snider 2001a; Zhang et al. 2001; Snider 2001; Bryan and Snider 2001b; Snider 2002; Snider 2003a; Snider and Xiong 2002; Xiong and Snider 2003; DOE 2004, Appendix BARRIERS). These experiments included hydration experiments under humid conditions, using a range of relative humidities and at temperatures up to 90°C. Inundated hydration experiments were carried out using deionized water, sodium chloride [NaCl] solutions and GWB and ERDA-6 brines at temperatures up to 90°C. The hydration products in deionized water, NaCl solutions, and ERDA-6 brine were identified as brucite using XRD. However, in experiments with GWB brine, a magnesium-chloride-hydroxide hydrate phase formed initially (Snider 2002). This phase was identified by XRD and scanning electron microscope examination as "phase 5" [$Mg_3(OH)_5Cl{\bullet}4H_2O$][8] (DOE 2004, Appendix BARRIERS-2.3.2.1). In longer-term experiments, there was XRD evidence that this material was slowly being replaced by brucite (Snider 2003a; DOE 2004, Appendix BARRIERS-2.3.2.1).

Magnesium oxide (MgO) carbonation experiments were carried out under inundated conditions at CO_2 concentrations that ranged from atmospheric conditions up to 5%, using deionized water, 4 M NaCl, GWB brine, and ERDA-6 brine. Nesquehonite formation [reaction (19)] was only observed at the highest CO_2 partial pressure, and nesquehonite apparently was being replaced by hydromagnesite as these experiments progressed (DOE 2004, Appendix BARRIERS-2.3.2.2). In all GWB and ERDA-6 inundated experiments with Premier MgO at atmospheric CO_2 partial pressures, hydromagnesite was the only magnesium-carbonate phase detected.

EPA (2006c) reviewed the MgO hydration and carbonation experiments. Based on this review, EPA concluded that DOE had adequately accounted for information developed since the CCA in their consideration of the magnesium-carbonate phases most likely to control pH and CO_2 fugacities in the WIPP repository. The formation of brucite and possibly a magnesium-chloride-hydroxide hydrate phase is likely to control pH in the repository. Based on the experimental results, nesquehonite formation, if it occurs, appears to be transient and hydromagnesite is likely

[8] This magnesium hydroxychloride is referred to as "phase 5" in the cement industry, and this term is adopted for consistency with other WIPP documents (e.g., Xiong et al. 2010a).

to be the most important magnesium-hydroxycarbonate phase in the repository during the regulatory time period.

4.3.3 MgO Excess Factor Calculations

The MgO EF calculations for the CRA-2004 were performed concurrently with the AMWTF review of issues associated with the CPR microbial degradation reactions and effects on the MgO EF (see Sections 3.3.2 and 4.2). Consequently, EPA's requirement that DOE should assume all CPR carbon could be completely converted to CO_2 was not included in these calculations. In addition, when calculating the amount of CPR in the repository for the CRA-2004 PA, DOE did not include the CPR materials external to the waste containers, such as shrink wrap placed around the 55-gallon drum 7-packs or the support sheets and packaging materials used for the MgO supersacks (Cotsworth 2004b, Comment G-2). EPA pointed out that the MgO EF had not been appropriately computed for the 2004 CRA (Cotsworth 2004b, Comment C-23-5). EPA reiterated the condition that DOE maintain a 1.67 MgO EF on a room-by-room basis, and requested that DOE provide a plan for implementing this condition (Cotsworth 2004b, Comment G-4). DOE responded that the necessary measures would be implemented to ensure that the required amounts of MgO are emplaced within the repository, and provided the emplacement plan EPA requested (Detwiler 2004a, Detwiler 2004d).

Under the MgO emplacement plan, DOE monitored the amounts of MgO backfill and CPR during their emplacement in each room to ensure that the required MgO EF of 1.67 is maintained on a room-by-room basis (Detwiler 2004a). During review of the CRA-2004 PA, EPA (2006c) noted that waste loading in Panel 1 demonstrated that waste placement in the repository is likely to be heterogeneous, and that tight panel seals could prevent brine mixing between panels. EPA (2006c) concurred with DOE's plan to emplace enough MgO in each room of each panel to ensure an adequate EF under heterogeneous waste loading conditions.

Because the AMWTF compressed waste contains higher than average concentrations of CPR, DOE was required to emplace additional MgO. Consequently, in addition to the one supersack per stack of waste that had previously been used in WIPP, DOE began emplacing additional MgO supersacks on racks placed in the repository to achieve the required EF in each room. Each rack contained five supersacks identical to those placed on top of the waste containers and spanned the same vertical distance normally occupied by the waste containers. Thus, emplacement of additional MgO in the repository has used space normally occupied by CH waste (DOE 2009, Section 44.6.1.2).

4.4 PLANNED CHANGE REQUEST TO REDUCE MgO EXCESS FACTOR

DOE submitted a PCR to EPA to reduce the MgO EF from the approved value of 1.67 to 1.20 (Moody 2006). Because of the importance of MgO as the only engineered barrier for WIPP, EPA requested additional information about the uncertainties related to MgO effectiveness, the size of these uncertainties and their potential impacts on WIPP's long-term performance (Gitlin 2006). DOE responded with an analysis of the uncertainties associated with the effectiveness of MgO and provided an assessment of the effects of these uncertainties on the calculation of required MgO quantities (Vugrin et al. 2006). Vugrin et al. (2006) divided these uncertainties into four categories:

- Uncertainties in the quantity of CPR that will be consumed
- Uncertainties associated with the quantities of CO_2 produced by microbial degradation of CPR
- Uncertainties related to the amount of MgO available to react with CO_2
- Uncertainties in the moles of CO_2 consumed per mole of available MgO, and in the moles of CO_2 that could be consumed by reaction with other materials

To evaluate the uncertainties associated with the performance of the MgO backfill, Vugrin et al. (2006) defined the Effective Excess Factor (EEF) as:

$$EEF = \frac{\left(m \times M_{MgO}\right)}{\left(g \times M_c\right)} \times r \qquad \textbf{(22)}$$

Where:

g = uncertainty in the moles of CO_2 produced per mole of consumed organic carbon
m = uncertainty in the moles of MgO available for CO_2 consumption
M_c = total moles of organic carbon in the emplaced CPR reported by DOE
r = uncertainty in the moles of CO_2 consumed per mole of emplaced MgO
M_{MgO} = total moles of emplaced MgO

If this EEF equals one or greater, then sufficient MgO is expected to be available to react with all CO_2 produced by CPR degradation and maintain low CO_2 concentrations in the repository. DOE (Vugrin et al. 2006) addressed the uncertainties associated with the parameters in equation (22). During their review of the proposed change in the MgO EF, EPA requested additional information that was provided by DOE during technical exchange meetings in September 2006, January 2007 and May 2007. DOE then provided a revised report describing the uncertainties associated with the MgO EF in the repository (Vugrin et al. 2007).

DOE (Vugrin et al. 2007) accounted for uncertainty in the CPR inventory masses using the results of an evaluation by Kirchner and Vugrin (2006). The results of this study indicated that the mean CPR quantity in a disposal room should equal the sum of the CPR quantities reported by DOE for the individual containers. This study also demonstrated that the standard deviation would be relatively small, because of the random nature of the differences between the reported and actual inventory contents. Because of uncertainty regarding the long-term degradation of CPR, Vugrin et al. (2006, 2007) made the bounding assumption that all CPR could degrade during the 10,000-year WIPP regulatory period.

SC&A (2008a) observed that the reported masses of CPR in the inventory must be converted to moles of carbon to determine the amount of CO_2 that could be produced by CPR degradation. These calculations require assumptions regarding the chemical composition of the CPR. Assumptions summarized by Wang and Brush (1996) have been used in the past to perform these calculations. Vugrin et al. (2006, 2007) did not consider the possible effects of these assumptions on the EEF. EPA (SC&A 2008a) used assumptions regarding the compositions of the CPR to develop reasonable upper-range and lower-range estimates of the moles of carbon in

the CPR inventory. Using these values, they determined that the estimated moles of CPR carbon in the inventory ranged from 0.97 to 1.09 times the value calculated using the Wang and Brush (1996) assumptions. SC&A (2008a) stated that this range should be included in the EEF calculations as an uncertain parameter with a uniform distribution.

Vugrin et al. (2006, 2007) assumed that sufficient sulfate was present in the waste, brines and Salado minerals for complete degradation of all CPR carbon in the repository through sulfate reduction and denitrification. Consequently, they assumed that each mole of organic carbon consumed would produce a mole of CO_2. Because of the lower CO_2 yield from methanogenic CPR degradation, this assumption conservatively bounds the uncertainties related to the microbial reactions that may degrade CPR in the repository.

EPA (SC&A 2008a) concluded that the MagChem 10 WTS-60 MgO from Martin Marietta Magnesia Specialties, Inc. (Martin Marietta MgO), currently being used as backfill, has been reasonably well characterized. Preliminary hydration data provided by Wall (2005) indicated the Martin Marietta MgO will likely hydrate and carbonate more rapidly than MgO from previous suppliers (National Magnesia Chemicals and Premier Chemicals). Deng et al. (2006) used chemical analysis results, loss on ignition (LOI), thermogravimetric tests and assumptions regarding the chemical composition of the nonreactive phases in the MgO to calculate the amounts of reactive periclase and lime in Martin Marietta MgO samples. The results indicated that the Martin Marietta MgO contained 96 ± 2 (1σ) mole percent reactive periclase plus lime, with periclase making up 95 mole % and lime making up 1 mole % of the Martin Marietta MgO. SC&A (2008a) noted that the results reported by Deng et al. (2006) were based on analysis of eight samples from a single shipment (shipment SL2980076). Although limited data were available at that time regarding potential variability of the physical and chemical properties of the Martin Marietta MgO, SC&A (2008a) concluded based on information regarding the manufacturing processes and feedstock that this MgO would be expected to meet the performance specification of 96 ± 2 mole % reactive periclase plus lime included in the EEF calculations of Vugrin et al. (2007). However, SC&A (2008a) noted that the reactivity test (Krumhansl et al. 1997) included in the MgO specifications at that time (WTS 2005) was unlikely to be sufficient to ensure adequate reactivity of the materials in each MgO shipment, so an improved reactivity test was necessary.

The MgO backfill can react with brine and thereby control repository chemical conditions only if the brine and MgO remain in physical contact. There is no evidence that significant physical segregation of MgO by room roof collapse will occur. Similarly, the MgO supersacks appear very likely to rupture and expose MgO to any brine that enters the repository. An analysis presented by Clayton and Nemer (2006) of loss of MgO with brine from the repository was consistent with previous evaluations of the effects of drilling events on repository performance, and the effects of MgO loss to brine are likely to be relatively small. A very small fraction of the MgO appears likely to carbonate before emplacement, and this fraction was accounted for in the EEF calculation. Only a small amount of MgO dissolved in Salado brine is likely to enter the repository and react with CO_2, reducing the required amount of MgO; this effect was conservatively omitted from the calculations. Formation of impermeable rims of reaction products on individual periclase grains and impermeable reaction rinds on the masses of MgO in the repository would have the potential to limit the availability of MgO for complete reaction. The possible formation of such reaction rims on individual periclase grains or impermeable rinds

on masses of MgO was previously considered by the CCA Conceptual Models Peer Review Panel (Wilson et al. 1996a, 1996b, 1997a, 1997b). The Panel concluded that formation of magnesium-carbonate reaction products would not inhibit the access of brine to the surfaces of the MgO, and would not render any of the MgO unavailable for reaction with brine and CO_2. SC&A (2008a) determined that no new data had been developed since the time of the peer review to contradict this assumption, and concluded that it was reasonable to assume that essentially all MgO in the backfill will be available for reaction with brine and CO_2. Kanney and Vugrin (2006) evaluated aqueous diffusion of CO_2 in the repository; their results indicated that the gases and liquids in the repository will be sufficiently well mixed to permit contact and reaction of the MgO with brine and CO_2.

After MgO has eventually converted to hydromagnesite, the rate at which it will convert to magnesite is important, because it affects the moles of CO_2 consumed per mole of MgO reacted during the 10,000-year repository regulatory period, which in turn affects the EEF calculation. SC&A (2008a) examined the available experimental and natural analogue data that indicated the hydromagnesite to magnesite reaction rate could be relatively slow, so this reaction may not be complete during the WIPP repository regulatory period. Vugrin et al. (2007) accordingly used an uncertain variable with a uniform distribution to represent the moles of CO_2 consumed per mole of reacted MgO. This variable ranged from 0.8 (hydromagnesite only) to 1.0 (magnesite only).

Significant amounts of CPR degradation by sulfate reduction would require dissolution of sulfate minerals in the Salado Formation, including anhydrite, gypsum and polyhalite. Dissolution of these solid phases would release relatively large quantities of calcium ion into the brine. Elevated calcium concentrations would in turn be expected to cause calcium-carbonate precipitation and increased net consumption of CO_2 per mole of MgO in the backfill. DOE carried out EQ3/6 geochemical computer code calculations to estimate the proportions of CO_2 that would be consumed by magnesite or hydromagnesite and calcium carbonate precipitation (Brush et al. 2006). However, limitations in the EQ3/6 database resulted in modeling calculations that inadequately represented repository conditions. Because of the difficulties associated with quantifying the calcium-carbonate solids that would precipitate, a limiting assumption was made for the EEF calculation that no calcium carbonate precipitation would occur. This is undoubtedly a conservative, bounding assumption, and will lead to an underestimation of the EEF.

DOE (Vugrin et al. 2007) calculated a mean EEF of 1.03, with a standard deviation of 0.0719. EPA SC&A (2008a) found that incorporating the effects of uncertainty associated with the chemical composition of the CPR reduced the EEF to 1.00, with a standard deviation of 0.078. This EEF might seem to indicate that if the EF is reduced to 1.20, the average amount of MgO in a disposal room would equal the quantity required to react with CO_2. The EEF calculation, however, includes several conservative assumptions, including the assumptions that all CPR will degrade, all carbon in the CPR will react to form CO_2, and carbonate minerals other than hydromagnesite or magnesite will not precipitate, including calcite, iron carbonates, or lead carbonates. SC&A (2008a) determined that given these conservative, bounding assumptions, it was probable that if the EF was reduced to 1.20, the EEF in the disposal rooms will be greater than the mean bounding value of 1.00. Consequently, SC&A (2008a) determined that reduction of the EF to 1.20 would have no significant effects on repository chemistry.

After a review of the PCR to decrease the amount of MgO backfill emplaced at WIPP, which reduced the MgO EF from 1.6 to 1.2, and supporting documentation, EPA concluded that the available data supported a 1.20 MgO EF (Reyes 2008). EPA approved this planned change, stipulating that DOE should continue to calculate and track both the CPR carbon disposed and the required MgO needed on a room-by-room basis. EPA also required DOE to annually verify the reactivity of the MgO and ensure that it is maintained at 96%, as assumed in DOE's supporting documentation.

4.5 CRA-2009 MGO BACKFILL EFFICACY REVIEW

The WIPP engineered barrier was described in CRA-2009, Section 44.6.1, Appendix MgO-2009, and Appendix SOTERM-2009, Section 2.3 (DOE 2009). Descriptions of the MgO supersacks and their placement in the disposal system were provided in the CRA-2004 (DOE 2004, Section 3.3.1) and Section 44.6.1.2 of the CRA-2009 (DOE 2009).

The CRA-2009 included additional information regarding the Martin Marietta MgO now used as backfill at WIPP (DOE 2009, Appendix MgO-3.3.2). Deng et al. (2007) reported the results from characterization and accelerated inundated hydration testing of the MgO. The characterization and hydration results were obtained using samples from the same lot used by Deng et al. (2006). Particle-size analysis was carried out by sieving the Martin Marietta MgO through a series of sieves with openings of 2 mm (10 mesh) and less. The particle-size analysis results indicated that 53% of the MgO particles were between 0.60 and 1 mm.

Deng et al. (2007) reported results of hydration tests in deionized water at 70ºC. These tests were designed to evaluate the potential influence of MgO particle size, stirring rate, and solid-to-liquid ratio. Deng et al. (2007) observed that the Martin Marietta MgO hydrated more quickly in deionized water at 70°C than the Premier MgO. Deng et al. (2007) also observed that diffusion mechanisms may be important for small MgO particle sizes, whereas surface area appeared to be an important control for the rate of hydration for larger MgO particle sizes. The results of the Deng et al. (2007) investigation were used to design long-term hydration and carbonation experiments.

Deng et al. (2009) described preliminary results from long-term MgO inundated hydration experiments using Martin Marietta MgO currently used as WIPP backfill. These experiments included two MgO to brine ratios (3 g/11 ml and 3.1 g/77 ml), three brines (GWB, ERDA-6, and simplified GWB), and three particle-size ranges (as received, 1.0 to 2.0 mm, and less than 0.075 mm). All experiments were conducted at the predicted repository temperature of 28°C. Based on XRD examination, the MgO hydration reaction products were brucite in ERDA-6 brine and brucite plus phase 5 in GWB and simplified GWB brines. The results showed that MgO particle size affected the hydration rates, with more rapid hydration of smaller particles. The MgO hydration rate was faster in simplified GWB than in GWB or ERDA-6.

During review of the CRA-2009, EPA requested that DOE provide additional characterization data for the Martin Marietta MgO (Cotsworth 2009a, Comment 1-C-1). EPA noted that the information provided in the CRA-2009 was based on a single lot of this material, and questioned whether analysis of a single lot would be representative. EPA also questioned whether the reactivity test developed by Krumhansl et al. (1997) for MgO material acceptance was likely to

reliably detect MgO with insufficient reactive periclase plus lime (Cotsworth 2009a, Comment 1-C-2). In response, DOE provided their revised procedure for MgO acceptance testing (Nemer 2008), and confirmed that characterization and reactivity testing are performed on all shipments of the Martin Marietta MgO (Moody 2009b). The procedure outlined by Nemer (2008) determines the reactive mole percents of periclase and lime by first hydrating a sample of MgO in deionized water at approximately 245°C to form brucite and portlandite [$Ca(OH)_2(s)$]. The hydrated MgO sample is then dehydrated and the mass of dehydrated MgO and the mass of water are measured. The mass of water lost during dehydration and the mass of MgO, when converted to moles, provide the mole percents of periclase and lime available to react in the Martin Marietta MgO sample. The procedure Nemer (2008) provided is adequate for testing the moles of periclase plus lime that would rapidly react with brine in the repository.

DOE (Nemer 2009) performed a study to demonstrate that the current MgO acceptance test (Nemer 2008) would reliably detect MgO shipments with insufficient reactive periclase plus lime. In this investigation, the MgO acceptance test was performed on six samples composed of different ratios of high-purity MgO and non-reactive $Al_2O_3(s)$. The results established that the MgO acceptance test reliably determined known concentrations of reactive MgO with maximum errors of approximately 1%. These results demonstrated that the MgO acceptance test would detect MgO shipments with a percentage of reactive MgO less than the specified 96 ± 2 mole % reactive periclase plus lime.

DOE provided the results of testing of 127 samples from 105 MgO shipments (Moody 2009b). These tests were performed by an outside laboratory or by Sandia National Laboratories (SNL). The results indicated that the minimum measured reactivity of the Martin Marietta MgO was 96.2 mole %. The mean and standard deviation (1σ) calculated using all reported results were 97.9 ± 0.7 mole %, which exceeds the specified 96 ± 2 mole % reactive periclase plus lime. Based on the results of MgO acceptance testing reported by Moody (2009b), the Martin Marietta MgO backfill material will have sufficient reactivity to control chemical conditions in the WIPP repository.

EPA noted DOE's statement in Appendix MgO-2009, Section 4.2.2, that hydromagnesite will completely convert to magnesite during the 10,000-year WIPP regulatory time period (Cotsworth 2009a, Comment 1-C-18). EPA observed that a recent evaluation of the likely conversion rate for hydromagnesite to magnesite cited data from Vance et al. (1992) showing hydromagnesite may persist under some conditions for up to 6,200 years (SC&A 2008a). DOE's arguments supporting the formation of magnesite for most of the WIPP regulatory period in Appendix MgO-2009, Section 4.4.2, were considered in detail by SC&A (2008a) and found to be inadequate for establishing that hydromagnesite would rapidly convert to magnesite during the WIPP regulatory period. EPA pointed out that relatively slow CPR degradation rates could result in the formation of hydromagnesite throughout the 10,000-year regulatory period (Cotsworth 2009a). Consequently, even if hydromagnesite converts to magnesite in the repository within hundreds to thousands of years, hydromagnesite formed relatively late in the regulatory period by CPR degradation may be available to influence repository chemical conditions.

DOE responded that it is unclear whether hydromagnesite will persist or convert to magnesite during the 10,000-year WIPP regulatory period (Moody 2009a). This statement is consistent with the calculation of the EEF by Vugrin et al. (2007), who randomly sampled the uncertainty in the

moles of CO_2 consumed per mole of MgO reacted (see Section 4.4). Because of the uncertainty in whether hydromagnesite or magnesite formation will control CO_2 fugacity, EPA has specified that the CO_2 fugacity used to calculate actinide solubilities should be established by the brucite-hydromagnesite buffer [reaction (12)], which should provide an upper bound on actinide solubilities (see Section 6.0). DOE stated that information clarifying the uncertainties associated with the rate of conversion of hydromagnesite to magnesite would be attached as an erratum to CRA-2009, Appendix MgO (Moody 2009a).

EPA also observed that the CRA-2009 discussion of MgO uncertainties (Appendix MgO-2009, Section 6.2.4.4) did not include the uncertainties associated with the chemical composition of the CPR in the WIPP inventory (Cotsworth 2009a, Comment 1-C-20). DOE responded that although Vugrin et al. (2006) did not address uncertainties associated with the chemical composition of CPR materials in the WIPP inventory, DOE acknowledges that such uncertainties exist (Moody 2009a). Consequently, DOE will include a statement adding chemical composition uncertainties to the errata attached to Appendix MgO (DOE 2009).

4.6 PLANNED CHANGE NOTIFICATION REGARDING ALTERNATIVE PLACEMENT OF MgO SUPERSACKS

DOE (Franco 2012) notified EPA of planned changes in the emplacement of MgO and MgO supersack weight. Since EPA's approval of the PCR reducing the MgO EF from 1.67 to 1.2 (Section 4.4), 4,200 lb supersacks were placed on top of each waste stack and the EF was calculated at the end of each shift after data was uploaded to the WDS. Based on this EF calculation, additional MgO was placed during the next waste disposal shift to maintain a minimum EF of 1.2. Franco (2012) noted that using this emplacement process, a large excess of MgO was sometimes emplaced, resulting in a range of EF values from 1.22 to 2.85. DOE requested a change to 3,000 lb supersacks placed on alternating waste stacks, with additional supersacks emplaced if required to maintain a minimum EF of 1.2 based on calculations at the end of a waste emplacement shift.

Franco (2012) supported this change with an analysis based on calculations by Kanney and Vugrin (2006). These calculations, performed for the PABC04, showed that the minimum diffusion length of CO_2 generated by CPR degradation (3.37 m) would exceed the diameter of typical waste stacks (1.4 – 1.9 m) during time periods less than the hydraulic residence time. Because diffusion alone will be sufficient for CO_2 to reach MgO placed on an adjacent waste stack and advection would be expected to increase mixing, emplacement of MgO supersacks on alternating waste stacks was found to be a reasonable emplacement process. DOE also demonstrated using data from a Comprehensive Inventory Database query as of December 31, 2010, that approximately half of the stored and projected waste inventory would require 0.5 or fewer 3,000 lb MgO supersacks per waste stack to maintain an EF of 1.2 (Franco 2012). On this basis, Franco (2012) concluded that emplacing a 3,000 lb supersack on alternating waste stacks and using data uploaded to the WDS at the end of each shift to calculate if additional supersacks are required would ensure that a minimum EF of 1.2 was maintained.

EPA reviewed the information provided by DOE related to the PCR for MgO emplacement and supersack weight and had no objection to this modification of site procedures (Peake 2012). Peake (2012) noted that EPA would review the emplacement procedure revisions and verify that

the 2008 approval conditions continued to be met during the next scheduled Emplacement Inspection.

4.7 CRA-2014 MGO BACKFILL EFFICACY REVIEW

The MgO backfill that serves as an engineered barrier in the WIPP repository was described in CRA-2014 Section 44.0, Appendix MgO-2014, and Appendix SOTERM-2014 Section 2.3.3 (DOE 2014b).

4.7.1 MgO Placement

CRA-2014 Appendix MgO-2014 (DOE 2014b) describes the current emplacement of MgO backfill. WTS (2009a) specifies both 3,000- and 4,200-lb MgO supersacks because using both sizes is more economical and decreases the number of MgO supersack racks required to maintain a minimum EF of 1.2. Supersacks are now placed on every other row of waste stacks and WDS information is used to calculate the sizes of the emplaced supersacks to maintain a minimum EF of 1.2 and minimize the use of supersack racks.

As of December 31, 2012, the overall EF in the WIPP repository was 1.81 (Kouba 2013, DOE 2014b Appendix MgO-2014). The EF in individual WIPP panels has changed over time because of the elimination of minisacks with reduction of the minimum EF from 1.95 to 1.67 (Section 4.2), the approved PCR for reduction of the minimum EF from 1.67 to 1.2 (Section 4.4) and increased efficiency achieved by placing supersacks on alternating waste stack rows (Section 4.6). The highest EF (2.186) was calculated for Panel 2, which was filled in October 2005, and the lowest EF (1.557) was calculated for Panel 6, which was filled in March 2013 (Kouba 2013). The information provided by Kouba (2013) demonstrates that DOE has maintained EF values in each panel that exceed the minimum 1.2 EF.

EPA requested additional information about whether the larger lateral distance between MgO supersacks resulting from the emplacement changes since the PABC09 still allows sufficient reaction between MgO and CO_2 (Edwards 2015b, Comment 2-44-1). DOE responded with an update of the calculations performed by Kanney and Vugrin (2006) using BRAGFLO output data for waste panel porosity, waste panel pore volume and cumulative brine flow up the intrusion borehole for each of the 100 vectors in Replicate 1 Scenario 2 of the CRA-2014 (Franco 2015c). Scenario 2 has a borehole intrusion that intersects the waste panel and a brine pocket in the Castile at 350 years after closure. DOE selected Scenario 2 because its high flow up the intrusion borehole results in lower hydraulic residence times and lower diffusion penetration lengths compared to an undisturbed scenario. The shortest diffusion length was 1.43 m with a residence time of 320 years (Franco 2015c, Attachment A). DOE demonstrated that this minimum lateral diffusion length of 1.43 m will allow sufficient reaction between MgO and CO_2 using the as-emplaced waste in Panel 7, Room 7 (Franco 2015c).

4.7.2 MgO Characteristics and Reactivity Testing

DOE has used MgO from Martin Marietta (Section 4.4) in the repository since January 2005 (DOE 2014b, Appendix MgO-2014). In response to EPA comments regarding reactivity testing of MgO (Sections 4.4 and 4.5), Nemer (2008) developed a testing procedure incorporated into

the MgO specifications (WTS 2009b). A total of 370 reactivity tests have been carried out on 37 shipments received from April 2009 to December 2012, which yielded an average reactivity of 97.4 mole percent (DOE 2014b, Appendix MgO-2014) that exceeds the minimum required reactivity of 96 ± 2 mole percent (Reyes 2008).

4.7.3 MgO Hydration Reactions

MgO hydration experiments conducted in ERDA-6 brine have produced brucite as the hydrated solid phase [reaction (14)] (Snider 2002, Deng 2009). However, in GWB and simplified GWB brines, MgO hydration produced brucite plus phase 5 (Snider 2002, Deng 2009). Phase 5 solubility data was not included in the geochemical modeling database used for the CCA PAVT, PABC04 or PABC09. Phase 5 solubility data (Xiong 2009, Xiong et al. 2009b, Xiong et al. 2010a) was added to the geochemical modeling database used for the CRA-2014 PA (DATA0.FM1, Section 6.6.4).

4.7.4 MgO Carbonation Reactions

Assumptions regarding MgO carbonation reactions are unchanged since the PABC09 (Section 4.5). For the purposes of calculating dissolved actinide solubilities, DOE continues to assume that reaction between brucite and hydromagnesite [reaction (17)] will buffer CO_2 fugacity. New studies have examined hydromagnesite solubility (Cheng and Li 2010, Xiong 2011a, Berninger et al. 2014, Gautier et al. 2014). These solubility studies are reviewed in Section 6.6.4.1.

DOE included the rate of conversion of hydromagnesite to magnesite in their revised water balance calculations (Clayton 2013, DOE 2014b Appendix PA Section PA-4.2.5). DOE's assumptions regarding the conversion rate of hydromagnesite to magnesite are examined in Section 12.4.3.

4.8 BACKFILL EFFICACY CONCLUSIONS

The available data indicates that the MgO backfill will continue to control CO_2 fugacities under inundated conditions and maintain chemical conditions in WIPP brines that limit actinide solubilities. There are no data available regarding the carbonation rate of MgO under humid conditions in the WIPP repository, but maintenance of low CO_2 partial pressures is relatively unimportant for these conditions.

EPA has reviewed the current characterization, testing and emplacement of MgO in the repository and concluded:

- The current emplacement plan ensures adequate amounts of MgO, because the quantities of CPR and MgO are monitored in each room of the repository during emplacement, and additional MgO is emplaced if necessary to maintain the MgO EF of 1.2.
- Because of uncertainties regarding the rate at which hydromagnesite will convert to magnesite in the repository environment, PA calculations of actinide solubilities assume that the brucite-hydromagnesite reaction will buffer CO_2 fugacity at levels consistent with

relatively low actinide solubilities under inundated conditions over the 10,000-year regulatory time period.

- EPA has reviewed additional documentation from DOE regarding the characterization of the Martin Marietta MgO currently used as WIPP backfill and the acceptance testing that is carried out for this material. The MgO reactivity testing procedure and test results provided by DOE (Moody 2009b) demonstrates that the current Martin Marietta backfill material contains a sufficient percentage of reactive periclase plus lime to control chemical conditions in the repository, and that the testing procedure would detect any MgO shipments with inadequate percentages of reactive periclase plus lime. The testing procedure has been incorporated in the MgO specifications (WTS 2009b). DOE provided the results of 370 reactivity tests carried out on 37 MgO shipments received from April 2009 to December 2012 (DOE 2014b, Appendix MgO-2014). These results demonstrate the MgO reactivity has exceeded the minimum 96 ± 2 mole percent reactivity specified by EPA (Reyes 2008).
- DOE has not completed an experimental determination of MgO hydration rates using Martin Marietta MgO. Because the majority of MgO in the repository is Martin Marietta MgO and MgO hydration rates are important to repository water balance calculations (Section 12.4.1), EPA would like to see updated hydration rates reflective of the different types of MgO used.

5.0 ACTINIDE OXIDATION STATES

The actinide oxidation states assumed in the CRA-2014 PA have remained unchanged since the CCA (DOE 2009, Appendix SOTERM-3.9). Assumptions regarding the actinide oxidation states were peer reviewed and approved for the CCA as part of the Dissolved Actinide Source Term and Chemical Conditions conceptual models (Wilson et al. 1996a, 1996b, 1997a, 1997b).

The Chemical Conditions conceptual model does not assume equilibrium for redox reactions among the actinides. Actinide oxidation states were determined based on the assumption that reducing conditions would be established relatively quickly in the WIPP repository, combined with the results of a literature review and experimental investigations. The actinide oxidation states that were predicted to persist in the WIPP repository environment over the long term were (DOE 1996, Appendix SOTERM):

- Am(III), Cm(III) and Th(IV)
- Pu(III) and Pu(IV)
- Np(IV) and Np(V)
- U(IV) and U(VI)

Actinide solubilities were calculated for the CCA PAVT, PABC04 and PABC09 using the Fracture-Matrix Transport code (FMT) and were calculated for the CRA-2014 PA using the EQ3/6 code. FMT does not include the calculation of redox states. Consequently, the redox states of the actinides for the CCA PAVT, PABC04 and PABC09 were based on sampling of an oxidation-state parameter. The EQ3/6 code can be used to calculate redox states, but the same approach for assigning redox states for plutonium, neptunium and uranium was retained for the CRA-2014 PA to remain consistent with the Chemical Conditions conceptual model.

Because PA assumes that plutonium, neptunium and uranium may be present in either of two oxidation states, the parameter GLOBAL:OXSTAT is sampled from a uniform distribution (DOE 2014b, Appendix SOTERM-2014 Section 5.2; Kicker and Herrick 2013). Calculated solubilities for the Pu(III), Np(IV) and U(IV) oxidation states are assumed for half of the PA realizations, and calculated solubilities for the Pu(IV), Np(V) and U(VI) oxidation states are assumed for the other half of the PA realizations.

The actinide oxidation states assumed for the PA calculations are important because of the effects of redox state on actinide solubilities and total mobilized actinides (Section 6.0). Reduced actinides [Pu(III), Pu(IV), Np(IV), and U(IV)] form solids that have lower solubilities than actinides in higher oxidation states [plutonium(V), plutonium(VI), Np(V), and U(VI)]. However, Pu(III) is generally more soluble than Pu(IV). Actinide oxidation states also affect colloidal concentrations (Section 7.0).

5.1 ACTINIDE OXIDATION STATE INFORMATION DEVELOPED FOR THE CCA PAVT AND PABC04

EPA (1998d) reviewed and agreed with the expected oxidation states used in the CCA PA and PAVT. At the time of the CCA, most stakeholder questions about actinide oxidation states concerned the possible persistence of plutonium(VI) in the WIPP repository. EPA (1998d)

considered several experimental studies indicating that reductants, including soluble iron, metallic iron, humics and other organic ligands, would reduce plutonium to the (III) and (IV) oxidation states under equilibrium conditions in the repository (Weiner 1996; Felmy et al. 1989; Rai and Ryan 1985; Choppin 1991).

For the CRA-2004 PABC, EPA (2006c) reviewed information regarding likely actinide oxidation states in WIPP brines that became available after the CCA. The investigations considered by EPA (2006c) included Grambow et al. (1996), Villareal et al. (2001), Haschke et al. (2000), Slater et al. (1997), Xia et al. (2001), Reed et al. (1997), ANL (1997) and André and Choppin (2000). Based on this review, EPA (2006c) concluded that the available evidence continued to support the actinide oxidation state assumptions used for the WIPP PABC04 calculations.

5.2 ACTINIDE OXIDATION STATE INFORMATION DEVELOPED FOR THE PABC09

For the PABC09, DOE (2009) assumed that uranium may exist in either the +IV or +VI oxidation state. EPA (2010b) concluded that this assumption remained valid based on a review of data from numerous uranium studies, including Grambow et al. (1996), Gu et al. (1998), Dodge et al. (2002), O'Loughlin et al. (2003) Fiedor et al. (1998), Xia et al. (2001), Hua et al. (2006), Lovley and Phillips (1992), Frederickson et al. (2000), Suzuki et al. (2003), Brooks et al. (2003), Neiss et al. (2007), Francis and Dodge (2008) and Francis et al. (2000). EPA (2010b) concluded that U(IV) is likely to be the most stable oxidation state under the reducing conditions in the WIPP repository, but U(VI) may persist because of the effects of aqueous speciation on uranium reduction.

The PABC09 assumed that neptunium will be present in the WIPP repository in either the +IV or +V oxidation state. EPA (2010b) reviewed neptunium oxidation state investigations that included Rai and Ryan (1985), Xia et al. (2001), Banaszak et al. (1999), Rittmann et al. (2002) and Icopini et al. (2007). EPA (2010b) concluded that neptunium will most likely be present in the +IV oxidation state and the assumption that neptunium may be present in the +V oxidation state in the WIPP repository brines is conservative, because of the greater solubility of Np(V) solid phases. Because of the relatively small neptunium inventory, EPA (2010b) observed that the assumption of higher neptunium solubility in half of the PA realizations is unlikely to affect PA results.

EPA (2010b) found that the available data continued to support DOE's assumption that plutonium will be present in the less-soluble +III and +IV oxidation states, rather than the more-soluble +V and +VI oxidation states. Investigations related to plutonium oxidation states reviewed by EPA (2010b) included Rai et al. (2002), Ding et al. (2006), Reed et al. (2006), Neck et al. (2007), Altmaier et al. (2009), Xia et al. (2001), Reed et al. (2010), Reed et al. (2007), Boukhalfa et al. (2007), Ohnuki et al. (2007) and Icopini et al. (2009). EPA (2010b) noted that the relatively more soluble Pu(III) oxidation state may be stable or may metastably persist under anticipated WIPP repository conditions. Radiolytic effects on actinide oxidation states have been assumed to be mitigated by the effects of reducing materials, mainly iron metal, in the WIPP repository and EPA (2010b) stated that the available data continued to support this assumption.

5.3 ACTINIDE OXIDATION STATE INFORMATION DEVELOPED FOR THE CRA-2014 PA

Actinide oxidation state assumptions used in the CRA-2014 PA remained unchanged from previous PA assumptions.

5.3.1 Uranium and Neptunium Oxidation States

DOE (2014b) summarized the redox chemistry of uranium in Appendix SOTERM-2014, Section SOTERM-3.4.1.1. Du et al. (2011) demonstrated that U(VI) can be reduced to U(IV) by aqueous Fe(II). Latta et al. (2012) investigated U(VI) reduction by magnetite and determined that magnetite stoichiometry influenced the extent of U(VI) reduction. Singer et al. (2012a, 2012b) found that formation of Ca-U(VI)-CO_3 aqueous species limited U(VI) reduction by magnetite.

In addition to the studies cited by DOE (2014b, Appendix SOTERM-2014), Regenspurg et al. (2009) performed experiments that showed Fe(II), whether structurally bound in magnetite or sorbed on a mineral surface, reduced U(VI) to U(IV) in the presence of bicarbonate. Hyun et al. (2012) performed experiments demonstrating that mackinawite [FeS(s)] reduced aqueous U(VI) to solid U(IV) in oxygen- and carbonate-free solutions from pH 5 to 11. Gallegos et al. (2013) found that mackinawite reduced aqueous U(VI) to U(IV) in anoxic solutions with 0.012 M bicarbonate. These data indicate that U(IV) is likely to be present in WIPP brines under the highly reducing conditions established by iron metal and iron sulfides in the repository. The relatively low calcium and carbonate concentrations anticipated in WIPP brines are also likely to be conducive to uranium reduction and low solubilities. Consequently, the assumption that U(VI) will be present in half of the PA realizations is likely to be conservative.

No new data have been identified regarding neptunium oxidation states. Consequently, the assumption that neptunium will be present as either Np(IV) or Np(V) continues to be appropriate.

5.3.2 Plutonium Oxidation States

DOE (2014b, Appendix SOTERM-2014) stated that Pu(IV) was the most likely oxidation state in WIPP brines and equilibrium solid phases. DOE indicated that inclusion of the Pu(III) oxidation state in the actinide solubility calculations used in PA was a conservative assumption because of the generally higher solubilities of Pu(III) solids in WIPP brines. However, more recent data (e.g., Altmaier et al. 2009 and Reed et al. 2011) show that Pu(III) in WIPP repository brines and equilibrium solid phases may be more important than was previously recognized. Accordingly, EPA requested that DOE provide an assessment of all available data relevant to the assumed plutonium oxidation states for PA (Edwards 2015c, Completeness Comment 3-C-1).

In response, DOE acknowledged that data developed since the CRA-2009 PA suggest that Pu(III) may be more important for WIPP PA than previously understood (Shrader 2015). In this response, DOE discussed the likely effects of reduced iron, organic ligands such as EDTA, and microbial processes on plutonium oxidation states. DOE concluded that although Pu(III) could be formed under some conditions, Pu(IV) would continue to be important because of its stabilization by EDTA and its production by radiolysis (Shrader 2015). Because DOE's response

(Shrader 2015) raised issues related to radiolytic effects on actinide oxidation states and the potential effects of reductive dissolution of Pu(IV) solid to form Pu(III) aqueous species, EPA carried out a comprehensive review of the available data.

5.3.2.1 Long-Term WIPP Repository Conditions

Within 100 years of closure, the WIPP repository is expected to become anoxic because of degradation of waste, packaging and emplacement CPR and corrosion of iron metal in the waste and waste containers. Reductants in the WIPP repository that could affect plutonium oxidation states include large quantities of iron metal present in the waste and steel waste drums, iron corrosion products, organic ligands in the waste and humic substances present in waste soils or produced during waste degradation. Microbial reduction of plutonium may also occur under some conditions.

Because MgO backfill is added to the repository, repository brines are expected to be mildly alkaline, with pH values of approximately 9 and low total inorganic carbon concentrations (less than 5×10^{-4} M, Brush and Domski 2013b). Brines included in WIPP PA are two end-member brine compositions: GWB represents the composition of Salado Formation brine from the repository horizon, and ERDA-6 represents the composition of Castile brine that may enter the repository from a pressurized region below the repository.

An Eh-pH diagram illustrates the possible effects of expected oxidation-reduction potential (Eh) and brine pH on aqueous plutonium redox speciation at low ionic strength and 1 atm pressure. (Figure 5-1). Although the coniditons in this diagram are not directly reflected at WIPP, the aqueous species will follow similar trends at higher ionic strengths and pressures. The blue-shaded area in Figure 5-1 represents conditions between the upper stability limit of water [O_2(g) pressure of 1 atm] and the lower stability limit of water [H_2(g) pressure of 1 atm]. Because of anoxic corrosion and the approximately 80 atm hydrostatic pressure in the WIPP repository after closure, repository hydrogen gas [H_2(g)] pressures are expected to be much greater than 1 atm. Consequently, WIPP Eh-pH conditions are likely to fall below the blue-shaded area around pH 9 in Figure 5-1, near the boundary between $PuOH^{2+}$ and $Pu(OH)_4$(aq) in Figure 1, which indicates that the stable aqueous plutonium oxidation state may be Pu(III) [$Pu(OH)^{2+}$] or Pu(IV) [$Pu(OH)_4$(aq)].

The plutonium isotope used in many of the reviewed investigations was ^{239}Pu, which could cause increased plutonium oxidation states through radiolysis because of its shorter half life (24,110 years) compared to ^{242}Pu (374,000 years). Other isotopes used in the experiments included ^{238}Pu (87.74 years) and ^{240}Pu (6,537 years), which could also cause significant radiolysis. Many studies were carried out in low ionic strength solutions, which could affect their applicability to brines. Finally, many studies were conducted for time periods on the order of hours to weeks, which are extremely short relative to the 10,000-year period of performance for the WIPP repository. These possible limitations are considered in the evaluation of the experimental data.

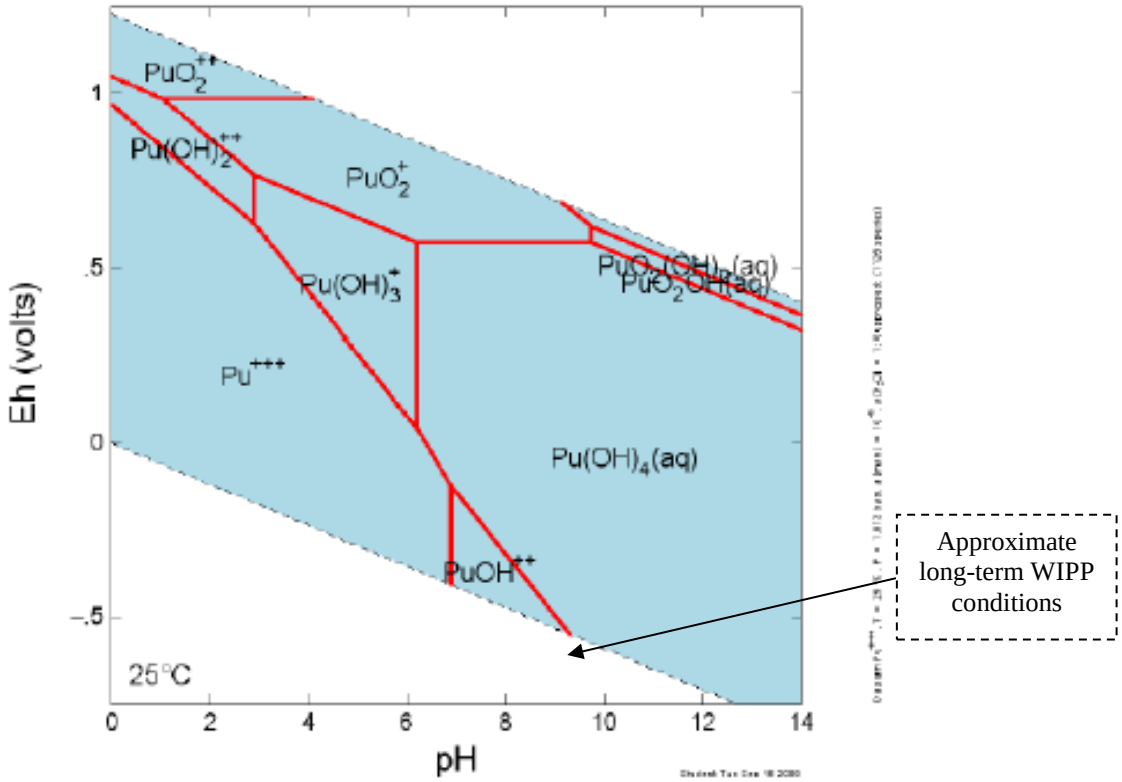

Figure 5-1. Plutonium Eh-pH Diagram Showing Plutonium Aqueous Speciation (Simpkins 2011) [9]

5.3.2.2 Effects of Iron Solids and Aqueous Species

Iron metal in the WIPP waste produces Fe solids and aqueous species capable of Pu reduction:

$$Fe(s) + (x+2)\ H_2O(l) \rightarrow Fe(OH)_2 \bullet xH_2O(s) + H_2(g) \quad \textbf{(23)}$$

$$Fe(s) + H_2S(g) \rightarrow FeS(s) + H_2(g) \quad \textbf{(24)}$$

$$Fe(s) + 2\ H^+ \rightarrow Fe^{2+} + H_2(g) \quad \textbf{(25)}$$

[9] This diagram is shown for discussion purposes only, and was not developed using WIPP solubility or aqueous speciation data. The diagram was generated using a total plutonium concentration of 1×10^{-9} M in 0.1 M NaCl, with solid phase precipitation not allowed.

Consequently, iron solids and aqueous species anticipated in the repository include iron metal [Fe(s)], solid ferrous hydroxide [$Fe(OH)_2 \cdot xH_2O(s)$], iron sulfides such as mackinawite [FeS(s)] and aqueous ferrous iron [Fe^{2+}]. Significant quantities of other iron solids such as magnetite [$Fe_3O_4(s)$] or ferrihydrite [$Fe(OH)_3(s)$] are not expected to be present in the long-term WIPP environment. However, experimental data for plutonium reduction by phases such as magnetite and ferrihydrite are relevant to WIPP if they demonstrate plutonium reduction through reaction with aqueous ferrous iron in equilibrium with these solids.

CCA Appendix SOTERM (DOE 1996) reviewed data reported by Clark and Tait (1996) and Weiner (1996), which demonstrated that iron metal and aqueous ferrous iron reduce Pu(VI) to Pu(IV). DOE (1996) determined that Pu(IV) would be the dominant oxidation state under WIPP repository conditions based on results reported by Weiner (1996). However, DOE (1996) reported ^{239}Pu(III) stabilization in brines by metallic iron in experiments equilibrated for up to 24 days (Felmy et al. 1989), so the persistence of Pu(III) in the long-term WIPP repository could not be ruled out. Accordingly, both Pu(III) and Pu(IV) were included in the CCA PA actinide solubility calculations. Recent experiments outlined below suggest however, that Pu(III) may be more dominant through the process of reductive dissolution.

Xia et al. (2001) demonstrated that powdered metallic iron reduces Pu(VI) to Pu(IV) and Pu(III) solids in ERDA-6 brine. The plutonium stock solution used in these experiments was 93.6% ^{239}Pu and 6.3% ^{240}Pu.The experiments were carried out under an inert (argon) atmosphere over a pH range from approximately 8 to 12 for up to 76 days. In the dilute NaCl solution, Pu(VI) reduction and precipitation took place within a few days to a few months. The low aqueous plutonium concentrations prevented direct determination of the aqueous plutonium oxidation state, but the precipitated solid phase was believed to be either $PuO_2 \cdot xH_2O(s)$ or $Pu(OH)_3(s)$. In the ERDA-6 brine with powdered metallic iron, the Pu(VI) reduction rate was much slower, the dominant oxidation state in solution was Pu(V) and the precipitated solid phase appeared to be $PuO_2 \cdot xH_2O(s)$. Incomplete reduction of the aqueous plutonium in the brine experiments appeared to be caused by formation of oxide coatings on the iron metal surface, which limited its reducing capacity.

Reed et al. (2006) also demonstrated Pu reduction by iron coupons and aqueous ferrous iron in WIPP brines containing ^{239}Pu(VI) at pcH[10] values from 5 to 10. The zero-valent iron experiments were equilibrated for 19 days after an iron coupon was added, and the aqueous ferrous iron experiments were equilibrated for 9 days after addition of Fe^{2+}. In these experiments, solid iron addition resulted in rapid decreases in aqueous plutonium concentrations due to precipitation of Pu(IV) solid. The oxidation state of the plutonium remaining in the aqueous phase was not directly determined, but was believed to be Pu(IV) or Pu(III), based on the low plutonium concentrations. Reed et al. (2006) noted that the preponderance of Pu(IV) in the system was inconsistent with the thermodynamic data that would predict the existence of Pu(III) under anoxic conditions in the presence of metallic iron. They suggested that the presence of Pu(IV) may have been caused by buildup of radiolytically produced oxychlorides during the 2-year

[10] pcH is the negative logarithm of the hydrogen ion concentration (moles/L); in WIPP repository brines, pcH is approximately 9.5 (Brush and Domski 2013b), compared to an approximate pH (negative logarithm of the hydrogen ion activity) of 9.0.

stabilization period before addition of the iron coupon. Addition of aqueous ferrous iron to the WIPP brines containing Pu(VI) resulted in rapid Pu(VI) reduction and low aqueous plutonium concentrations in all experiments conducted in alkaline brines. The extent of plutonium concentration decrease was less for experiments with added aqueous ferrous iron than for the zero-valent iron experiments.

Ding et al. (2006) further demonstrated Pu reduction by iron. Their experiments investigated the speciation of ^{239}Pu solids heterogeneously precipitated by iron metal and aluminum metal in water, NaCl solutions and ERDA-6 brine. Their results indicated that reductive precipitation of Pu(VI) over the course of four weeks produced a solid precipitate identical to the $PuO_{2+x-y}(OH)_{2y}•zH_2O(s)$ produced by hydrolysis of Pu(IV). In another investigation, Reed et al. (2010) demonstrated the reduction of ^{242}Pu(VI) in brine by iron solid phases. These experiments were carried out for 4 weeks at room temperature under anoxic conditions in ERDA-6 brine and GWB brine in the presence of iron powder or an iron coupon. In experiments at pcH 7 (GWB) and 8 (ERDA 6), plutonium concentrations decreased rapidly in the brines when either iron powder or an iron coupon was present. At pcH 10, the plutonium concentration decreased more slowly, and the concentration was still decreasing at the time of the report.

Reed et al. (2010) summarized the results of experiments in ERDA-6 brine to evaluate the effects of iron oxidation state on ^{242}Pu(VI) reduction. These experiments were carried out with carbonate ion at pcH 9, with addition of an iron coupon, iron powder, colloidal iron(II), colloidal iron(III), iron(III) oxide or magnetite. In these experiments, the iron powder, iron coupons or magnetite rapidly reduced plutonium concentrations in solution. X-ray absorption near-edge structure (XANES) analysis showed that aqueous Pu(VI) was reduced to form solid Pu(IV) phases by the zero-valent iron and Fe(II). A smaller decrease in the aqueous plutonium concentration was observed in the Fe(III) oxide experiment. Because no reductant was available in these experiments, the decreased plutonium concentration was believed to be caused by sorption.

Kirsch et al. (2010, 2011) demonstrated Pu reduction by Fe. They carried out a series of experiments in which solutions of ^{242}Pu(III) in 0.1 M NaCl were contacted with magnetite at pH values of approximately 6 and 8, and solutions of ^{242}Pu(V) in 0.1 M NaCl were contacted with magnetite or mackinawite at pH values of approximately 8. Experiments were conducted for approximately 40 days, at which time aqueous plutonium concentrations were below the analytical detection limit of 1×10^{-9} M. Pu(III) and Pu(V) added to magnetite were immobilized on the magnetite surface as a Pu(III) surface complex. The Pu(V) added to mackinawite was immobilized as $PuO_2(s)$.

5.3.2.3 Evidence of Pu Reductive Dissolution

The studies that are most applicable to the WIPP repository are the long-term Reed et al. (2011) investigation with iron coupons or iron powder in WIPP brines with ^{242}Pu to limit radiolytic effects and the experiments with ^{242}Pu by Altmaier et al. (2009) and Altmaier and Geckeis (2011) in $MgCl_2$ brine. These experiments indicated that Pu(III) was present in solution; in the solid phase, either Pu(III) or Pu(IV) solids were observed or inferred. Consequently, the available data indicate that metallic iron, iron sulfides and aqueous ferrous iron in the WIPP

repository brines are likely to result in the formation of Pu(III) and/or Pu(IV) solids in equilibrium with aqueous Pu(III).

While multiple experiments have established that the Fe present in the waste will reduce Pu, further experiments provide evidence that reductive dissolution is a very important process that may increase the importance of Pu(III) the WIPP. Rai et al. (2002)[11] for example, evaluated the reductive dissolution of amorphous $^{239}PuO_2$(am) by aqueous Fe^{2+} in dilute NaCl solution for up to 43 days. In these experiments, reductive dissolution was observed in less than 4 days. Pu(III) was present in the experimental solutions based on spectroscopic, solvent extraction and thermodynamic analysis of the data. The dominant solubility-controlling reaction determined for these experiments was:

$$PuO_2(am) + 4\ H^+ + e^- = Pu^{3+} + 2\ H_2O \qquad \textbf{(26)}$$

Further evidence of reductive dissolution was reported by Altmaier et al. (2009). This investigation examined the solubility of ^{242}Pu(IV) hydrous oxide in 0.25 M and 3.5 M $MgCl_2$ solutions at approximately pcH 9 in the presence of metallic iron powder for periods of 4 to 582 days. In these experiments, Pu(III) was the dominant oxidation state in solution. The solid phase was indirectly determined to be $PuO_2 \cdot xH_2O$(s) based on solubility calculations.

Reed et al. (2011) further demonstrated Pu reduction, and possibly reductive dissolution, in ^{242}Pu(VI)-brine experiments with added magnetite, iron coupons and iron powder that were allowed to equilibrate for about 5.8 years. Analysis of the plutonium solid phase indicated that plutonium was present predominantly as Pu(III), ranging from 87% to 100% Pu(III). Transformation over time from Pu(IV) to Pu(III) solids coincided with an increase in aqueous plutonium concentrations, consistent with higher Pu(III) hydrous oxide solubility suggesting that reductive dissolution was occurring.

Altmaier and Geckeis (2011) investigated the plutonium solid phases, solubility, and aqueous speciation in 3.5 M $MgCl_2$ solutions under strongly reducing conditions with and without the presence of aqueous carbonate. The experimental results showedPu reduction by Fe resulting in Pu(III) solids in equilibrium with Pu(III) aqueous species as well as PuO_2(s) reductive dissolution, with Pu(IV) solids in equilibrium with Pu(III) aqueous species (Figure 5-2). Powdered metallic iron was used in the experiments to establish strongly reducing conditions and experiments were conducted with ^{242}Pu for up to 582 days. In samples with Pu(IV) solid under carbonate-free conditions, solubilities were consistent with Pu(III) aqueous species in equilibrium with Pu(IV) solid. In the carbonate-free experiment with Pu(III) added to the brine, short equilibration times produced solution concentrations consistent with Pu(III) aqueous species in equilibrium with Pu(III) solid. However, in these carbonate-free experiments, plutonium concentrations decreased over time because of the formation of Pu(IV) solid. The third set of experiments was carried out with addition of aqueous Pu(III) to systems containing precipitated Mg-OH-CO_3 solids to maintain carbonate concentrations in the brine. In these

[11] In their response to EPA Comment 3-C-1, DOE (Shrader 2015) referred to this study as Felmy et al. (1989).

experiments, Pu(III) solid was in equilibrium with Pu(III) aqueous species over the entire 582-day experiment duration. Altmaier and Geckeis (2011) stated that "formation of the Pu(III) solid phase can be explained by a stabilization of Pu(III) by coordinated carbonate ligands in the solid but this needs further investigation."

Felmy et al. (2011) evaluated the effects of goethite [FeOOH(s)] addition on the reductive dissolution of PuO_2(am) by aqueous Fe^{2+} in dilute NaCl solutions over a pH range from approximately 2 to 6. The stock solution used in this investigation was 93% ^{239}Pu and 7% ^{240}Pu. Goethite was found to enhance Pu(IV) reduction in experiments carried out for up to 61 days. Aqueous plutonium was found to be present predominantly as Pu(III), in equilibrium with PuO_2(am). Felmy et al. (2012) similarly evaluated the effects of magnetite nanoparticles on the reductive dissolution of PuO_2(am) by aqueous Fe^{2+} in dilute NaCl solutions at pH values from approximately 4.5 to 10. The stock solution used in this investigation was 93% ^{239}Pu and 7% ^{240}Pu. In experiments that were equilibrated up to 56 days, much less Pu(III) was released into solution through reductive dissolution than predicted by thermodynamic calculations. The results of these experiments with reduced iron solids and aqueous Fe(II) demonstrate that Pu(VI) and Pu(V) will be reduced to Pu(III) or Pu(IV) in the WIPP repository.

5.3.2.4 Effects of Organic Ligands

EDTA can reduce higher oxidation states of Pu to either Pu(IV) or Pu(III). AlMahamid et al. (1996) evaluated the effect of EDTA addition to Pu(III) present in solution at an initial plutonium concentration of 7.9×10^{-4} M at pH 6 and an initial Pu/EDTA concentration ratio of 1/6. Under these conditions with relatively high plutonium concentrations, Pu(III) was rapidly oxidized to form Pu(IV)-EDTA in solution. Additional experiments were conducted with an initial Pu(IV) concentration of 5×10^{-7} M at pH 7 to 8 with Pu/EDTA ratios of 1/10 and 1/100. In these experiments, 12% to 29% of the Pu(IV) was reduced to Pu(III) after 10 days. The +IV actinide concentrations modeled for the CRA-2014 PA range from 6.05×10^{-7} M to 7.20×10^{-8} M (Brush and Domski 2013a) and the +IV actinide/EDTA ratio ranges from 1/244 to 1/1,223, so the more dilute experiments are more consistent with WIPP conditions. These experiments indicate that at the lower concentrations anticipated in WIPP brines, aqueous Pu(IV) may be reduced to Pu(III) by EDTA.

Reed et al. (1996) demonstrated that EDTA can reduce oxidized forms of Pu to Pu(IV). They investigated the effects of oxalate, citrate or EDTA on 1×10^{-4} M solutions of Pu(VI) in WIPP brines over the course of 10 days. Oxalate reduced about 60% of the Pu(VI) to Pu(V), with no evident Pu(IV) in solution. Citrate reduced approximately 70% of the Pu(VI) to Pu(IV). EDTA rapidly reduced Pu(VI) to Pu(V), with slower reduction to Pu(IV), which comprised about 35% of the aqueous plutonium after 10 days.

Reed et al. (1998) also evaluated reduction rates, comparing the efficacy of different ligands for reducing oxidized Pu to Pu(IV). Reed et al. (1998) reported the results of ^{242}Pu(VI) stability experiments in low ionic strength solutions and WIPP brines with added citrate, oxalate or EDTA. The low ionic strength experiments were carried out at pH 6 for 110 days, and all three organic ligands reduced Pu(VI) to Pu(V), with rates that decreased in the order EDTA > citrate > oxalate. Reduction of Pu(VI) to Pu(IV) occurred with rates that decreased in the order citrate > EDTA > oxalate. Five experiments were conducted with Pu(VI) in simulated WIPP brine with

addition of a mixture of EDTA, citrate and oxalate: ERDA-6 brine at pH 8 or 10 with 10^{-4} M carbonate, ERDA-6 brine at pH 10 with no carbonate and G-Seep (Salado Formation) brine at pH 5 or 7. The initial plutonium concentrations were 1×10^{-4} M and the experiments were equilibrated for 2 months under anoxic conditions. In the pH 8 ERDA-6 experiment with carbonate, Pu(VI) was slowly reduced to Pu(V) and Pu(IV), but no reduction of Pu(VI) was observed in the ERDA-6 pH 10 experiment with carbonate. In the ERDA-6 pH 10 experiment without carbonate, the Pu(VI) appeared to be reduced to Pu(IV) polymer. In the G-Seep brine at both pH 5 and 7, Pu(VI) was rapidly reduced to Pu(V) and Pu(IV). No reduction of Pu(IV) to Pu(III) was noted in these experiments.

Rai et al. (2008b) posit the importance of Pu(III) over Pu(IV) in the environment due to EDTA complexes. Their experiments examined stability constants developed by Boukhalfa et al. (2003, 2004), who used spectrophotometric and potentiometric titration methods to show that in acidic solutions, the Pu(III)-EDTA complex dissociates and Pu(III) is oxidized to Pu(IV) because of the stability of the Pu(IV)-EDTA complex. However, the experiments by Boukhalfa et al. (2003, 2004) contained 93% ^{239}Pu and 7% ^{240}Pu, indicating radiolysis may have oxidized the Pu(III). Rai et al. (2008b) determined that the Boukhalfa et al. (2003, 2004) experiments do not adequately predict the experimentally determined solubility of PuO_2(am) as a function of pH and EDTA concentrations. Rai et al. (2008b) further evaluated the solubility of $^{239}PuO_2$(am) in the presence of ferrihydrite and EDTA in dilute solutions from pH 2.3 to 11.5. The measured total plutonium concentrations in these experiments were much higher than predicted based on the complexation of Pu(IV) and Fe(III) by EDTA. Oxidation state analysis by solvent extraction showed that significant amounts of Pu(III) were in solution below about pH 8 and Pu(V) or Pu(VI) was in solution above about pH 8. Reduction of Pu(IV) to Pu(III) in the absence of an added reductant was attributed to reaction with small amounts of ferrous iron in the ferrihydrite. Rai et al. (2008b) concluded from their experimental data and calculations that the importance of Pu(IV)-EDTA complexes had been overstated and that Pu(III)-EDTA complexes may play an important role in plutonium mobility in reducing environments.

5.3.2.5 Effects of Humic Substances

Studies indicate that Pu(V) and Pu(VI) likely will be reduced by humic substances to a mixture of Pu(III) and Pu(IV). Choppin (1991) and André and Choppin (2000) experimentally determined that humics in seawater and 5 M NaCl solutions reduced ^{238}Pu(V) to Pu(IV). Marquardt et al. (2004, 2008) and Banik et al. (2006) found that humic and fulvic acids in groundwater reduced Pu(V) and Pu(VI) to a mixture of Pu(IV) and Pu(III). Dardenne et al. (2009) added Pu(III), Pu(IV) and Pu(VI) to Gorleben groundwater and found that the humic substances in the groundwater produced mostly Pu(IV) regardless of the initial plutonium oxidation state.

5.3.2.6 Effects of Microorganisms

Microbial metal reduction may occur through direct enzymatic reduction or may occur indirectly, for example if microbes produce aqueous ferrous iron or organic compounds that can reduce another metal such as plutonium. A large body of evidence demonstrates microbial reduction of higher oxidation states of plutonium [Pu(VI) and Pu(V)] to Pu(IV) and/or Pu(III) in low ionic strength solutions. Rusin et al. (1994) reported that *Bacillus* strains solubilized hydrous

PuO_2(s) under anaerobic conditions through apparent Pu(IV) reduction to Pu(III). Boukhalfa et al. (2007) determined that addition of EDTA promoted the reduction of $Pu(OH)_4$(am) to Pu(III) by *Shewanella oneidensis* and *Geobacter sulfurreducens.*

Experiments have demonstrated that microbially produced ligands can reduce Pu to Pu(III). Bolton et al. (2006) and Plymale et al. (2012) investigated abiotic and biotic (*Shewanella oneidensis* and *Geobacter sulfurreducens*) reduction and solubilization of hydrous PuO_2(am) with and without the presence of EDTA and anthraquinone-2,6-disulfonate (AQDS), an electron shuttle included to simulate humic compounds. All experiments were conducted with excess H_2 as an electron donor. In the presence of EDTA and AQDS in the abiotic experiments, 98% of the hydrous PuO_2(am) was dissolved after 418 days, with Pu(III) detected in solution along with additional colloidal material that may have been Pu(IV) or Pu(III). Addition of EDTA and AQDS to the biotic experiments resulted in complete reductive dissolution of hydrous PuO_2(am) in about 24 hours. With only EDTA added to the biotic experiments, the bioreductive dissolution was slower and less extensive, reaching 83 to 94% in about 22 days.

Other experiments are unclear about microbial Pu reduction mechanisms. Francis et al. (2007) observed reduction of Pu(IV) to Pu(III) by the anaerobic bacterium *Clostridium*. Icopini et al. (2009) investigated microbial reduction of Pu(VI) and Pu(V) by *Shewanella oneidensis* and *Geobacter sulfurreducens* in low-ionic-strength solutions at pH 7. The Pu(VI) and Pu(V) were reduced to nanoparticulate Pu(IV), with no evidence of Pu(III) after 24 hours. Renshaw et al. (2009) investigated the effects of *Shewanella oneidensis* and *Geobacter sulfurreducens* on plutonium solution concentrations in the presence of acetate and lactate. The presence of the bacteria resulted in much lower plutonium concentrations in solution because of its association with the biomass. The plutonium, initially added as either Pu(IV) or Pu(VI) was present as sorbed or precipitated Pu(IV) and a small amount of Pu(III).

Although extensive data are available showing that biotic plutonium reduction can occur under low-ionic-strength conditions and that EDTA or other ligands can promote dissolution and reduction, only limited data are available for high-ionic-strength solutions such as WIPP repository brines. Reed et al. (2011) observed reduction of Fe(III) to Fe(II) by a mixed culture of halophilic *Bacteria* and *Archaea*. Production of aqueous ferrous iron could cause indirect reduction of Pu(IV) to Pu(III). However, iron reduction appears to have been caused by the halophilic *Bacteria* (up to 2.5 M ionic strength) rather than *Archaea* (greater than 3.5 M ionic strength) so it is not certain that this bacterial iron reduction would occur in WIPP repository brines. Emmerich et al. (2012) performed experiments demonstrating microbial reduction of Fe(III) in up to 5 M NaCl. However, whether the microbes identified in WIPP halite (Swanson 2013) can cause either direct or indirect reduction of plutonium remains uncertain.

5.3.2.7 Effects of Plutonium Oxidation States on PA

All WIPP PAs performed since the CCA have assumed plutonium oxidation states in both the solid phases and brines as Pu(III) in 50% of the realizations and Pu(IV) in 50% of the realizations. Plutonium solubilities in WIPP repository brines have been calculated using the reactions:

$$PuO_2(am) + 4\ H^+ = Pu^{4+} + 2\ H_2O \quad \textbf{(27)}$$

$$Pu(OH)_3(s) + 3\ H^+ = Pu^{3+} + 3\ H_2O \quad \textbf{(28)}$$

Because of the oxidation-state analogy, the solubility of $PuO_2(am)$ is assumed equal to the solubility of $ThO_2(am)$ and the solubility of $Pu(OH)_3(s)$ is assumed equal to the solubility of $Am(OH)_3(s)$. For the CRA-2014 PA, calculated baseline +III actinide solubilities ranged from 3.92×10^{-7} M to 2.59×10^{-6} M and calculated baseline +IV actinide solubilities were significantly lower, ranging from 6.05×10^{-8} M to 7.20×10^{-8} M (Table 5-1).

Table 5-1. CRA-2014 Baseline Actinide Solubilities (Brush and Domski 2013a) in mol/L (M). Actinide concentrations in brine are calculated by equilibrating a representative brine (GWB or ERDA-6) with WIPP-relevant solid phases (such as minerals), organic ligands, and actinides. Solubilities are calculated for different brine volumes released from the repository, ranging from the minimum brine volume needed for a release to 5-times that volume (discussed in Section 6.6.3).

Brine Volume	GWB Am(III)	GWB Th(IV)	ERDA-6 Am(III)	ERDA-6 Th(IV)
1 × minimum	2.59×10^{-6}	6.05×10^{-8}	1.48×10^{-6}	7.02×10^{-8}
2 × minimum	1.38×10^{-6}	6.06×10^{-8}	8.59×10^{-7}	7.14×10^{-8}
3 × minimum	9.74×10^{-7}	6.07×10^{-8}	5.99×10^{-7}	7.17×10^{-8}
4 × minimum	7.69×10^{-7}	6.07×10^{-8}	4.69×10^{-7}	7.19×10^{-8}
5 × minimum	6.47×10^{-7}	6.07×10^{-8}	3.92×10^{-7}	7.20×10^{-8}

In the reducing environment of the WIPP repository, the evidence reviewed above demonstrates that the more soluble Pu(V) and Pu(VI) oxidation states will be reduced to the less-soluble Pu(III) and Pu(IV) oxidation states. Review of the available data also shows that plutonium reduction by iron metal, ferrous hydroxide solid, mackinawite, aqueous ferrous iron and humic substances is likely to result in Pu(III) and Pu(IV) solids in equilibrium with Pu(III) aqueous species. The presence of EDTA in the WIPP brines does not appear likely to stabilize Pu(IV) in solution, and the effects of microbial processes on plutonium oxidation states in the brines are uncertain. Consequently, instead of reaction (27), the solubility of Pu(IV) solid in the repository should be represented by the reductive dissolution reaction:

$$PuO_2(am) + 3\ H^+ + 0.5\ H_2 = Pu^{3+} + 2\ H_2O \quad \textbf{(29)}$$

The solubility reactions (28) and (29) likely to control plutonium concentrations in WIPP repository brines are illustrated in Figure 5-2. This figure is adapted from Altmaier and Geckeis (2011), who discussed ongoing research at Karlsruhe Institute of Technology – Institute for Nuclear Waste Disposal (KIT-INE) concerning the stability of $Pu(OH)_3(s)$ in highly reducing brines containing carbonate.

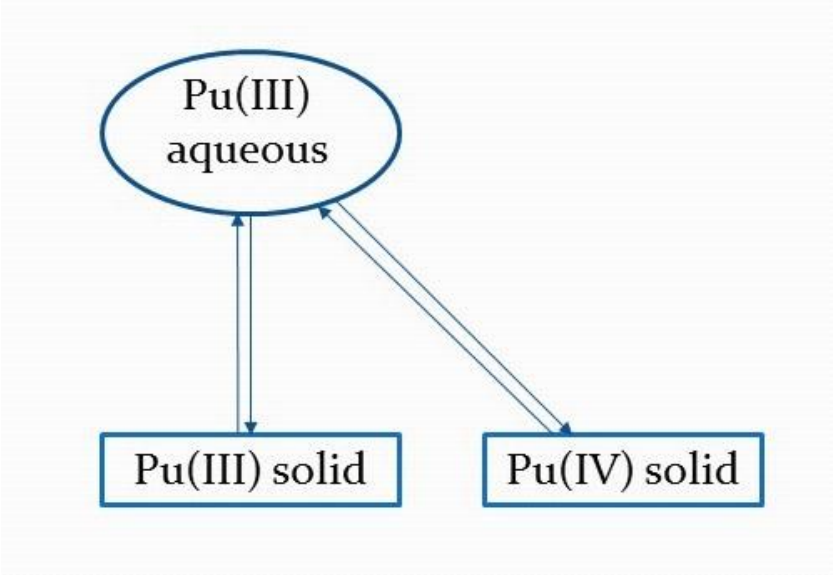

Figure 5-2. Reactions Controlling the Solubility of Plutonium in WIPP Brines

Because of uncertainties associated with the plutonium oxidation state in the solid phase [either Pu(III) or Pu(IV)], the 50% of the PA realizations with lower actinide oxidation states should use the dissolution of Pu(III) solid [reaction (28)] and the 50% of the PA realizations with higher actinide oxidation states should use the reductive dissolution of Pu(IV) solid [reaction (29)] to calculate baseline aqueous plutonium concentrations.

The effects of redox conditions on the solubilities of $Pu(OH)_3(s)$ and $PuO_2(am)$ in WIPP brines can be illustrated using the solubilities calculated for GWB (1× brine volume) for the CRA-2014 (Figure 5-3). Under the most reducing conditions anticipated in the WIPP repository, the solubility of $Pu(OH)_3(s)$ controls aqueous plutonium concentrations in GWB brine at 2.59×10^{-6} M [reaction (28)]. At higher redox conditions in the repository, $PuO_2(am)$ becomes the stable plutonium solid and reductive dissolution of $PuO_2(am)$ [reaction (29)] controls aqueous plutonium concentrations. During reductive dissolution of $PuO_2(am)$, the Pu^{3+} activity $\{Pu^{3+}\}$ and the Pu^{3+} concentration (Pu^{3+})[12] will decrease as a function of increasing redox conditions (pe)[13] based on the relationship between the equilibrium constant (log K) for reaction (26) and pe at constant pH:

$$\text{Log } \{Pu^{3+}\} = \log K - 4\,pH - pe \qquad \textbf{(30)}$$

[12] The activity of the Pu^{3+} ion, or its "effective concentration," equals the Pu^{3+} concentration multiplied by the Pu^{3+} activity coefficient (γ_{Pu3+})

[13] The redox conditions are indicated by the pe, which is the negative logarithm of the electron activity

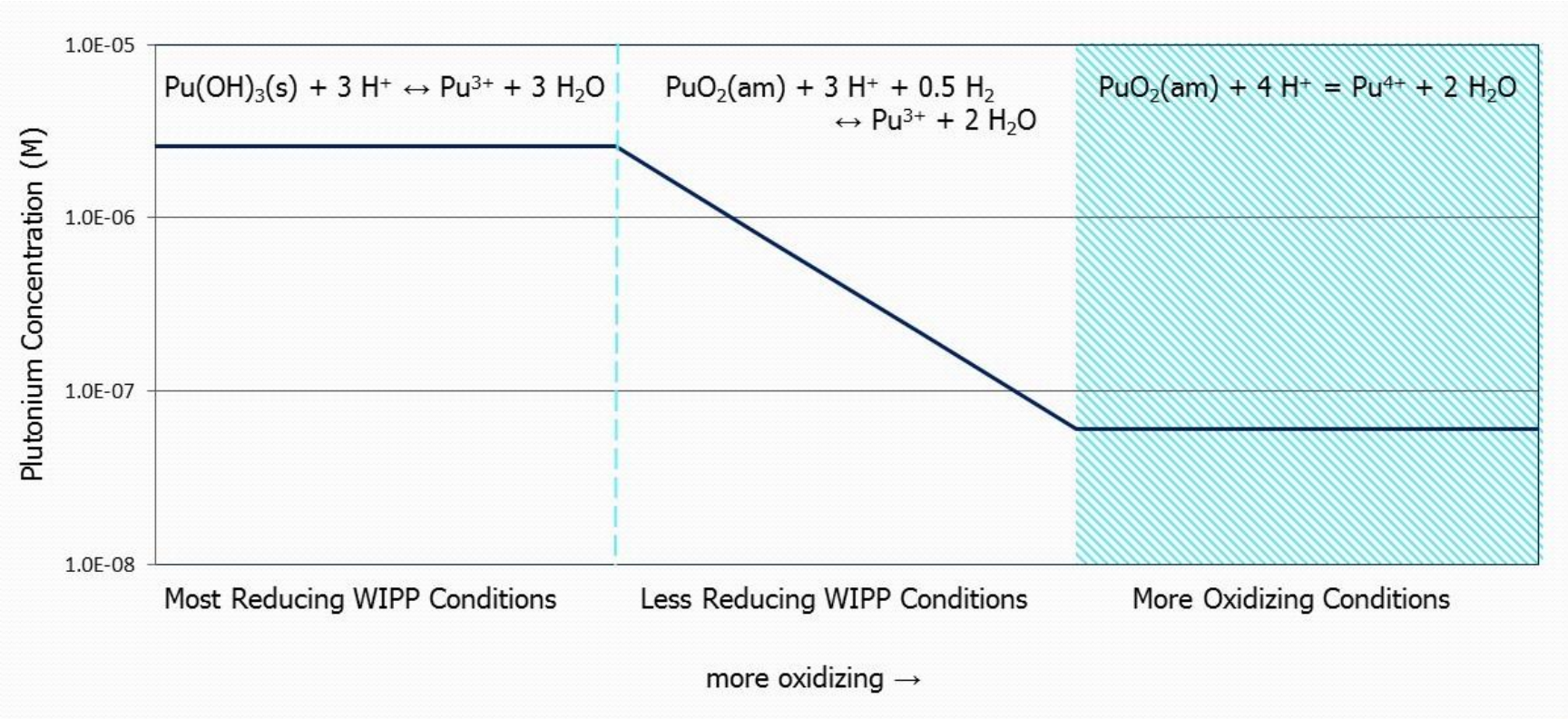

Figure 5-3. Effects of Redox Conditions on Baseline Plutonium Concentrations for WIPP PA, Illustrated Using CRA-2014 Am(III) and Th(IV) Baseline Solubilities (GWB, 1× brine volume). WIPP Repository Brine Aqueous Plutonium Concentrations Are Controlled by $Pu(OH)_3(s)$ Solubility Under the Most Reducing WIPP Conditions and by Reductive Dissolution of $PuO_2(am)$ Under the Less Reducing WIPP Conditions

This relationship can be plotted as shown in Figure 5-3. Because log K is a constant, and assuming a constant pH, increasing pe (i.e., creating more oxidizing conditions) results in lower Pu^{3+} concentrations when pH is also constant. Finally, as conditions become sufficiently oxidizing, aqueous Pu^{4+} becomes more stable than aqueous Pu^{3+} and reaction (27) controls aqueous plutonium concentrations in GWB brine at 6.05×10^{-8} M (Figure 5-3). Consequently, under redox conditions where reductive dissolution of PuO_2(am) controls aqueous plutonium concentrations [reaction (29)], the upper limit of the plutonium concentration in brine is the aqueous Pu(III) concentration in equilibrium with $Pu(OH)_3$(s), and the lower limit is the aqueous Pu(IV) concentration in equilibrium with PuO_2(am) (Figure 5-3).

Given the EPA analysis, instead of using the current 50/50 assumption, PA realizations with the lower oxidation state assumption, baseline plutonium concentrations could continue to be set equal to the baseline +III actinide concentrations for GWB and ERDA-6 brine. For each PA realization with the higher oxidation state assumption, baseline plutonium concentrations would ideally be determined by random sampling of the range of baseline plutonium concentrations consistent with reductive dissolution of PuO_2(s). The plutonium concentration ranges for the higher oxidation state conditions based on the CRA-2014 PA baseline actinide concentrations are summarized in Table 5-2.

Table 5-2. Higher Oxidation State Assumption Plutonium Concentration Ranges Using CRA-2014 Baseline Concentrations

Brine Volume	GWB Concentration Range (M)		ERDA-6 Concentration Range (M)	
	Minimum[a]	Maximum[b]	Minimum[a]	Maximum[b]
1 × minimum	6.05E-08	2.59E-06	7.02E-08	1.48E-06
2 × minimum	6.06E-08	1.38E-06	7.14E-08	8.59E-07
3 × minimum	6.07E-08	9.74E-07	7.17E-08	5.99E-07
4 × minimum	6.07E-08	7.69E-07	7.19E-08	4.69E-07
5 × minimum	6.07E-08	6.47E-07	7.20E-08	3.92E-07

a – equal to baseline CRA-2014 Th(IV) solubility (Brush and Domski 2013b)
b – equal to baseline CRA-2014 Am(III) solubility (Brush and Domski 2013b)

5.3.2.8 Technical Exchanges with DOE

The results of EPA's review of plutonium oxidation states and the conclusion that reductive dissolution of Pu(IV) solid more accurately represents likely plutonium redox states under the higher oxidation state conditions were addressed in an email dated July 28, 2016 (Economy 2016) and discussed with DOE during a conference call held on August 9, 2016 and during a EPA/DOE technical exchange meeting held on August 31 and September 1, 2016.

During this technical exchange, differences of opinion were voiced related to modifying the Pu(III)/(IV) proportions in PA calculations. EPA indicated there is experimental data that suggests amorphous PuO_2(am) is dissolved to aqueous Pu(III) via reductive dissolution in WIPP pcH/Eh conditions. Translating this to WIPP PA calculations, EPA suggested it is likely that the percent of PA realizations with actinides assigned the lower oxidation states [Pu(III), Np(IV) and U(IV)] should increase from the current value of 50%. This would then mean the percent of

realizations with the higher oxidation state [Pu(IV), Np(V) and U(VI)] would decrease from 50%. DOE contractor staff thought there was contradictory literature on this issue and they do not support the technical argument presented by EPA justifying changing the proportions of Pu III/IV oxidation states. Given these reasons, DOE indicated they continue to support the current oxidation state distribution as 50/50 and documented in Appendix SOTERM. DOE indicated any modification to the current oxidation sate proportions would require modifications to the PANEL code, a time consuming task (Patterson 2016a).

DOE cites Pu(IV)-EDTA stability as a reason for the importance of Pu(IV). An investigation of Pu(IV)-EDTA stability constants by Meyer et al. (2007) is cited in DOE's response to Comment 3-C-1 as evidence that Pu(IV) reduction is not observed under acidic conditions (Shrader 2015). However, these titration experiments were carried out in nitric acid (a strong oxidant), likely over the course of hours rather than weeks or years. Consequently, this study does not provide information relevant to potential long-term reduction of Pu(IV) by EDTA in alkaline brines under reducing conditions, such as those that will occur in WIPP.

Thakur et al. (2009), Rai et al. (2008b)[14] and Rai et al (2010)[15] were cited in DOE's response to Comment 3-C-1 (Shrader 2015) as evidence that Pu(IV) would not be reduced by EDTA "and strong measures were needed to suppress the oxidation of Pu(III) to Pu(IV) in the presence of EDTA." However, the experimental section of Thakur et al. (2009) states that an oxidant – not a reductant – was added to prevent reduction of Pu(IV) to Pu(III) in very short-term (1 hour) solvent extraction experiments evaluating Pu(IV)-EDTA complexation constants. Rai et al. (2008b) did not report the use of a reductant in their experiments and in fact noted the reduction of Pu(IV) to Pu(III) in experiments with added ferrihydrite. Rai et al. (2010) did include reductants (hydroquinone and sodium dithionite) to maintain reducing conditions and ensure all plutonium remained in the Pu(III) oxidation state in their solubility study for $PuPO_4(s)$ in the presence of EDTA. However, the precaution taken in these experiments does not constitute proof that EDTA will oxidize Pu(III) to Pu(IV). Rai et al. (2010) appears to draw a much different conclusion than Shrader (2015), stating "Our recent study [Rai et al. 2008b] with ethylenediaminetetraacetic acid (EDTA) complexes of Pu(IV), and other environmentally important metal ions Fe(III) and Ca(II), showed that Pu(IV)-EDTA complexes are not expected to be the significantly mobile Pu species under environmental conditions. This study also showed the likelihood of Pu(III) species being potentially mobile under environmental conditions where Pu and EDTA have been co-disposed."

Experiments have demonstrated that EDTA will reduce Pu(VI) and Pu(V) to Pu(III) or Pu(IV). The Thakur et al. (2009), Rai et al. (2008b) and Rai et al (2010) investigations cited by Shrader (2015) do not demonstrate that EDTA will stabilize Pu(IV) and prevent reduction to Pu(III). In fact, the results of Rai et al. (2008b) indicate that in the presence of aqueous ferrous iron and EDTA, Pu(IV) solids will be reduced to form aqueous Pu(III).

DOE provided additional justification for not revising the actinide oxidation state distribution implementation by stating that there are no data that show a mixed oxidation state solubility

[14] referenced as Rai et al. (2007) by Franco (2015b)
[15] referenced as Rai et al. (2009) by Franco (2015b)

model (Patterson 2016b). However, as explained in Section 5.3.2.6 and illustrated in Figure 5-3, plutonium concentrations resulting from reductive dissolution will vary between the limits of Pu(IV) solid solubility [reaction (27)] and Pu(III) solid solubility [(reaction (28)]. Consequently, no new solubility model is required.

DOE also objects that there "is no high-ionic strength capability or accepted approach to support an Eh driven (i.e., calculational) approach to defining the redox conditions in the WIPP using the Pitzer approach" (Patterson 2016b). However, EPA has not recommended such an approach, and instead recommends an independent technical review to assess the best possible changes to the model.

The data reviewed this section:

- Demonstrate a high likelihood that plutonium concentrations in WIPP repository brines will be controlled by the solubility of Pu(III) solids [reaction (28)] or reductive dissolution of Pu(IV) solids [reaction (29)].
- Underestimate plutonium solubilities because more oxidizing realizations will be underestimated.
- Underestimate plutonium concentrations in a DBR because the underestimation of plutonium solubilities in the more oxidizing realizations is significant (Table 5-1).
- Show the need for an independent technical review to resolve this this issue.

5.3.3 Incorrect Citations

DOE (2014b, Appendix SOTERM-2014, Section 3.6.1.1) stated that "Clark and Tait (Clark and Tait 1996) and Felmy et al. (Felmy et al. 1996) have experimentally observed the reduction of Pu(VI) carbonates by either Fe^0 or Fe^{2+} to Pu(IV)." EPA requested that DOE correct these references, noting that Felmy et al. (1996) was a study of Th(IV) hydrous oxide solubility, whereas Clark and Tait (1996) found that plutonium(VI) chloride complexes were reduced to plutonium(V) by Fe^0 or Fe^{2+} (Edwards 2015c, Comment 3-C-8). DOE responded that the correct references are Reed et al. (2006) and Reed et al. (2010), and included the correction to Appendix SOTERM-14 in their list of errata (Shrader 2015).

5.4 ACTINIDE OXIDATION STATES SUMMARY AND CONCLUSIONS

The actinide oxidation states have remained the same for all WIPP PAs. EPA has reviewed the available data related to actinides oxidation states in WIPP brines:

- Am(III), Cm(III), and Th(IV) are assumed to be the only redox states for these actinides. Uranium is assumed present in the +IV and +VI states while neptunium is assumed present in the +IV and +V states. Plutonium is assumed present in the +III and +IV states.
- Half of PA realizations assume the more reduced state (Pu(III), Np(IV), and U(IV)) while the other half assume the more oxidized state (e.g., Pu(IV), Np(V), and U(VI). This is important as Pu(III) is more soluble than Pu(IV).

- Iron metal present in the waste containers and waste will quickly create reducing conditions allowing for the +III and +IV plutonium oxidation states to persist instead of the +V and +VI states.
- Data that has become available since the CRA-2009 indicates that under WIPP conditions, Pu(III) will exist in equilibrium with the Pu(III) solid $Pu(OH)_3$ or with the Pu(IV) solid PuO_2 (reductive dissolution).
- Organic ligands, humics, and microbes also have the potential to enhance reductive dissolution and increase the likelihood of Pu(III) existing in the repository.
- In order to further resolve this issue, it would be beneficial to have an independent technical review of the likely Pu oxidation states at the WIPP with the recommendations from this review implemented as soon as possible.

6.0 DISSOLVED ACTINIDE SOURCE TERM

Actinides in the WIPP waste inventory may dissolve in brine that flows into the repository from the DRZ in the Salado Formation, or in brine that flows up a borehole that intersects both the repository and a pressurized brine region in the underlying Castile Formation. The actinide solubilities calculated for PA include americium, curium, neptunium, plutonium, thorium and uranium. Actinide solubilities are calculated using thermodynamic modeling that depends on a number of assumptions related to chemical conditions in the repository and to the chemical behavior of the actinides in solution. Consequently, both the Chemical Conditions and Dissolved Actinide Source Term conceptual models are important for calculating dissolved actinide concentrations used in PA. These conceptual models are described in detail by SC&A (2008b, Appendix A).

The Chemical Conditions conceptual model includes assumptions related to the mineralogy of the Salado Formation in contact with WIPP brines, the compositions of the Salado and Castile brines that may enter the repository and contact waste, organic ligand concentrations and the reactions that may control important chemical parameters, such as pH, redox and CO_2 fugacities. The Chemical Conditions conceptual model also includes assumptions regarding the redox states of actinides and metals in solution. The Dissolved Actinide Source Term conceptual model includes a number of assumptions, including assumptions about the oxidation states of the actinides, equilibrium of the brine with respect to precipitation-dissolution reactions, the existence of reducing conditions in the repository, the important inorganic and organic constituents for determining actinide speciation in brines and use of the Pitzer activity coefficient model.

The FMT code was used to calculate actinide solubilities for the CCA PAVT, PABC04 and PABC09. FMT was replaced by EQ3/6 for the CRA-2014 PA. The FMT and EQ3/6 calculations of aqueous concentrations in WIPP brines are based on calculations of aqueous speciation and solubility equilibria performed using the Pitzer activity coefficient model. Because thermodynamic equilibrium is not assumed for redox reactions among the actinides as part of the Chemical Conditions conceptual model (SCA 2008), the actinide solubility calculations do not include reactions representative of redox processes and the oxidation state of each actinide is instead assumed for the calculations (Section 5.0).

6.1 CCA AND PAVT DISSOLVED ACTINIDE SOURCE TERM

The Dissolved Source Term and Chemical Conditions conceptual model assumptions were peer reviewed and approved for the CCA PA (Wilson et al. 1996a, 1996b, 1997a, 1997b). DOE performed FMT modeling calculations to determine the solubilities of Am(III), Th(IV) and Np(V) in end-member Salado (Brine A) and Castile (ERDA-6) brine. DOE assumed that actinide solubilities in brine mixtures would be adequately represented by calculations with the end-member brines. For these solubility calculations, DOE assumes that the brines would be in equilibrium with the Salado minerals anhydrite, halite and magnesite, as well as brucite and magnesite that would form from hydration and carbonation, respectively, of the MgO backfill. The minerals glauberite [$Na_2Ca(SO_4)_2$] and korshunovskite [$Mg_2Cl(OH)_3 \cdot 4H_2O$(cr) or phase 3] were allowed to precipitate from the brines.

6.1.1 FMT Code and Database

The CCA actinide solubility calculations were performed with FMT Version 2.0. EPA (1998d) identified the database used for the CCA calculations as FMT_HMW_345_960501FANG.CHEMDAT, but noted that it was not clear which database had been used. Based on the date indicated in the file name, EPA (1998d) believed the database was representative of the database used for the CCA PA actinide solubility calculations. Novak and Moore (1996), however, stated that HMW_3456_960318.CHEMDAT and HMW_3456_960325.CHEMDAT were used for the FMT calculations, and that the data in these two files were identical.

6.1.2 Oxidation-State Analogy

The oxidation-state analogy was used to extend the calculated Am(III), Th(IV) and Np(V) solubilities to the other actinides and oxidation states important to WIPP PA. The oxidation-state analogy, part of the Dissolved Actinide Source Term conceptual model, is the assumption that all actinides in the same oxidation state will form the same aqueous species and isostructural compounds. Consequently, Pu(III) and Cm(III) solubilities in WIPP brines are assumed to be equal to calculated Am(III) solubilities, and U(IV), Pu(IV) and Np(IV) solubilities are assumed to be equal to calculated Th(IV) solubilities. Calculated Np(V) solubilities are used only for neptunium, because it is the only actinide predicted to be present in WIPP brines in the +V oxidation state.

6.1.3 Uranium(VI) Solubility

Because DOE could not develop an adequate thermodynamic model for U(VI), fixed concentrations of 8.7×10^{-6} M (Salado brine) and 8.8×10^{-6} M (Castile brine) were used for PA. EPA (1998d) reviewed DOE's predictions of U(VI) solubilities, including the information in the CCA and supporting documents (Hobart and Moore 1996, Novak and Moore 1996), and additional information that became available after the CCA. EPA (1998d) noted two assumptions that DOE relied on in selecting this U(VI) concentration for PA. One of DOE's assumptions was that carbonate would be completely absent from repository brines, when in fact the brucite-hydromagnesite reaction will control carbonate concentrations at relatively low but non-zero levels. Another assumption made by DOE was that a model for U(VI) could not be developed because of uncertainties regarding U(VI) hydrolysis species; EPA (1998d) noted that the dominant species in the pH range relevant to the WIPP repository are likely to be carbonate complexes, such as $UO_2CO_3^0$, $UO_2(CO_3)_2^{2-}$ and $UO_2(CO_3)_3^{4-}$. Therefore, precise knowledge of the stabilities of the hydrolysis species may not be necessary to model U(VI) solubility under the expected repository conditions, because only a small fraction of the total dissolved U(VI) exists as hydrolysis species. However, EPA (1998d) accepted the use of a single U(VI) concentration in PA because it was consistent with the available data presented in Reed and Wygmans (1997) and Hobart and Moore (1996) and uncertainties associated with this estimated concentration were believed to be adequately accounted for by the sampled uncertainty distribution.

6.1.4 CCA PA and PAVT Actinide Solubility Uncertainties

The actinide solubilities used in WIPP PA are constants; uncertainties in these values are accounted for by sampling a cumulative distribution function (CDF) representing uncertainty and multiplying the solubilities by the antilog of the sampled value to determine the actinide concentrations used in PA for each realization. EPA reviewed the determination of the actinide solubility uncertainty distribution used in the CCA PA and PAVT (1998d). To obtain this distribution, DOE compared experimentally measured solubility data used to develop the solubility models in FMT to the concentrations predicted by curve-fitting with the code NONLIN (Babb 1996). DOE also compared solubilities reported in the literature with concentrations predicted using FMT for the conditions of the experiments. Difference values between the predicted (S_p) and measured (S_m) solubilities were calculated using the equation:

$$D = \log_{10} S_m - \log_{10} S_p \quad \textbf{(31)}$$

Using this equation, the difference value is negative if the FMT-calculated solubility is greater than the measured solubility, positive if the FMT-calculated solubility is less than the measured solubility and zero if the FMT calculated solubility and the measured solubility are equal.

The population of difference values from these comparisons was accumulated and used to generate a cumulative distribution. DOE excluded data for the +IV and +VI actinides from the evaluation, because they believed these datasets to be inconsistent or technically deficient. The remaining data consisted of +III actinide solubility measurements (139 values) and +V actinide solubility measurements (11 values). These data were combined to generate a single distribution, which ranged from -2.0 to 1.4, with a median of -0.09 (DOE 2004, Appendix PA, Attachment SOTERM). This distribution was used to represent the uncertainties associated with the solubilities for all four actinide oxidation states.

6.1.5 Effects of Organic Ligands on Actinide Solubilities

Acetate, citrate, EDTA and oxalate were identified as organic ligands that could potentially affect actinide solubilities, because these ligands are water soluble and present in significant quantities in the WIPP inventory (DOE 1996). DOE (1996) estimated the possible concentrations of these ligands using the inventory amounts and a brine volume of 29,841 m^3, which was the smallest quantity of brine required to be in the repository that will support transport away from the repository (Larson 1996). The organic ligand concentrations DOE (1996) calculated are listed in Table 6-1. DOE (1996, Appendix SOTERM, Section 5) determined that actinide solubilities would not be significantly affected by the presence of organic ligands because other constituents, including transition metals in the waste and magnesium from the MgO backfill, would compete with the actinides for binding sites on the organic ligands.

Table 6-1. Organic Ligand Concentrations Calculated for the CCA PAVT, PABC04, PABC09 and CRA-2014 PA Using Brine Volumes and Organic Ligand Inventories That Were Updated for Each PA

	Brine Volume (m^3)	Acetate[a]	Citrate[b]	EDTA[c]	Oxalate[d]
CCA PA [m] (DOE 1996)	29,841	1.1×10^{-3}	7.4×10^{-3}	4.2×10^{-6}	4.7×10^{-4}
PABC04 [M] (Brush 2005)	10,011	1.06×10^{-2}	8.06×10^{-4}	8.14×10^{-6}	4.55×10^{-2}
PABC09 [M] (Brush and Xiong 2009)	17,400	1.94×10^{-2}	2.38×10^{-3}	6.47×10^{-5}	1.73×10^{-3}
CRA-2014 PA [M] (Brush and Domski 2013a)	17,400	2.30×10^{-2}	2.33×10^{-3}	7.40×10^{-5}	1.18×10^{-2}
	34,800	1.15×10^{-2}	1.16×10^{-3}	3.70×10^{-5}	5.90×10^{-3}
	52,200	7.68×10^{-3}	7.76×10^{-4}	2.47×10^{-5}	3.93×10^{-3}
	69,600	5.76×10^{-3}	5.82×10^{-4}	1.85×10^{-5}	2.95×10^{-3}
	87,000	4.61×10^{-3}	4.65×10^{-4}	1.48×10^{-5}	2.36×10^{-3}

a – Sum of acetic acid (CH_3COOH) and sodium acetate ($NaCH_3COO$)
b – Sum of citric acid ($C_6H_8O_7$) and sodium citrate ($NaC_6H_7O_7$)
c – Assumed monosodium EDTA
d – Sum of oxalic acid ($H_2C_2O_4$) and sodium oxalate ($NaHC_2O_4$)

6.1.6 Actinide Solubility Calculations for the CCA PAVT

After review of the conceptual model and CCA PA results, EPA (1997a, 1997b, 1998a, 1998d) directed DOE to use the assumption that reaction of brucite to form metastable hydromagnesite would control CO_2 fugacities in the WIPP repository, rather than the brucite-magnesite reaction. DOE also incorporated more realistic thermodynamic data for Th(IV) and Np(V) in the FMT database, based on information that had become available since the CCA PA (EPA 1998d). The results of these actinide solubility calculations, carried out for the CCA PAVT, are summarized in Table 6-2.

Table 6-2. Actinide Solubility Calculations for the CCA PAVT, PABC04, PABC09 and CRA-2014 PA (1× brine volume)

Property or Actinide Oxidation State	CCA PAVT No Organic Ligands		PABC04 With Organic Ligands		PABC09 With Organic Ligands		CRA-2014 PA With Organic Ligands	
Brine	Salado (Brine A)	Castile (ERDA-6)	Salado (GWB)	Castile (ERDA-6)	Salado (GWB)	Castile (ERDA-6)	Salado (GWB)	Castile (ERDA-6)
pH	8.69	9.24	8.69	8.94	8.69	8.98	8.82	8.99
pcH	--	--	9.39	9.64	9.40	9.68	9.54	9.69
Log CO_2 fugacity	-5.50	-5.50	-5.50	-5.50	-5.50	-5.50	-5.50	-5.50
Total Carbon (M)	--	--	2.16×10^{-5}	5.18×10^{-5}	3.50×10^{-4}	4.48×10^{-4}	3.79×10^{-4}	4.55×10^{-4}
III (M)	1.2×10^{-7}	1.3×10^{-8}	3.87×10^{-7}	2.88×10^{-7}	1.66×10^{-6}	1.51×10^{-6}	2.59×10^{-6}	1.48×10^{-6}
IV (M)	1.3×10^{-8}	4.1×10^{-8}	5.64×10^{-8}	6.79×10^{-8}	5.63×10^{-8}	6.98×10^{-8}	6.05×10^{-8}	7.02×10^{-8}
V (M)	2.4×10^{-7}	4.8×10^{-7}	3.55×10^{-7}	8.24×10^{-7}	3.90×10^{-7}	8.75×10^{-7}	2.77×10^{-7}	8.76×10^{-7}
VI (M)[a]	8.7×10^{-6}	8.8×10^{-6}	10^{-3}	10^{-3}	10^{-3}	10^{-3}	10^{-3}	10^{-3}
Equilibrium Nonradionuclide Solid Phases	Anhydrite, halite, brucite, hydromagnesite, korshunovskite	Anhydrite, halite, brucite, glauberite, hydromagnesite	Anhydrite, halite, brucite, hydromagnesite, whewellite, korshunovskite	Anhydrite, halite, brucite, hydromagnesite, whewellite, glauberite	Anhydrite, halite, brucite, hydromagnesite, whewellite, korshunovskite	Anhydrite, halite, brucite, hydromagnesite, whewellite, glauberite	Anhydrite, halite, brucite, hydromagnesite, whewellite, phase 5	Anhydrite, halite, brucite, hydromagnesite, whewellite, glauberite
Equilibrium Radionuclide Solid Phases	$AmOHCO_3$(cr), ThO_2(am), $KNpO_2CO_3$(s)		$Am(OH)_3$(s), ThO_2(am), $KNpO_2CO_3$(s)		$Am(OH)_3$(s), ThO_2(am), $KNpO_2CO_3$(s)		$Am(OH)_3$(s), ThO_2(am), $KNpO_2CO_3$(s)	
Database	FMT_970407.CHEMDAT		FMT_050405.CHEMDAT		FMT_050405.CHEMDAT		DATA0.FM1 (DATA0.FMT.R2)	
Output filename	--	--	FMT_CRA1BC_GWB_HMAG_ORGS_007	FMT_CRA1BC_ER6_HMAG_ORGS_007	FMT_PABC09_GWB_HMAG_ORGS_005.OUT	FMT_PABC09_E6_HMAG_ORGS_013	gwb_1x.6o	erda_1xb.6o

a – DOE did not develop a solubility model for the +VI actinides. Therefore, for all PAs, a fixed concentration was assumed for U(VI), which is the only +VI actinide predicted to be present in the WIPP repository in significant concentrations.

6.2 CRA-2004 PA DISSOLVED ACTINIDE SOURCE TERM

DOE revised the assumptions used to calculate actinide solubilities for the CRA-2004 PA (DOE 2004, Appendix PA, Attachment SOTERM). DOE's revisions to the conceptual model for these calculations included a change in the Salado brine composition from Brine A to GWB, and the assumption that the mineral assemblage that buffers CO_2 fugacity in the absence of significant microbial activity would be brucite-calcite instead of brucite-hydromagnesite. DOE (2004, Appendix PA, Attachment SOTERM) also updated the FMT database and incorporated calculations of the effects of organic ligands (acetate, citrate, EDTA and oxalate), using newly developed data for actinide-organic ligand complex formation and the formation of magnesium-organic ligand complexes. Consequently, the potential effects of organic ligands on actinide solubilities were included in the calculations, instead of being assumed to be negligible.

6.2.1 FMT Code and Database

FMT Version 2.4 was used for the CRA-2004 PA actinide solubility calculations; the database was FMT_021120.CHEMDAT (Brush and Xiong 2003a; DOE 2004, Appendix PA, Attachment SOTERM-3.3). Giambalvo (2002a, 2002b, 2002c, 2002d, 2002e, 2003) documented changes to the FMT database between the CCA PAVT and CRA-2004 PA and EPA (2006c) reviewed these changes. Changes to the database since the CCA PAVT included revisions to the thermodynamic data for Am(III) aqueous species and americium solids, and minor revisions to the thermodynamic data for some Th(IV) aqueous species and Pitzer interaction parameters. A more significant change was incorporation of thermodynamic data for the protonation of organic ligands and complexation of organic ligands with actinides and with magnesium, based on data from Choppin et al. (2001).

6.2.2 Salado Brine Formulation

For the CCA PAVT actinide solubility calculations, the brine formulation referred to as Brine A was used to simulate intergranular Salado brines. However, the GWB Salado brine formulation was used in the CRA-2004 PA actinide solubility calculations. Brush and Xiong (2003a) discussed the use of both GWB and Brine A in the CRA-2004 PA to simulate intergranular Salado brines, and provided the compositions of these brines. Snider (2003b) provided a detailed discussion of GWB brine and a comparison of this brine to Brine A.

6.2.3 Carbon Dioxide Buffering in the Absence of Significant Microbial Activity

DOE (2004, Appendix PA, Attachment SOTERM, Section 2.2.2 and Appendix BARRIERS, Section 2.3.2.4) addressed the different reactions likely to buffer CO_2 fugacity. DOE stated that calcite is stable under WIPP conditions, and has formed readily at low temperatures in GWB and ERDA-6 brines because of the rapid carbonation of lime or portlandite from cements in waste containers. In PA realizations with significant microbial production of CO_2, DOE stated that the amount of calcium ion available is likely to be overwhelmed by the amount of CO_2, so the brucite-calcite reaction:

$$Mg(OH)_2 + Ca^{2+} + CO_2 \leftrightarrow CaCO_3 + Mg^{2+} + H_2O \quad \textbf{(32)}$$

was suppressed to allow the brucite-hydromagnesite reaction to control CO_2 fugacities. However, in the absence of significant microbial CO_2 production, DOE stated that sufficient calcium ions would be available to allow control of CO_2 fugacities by the brucite-calcite reaction.

EPA (2006c) reviewed the documentation and FMT modeling calculations DOE provided related to the assumption that brucite-calcite would control CO_2 fugacities in PA realizations without significant microbial activity. EPA (2006c) concluded that DOE had not provided adequate information to support the assumption that the brucite-calcite reaction would control the CO_2 fugacity in the absence of significant microbial consumption of CPR. EPA (2006c) noted that because the microbial degradation probability would be increased for subsequent PA calculations, essentially including some microbial degradation in all realizations (Section 3.3.3.1), the assumption that brucite-calcite will buffer CO_2 fugacities in some realizations would not be included in the PABC04 calculations, so further consideration of this assumption was no longer warranted.

6.2.4 Uranium(VI) Solubility

For the CRA-2004 PA, DOE used the same estimated uranium (VI) concentration as for the CCA PA and PAVT. EPA (2006c) noted that DOE had not conducted a review of new data regarding the solubility of the +VI actinides since the CCA, and reviewed U(VI) solubility data in NaCl brines to determine whether the assumed U(VI) concentration used in the CRA-2004 PA was still justified. EPA (2006c) reviewed solubility data and determined that the presence of free carbonate ion at the concentration calculated in GWB brine for the CRA-2004 PA (2.16×10^{-5} M, run 18) would increase U(VI) concentrations by a factor of about 250, relative to the concentration without carbonate. Table 6-3 summarizes this review. EPA (2006c) also noted that Díaz Arocas and Grambow (1998) reported a solubility of 3×10^{-5} M for sodium uranate in 5 M NaCl brine at pH 8.9 in the absence of carbonate. This concentration is probably a reasonable upper limit for the solubility of an alkali or alkaline-earth uranate solid in NaCl brines in the absence of carbonate. This upper limit was increased by approximately two orders of magnitude to be consistent with the carbonate concentrations expected in the WIPP repository, based on the speciation calculations mentioned above carried out with low-ionic-strength data. Thus, EPA (2006c) determined that a reasonable upper limit for U(VI) solubility in WIPP brines would be approximately 10^{-3} M. This concentration is approximately two orders of magnitude higher than the mid-range value used in the CCA PA, PAVT, and CRA-2004 PA, and exceeds the upper limit of the solubility uncertainty range used in these assessments. EPA directed DOE to use the revised, higher U(VI) of 10^{-3} M for the PABC04 (Cotsworth 2005).

Table 6-3. High Ionic Strength Uranium Solubility Data Evaluated by EPA (2006c)

U(VI) concentration	pH	Carbon Dioxide	Solution	Solid	Reference
3×10^{-5} M	8.9	Absent	5 molal NaCl	$Na_{0.68}UO_{3.34}\cdot 2.15H_2O$(s)	Díaz Arocas and Grambow (1998)
9×10^{-5} M	7.6	Absent	5 molal NaCl	$Na_{0.45}UO_{3.23}\cdot 4.5H_2O$(s)	Díaz Arocas and Grambow (1998)
~ 5×10^{-3} m	not specified[a]	10^{-5} $[CO_3^{2-}]$	5 M NaCl	UO_2CO_3(s)	Lin et al. (1998)

U(VI) concentration	pH	Carbon Dioxide	Solution	Solid	Reference
4.5×10^{-7} and 2×10^{-6} M[b]	7	10^{-4} M Carbonate	G-Seep brine	Not determined	Reed and Wygmans (1997)
5.0×10^{-7} and 2×10^{-6} M[b]	7	Absent	G-Seep brine	Not determined	Reed and Wygmans (1997)
1.1×10^{-8} M	8	10^{-4} M Carbonate	ERDA-6 brine	Not determined	Reed and Wygmans (1997)
5.5×10^{-7} M	10	Absent	ERDA-6 brine	Not determined	Reed and Wygmans (1997)
$> 1 \times 10^{-4}$ M	10	10^{-4} M Carbonate	ERDA-6 brine	None formed	Reed and Wygmans (1997)
2.8×10^{-6} molal	9.8	Absent	5.2 molal WIPP brine	UO_2OH_2[c]	Palmer (1996)[d]
1.82×10^{-3} M	8.4 (pcH)	$10^{-3.5}$ atm	Brine A	Schoepite (oversaturation)	Yamazaki et al. (1992)
1.81×10^{-3} M	8.4 (pcH)	$10^{-3.5}$ atm	Brine A	Schoepite (oversaturation)	Yamazaki et al. (1992)
1.4×10^{-3} M	8.4 (pcH)	$10^{-3.5}$ atm	Brine A	Schoepite (undersaturation)	Yamazaki et al. (1992)
1.8×10^{-3} M	8.4 (pcH)	$10^{-3.5}$ atm	Brine A	Schoepite (undersaturation)	Yamazaki et al. (1992)
3.8×10^{-7} M	10.4 (pcH)	Low	Brine A	$K_2U_2O_7$ (oversaturation)	Yamazaki et al. (1992)
3.1×10^{-7} M	10.4 (pcH)	Low	Brine A	$K_2U_2O_7$ (oversaturation)	Yamazaki et al. (1992)
1.8×10^{-7} M	10.4 (pcH)	Low	Brine A	$K_2U_2O_7$ (undersaturation)	Yamazaki et al. (1992)
1.7×10^{-7} M	10.4 (pcH)	Low	Brine A	$K_2U_2O_7$ (undersaturation)	Yamazaki et al. (1992)

a – Probably less than 7

b – The lower concentration was reported on page 4 of the text, but a higher concentration was illustrated in Figure 1A

c – Solid should probably have been identified as $UO_2(OH)_2$(s), U(VI) concentration as cited by Hobart and Moore (1996)

d – Hobart and Moore (1996) table cites Palmer et al. (1996), but reference list cites Palmer (1996) personal communication

6.2.5 Actinide Solubility Uncertainties Used in PA

The uncertainty distribution determined for the CCA PA and PAVT was used to represent the actinide solubility uncertainties for the CRA-2004 PA (DOE 2004, Appendix PA, Attachment SOTERM, Section 3.6). Because the available solubility data and the FMT database had changed since the CCA PA and PAVT, EPA requested that DOE re-evaluate the uncertainties associated with the actinide solubilities, using the currently available actinide solubility data (Cotsworth 2004a, Comment C-23-16).

DOE re-evaluated the uncertainties associated with actinide solubilities (Triay 2005, Xiong et al. 2004). The database used for this evaluation was FMT_040628.CHEMDAT. This database was modified from the version used for the CRA-2004 PA (FMT_021120.CHEMDAT) by correcting the molecular weight of oxalate and adding solid calcium oxalate (whewellite, $CaC_2O_4 \bullet H_2O$) to the database (Xiong 2004). Because none of the calculations used in the uncertainty evaluation

involved oxalate or other ligands, using either database would have yielded the same results (Xiong et al. 2004).

Separate evaluations of the solubility uncertainty distribution were carried out for the +III, +IV and +V actinide oxidation states. Solubility data used to develop the FMT database as well as literature data were evaluated. The +III evaluation was based on 243 solubilities, the +IV evaluation included 159 solubilities, and the +V evaluation included 136 solubilities (Xiong et al. 2004).

For the +III actinides, the difference values ranged from -2.85 to +2.85, with a median of slightly less than 0 (Xiong et al. 2004). The difference values for the +IV actinides ranged from -2.85[16] to +3.3, with a median value between 0.6 and 0.75 (Xiong et al. 2004). DOE investigated the likely cause of the positive median difference value and determined a revision was necessary to the μ^0/RT value for $Th(OH)_4(aq)$ in the FMT database. This revision to the aqueous speciation data (database FMT_050405.CHEMDAT) was found by Xiong et al. (2005) to result in a significant improvement in the ability of the +IV actinide solubility model to predict the available solubility data at high ionic strength.

The difference values for the +V actinide solubilities ranged from -1.8 to +1.95, with a median value slightly less than 0 (Xiong et al. 2004). Xiong et al. (2005) stated that the uncertainty distribution for the +V actinides would not be used for PA, because neptunium is the only actinide expected to be present in the +V oxidation state in the equilibrium WIPP repository (see Section 5.0). Neptunium solubility is not considered in future PA calculations, because the neptunium inventory is insufficient to affect the long-term performance of the repository, regardless of its solubility (Xiong et al. 2005, EPA 2006d).

EPA (2006c) determined that the revised uncertainty ranges were adequate and these uncertainty distributions for the +III, +IV and +V actinides were used for the PABC04 (see Section 6.3.5).

6.2.6 Temperature Effects on Actinide Solubilities

EPA (2006c) addressed the potential effects of temperature on actinide solubilities in the WIPP repository. Temperature effects on actinide solubilities were assumed negligible for the CRA-2004 PA, based on calculations performed at the time of the CCA (DOE 2004, Appendix PA, Attachment SOTERM, Section 2.2.4). DOE has not subsequently revised these calculations to account for the potential effects of inventory changes since the CCA and for the effects of non-uniform waste loading, e.g., the high proportion of pipe overpack waste in Panel 1. Although DOE has not quantitatively assessed the possible effects of these changes, EPA (2006c) concluded that it is reasonable to assume that repository temperature will not be significantly affected by these changes, and that it remains reasonable to assume that the effects of temperature on actinide solubilities will be negligible. However, in the event that heat-source plutonium or wastes containing significant heat-generating fission products are placed in WIPP

[16] Figure 3 and Table 2 of Xiong et al. (2004) indicate that one value of -4.95 was observed; however, the text noted that this value was in error and should have been 0.65.

in excess of the amounts assumed during the CCA, the CCA calculations that were used to estimate temperature increases may require re-evaluation (EPA 2006c).

6.2.7 Effects of Organic Ligands on Actinide Solubilities

DOE used inventory estimates available at the time of the CCA to identify acetate, citrate, EDTA and oxalate as organic ligands that could affect actinide solubilities (DOE 2004, Appendix PA, Attachment SOTERM, Section 5.0). EPA (2006c) noted that DOE (2004) did not address whether new inventory information, such as new waste streams included since the CCA, might affect identification of complexing agents that should be addressed in the calculations. Reported inventories of the four ligands evaluated for the CRA-2004 changed between the CCA and the CRA-2004, including increased concentrations of acetate, changes in oxalate and citrate inventories that appear to have been caused by transposing the data during the CCA, and a decrease in the estimated inventory of EDTA (DOE 2004, Appendix PA, Attachment SOTERM, Table SOTERM-4).

DOE (2004, Appendix PA, Attachment SOTERM, Sections 3.5 and 5.0) included the effects of acetate, citrate, EDTA and oxalate on the calculated solubilities of the +III, +IV and +V actinides used in the CRA-2004 PA. Brush and Xiong (2003c) calculated the organic ligand concentrations used in the actinide solubility calculations by dividing the total reported ligand inventory by 29,841 m^3 of brine, which was the smallest volume of brine reported to be required in the repository for transport away from the repository (Larson 1996, DOE 1996). DOE (2004, Appendix PA, SOTERM, Section 5.0) stated that organic ligands would not significantly affect the +III and +IV actinide solubilities. EPA (2006c) evaluated the likely effects of organic ligands on actinide solubilities.

EPA (2006c) concluded in its CRA-2004 review that the concentrations of the +III and +V actinides could be affected by the concentrations of EDTA or oxalate and acetate in the repository, respectively. The available evidence showed that the +IV actinides were relatively insensitive to organic ligands over the range of evaluated organic ligand concentrations, and that microbially produced lactate is unlikely to significantly affect actinide solubilities at the concentrations expected, based on the microbial degradation experiments carried out for the WIPP program. The effects of EDTA concentrations on the modeled +III actinide concentrations indicate that the assumed concentrations, and hence the inventory, of organic ligands are potentially important for PA. However, the potential effects of oxalate and acetate on the solubility of the +V actinides are less important for PA, because neptunium is the only actinide assumed to be present in the equilibrium WIPP repository in the +V oxidation state, and the neptunium inventory is too low to significantly contribute to radionuclide releases (EPA 2006d). Evaluation of the available data regarding the complexation of U(VI) under anticipated WIPP repository conditions indicated that organic ligands are unlikely to significantly affect U(VI) solubilities in WIPP brines, because of the formation of relatively stable U(VI)-carbonate species.

6.3 PABC04 DISSOLVED ACTINIDE SOURCE TERM

At the direction of EPA (Cotsworth 2005), DOE incorporated a number of changes in the prediction of actinide solubilities for the PABC04 relative to the CRA-2004 PA. These changes

included use of the updated FMT thermodynamic database, revised estimated concentrations of organic ligands, revised actinide solubility uncertainties and a revised U(VI) concentration.

6.3.1 FMT Code and Database

FMT Version 2.4 was used for both the CRA-2004 PA and the PABC04 actinide solubility calculations (Brush and Xiong 2003b; Brush and Xiong 2005a). The FMT database used in the CRA-2004 PA actinide solubility calculations (FMT_021120.CHEMDAT) was revised several times, ultimately resulting in the version used in the PABC04 actinide solubility calculations (FMT_050405.CHEMDAT). The database changes since the CRA-2004 PA actinide solubility calculations included a revision of the thermodynamic data for one thorium aqueous species (Section 6.2.5), correction of the molecular weight of oxalate, and addition of a calcium-oxalate solid phase (whewellite).

6.3.2 Carbon Dioxide Buffering Reactions

The MgO hydration and carbonation phases assumed to be present in solubility calculations with Salado (GWB) brine were brucite, korshunovskite and hydromagnesite. For actinide solubility calculations with Castile (ERDA-6) brine, brucite and hydromagnesite were assumed present. These MgO hydration and carbonation phases were the same as those assumed to control pH and CO_2 fugacity for the CRA-2004 PA calculations that included significant microbial activity (DOE 2004, EPA 2006c). EPA (2006c) reviewed the results of DOE's MgO hydration and carbonation experiments and agreed that these phases are the most likely to control pH and CO_2 fugacities in the WIPP repository brines during the 10,000-year regulatory period. For CRA-2004 PA realizations without significant microbial activity, DOE had assumed that the brucite-calcite reaction would control CO_2 fugacity (DOE 2004, Appendix PA, Attachment SOTERM). EPA (2006c) determined that DOE had not adequately supported the assumption that the brucite-calcite reaction would control CO_2 fugacities in the absence of significant microbial activity. However, because the microbial degradation probability was changed for the PABC04 so all realizations included microbial activity (Section 3.3.3.1), it was appropriate to use the brucite-hydromagnesite reaction to buffer CO_2 fugacity in all actinide solubility calculations for the PABC04 (Brush 2005, Brush and Xiong 2005a).

6.3.3 Uranium(VI) Solubility

EPA (2006c) reviewed the available literature to determine whether the assumed +VI actinide solubility should be revised (Section 6.2.4). Based on the results of this review, EPA specified the use of a fixed upper-limit value of 10^{-3} M for the U(VI) concentration in the PABC04 (Cotsworth 2005).

6.3.4 Actinide Solubility Uncertainties Used in PA

Xiong et al. (2004, 2005) developed separate uncertainty distributions for the +III, +IV and +V actinide solubilities (Table 6-4). EPA (2006b) concluded that the overall approach used in the PABC04 for estimating the uncertainties associated with the actinide solubilities was a substantial improvement over the approach used for the CCA PA and PAVT. The use of a larger dataset and the determination of separate uncertainty distributions for the +III, +IV and +V

actinide solubilities for the PABC04 were more likely to provide reasonable estimates of the uncertainties than the approach taken for the CCA PA, PAVT and CRA-2004 PA. However, the approach of Xiong et al. (2004, 2005) for selecting the data for the evaluation may not have included all available experimental data. In addition, EPA (2006b) noted that a number of inconsistencies appear to have occurred because of the inclusion of data used to develop the FMT database in some cases and its exclusion in others. Comparison of the separate PABC04 uncertainty distributions developed for the three modeled actinide oxidation states with the single uncertainty distribution used in the CCA PA, PAVT, and CRA-2004 PA showed that the revised ranges were generally wider, particularly on the upper end of the distributions. Therefore, EPA (2006b) concluded that the revised actinide solubility uncertainty distributions would likely result in the more frequent use of higher actinide solubilities in PA. EPA (2006b) also observed that the larger amount of experimental data used to develop the distributions, the development of uncertainty distributions for each of the modeled actinide oxidation states and the large ranges developed for the uncertainties indicate that these uncertainty distributions were reasonable and acceptable for use in the PABC04.

Table 6-4. Cumulative Density Function Ranges Established by the PABC04 Actinide Solubility Uncertainty Analysis

Actinide Oxidation State	Cumulative Density Function Range[a]
III	-3.00 to 2.85
IV	-1.80 to 2.40
V	-1.95 to 1.95

a – At the lower end of the range, there is a zero probability that a difference value is less than or equal to this number; at the upper end of the range, the probability is equal to one because all difference values were less than or equal to this number (Brush et al. 2005).

Source: Xiong et al. 2005

6.3.5 Organic Ligand Concentrations

The concentrations of organic ligands were re-evaluated for the PABC04 actinide solubility calculations based on a revised estimate of the minimum amount of brine that could lead to a release from the repository. For the PABC04, Stein (2005) predicted that the minimum amount of brine that could lead to a brine release from the WIPP repository was 10,011 m^3. EPA (2006b) noted that this volume was calculated assuming the brine release occurred from the entire repository. EPA (2006b) ultimately concluded that the use of the minimum amount of brine that could be released from the entire repository, and assuming that all ligands are dissolved in this amount of brine, is likely to be a reasonable approximation for calculating ligand concentrations and the resulting actinide solubilities.

The masses of organic ligands used to calculate concentrations for the CRA-2004 PA were found to be overestimates of the amounts likely to be in the repository (Brush and Xiong 2003d). However, because these higher concentrations would overestimate releases from the repository, the actinide solubilities calculated using these higher organic ligand masses were used in the CRA-2004 PA (DOE 2004). For the PABC04, the corrected masses of organic ligands reported by Crawford and Leigh (2003) were used to calculate ligand concentrations (Brush and Xiong 2005b). Leigh (2005) found that none of the revisions to the WIPP inventory for the PABC04 had resulted in changes to the total masses of organic ligands expected in the WIPP inventory;

therefore, Leigh (2005) recommended the use of the ligand inventories listed in Leigh (2003), which are the same as those listed in Crawford and Leigh (2003). These masses were converted to moles and divided by 10,011 m^3 to yield the organic ligand concentrations used in the actinide solubility calculations. The resulting organic ligand concentrations used for the PABC04 solubility calculations are compared to the PAVT organic ligands concentrations in Table 6-1.

6.3.6 Results of the PABC04 Actinide Solubility Calculations

Changes and improvements incorporated into the calculation of actinide solubilities for the PABC04 implemented after the CCA PAVT included:

- Incorporation of organic ligand complexation data into the FMT database, so the effects of organic ligands on +III, +IV, and +V actinide solubilities could be calculated directly
- Refinement of the FMT database using new +III, +IV and +V actinide data
- Use of GWB instead of Brine A as the Salado Brine formulation for actinide solubility calculations
- Correction of the minimum brine volume necessary for DBR
- Revision of the estimated U(VI) solubility to account for new data
- Recalculation of actinide solubility uncertainties based on a much larger number of solubility measurements, with separate distributions developed for the +III, +IV and +V actinide solubilities, instead of the single distribution used for the CCA PAVT

As a result of these changes and improvements, the calculated +III, +IV and +V actinide solubilities for the PABC04 were slightly higher than the solubilities calculated for the CCA PAVT (Table 6-2). The uncertainties associated with these solubilities were also greater than the single uncertainty distribution used in the CCA PAVT. The results of the calculations also indicated that organic ligands could significantly affect actinide solubilities, particularly EDTA complexation of the +III actinides. As a consequence of the higher calculated solubilities and associated uncertainties, the importance of DBR to total releases was increased in the PABC04, compared to the CRA-2004 PA and the CCA PAVT. However, cuttings and cavings releases continued to dominate total radionuclide releases, except at low probabilities (Leigh et al. 2005a).

EPA (2006b) concluded that although the actinide solubility calculations carried out for the PABC04 were significantly improved over the calculations for the CCA PAVT, some areas of uncertainty remained. EPA (2006b) recommended that DOE obtain additional data related to the likely solubility of U(VI) in WIPP brines and use these data to develop a thermodynamic solubility model. The relatively large uncertainty associated with +IV actinide solubilities, even though the uncertainty was determined with data used in the development of the FMT database, indicates that the +IV actinide solubility model could be improved for future PA calculations. Finally, EPA (2006b) also recommended that a more thorough and systematic approach should be implemented for identifying and selecting data for development of the actinide solubility uncertainty distributions for future WIPP PAs.

6.4 CRA-2009 PA DISSOLVED ACTINIDE SOURCE TERM

The actinide solubilities calculated for the PABC04 were also used for the CRA-2009 PA dissolved actinide source term. Use of the PABC04 actinide solubilities for the CRA-2009 PA did not consider updated inventory data or new aqueous speciation or solubility data published since the PABC04.

6.4.1 Waste Inventory

The components in the WIPP waste inventory and emplacement materials are relevant to calculating actinide solubilities, because some components may affect the WIPP repository chemistry and actinide source term. The information needed for PA that may influence repository chemistry includes the amounts of iron-based metals/alloys, aluminum-based metals/alloys, other metals/alloys (including lead), CPR, oxyanions (nitrate, sulfate and phosphate), complexing agents (organic ligands) and cement.

Appendix TRU WASTE in the CRA-2004 (DOE 2004) and Leigh et al. (2005b) describe theWIPP waste inventory used for the PABC04. The waste inventory used for the CRA-2009 PA was the same inventory used for the PABC04, except for the addition of waste emplacement materials that had been inadvertently omitted from the PABC04 (DOE 2009, Section 24.6.2). The PABC04 inventory was based on data received by September 30, 2002, from the waste-generator sites, with updates identified by EPA during their review of the CRA-2004 (Leigh et al. 2005b). The actinide solubilities calculated for the PABC04 using these inventory data were also used for the CRA-2009 PA (Table 6-2).

Updated inventory information available for the CRA-2009 PA was developed using data received from the TRU waste sites as of December 31, 2007 (Crawford et al. 2009). Comparison of this inventory data for organic ligands (Crawford et al. 2009) with the quantities used to calculate actinide solubilities for the PABC04 shows that organic ligand quantities had increased for acetic acid, citric acid, sodium citrate, and sodium EDTA (Table 6-5). Because of the potential effects of organic ligands on actinide solubilities, EPA instructed DOE to include the revised inventory of organic ligands in the PABC09 actinide solubility calculations (Cotsworth 2009a, Comments 1-23-1 and 1-23-4). In addition, EPA requested that DOE include the updated inventory of organic ligands in their identification of ligands most likely to influence actinide solubilities in the repository, and in their discussion of the extent to which ligands are likely to affect actinide solubilities (Cotsworth 2009a, Comments 1-C-6 and 1-C-14). Moody (2009a) responded that DOE would perform the PABC09, which would include updated EDTA, acetate, citrate and oxalate concentrations, based on the information provided in Crawford et al. (2009) and provide documentation of this PA to EPA.

Table 6-5. Reported Ligand Inventories for the PABC04, PABC09 and CRA-2014 PA

Compound	PABC04 Inventory [kg] (Leigh 2005)	PABC09 Inventory [kg] (Crawford et al. 2009)	CRA-2014 Inventory [kg] (Van Soest 2012)
Acetic acid	142	13,200	14,100
Sodium acetate	8,510	9,700	9,960
Citric acid	1190.5	5,680	5,230
Sodium citrate	400	2,550	2,550

Sodium EDTA	25.6	354	376
Oxalic acid	13,796	26,600	17,800
Sodium oxalate	33,940	646	650

Previous inventory data has shown that curium is present in quantities below its predicted solubility, when dissolved in the minimum brine volume. Neptunium-237 is also present in relatively low quantities. EPA (2010b) calculated the concentrations of these actinides from their inventories decayed through repository closure at 2033 (Crawford et al. 2009) and the minimum brine volume of 17,400 m^3 (Clayton 2008). The resulting curium concentration was less than the +III actinide solubilities calculated for the PABC09, but the inventory-based neptunium-237 concentration exceeded the +V actinide solubilities calculated for the PABC09. These results were consistent with previous evaluations of the inventories of curium and neptunium, which have concluded that curium will be present at concentrations below its calculated solubility, and neptunium will be of little significance to repository performance because of its low total curies (EPA 2006d).

6.4.2 Minimum Brine Volume

The minimum brine volume necessary for a brine release is used with the inventory data to calculate organic ligand concentrations for the actinide solubility calculations. The minimum brine volume used for these calculations was originally 29,841 m^3 (Larson 1996), but was changed to 10,011 m^3 based on an evaluation by Stein (2005) for the PABC04 and the CRA-2009 PA dissolved actinide source term calculations (Section 6.3.5). Clayton (2008) recalculated the minimum brine volume and obtained a value of 17,400 m^3. Increasing the minimum brine volume decreases the organic ligand concentrations calculated for the actinide solubility calculations. However, increasing the minimum brine volume from 10,011 m^3 to 17,400 m^3 did not completely offset the increase in reported organic ligand inventories (Table 6-5).

EPA requested additional information regarding the minimum brine volume calculations (Cotsworth 2009b, Comment 2-23-7). DOE's response (Moody 2009b) demonstrated that the assumed minimum brine volume of 17,400 m^3 is a bounding lower limit for DBR by comparing the overall repository-scale brine volume to the DBR volumes for the CRA-2009 PA, replicate R1. This comparison showed that non-zero DBR volumes were not observed unless the repository-scale brine volume was significantly in excess of 20,000 m^3. DOE also calculated that the DBR volume-weighted average of the overall repository-scale brine volume was 64,300 m^3. Consequently, EPA (2010b) found that use of the 17,400 m^3 minimum brine volume to calculate organic ligand concentrations appeared to be conservative and acceptable.

6.4.3 Repository Chemical Conditions

DOE (2009, Appendix SOTERM-2009, Section SOTERM-2.2) summarized repository conditions that could potentially affect actinide solubilities. Assumptions regarding many of these conditions are addressed in the Chemical Conditions conceptual model, which was summarized by SC&A (2008b, Appendix A.2).

6.4.3.1 WIPP Brines

WIPP brine formulations used for the CRA-2009 PA was GWB for Salado brine and ERDA-6 for Castile brine. These brine formulations remained unchanged from the CRA-2004 PA and the PABC04.

DOE reviewed a study by Altmaier et al. (2003) that addressed the pH buffering capacity of Mg-rich brines (2009, Appendix SOTERM-2009, Section SOTERM-2.3.2). Altmaier et al. (2003) determined the solubility of $Mg(OH)_2$(cr) in $MgCl_2$ and NaCl solutions, as well as in $MgCl_2$-NaCl mixtures. In experiments with $MgCl_2$ concentrations above 2 molal, they observed $Mg(OH)_2$ converted to korshunovskite. This phase has been predicted to precipitate from GWB brine during FMT modeling calculations, although GWB has a lower initial magnesium concentration of 1 M. In $MgCl_2$ solutions from 0.01 to 1.0 molal, pmH values measured in solution ranged from approximately 9 to 9.7, which is consistent with the PABC09 pmH values predicted for GWB and ERDA-6 of 9.34 and 9.63, respectively. Although phase 5 is expected to form in GWB under WIPP conditions (Section 4.3.2), these results indicate that formation of phase 5 or korshunovskite will maintain slightly alkaline brine pH.

6.4.3.2 Cement Inventory

DOE (2009, Appendix SOTERM-2009, Section SOTERM-2.3.3) did not directly address the influence of the cementitious waste inventory on brine pH in the WIPP repository. The potential effects of cementitious materials in the repository are addressed within the Chemical Conditions conceptual model, where it acknowledges that portlandite ($Ca(OH)_2$) in cementitious materials could react with CO_2 to form calcite. This reaction could buffer pH at relatively high values, compared to the brucite dissolution reaction. Evaluation of the effects of portlandite on brine pH at the time of the CCA showed that the effects of cementitious waste on pH will be minimal because of calcite precipitation and reaction of the portlandite with $MgCl_2$ in the brine to form $CaCl_2$ (SC&A 2008b, Appendix A.2; DOE 1996, Appendix SOTERM, Section 2.2.2):

$$Ca(OH)_2(s) + MgCl_2 \leftrightarrow CaCl_2 + Mg(OH)_2(s) \quad \textbf{(33)}$$

For the CCA, DOE calculated that 2×10^9 moles of MgO would be added to the repository, and 8×10^6 moles of portlandite would be present as cementitious material in the waste (DOE 1996, Appendix SOTERM-2009, Section SOTERM-2.2.2). DOE used these fixed quantities of MgO and portlandite to calculate the pH and CO_2 fugacity as a function of the amount of CO_2 produced by microbial reaction, the volume of brine in the repository, and the type of brine (DOE 1996, Appendix SOTERM, Section 2.2.2). The mass of cement reported for the CCA was 8.54×10^6 kg (Storz 1996), whereas the mass of cement reported by Crawford et al. (2009) based on more recent inventory information increased to 1.23×10^7 kg. EPA noted this increase in the reported cement inventory and the decreased quantities of MgO likely to be placed in the repository because of the decrease in the MgO EF from 1.95 to 1.2 (Section 4.4) (Cotsworth 2009b, Comment 2-C-24). Accordingly, EPA requested additional information from DOE regarding the possible consequences of the changed amounts of MgO and cement on pH buffering in WIPP brines and potential impacts on actinide solubilities.

DOE responded that the MgO excess factor has been demonstrated as sufficient to prevent acidification of the repository (Moody 2009b). However, the effect of portlandite in cement would be to raise, not lower, brine pH. DOE stated portlandite will react with CO_2 first, before the reaction of MgO, and that degradation of 11.5% of cellulosic materials is sufficient to react with all the portlandite reported in the PABC09 inventory. This explanation is not completely consistent with previous evaluations of the effects of portlandite, which indicated that portlandite would dissolve in brine, react with $MgCl_2$ in solution via reaction (33), and precipitate brucite. Consequently, portlandite dissolution would result in lower magnesium concentrations. If excessive quantities of portlandite dissolve, the available magnesium in solution could be completely consumed, resulting in relatively high pH values such as those predicted by DOE (1996) and Schuessler et al. (2001) for systems with high proportions of $Ca(OH)_2(s)$ relative to $Mg(OH)_2(s)$.

EPA (2010b) evaluated the potential effects of cement in the CRA-2009 waste inventory (Crawford et al. 2009) in the presence of the predicted amount of MgO backfill using mass balance calculations to determine if the amount of portlandite in the cement could exceed the amount of magnesium in the brine and in polyhalite in the Salado Formation. The amount of portlandite in the cement was estimated by assuming the cement contains 5%, 7.5%, or 10% by weight $Ca(OH)_2$ (Storz 1996), resulting in repository-wide estimates of 8.30×10^6 moles, 1.25×10^7 moles, and 1.66×10^7 moles of $Ca(OH)_2$, respectively. The repository brine volume was assumed equal to 17,400 m^3, the minimum volume necessary for DBR. The amounts of Salado polyhalite in the system were calculated assuming a DRZ volume of 1.58×10^6 m^3, a rock density of 1,180 kg/m^3 (Brush et al. 2006), and the assumption that Salado Formation contains 1.7% polyhalite by weight (Brush 1990). The moles of portlandite from cement dissolution, polyhalite from the Salado Formation and magnesium in the brine were calculated based on 1 kg of H_2O for both GWB and ERDA-6 (Table 6-6).

Table 6-6. Mass Balance Calculations Comparing Moles of Portlandite in Cement to Moles of Magnesium Available from Brine and Polyhalite, Minimum Brine Volume of 17,400 m^3

Brine	Portlandite in Cement (%)	Portlandite (moles/kg H_2O)	Magnesium in Brine (moles/kg H_2O)	Magnesium in Polyhalite (moles/kg H_2O)	Magnesium in Brine and Polyhalite (moles/kg H_2O)
GWB	0	0.000	1.217	6.662	7.879
GWB	5	0.569	1.217	6.662	7.879
GWB	7.5	0.854	1.217	6.662	7.879
GWB	10	1.138	1.217	6.662	7.879
ERDA-6	0	0.000	0.021	6.150	6.171
ERDA-6	5	0.525	0.021	6.150	6.171
ERDA-6	7.5	0.788	0.021	6.150	6.171
ERDA-6	10	1.051	0.021	6.150	6.171

Portlandite dissolution results in brucite precipitation (reaction 33). This reaction maintains the moderately alkaline pH predicted for the WIPP brine in the presence of the MgO backfill,

provided sufficient magnesium is available in the brine or in polyhalite, which can dissolve and release additional magnesium:

$$K_2MgCa_2(SO_4)_4 \cdot 2H_2O \leftrightarrow 2K^+ + Mg^{2+} + 2Ca^{2+} + 2SO_4^{2-} + 2H_2O \quad \textbf{(34)}$$

For GWB brine, which has a relatively high magnesium concentration, the moles of magnesium in the brine alone are greater than the moles of portlandite in cement (Table 6-6), so sufficient magnesium would be present to maintain moderately alkaline conditions. ERDA-6 has a much lower magnesium concentration than GWB, and the amount of magnesium initially present in the brine may not be sufficient to maintain the pH. However, magnesium released by polyhalite dissolution would be available to react with hydroxide ion released by portlandite dissolution, precipitating brucite according to reaction (33). The increased potassium, calcium and sulfate from polyhalite dissolution would be expected to result in precipitation of anhydrite [$CaSO_4$(s)] and syngenite [$K_2Ca(SO_4)_2 \cdot H_2O$(s)]. Because the moles of magnesium in polyhalite significantly exceed the moles of portlandite in these calculations, the increased cement inventory would be unlikely to cause high brine pH.

6.4.3.3 Organic Ligands

Because the actinide solubilities used in the CRA-2009 PA were based on calculations performed for the PABC04, CRA-2009 PA actinide solubilities (Section 6.4.1) did not account for the most recent inventory. The Crawford et al. (2009) inventory data showed that the masses of organic ligands increased significantly between the PABC04 and CRA-2009 PA (Table 6-5). Brush and Xiong (2009) calculated organic ligand concentrations used for the PABC09 (Table 6-1) from the masses of organic ligands in the PABC09 inventory (Crawford et al. 2009) and the 17,400 m^3 minimum brine volume required for a release (Clayton 2008). EPA requested additional information from DOE regarding the sensitivity of normalized releases to the increased organic ligands inventory (Cotsworth 2009a, Comment 1-23-4). Moody (2009a) responded to this request by providing a sensitivity analysis performed by Brush et al. (2008).

Brush et al. (2008) used the brine compositions, assumptions and FMT code and database used to calculate actinide solubilities for the PABC04 to calculate actinide solubilities with an assumed EDTA concentration of 10 times and 100 times the concentrations calculated by Brush and Xiong (2005b) for the PABC04. Brush et al. (2008) considered the likely effects on PA of higher +III, +IV and +V actinide solubilities caused by increased EDTA concentrations. Brush and Xiong (2005b) calculated an EDTA concentration of 8.14×10^{-6} M, so EDTA concentrations of 8.14×10^{-5} M and 8.14×10^{-4} M were used to calculate actinide solubilities for comparison with the solubilities calculated for the PABC04 (Table 6-7).

Table 6-7. PABC09 Organic Ligand Concentrations and Concentrations Used in the Sensitivity Calculations by Brush and Xiong (2004) and Brush et al. (2008)

Organic Ligand	PABC09 (Brush and Xiong 2009) (moles/L)	Brush and Xiong (2004) (moles/L)	Brush et al. (2008) (moles/L)
Acetate	1.94×10^{-2}	5.05×10^{-3} to 7.89×10^{-2}	1.06×10^{-2}
Citrate	2.38×10^{-2}	2.71×10^{-4} to 3.83×10^{-3}	8.06×10^{-4}

EDTA	6.47×10^{-5}	2.73×10^{-6} to 3.87×10^{-5}	8.14×10^{-6} to 8.14×10^{-4}
Oxalate	1.73×10^{-2}	2.16×10^{-2} to 2.16×10^{-1}	4.55×10^{-2}

The results indicated that the increased EDTA concentrations affected only the predicted Am(III) solubilities in both GWB and ERDA-6 brine, because of increased formation of the $AmEDTA^-$ aqueous species (Brush et al. 2008). Because the solubility of Pu(III) is predicted by analogy to Am(III), the results of these calculations indicate that increased EDTA concentrations would increase americium solubility in all PA realizations and plutonium solubility in the 50% of realizations that have an assumed +III oxidation state for plutonium. The speciation calculations did not include the potential effects of competition with the +III actinides for organic ligands by metals, such as iron and nickel from steel corrosion or sodium present in the brines. Consequently, the FMT calculation results presented by Brush et al. (2008) provide upper-bound estimates of the effects of EDTA on dissolved actinide concentrations in WIPP brines.

Brush et al. (2008) determined that mean DBR and total releases are increased by increasing EDTA concentrations, with effects on mean total releases most evident at probabilities of 0.1 or less. The results of these calculations showed that although increasing EDTA concentrations may increase mean total releases at relatively low probabilities, mean total releases still remain well below release limits.

6.4.3.4 Changes in WIPP Repository Chemical Conditions Between the PABC04 and CRA-2009 PA

There were no significant changes to assumptions in the Chemical Conditions conceptual model between the PABC04 and CRA-2009 PA. PAs since the CCA have assumed that CPR degradation and iron corrosion would establish and maintain reducing conditions. They have also assumed that radiolysis will not lead to oxidizing conditions and actinides in higher oxidation states, such as plutonium(V) or plutonium(VI). Although DOE (2009, Appendix SOTERM-2009, Section SOTERM-2.5) correctly pointed out that the WIPP TRU inventory was updated, the inventory changes were not accounted for in the CRA-2009 PA calculations of actinide solubilities. These changes were incorporated into the PABC09 calculations.

6.4.4 Actinide Aqueous Speciation and Solubility Data

DOE (2009, Appendix PA-2009, Sections PA-3.0 and PA-4.0) provided summaries of the chemistry of thorium, uranium, neptunium, plutonium, americium and curium under WIPP-relevant conditions. These data and additional literature data were reviewed by EPA (2010b) to determine if the aqueous speciation and solubility data in the FMT database used for the CRA-2009 PA and PABC09 remained adequate for PA calculations.

6.4.4.1 Thorium

The thorium solubility and aqueous speciation data included in the FMT database are important to PA, because the solubilities calculated for Th(IV) are also used to predict the solubilities of U(IV), Np(IV) and Pu(IV) (Section 6.1.2). Solubility data reported by Felmy et al. (1991) were used to derive the standard chemical potential (μ^0/RT) value for ThO_2(am) in the FMT database

FMT_050405.CHEMDAT (Giambalvo 2002c). $Th(OH)_4^0$ is the only hydrolysis species included in the FMT database, and the hydrolysis constant reported by Neck et al. (2002) was used to calculate the μ^0/RT value for this species (Nowak 2005, Xiong et al. 2005). Since the last revision of the WIPP thermodynamic database, significant amounts of experimental data have become available regarding Th(IV) aqueous speciation and solids solubilities and regarding the effects of intrinsic colloids on Th(IV) solubility measurements.

Two studies, Neck et al. (2002) and Altmaier et al. (2004), indicate that the higher dissolved thorium concentrations calculated with the current FMT database (FMT_050405.CHEMDAT) likely include not only dissolved thorium, but also a significant contribution from intrinsic Th(IV) colloids. Neck et al. (2002) determined the solubility of amorphous thorium hydroxide in 0.5 M NaCl using titration with laser-induced breakdown detection (LIBD) of colloid formation. Using this approach at pH 3 to 5, the H^+ and thorium concentrations at the onset of colloid formation provided the solubility of $Th(OH)_4(am)$ without any influence from colloidal thorium species. Neck et al. (2002) used LIBD to establish that the presence of intrinsic colloids caused the higher log K_{sp}^0 values reported by other studies, including Felmy et al. (1991) and Rai et al. (1997). Rothe et al. (2002) used x-ray absorption fine structure (XAFS) spectroscopy to evaluate the aqueous speciation under chemical conditions comparable to these studies and also identified thorium intrinsic colloids as the cause of the higher thorium solution concentrations. Altmaier et al. (2004) evaluated the solubility of amorphous hydrated thorium hydroxide in dilute to concentrated NaCl and $MgCl_2$ solutions equilibrated with brucite or korshunovskite and demonstrated that stable intrinsic Th(IV) colloids were also present in 5 M NaCl solutions. In concentrated $MgCl_2$ solutions, pseudocolloids were observed to form through thorium adsorption onto magnesium hydroxychloride colloids.

Altmaier et al. (2004) stated that, based on the experimental data from Neck et al. (2002) for the solubility of $Th(OH)_4(am)$ and the stability constant for the $Th(OH)_4^0$ aqueous species derived by Ekberg et al. (2000), the aqueous concentration of thorium determined by the reaction,

$$Th(OH)_4(am) \leftrightarrow Th(OH)_4^0 \quad \textbf{(35)}$$

would be log $[Th(OH)_4^0] = -8.8 \pm 0.6$. This is the same concentration used by Giambalvo (2002c) based on data from Ryan and Rai (1987) to develop the +IV actinide data in the CRA-2004 PA FMT database (FMT_021120.CHEMDAT). The FMT database was revised prior to the PABC04, CRA-2009 PA and PABC09 to include a different stability constant for $Th(OH)_4^0$ that yields log$[Th(OH)_4^0] = -7.0$ in equilibrium with amorphous thorium hydroxide (Nowak 2005). The potential effects on PA of the formation of intrinsic Th(IV) colloids are considered in Sections 7.0 and 8.0.

The Th(IV)-carbonate aqueous species included in FMT_050405.CHEMDAT are $Th(CO_3)_5^{6-}$ and $Th(OH)_3CO_3^-$. Giambalvo (2002c) stated that these species were included in the database based on an evaluation by Novak (1996) of solubility data in the presence and absence of carbonate from Felmy et al. (1991, 1997). DOE (2009, Appendix SOTERM-2009, Section SOTERM-3.2.1) observed that use of $Th(CO_3)_5^{6-}$ for the +IV actinide speciation in WIPP PA is a conservative assumption that overpredicts the solubility of the +IV oxidation state at pH greater than 10. However, at the total carbonate concentrations and pcH values predicted for the

PABC09 (9.40 for GWB and 9.68 for ERDA-6), significant concentrations of $Th(CO_3)_5^{6-}$ are not present in the brines. Consequently, inclusion of the $Th(CO_3)_5^{6-}$ aqueous species in the FMT database does not appear to cause overprediction of the +IV actinide solubilities under WIPP conditions.

Two studies (Altmaeier et al. 2005 and Altmaier et al. 2006) had since examined Th(IV) solid dissolution and Th(IV)-carbonate complexation. Altmaier et al. (2005) performed $ThO_2 \cdot xH_2O(am)$ solubility experiments in 0.5 M NaCl from pcH 4.5 to 13.5, and determined that in solutions with total carbonate equal to 0.015, 0.04 and 0.1 M, the aqueous speciation of thorium was dominated by $Th(OH)_4^0$ and the thorium species $ThOH(CO_3)_4^{5-}$ and $Th(OH)_2(CO_3)_2^{2-}$, with additional minor contributions from $Th(OH)_2CO_3^0$, and $Th(OH)_3CO_3^-$. At pH greater than 11, $Th(OH)_4CO_3^{2-}$ also became important. Although $Th(CO_3)_5^{6-}$ is known to form at high bicarbonate and carbonate concentrations, significant concentrations of this species did not form at total carbonate concentrations less than or equal to 0.1 M.

Altmaier et al. (2006) experimentally determined the solubility of $ThO_2 \cdot xH_2O(am)$ in 0 to 4 M NaCl solutions containing carbonate and bicarbonate. Total carbonate concentrations in these experiments were 0.02 M and 0.1 M and pcH was varied from 8 to 11. Their results from experiments with a total carbonate concentration of 0.02 M are reproduced in Figure 6-1. These results were obtained at a higher total carbonate concentration than predicted for GWB (3.5×10^{-4} M) and ERDA-6 (4.5×10^{-4} M) for the PABC09. However, this figure shows that increasing ionic strength from 0.1 to 4 M significantly increased $ThO_2 \cdot xH_2O(am)$ solubility at the pcH values from 9.4 to 9.7 expected in repository brines. The effects of higher ionic strength in WIPP repository brines (6.8 to 7.6 M) would be expected to be partially if not completely offset by the low total carbon concentrations in WIPP brines compared to 0.02 M in the experiments included in Figure 6-1. However, because the repository brines have ionic strengths higher than the maximum ionic strength in Figure 6-1, the possibility that carbonate may affect total thorium concentrations under repository conditions cannot be ruled out.

In response to Comment 1-23-3 (Cotsworth 2009a), Borkowski and Richmann (2009) compared the thorium data provided in the literature with the data in the FMT database (FMT_050405.CHEMDAT) and evaluated the difference in the $Th(CO_3)_5^{6-}$ stability constant. Although the stability constant in the FMT database is four orders of magnitude less than the $Th(CO_3)_5^{6-}$ stability constant selected by a recent critical review of thorium solubility and aqueous speciation data (Rand et al. 2008), this difference is unlikely to affect total thorium concentrations under repository conditions. Borkowski and Richmann (2009) noted that the FMT_050405.CHEMDAT database included the hydroxycarbonate species $Th(OH)_3CO_3^-$, but did not include stability constants for the other hydroxycarbonate species such as $ThOH(CO_3)_4^{5-}$ and $Th(OH)_2(CO_3)_2^{2-}$. Borkowski and Richmann (2009) stated that the presence of these other hydroxycarbonate species in the FMT database "could improve the accuracy but not the conservatism" of the current thorium model, but did not provide the basis for this conclusion.

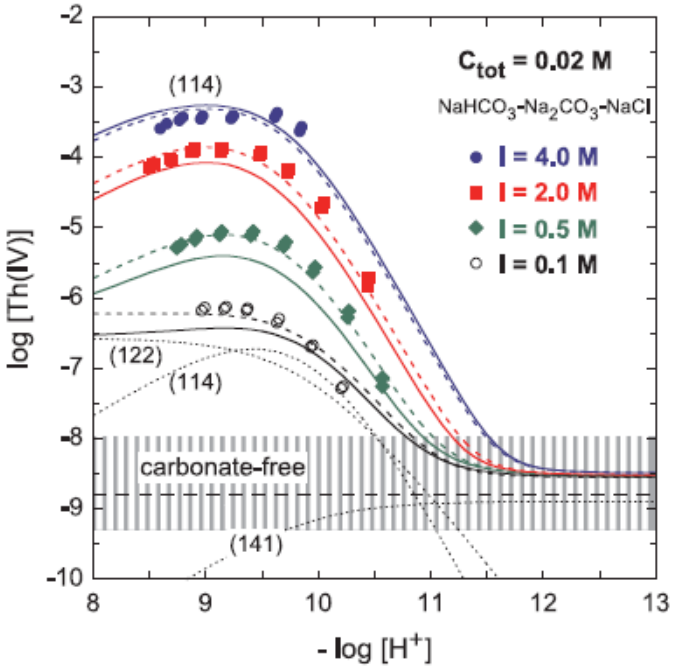

The experimental data are compared with model predictions (solid lines) based on the equilibrium constants and SIT coefficients from Altmaier et al. (2005); the speciation (dotted lines) shown is for 0.1 M NaCl. The dashed lines represent best fits to the data at the different ionic strengths.

Figure 6-1. Solubility of ThO_2•xH_2O(am) in 0.1 M to 4 M NaCl with a Total Carbonate Concentration of 0.02 M
(Source: Altmaier et al. 2006, Figure 2)

EPA noted the additional literature data regarding Th(IV)-carbonate speciation and suggested that this information may necessitate an update to the thorium speciation data in the FMT database (Kelly 2010, Comment 4-C-35). EPA also observed, however, that it was uncertain whether revising the thorium data in the FMT database would significantly affect calculated total thorium concentrations under repository conditions. EPA requested that DOE compare thorium concentrations in solubility experiments that included carbonate (Ősthols et al. 1994, Rai et al. 1995, Felmy et al. 1997, Altmaier et al. 2005, Altmaier et al. 2006) to FMT-calculated thorium concentrations under the same conditions (Kelly 2010). Comparison of the FMT calculation results to the experimentally measured concentrations would allow for an evaluation of whether the FMT results were reasonably consistent with these data, or consistently over- or underpredicted thorium concentrations in carbonate solutions. EPA also recommended that DOE evaluate the available data in an effort to derive Pitzer parameters for the thorium-hydroxycarbonate species not currently in the FMT database and to update the thorium aqueous speciation data in the FMT database for future PAs.

DOE (Xiong et al. 2010b) presented the results of FMT modeling calculations carried out to predict thorium concentrations at the conditions reported for the experiments carried out by Rai et al. (1995), Altmaier et al. (2005) and Altmaier et al. (2006). The data used by Felmy et al.

(1997) were previously reported by Rai et al. (1995). The results reported by Őssthols et al. (1994) were from experiments carried out in 0.5 M $NaClO_4$ solutions. These results were not compared to FMT-calculated Th(IV) concentrations because a previous evaluation had shown that the current FMT database does not provide accurate predicted thorium concentrations in solutions with ionic strength less than 3 M (Xiong et al. 2005).

DOE also compared FMT-calculated thorium solubilities for 26 measurements from Rai et al. (1995), which were carried out at high Na_2CO_3 concentrations (0.98, 1.0 and 1.48 molal) and high pcH (11.57 to 13.14) (Xiong et al. 2010b). The calculated and measured Th(IV) concentrations were in reasonable agreement and the calculated solubilities were not consistently greater or less than the measured concentrations. This result is as expected, because data reported by Rai et al. (1995) and reiterated by Felmy et al. (1997) were used to derive the μ^0/RT data in the FMT database for $Th(CO_3)_5^{6-}$ and $Th(OH)_3CO_3^-$ (Giambalvo 2002c).

Xiong et al. (2010b) also compared FMT-calculated thorium solubilities with measured solubilities reported by Altmaier et al. (2005) and Altmaier et al. (2006). Xiong et al. (2010b) stated that Altmaier et al. (2005) provided results for four experiments in which the ionic strength equaled or exceeded 3 M. These experiments had pcH values ranging from 12.44 to 12.52 and Na_2CO_3 concentrations from 1.35 to 1.82 M. The FMT-calculated results exceeded the measured Th(IV) concentrations in these experiments by a factor of 1.7 to 10. Altmaier et al. (2006) performed solubility experiments with amorphous Th(IV) hydrous oxide in carbonate solutions at ionic strengths up to 4 M (Figure 6-1). Xiong et al. (2010b) compared FMT-calculated solubilities to the measured solubilities in the 4 M NaCl experiments and found that the FMT calculations were consistently less than the measured solubilities by an order of magnitude or more. This consistent under-prediction is particularly significant because these experiments were conducted at pcH values that span those expected in WIPP repository brines rather than the high pcH values of the data from Rai et al. (1995) and Altmaier et al. (2005); on the other hand, the total carbonate concentrations were significantly greater than those predicted in WIPP repository brines. These results indicate that the Th(IV)-carbonate speciation data in the current FMT database are not completely consistent with the available experimental data. Xiong et al. (2010b) correctly noted that the total carbonate concentrations in WIPP brines are much lower than the concentrations used in the Altmaier et al. (2006), but neglected the enhanced stability of the $ThOH(CO_3)_4^{5-}$ aqueous species with increasing ionic strength. However, the effects of much lower carbonate concentrations are likely to outweigh the effects of higher ionic strength in WIPP repository brines. Consequently, carbonate complexation of Th(IV) is likely to have relatively small effects on total thorium concentrations under WIPP repository conditions and will not have large effects on WIPP PA results. However, based on this evaluation, EPA (2010b) stated that DOE should update the Th(IV)-carbonate aqueous speciation data in the geochemical modeling database for the CRA-2014 PA to be consistent with currently available data and to minimize uncertainty associated with this issue.

Brendebach et al. (2007) identified the formation of calcium-thorium-hydroxide complexes that resulted in high solubilities of Th(IV) hydrous oxides in alkaline $CaCl_2$ solutions. Under the investigated conditions, pcH 11 to 12 and $CaCl_2$ concentrations greater than 0.5 M, the dominant aqueous thorium species was identified as $Ca_4[Th(OH)_8]^{4+}$. Altmaier et al. (2009) reported the analogous Pu(IV) aqueous species $Ca_4[Pu(OH)_8]^{4+}$ in 3.5 M $CaCl_2$ solutions at pcH 11 to 12. Although formation of the $Ca_4[Th(OH)_8]^{4+}$ or $Ca_4[Pu(OH)_8]^{4+}$species could result in relatively

high thorium or plutonium concentrations under pcH and calcium concentrations controlled by the interaction of cementitious waste forms with brine, these high pcH and high calcium concentration conditions are not predicted to occur in the WIPP repository environment.

On the basis of their CRA-2009 review of the available data for Th(IV) solubility and aqueous speciation, EPA concluded that:

- The solubility of Th(IV) solids in the thermodynamic database might be affected by intrinsic colloid formation and should be re-assessed
- Recent literature data indicated that the aqueous Th(IV)-carbonate speciation used in the thermodynamic database should be revised
- Formation of calcium-thorium-hydroxide complexes would likely be unimportant under WIPP pH conditions

6.4.4.2 Uranium

Uranium is assumed to be present in WIPP brines as U(IV) in 50% of the PA realizations, and as U(VI) in 50% of the PA realizations (Section 5.0). The solubility of U(IV) is assumed equal to the Th(IV) solubility (Section 6.1.2). Because DOE has not developed a model for calculating the solubility of U(VI), a fixed bounding concentration of 10^{-3} M is assumed for PA (Section 6.3.3).

DOE (2009, Appendix SOTERM-2009, Section 3.3.1.3) addressed the solubility and speciation of U(VI) and provided WIPP-specific experimental results from Lucchini et al. (2010). Lucchini et al. (2010) investigated the solubility of U(VI) solid phases in brine, using sequential addition of U(VI) stock solution to the brines to establish oversaturation with respect to potential U(VI) phases. Experiments were carried out in simulated GWB from approximately pcH 6 to 9 and in simulated ERDA-6 from approximately pcH 8 to 12. All experiments were carried out in a nitrogen atmosphere and CO_2 was excluded from the experiments. The concentrations of U(VI) in the carbonate-free GWB and ERDA-6 brines were approximately 10 to 100 times lower than previously reported for carbonate-free 5 M NaCl brines by Díaz Arocas and Grambow (1998). At moderately alkaline pcH values, the solubility of uranium was about one order of magnitude higher in GWB than in ERDA-6 brine (Figure 6-2).

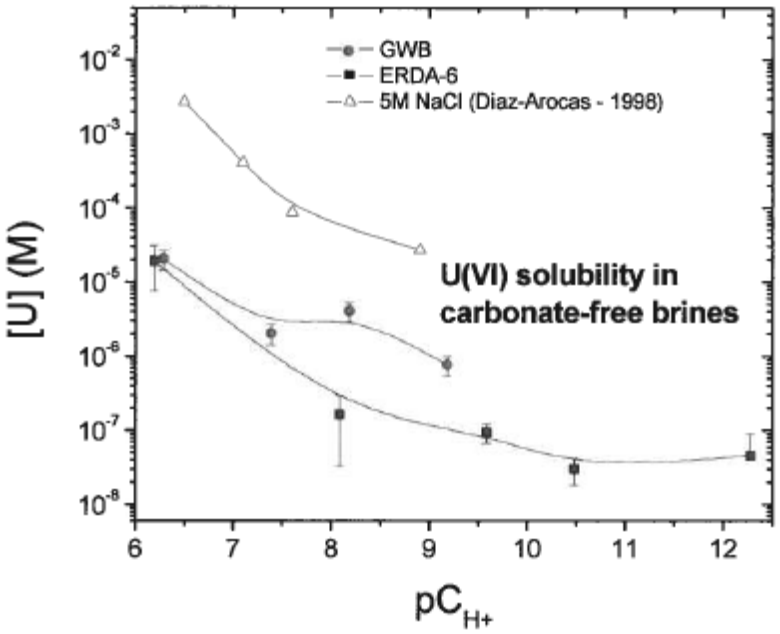

Figure 6-2. U(VI) Solubility Measured in Carbonate-Free Brine as a Function of pcH
(Source: Lucchini et al. 2010, Figure 4-9)

DOE (2009, Appendix SOTERM-2009, Section SOTERM-3.3.1.3) noted the higher solubility in GWB brine compared to ERDA-6 brine, and attributed the higher solubility to complexation by higher borate and sulfate ion concentrations in GWB. In a letter sent to DOE (Cotsworth 2009a, Comment 1-23-6c), EPA observed that higher concentrations in these experiments and in neodymium solubility experiments (Section 6.4.4.5) attributable to borate complexation do not appear to be consistent with the current Dissolved Actinide Source Term conceptual model assumption that states (SC&A 2008b, Appendix A.3):

> *The important ions in WIPP brines are H^+, Na^+, K^+, Mg^{2+}, OH^-, Cl^-, CO_3^{2-}, SO_4^{2-}, and Ca^{2+}. Other ions such as PO_4^{3-}, F^-, Al^{3+}, Fe^{2+}, and Fe^{3+} may be important, but their effects are included only in a qualitative understanding of the chemical environment.*

However, borate complexation of U(VI), if it occurs to a significant extent, would not substantially change the current understanding of likely U(VI) solubility in WIPP brines because uranyl carbonate species are expected to dominate aqueous speciation under WIPP repository conditions. DOE clarified that the potential effects of borate complexation on actinide solubilities were still under investigation, and that different solubilities predicted in GWB and ERDA-6 brine were likely caused by the many differences between the two brines and not solely by different borate concentrations (Moody 2010a).

Because of the probable importance of carbonate complexation on U(VI) concentrations in brine under repository conditions, the experiments reported by Lucchini et al. (2010) cannot be used to revise the upper limit of 10^{-3} M established for U(VI) at the time of the PABC04 (Section 6.3.3).

However, these experiments provide a baseline for experiments planned by DOE for uranium solids solubility in WIPP brines with carbonate.

6.4.4.3 Neptunium

Neptunium is in the +IV oxidation state in 50% of the PA realizations and in the +V oxidation state in the other 50% of the PA realizations. Np(IV) solubility is assumed equal to the solubility of Th(IV) (Section 6.1.2). Neptunium is the only actinide expected to be present in the +V oxidation state in the WIPP repository. Accordingly, a model was developed for calculating Np(V) solubilities under repository conditions. The neptunium aqueous species in the FMT database include inorganic hydrolysis and carbonate species, as well as complexes formed with the organic ligands acetate, citrate, EDTA, lactate and oxalate. The results of the PABC04 actinide solubility calculations indicated that the predominant aqueous Np(V) species under WIPP repository conditions would be NpO_2^+, $NpO_2CO_3^-$, NpO_2Acetate(aq), and NpO_2Oxalate$^-$.

Although a solubility model has been developed for Np(V), the inventory of neptunium-237 in the repository is relatively small and does not significantly affect repository performance (Section 6.4.1). For the CRA-2009, neptunium-237 was included in calculations of radionuclide releases through DBR, but not for cuttings, cavings or spallings or for calculations of releases by transport through the Salado or Culebra (DOE 2009, Appendix PA, Figure PA-21).

6.4.4.4 Americium and Curium

Americium, along with plutonium, constitutes a significant fraction of the total activity in the WIPP inventory. As a result, the solubility of americium solids in WIPP brines is important for calculating potential releases from the repository. The solubility of americium solids in WIPP brines is also used to predict the concentrations of Pu(III) and Cm(III) using the oxidation-state analogy (Section 6.1.2). Curium isotopes are present in the WIPP inventory in relatively small amounts. If the entire inventory of curium isotopes is dissolved in the minimum quantity of brine, the resulting concentration is below the predicted solubility (Section 6.4.1). Plutonium and americium isotopes were included in CRA-2009 calculations of all release mechanisms, whereas curium isotopes were included in calculated releases by cuttings and cavings, spallings and by DBR, but not in releases by transport through the Salado or Culebra (DOE 2009, Appendix PA, Figure PA-21).

Giambalvo (2002a) described the aqueous speciation and solid-phase solubility data for Am(III) included in the FMT_05405.CHEMDAT database. EPA (2006c) reviewed and accepted this for the PABC04. These data are primarily derived from studies involving americium and curium, although the K_{sp}^0 for one solid phase [$NaAm(CO_3)_2 \cdot 6H_2O$(cr)] was obtained from an investigation with a neodymium analogue. Giambalvo (2002a) compared Am(III) concentrations calculated with FMT to $Am(OH)_3$(s) solubility results in 5 M NaCl (Runde and Kim 1994) and found that the calculated solubilities were consistent with the measured solubilities. The results of both the PABC04 and PABC09 actinide solubility calculations indicated that the principal aqueous americium species under WIPP repository conditions are likely to be AmEDTA$^-$ and $Am(OH)_2^+$. Actinide solubility calculations in the absence of organic ligands for both the PABC04 and PABC09 indicated that the dominant aqueous americium species in the absence of organic ligands in WIPP brines would be $Am(OH)_2^+$. The stable americium solid under WIPP

repository conditions is $Am(OH)_3(s)$ based on the results of FMT calculations for both the PABC04 and PABC09.

There appear to be significant differences between Nd (and Am by analogy) values used in the FMT database and experimental data. Neck et al. (2009) performed solubility experiments with $Nd(OH)_3(s)$ in NaCl, $MgCl_2$ and $CaCl_2$ solutions of varying ionic strengths. These data were combined with existing solubility and hydrolysis data for Am(III) and Cm(III) to develop an aqueous speciation and solubility model covering a wide pH range in dilute to concentrated solutions. Ternary complexes of the +III actinides have been identified with calcium and hydroxide ion that were assumed to be $Ca[Cm(OH)_3]^{2+}$, $Ca_2[Cm(OH)_4]^{3+}$ and $Ca_3[Cm(OH)_6]^{3+}$ (Neck et al. 2009, Rabung et al. 2008). These ternary species are unlikely to be important under WIPP repository conditions because they affect the solubility of the +III actinides only at pcH greater than about 11 and at relatively high calcium concentrations, which are not anticipated in the WIPP repository environment. Neck et al. (2009) provided an internally consistent thermodynamic model including Pitzer parameters, and EPA (2010b) noted that there appeared to be significant differences between the data compiled by Neck et al. (2009) and the data included in the FMT database. EPA (2010b) noted that Neck et al. (2009) was not available for evaluation by DOE prior to the PABC09, but stated that these data should be considered with respect to possible revisions to the FMT database for the CRA-2014.

DOE (2009, Appendix SOTERM-2009, Section SOTERM-3.6.2) summarized the results of a WIPP-specific solubility investigation, carried out using Nd(III) as an analogue for Am(III), and by analogy Pu(III) and Cm(III). DOE (2009) stated that the solubility data for Nd(III) in WIPP brines support the current WIPP PA calculations of the solubilities of +III actinides because the calculated solubilities remain conservative. DOE (2009) observed that Nd(III) solubility in WIPP brine was not strongly influenced by carbonate concentrations as high as 0.01 M in the experiments because borate complexation masked the effects of carbonate. DOE also stated that borate is the predominant +III actinide complexing agent in brine in the WIPP-relevant pcH range from 7.5 to 10.

EPA (2010b) reviewed information provided by DOE on the aqueous solubilities and solubility-controlling solids in the Nd(III) solubility experiments (Borkowski et al. 2009, Borkowski 2010, Xiong et al. 2010b) and concluded:

- The identities of the solid phases present at the end of the carbonate-bearing experiments is uncertain. Only indirect evidence is available regarding the final composition and crystallinity of the solid phases in the experiments, because the solid phases were present in quantities that were too small to be characterized. FMT calculation results for the experiments conducted by Borkowski et al. (2009) predicted that not only $Nd(OH)_3(s)$ would form, but also $NdOHCO_3(s)$ and $NaNd(CO_3)_2 \cdot 6H_2O(cr)$ in some carbonate-bearing solutions.
- The results of the Nd(III) experiments and FMT modeling carried out by Xiong et al. (2010b) confirm that carbonate complexation of the +III actinides is unlikely to be significant at WIPP-relevant pcH (9 to 10) and total carbonate concentrations (1.0×10^{-4} to 0.001 M).

- Experimental results in ERDA-6 brine at WIPP-relevant pcH values and carbonate concentrations were approximately one order of magnitude higher than FMT-predicted concentrations under these conditions. This discrepancy was attributed to complexation of the +III actinides by borate. Experimental results in GWB brine were not obtained at WIPP-relevant pcH values, so the effects of borate complexation in GWB brine under WIPP-relevant conditions remain undetermined.
- Significant disagreement between measured and predicted concentrations at low pcH values (6.60 to 7.97) in carbonate-free GWB indicates that the FMT model is not well parameterized under these conditions. The cause of this disagreement between the measured and predicted solubilities is not known.

6.4.4.5 Actinide Solubility Uncertainty Distribution

For the CRA-2009, the uncertainty distributions for each oxidation state were sampled for each realization from the distributions developed for the PABC04 (Xiong et al. 2004, 2005) (Section 6.3.5). The +III, +IV and +V actinide solubilities used in each PA realization are the products of the antilog of the sampled uncertainties multiplied by the calculated solubilities. The U(VI) solubility used in PA remains equal to the fixed value of 10^{-3} M (Section 6.3.4).

During EPA's completeness review of the CRA-2009 (DOE 2009), EPA noted that additional data related to the solubilities of actinides had become available since the PABC04 (Cotsworth 2009a, Comment 1-23-3). EPA requested that DOE evaluate the possible effects of these additional data on the solubility uncertainty distributions developed for the PABC04. DOE prepared updated uncertainty distributions for the +III and +IV actinides that were sampled for the PABC09 (Xiong et al. 2009a). These updated uncertainty distributions are addressed in Section 6.5.5.

6.5 PABC09 DISSOLVED ACTINIDE SOURCE TERM

Brush et al. (2009) summarized the PABC09 actinide aqueous speciation and solubility calculations for the +III, +IV and +V actinides. Because DOE has not developed an aqueous speciation and solubility model for actinides in the +VI oxidation state, the U(VI) concentration of 10^{-3} M established by a review of the available literature (Section 6.2.4) was used in the PABC09.

6.5.1 FMT Code and Database

FMT version 2.4 was used to perform the actinide speciation and solubility calculations for the PABC09 (Brush et al. 2009), which is the same version used for the PABC04. The FMT database used for the PABC09 (FMT_050405.CHEMDAT) was the same version used for the PABC04 (Brush et al. 2009, Moody 2009a). DOE (2009, Appendix SOTERM-2009) reviewed aqueous speciation and solubility data that have become available since the development of FMT_050405.CHEMDAT, but did not revise the FMT database. Although EPA noted some differences between the chemical models in the FMT database and the published literature (EPA 2010b, Section 6.4), FMT calculations carried out with this database provided reasonable estimates of actinide solubilities in WIPP repository brines. Based on the available data relevant

to actinide solubilities and speciation in brines, and comparison of FMT-calculated solubilities to measured solubilities, EPA (2010b) recommended that a review and update of this database should be carried out prior to the CRA-2014, including consideration of:

- Information summarized by Neck et al. (2009) for the +III actinides (Section 6.4.4.4)
- Results of WIPP-specific Nd(III) experiments (Borkowski et al. 2009, Borkowski 2010) for the +III actinides
- Results for Th(IV) hydroxide solubility and carbonate speciation provided by Neck et al. (2002), Rothe et al. (2002) and Altmaier et al. (2004, 2005, 2006)
- Results from continuing WIPP-specific experiments regarding the speciation and solubility of U(VI) (Lucchini et al. 2010)
- Other literature data that become available in time for inclusion in the FMT database review before the CRA-2014 PA

6.5.2 Chemical Conditions Assumptions

The PABC09 aqueous speciation and solubility calculations were carried out using the GWB formulation of Salado brine and the ERDA-6 Castile brine formulation. Equilibrium with the Salado minerals halite and anhydrite and the MgO backfill hydration and carbonation reaction products brucite, korshunovskite and hydromagnesite was assumed in FMT calculations used for the PABC09 dissolved actinide source term.

6.5.3 Organic Ligand Concentrations

DOE used the most recent inventory data (Table 6-5) and the most recent estimate of the minimum brine volume necessary for DBR (Clayton 2008) to calculate organic ligand concentrations for the PABC09 (Table 6-1, Brush and Xiong 2009). The aqueous speciation and solubility calculations were carried out both with and without the predicted organic ligand concentrations. The results obtained with organic ligands were used to determine dissolved actinide source term concentrations for the PABC09. Results of the calculations without organic ligands provided an indication of the effects of organic ligands on actinide solubilities in WIPP brines and were also useful for comparisons to literature solubility and speciation data obtained without organic ligands.

6.5.4 Results of Actinide Solubility Calculations

The results of the actinide solubility calculations for GWB and ERDA-6 brine for the PABC09 are summarized in Table 6-2. The baseline actinide solubilities calculated for the PABC04 and PABC09 were higher than the solubilities used in the CCA PAVT. The increased concentrations of the +III actinides were primarily caused by increased inventories of organic ligands. Smaller increases in the +IV actinide solubilities resulted from changes in the Th(IV) data in the FMT database since the CCA PA. Th(IV) and Np(V) concentrations are predicted to be controlled by the solubilities of ThO_2(am) and $KNpO_2CO_3$(s), respectively, which has remained unchanged since the CCA PAVT. For the CCA PAVT, $AmOHCO_3$(cr) was predicted to be the solubility-controlling solid for the +III actinides. As a result of revisions to the FMT database between the

CCA PAVT and the PABC04, $Am(OH)_3(s)$ was predicted to be the solubility-controlling solid phase for the PABC04 and PABC09.

Experimental investigations of MgO hydration have shown that a magnesium-hydroxychloride solid phase forms in addition to brucite in GWB brine (Snider 2002, Deng et al. 2009). The phase korshunovskite [$Mg_2(OH)_3Cl•4H_2O(s)$] was included in the FMT database used for the PABC09 (FMT_050405.CHEMDAT), but experimental investigations with GWB brine and Martin Marietta MgO have detected the formation of phase 5 [$Mg_3(OH)_5Cl•4H_2O(s)$] rather than korshunovskite (Deng et al. 2009). Brush et al. (2009) used an FMT database that included both magnesium-hydroxychloride phases (FMT_090720.CHEMDAT, Xiong 2009) to calculate which phase would be stable under repository conditions and the potential effects of phase 5 formation on actinide solubilities. The results indicated that phase 5 is the stable magnesium-hydroxychloride phase, as observed in the MgO hydration experiments in GWB. Predicted formation of this phase in place of korshunovskite had only minor effects on calculated actinide solubilities. The FMT calculations with phase 5 were not used in the PABC09 dissolved actinide source term because the FMT_090720.CHEMDAT database had not yet been reviewed and approved by EPA.

6.5.5 Actinide Solubility Uncertainties

Xiong et al. (2009a) described the development of uncertainty distributions for the +III and +IV actinide solubilities sampled for the PABC09 calculations. Xiong et al. (2009a) did not develop an uncertainty distribution for the +V actinides because this distribution is not sampled in PA. Neptunium is the only actinide expected to be present in WIPP repository brines in the +V oxidation state and neptunium does not have a significant effect on PA (Section 9.0).

The process Xiong et al. (2009a) used to develop the uncertainty distributions included use of a set of criteria to select solubility data from the literature. These criteria are reviewed in detail in Section 6.7.1. During an EPA/DOE technical exchange meeting in February 2010, SNL staff stated that an additional requirement for the evaluation was that solubility data used to parameterize the FMT database were not included in the development of the uncertainty distributions. The FMT code (Version 2.4) and database (FMT_050405.CHEMDAT) were used to calculate the predicted solubility at the conditions of each experiment. These calculated solubilities were used with measured solubilities to generate difference values (Equation 31) for accumulation into a probability distribution.

The difference values calculated for the +III and +IV oxidation states were accumulated into separate probability distributions. These distributions were sampled during the PABC09 and used with the FMT-calculated baseline solubilities in GWB and ERDA-6 under repository conditions (Table 6-2) to calculate the concentrations of the +III and +IV actinides used for each brine in each PA realization.

6.5.5.1 +IV Actinide Solubility Uncertainty Distribution

The mean and median values are lower for the PABC09 +IV actinide solubility uncertainty distribution than for the PABC04 (Table 6-8). EPA (2010b) disagreed with some of the decisions made by DOE during development of the +IV actinide solubility uncertainty distribution. EPA

(2010b) did not agree with DOE's inclusion of uncentrifuged, unfiltered data and exclusion of ultracentrifuged results from Altmaier et al. (2004). EPA (2010b) also disagreed with DOE's decision to exclude high-ionic-strength solubility data carried out in carbonate-bearing solutions, specifically, data from Altmaier et al. (2005), Altmaier et al. (2006) and Rai et al. (1995). The difference values calculated for the PABC09, for individual investigations evaluated for the uncertainty distribution and the uncertainty distribution recalculated by EPA (2010b) are compared in Table 6-9. The mean and median of the uncertainty distributions calculated by EPA (2010b) are slightly higher than the mean and median values calculated by DOE for the PABC09. Although the higher overall difference values would tend to increase predicted repository releases, EPA (2010b) concluded that these increased releases would be relatively small, would likely occur only at low probabilities where DBR is important and would not significantly affect repository compliance.

Table 6-8. Comparison of the Th(IV) and Am(III) Solubility Uncertainty Distribution Statistics for the PABC04, PABC09, CRA-2014 PA and CRA14_SEN4 PA

(Xiong et al. 2009a, Brush and Domski 2013c, Xiong and Domski 2016a)

Actinide Oxidation State	Th(IV)				Am(III)			
Performance Assessment	PABC04	PABC09[a]	CRA-2014 PA	CRA14_SEN4 PA	PABC04	PABC09[b]	CRA-2014 PA	CRA14_SEN4 PA
Mean	0.108	-0.346	0.673	-0.011	0.035	-0.142	-0.678	0.484
Median	0.075	-0.520	1.029	-0.090	-0.031	0.072	-0.866	0.074
Standard Deviation	0.837	0.995	0.869	0.821	0.900	1.17	1.57	0.930
Maximum	2.40	3.30	-1.52	1.43	2.85	2.70	2.97	2.97
Minimum	-1.80	-2.25	3.19	-2.01	-3.00	-4.20	-3.55	-1.14

a – The PABC09 Th(IV) statistics listed in Xiong et al. (2009a) differed slightly from the summary statistics in the spreadsheet (PABC09 Th(IV) Uncertainty Analysis 091124.xls) provided to EPA: mean = -0.349, median = -0.517, standard deviation = 0.992, maximum = 3.19 and minimum = -2.21.

b – The PABC09 Am(III) statistics listed in Xiong et al. (2009a) differed slightly from the summary statistics in the spreadsheet (PABC09 Am(III) Uncertainty Analysis 091124.xls) provided to EPA: mean = -0.145, median = 0.090, standard deviation = 1.17, maximum = 2.68 and minimum = -4.16.

Table 6-9. Comparison of Th(IV) Difference Values Calculated for the PABC09 and for Individual Investigations

Data	Mean	Median	Standard Deviation	Maximum	Minimum	Number
PABC09[a]	-0.346	-0.520	0.995	3.30	-2.25	140
Felmy et al. (1991)	0.109	0.0577	0.844	2.39	-1.75	45
Rai et al. (1997)	-0.728	-0.793	0.745	1.37	-2.21	89
Altmaier et al. (2004)	1.82	1.40	1.09	3.19	0.778	6
Ősthols et al. (1994)	0.791	0.808	0.145	1.03	0.517	19
Rai et al. (1995)	0.0299	0.0772	0.447	0.778	-1.22	26
Altmaier et al. (2005)	-0.674	-0.733	0.381	-0.228	-1.00	4
Altmaier et al. (2006)	1.18	1.05	0.231	1.59	0.959	12
High-ionic-strength carbonate[b]	0.292	0.226	0.716	1.59	-1.22	42

PABC09 uncertainty data without uncentrifuged data and with high-ionic-strength carbonate data[c]	-0.271	-0.290	0.893	2.39	-2.21	176

a – Felmy et al. (1991), Rai et al. (1997), Altmaier et al. (2004)
b – Rai et al. (1995), Altmaier et al. (2005), Altmaier et al. (2006)
c – Felmy et al. (1991), Rai et al. (1997), Rai et al. (1995), Altmaier et al. (2005), Altmaier et al. (2006)

6.5.5.2 +III Actinide Solubility Uncertainty Distribution

The uncertainty distribution used for the PABC09 had a lower mean and a slightly higher median value than the uncertainty distribution used in the PABC04 (Table 6-8). EPA (2010b) did not agree with some of DOE's data selections for the +III actinide uncertainty distribution. DOE excluded data from one study (Silva 1982) based solely on its date of publication, which EPA found to be an inadequate basis for exclusion. More importantly, because the FMT database did not include Am(III)-borate aqueous speciation data, DOE excluded solubility data obtained at pcH greater than 7.4 in Salado brines and 8.1 in ERDA-6 brine. EPA (2010b) noted that excluding higher-pcH WIPP brine solubility data implies that the current WIPP thermodynamic database is inadequate for calculating +III actinide solubilities at the pcH values predicted in the WIPP repository, pcH 9.4 for GWB and pcH 9.7 for ERDA-6. EPA (2010b) also stated that because the lack of Am(III)-borate aqueous species in the FMT database might result in the underprediction of total americium concentrations in WIPP brine at higher pcH, including these data could result in a larger number of positive difference values in the PABC09 uncertainty distribution.

DOE included data from Borkowski et al. (2009) in the +III actinide solubility uncertainty distribution, even though only indirect means were used to identify the solid phases in the experiments. EPA (2010b) determined that these results should not have been included in the PABC09 uncertainty evaluation because the lack of solid phase characterization.

Table 6-10. Am(III) PABC09 Uncertainty Distribution and Range of Difference Values Calculated for Excluded Data

	Mean	Median	Standard Deviation	Maximum	Minimum	Number
PABC09[a]	-0.142	0.072	1.17	2.70	-4.20	346
Clayton (2010)[b]	-0.250	-0.225	not reported	2.70	-3.75	536
Silva (1982)	1.33	1.28	0.681	2.79	-1.35	38
Khalili et al. (1994) pcH 6.4 and 8.4	-0.297	-0.218	0.505	0.442	-1.47	29
Khalili et al. (1994) pcH 8.4	-0.085	0.098	0.185	0.442	-0.218	24
Khalili et al. (1994) pcH 6.4	-1.32	-1.34	0.104	-1.22	-1.47	5
Rao et al. (1999) all data	-0.244	-0.144	0.716	1.34	-2.93	105
Rao et al. (1999) pcH > 7.4 (G Seep), pcH > 8.1 (ERDA-6)	-0.645	-0.677	0.662	0.657	-1.778	28
Rao et al. (1999) pcH < 7.4 (G Seep), pcH < 8.1 (ERDA-6)	-0.0984	-0.0291	0.682	1.34	-2.93	77
Rao et al. (1999) pcH < 7.4 (G Seep)	-0.717	-0.704	0.427	-0.174	-1.31	7

Table 6-10. Am(III) PABC09 Uncertainty Distribution and Range of Difference Values Calculated for Excluded Data

	Mean	Median	Standard Deviation	Maximum	Minimum	Number
Borkowski et al. (2009) 5 M NaCl	-0.563	-0.695	0.957	1.64	-3.12	120
Borkowski et al. (2009) ERDA-6, pcH ≤ 8.1	-0.691	-0.540	0.818	0.360	-1.91	14
Borkowski et al. (2009) GWB, pcH ≤ 7.4	-1.51	-1.37	1.33	1.01	-3.67	28
Recalculated[c]	0.181	0.134	0.862	2.79	-2.93	354

a – Borkowski et al. (2009, 5 M NaCl, GWB 6.6 ≤ pcH ≤ 7.4, ERDA-6 7.9 ≤ pcH ≤ 8.1), Khalili et al. (1994, pcH 6.4), Meinrath and Kim (1991), Meinrath and Takeishi (1993), Rao et al. (1996a), Rao et al. (1996b), Rao et al. (1999, excluded G Seep brine pcH > 7.4, ERDA-6 pcH > 8.1), Runde and Kim (1994)

b– Borkowski et al. (2009), Khalili et al. (1994, pcH 6.4), Meinrath and Kim (1991), Meinrath and Takeishi (1993), Rao et al. (1996a), Rao et al. (1996b), Rao et al. (1999, excluded G Seep brine pcH > 7.4, ERDA-6 pcH > 8.1), Runde and Kim (1994)

c– Silva (1982), Khalili et al. (1994, pcH 6.4 and 8.4), Meinrath and Kim (1991), Meinrath and Takeishi (1993), Rao et al. (1996a), Rao et al. (1996b), Rao et al. (1999), Runde and Kim (1994)

EPA (2010b) recalculated the +III actinide solubility uncertainty distribution to determine the effects of excluding the Borkowski et al. (2009) data and including data from Silva (1982), Khalili et al. (1994) at pcH 6.4 and 8.4, Meinrath and Kim (1991), Meinrath and Takeishi (1993), Runde and Kim (1994), Rao et al. (1996a, 1996b) and all data from Rao et al. (1999). The recalculated +III actinide solubility distribution had a slightly higher mean, median and maximum than the uncertainty distribution used in the PABC09, and a significantly higher minimum (Table 6-10). Because the mean of the recalculated uncertainty distribution is only slightly higher than the mean of the distribution sampled for the PABC09, the effects on mean repository releases are likely to have been small.

6.5.5.3 Adequacy of the PABC09 Uncertainty Distribution Evaluation

The PABC09 actinide solubility uncertainty distribution was improved in some respects over the PABC04 distribution. An extensive literature search was carried out to identify actinide solubility data to include in the evaluation and the data selection process included clearly stated data-selection criteria. However, EPA (2010b) identified some issues in the application of these criteria, and some of these issues had non-conservative effects or effects that could not be determined using the available information. These issues included exclusion of the Silva (1982) Am(III) solubility data because of an arbitrarily selected date range for data inclusion, exclusion of Th(IV) solubility data because of ultracentrifugation to separate the dissolved species from the aqueous species, exclusion of Th(IV) solubility data from several studies because of different Th(IV)-carbonate species assumed by the studies' authors, inclusion of a large amount of data from Borkowski et al. (2009) despite uncertainty regarding the solubility-controlling phases and exclusion of solubility data measured in WIPP brines at WIPP-relevant pcH conditions because of concerns about borate complexation of the +III actinides at higher pcH.

The +IV and +III actinide solubility uncertainty distributions were recalculated to address these issues. Removing the uncentrifuged solubility data (Altmaier et al. 2004) and including high-

ionic-strength Th(IV)-carbonate data in the +IV actinide solubility uncertainty distribution increased the mean and median difference values. Recalculation of the +III actinide solubility uncertainty distribution only slightly increased the mean and median difference values. Although the increased mean difference values for the +III and +IV actinide solubility uncertainty distributions would increase mean releases relative to the mean releases calculated for the PABC09, these changes would be relatively small, would likely occur only at low probabilities where DBR is important and would not significantly affect repository compliance. Consequently, EPA (201b) determined that the actinide solubility uncertainty distributions sampled for the PABC09 were adequate.

6.6 CRA-2014 PA DISSOLVED ACTINIDE SOURCE TERM

DOE (2014b, Appendix SOTERM-2014) summarized the assumptions, data and calculations of the dissolved actinide source term concentrations used in the CRA-2014 PA. DOE did not revise the Dissolved Actinide Source Term or Chemical Conditions conceptual model assumptions for their calculations of dissolved actinide source term concentrations for the CRA-2014 PA. Solubility calculations were performed using Salado (GWB) and Castile (ERDA-6) brine compositions, and were performed for Am(III), Th(IV) and Np(V). U(VI) solubility was not calculated, but was instead assumed equal to the fixed upper-limit value of 10^{-3} M specified by EPA at the time of the PABC04 (Section 6.2.4).

DOE (2014b, Appendix SOTERM-2014, Sections SOTERM-2.2.1 and SOTERM-2.2.2) reviewed information about repository pressure and temperature. The information presented is consistent with the Chemical Conditions conceptual model assumption that pressure will not significantly affect actinide solubilities, and that temperature is not expected to significantly depart from ambient conditions. Consequently, these assumptions continue to be appropriate for PA.

New information developed since the PABC09 that may affect dissolved actinide source term concentrations include revisions to the waste inventory, implementation of a variable brine volume for calculating actinide solubilities for DBR and calculation of actinide solubilities using the EQ3/6 code instead of FMT. Investigations of the dependence of WIPP brine composition on pH and its long-term stability also have been performed.

Additional actinide solubility and aqueous speciation data have been published since the last revision of the WIPP geochemical modeling database. These data are reviewed for their potential effects on baseline calculated actinide solubilities and the uncertainty distributions for the Am(III) and Th(IV) actinide solubilities used in PA.

6.6.1 Waste Inventory

The WIPP CPR inventory can affect actinide solubilities because of its possible microbial degradation that produces CO_2. Van Soest (2012) reported the CPR inventory for the CRA-2014 PA. Because of the presence of MgO backfill (Section 4.0), CO_2 production by CPR degradation has relatively small effects on actinide solubilities. Actinide solubilities continue to be calculated assuming that hydromagnesite formation by reaction of CO_2 with the MgO backfill will maintain low CO_2 fugacities.

As described in Section 6.4.3.2, cementitious waste in the WIPP inventory could increase brine pH above values established by the brucite dissolution reaction. However, if sufficient magnesium is available in brine and polyhalite in the DRZ, the portlandite in cement is not expected to significantly affect brine pH. The moles of portlandite from cement dissolution and moles of magnesium available from polyhalite in the Salado Formation DRZ and in the brine were calculated on the basis of 1 kg of H_2O for both GWB and ERDA-6 using the cement inventory reported for the CRA-2014 PA and assuming 0%, 5% and 7.5% portlandite in the cementitious waste (Table 6-11). The results of these calculations indicate that the moles of magnesium in the brine and polyhalite are significantly greater than the moles of portlandite. Accordingly, the cementitious waste is not expected to have significant effects on repository brine pH.

Table 6-11. CRA-2014 PA Inventory Mass Balance Calculations Comparing Moles of Portlandite in Cement to Moles of Magnesium Available from Brine and Polyhalite Using Minimum Brine Volume of 17,400 m^3

Brine	Portlandite in Cement (%)	Portlandite (moles/kg H_2O)	Magnesium in Brine and Polyhalite (moles/kg H_2O)
GWB	0	0.000	7.879
GWB	5	0.498	7.879
GWB	7.5	0.747	7.879
GWB	10	0.997	7.879
ERDA-6	0	0.000	6.171
ERDA-6	5	0.460	6.171
ERDA-6	7.5	0.690	6.171
ERDA-6	10	0.920	6.171

Previous inventory data have shown curium to be present in quantities below its predicted solubility when dissolved in the minimum brine volume. Neptunium-237 is also present in relatively low quantities. The inventories of these actinides, decayed through repository closure at 2033, are provided in Table 6-12. Dissolution of these quantities of curium and neptunium in the minimum brine volume of 17,400 m^3 (Clayton 2008) results in a curium concentration less than the +III actinide solubilities calculated for the CRA-2014 PA, but the inventory-based neptunium-237 concentration exceeds the +V actinide solubilities calculated for the CRA-2014 PA (Table 6-12). These results are consistent with previous evaluations of the inventories of curium and neptunium, which have concluded that curium will be present at concentrations below its calculated solubility, and neptunium will be of little significance to repository performance because of its low total curies (EPA 2006d, EPA 2010b).

Table 6-12. CRA-2014 PA Curium and Neptunium Inventory Decayed through 2033

	Nuclide	Inventory Activity (Ci)[a]	Inventory Mass (g)	Concentration (M)	CRA-2014 PA Actinide Solubility (M)[b]
Curium	Cm-242	18.48	0.005435	1.23×10^{-7}	2.59×10^{-6} (GWB) 1.48×10^{-6} (ERDA-6)
	Cm-243	234.1	4.502		
	Cm-244	9,970	121.6		
	Cm-245	1.225	7.206		
	Cm-246	74.63	240.7		
	Cm-247	0.01120	119.2		
	Cm-248	0.1192	27.72		
	Cm-250	0.005910	0.02814		
Neptunium	Np-237	23.24	32,732	7.94×10^{-6}	2.77×10^{-7} (GWB) 8.76×10^{-7} (ERDA-6)

[a] Van Soest (2012), Tables 5-3 and 5-4
[b] Brush and Domski (2013b), Tables 5 and 6

Organic ligands inventories reported for the CRA-2014 PA are compared to organic ligands inventories for the PABC04 and PABC09 in Table 6-5. The CRA-2014 PA inventories are reasonably similar to the inventories used in the PABC09.

6.6.2 Brine Chemistry

DOE reported results of geochemical modeling calculations that simulated reaction of GWB and ERDA-6 brines with solids in WIPP disposal rooms (Brush et al. 2011). The calculations were carried out using EQ3/6 version 8.0a and the DATA0.FM1 database (Section 6.6.4). The simulations involved adding organic ligands (acetate, citrate, EDTA and oxalate) to GWB or ERDA-6, followed by reaction with halite, anhydrite, brucite, ThO_2(am), $KNpO_2CO_3$(s) and $Am(OH)_3$(s), which in turn was followed by titration to higher pcH values.

DOE investigated the long-term stability of WIPP brine by analyzing simulated brines that had been stored for up to 6 years. The analytical results showed that the stored WIPP brines remained stable, except for magnesium and borate precipitation from ERDA-6 brine at pcH values greater than 10 (Lucchini et al. 2013). DOE also evaluated the effects of pcH on brine chemistry by titrating GWB up to approximately pcH 13 and allowing the brine to equilibrate before analysis. The analyzed brine compositions were compared to the compositions predicted by Brush et al. (2011). Lucchini et al. (2013) observed that the predicted and measured calcium and magnesium concentrations diverged above pcH 10. Comparison of the borate and magnesium concentrations in the experiments (Lucchini et al. 2013) and calculations (Brush et al. 2011) indicated that

additional data are required to improve the modeling of magnesium and borate in WIPP brines at pcH values of 9.5 and greater.

6.6.3 Brine Volumes and Organic Ligand Concentrations

For the PABC04 and PABC09 actinide solubility calculations, the concentrations of organic ligands (Table 6-1) were determined by dissolving the ligand inventories (Table 6-5) in the minimum brine volumes required for a DBR. These concentrations were used to calculate actinide solubilities for all DBRs, regardless of the volume of brine released. For brine release volumes greater than the minimum brine volume, this approach resulted in larger total dissolved masses of organic ligands than were present in the inventory, and likely caused overestimation of the +III actinide solubilities.

For the CRA-2014 PA, Brush and Domski (2013a) calculated the organic ligand concentrations using the minimum brine volume of 17,400 m^3 established by Clayton (2008), as well as brine volumes that are factors of 2, 3, 4 and 5 times greater than this minimum volume. These volumes were determined to span the range of DBRs in the PABC09 (Brush and Domski 2013a). The resulting range of organic ligand concentrations used in the CRA-2014 PA actinide solubility calculations is summarized in Table 6-1. Use of variable brine volumes that more closely match release volumes diluted the organic ligand concentrations in brines and slightly decreased dissolved actinide concentrations for the higher release volumes.

6.6.4 EQ3/6 Code and Database

Wolery et al. (2010) qualified the EQ3/6 code for WIPP PA geochemical modeling calculations. EQ3/6 replaced FMT, which was used to calculate actinide solubilities for previous WIPP PAs. The EQ3/6 code qualification included reformatting the FMT database used for the PABC09 (FMT_050405.CHEMDAT) into a format compatible with EQ3/6 (Ismail et al. 2009). The reformatted EQ3/6 database file was named data0.fmt.r0. The data0.fmt.r0 database was revised by correcting the parameter A^{ϕ} from 0.39 to 0.392 and correcting the parameter $\beta^{(1)}$ for NaCl from 0.2644 to 0.2664 to create data0.fmt.r1. The database conversion from the FMT format to the EQ3/6 format (data0.fmt.r0) and the corrections made to the database to create data0.fmt.r1 were reviewed previously (SC&A 2011).

DOE measured the solubility of phase 5 in $MgCl_2$ – NaCl solutions (Xiong et al. 2010a). This Mg-chloride-hydroxide-hydrate solid is produced in addition to brucite by hydration of MgO in GWB brine (Section 4.7.3). Xiong (2011b) added the equilibrium constant for phase 5 to the data0.fmt.r1 database to create data0.fmt.r2. This database is also referred to as DATA0.FM1.

6.6.4.1 DOE and EPA Technical Exchanges Over FMT

EPA (Edwards 2015, Comment 3-C-10) requested additional information regarding the phase 5 solubility data added to DATA0.FM1, because the solubility in the database (42.96) differed slightly from the solubility (43.21) Xiong et al. (2010a) reported. In response, DOE explained that the 42.96 solubility value was based on extrapolating the experimental data to zero ionic strength using the Pitzer model, whereas the 43.21 solubility value was based on an extrapolation using the Specific Ion Interaction Theory model (Bryson 2015b). Consequently, the phase 5

solubility value of 42.96 incorporated in DATA0.FM1 is correct because it was based on the Pitzer ion activity model used in the WIPP solubility and aqueous speciation calculations.

The EQ3/6 code version 8.0a and the DATA0.FM1 database were used for the CRA-2014 PA actinide solubility calculations. EPA reviewed the information DOE provided (DOE 2014b Appendix SOTERM-2014, Sections SOTERM-3.0 and SOTERM-4.0) and requested additional information, including:

- Copies of the DATA0.FM1 database, EQ3/6 input and output files, Excel macros and Excel spreadsheets used for the actinide solubility calculations (Comment 1-23-11, Edwards 2014)
- Documentation for WIPP-specific data supporting Figure SOTERM-21 graphs depicting the effects of organic chelating agents on +III and +IV actinide solubilities in WIPP brines (Comment 1-23-12, Edwards 2014)
- An evaluation of boron speciation in WIPP brine (Comment 3-C-2, Edwards 2015c)

EPA noted that the +III and +IV actinide aqueous speciation and solubility data in the DATA0.FM1 was last updated using data available in 2002 (Comment 3-C-3, Edwards 2015c). EPA observed that Xiong (2011b) had experimentally determined the solubilities of natural and synthetic hydromagnesite samples and calculated a different solubility for synthetic hydromagnesite than the value in DATA0.FM1, Borkowski et al. (2010) had determined the stability constant for the Nd(III)-tetraborate aqueous species and Thakur et al. (2014) had determined a revised β^0_{101} for $AmEDTA^-$. EPA consequently requested that DOE carry out and document a review of available +III and +IV actinide aqueous speciation and solubility data and hydromagnesite solubility data, use the results of this review to defensibly update the EQ3/6 database and then use this revised database to recalculate the actinide solubilities and associated uncertainty distributions for the WIPP PA.

In response to these EPA comments, DOE revised DATA0.FM1 to create DATA0.FM2 (Xiong and Domski 2016b) following the procedure summarized in analysis plan AP-173 Revision 1 (Domski and Xiong 2015a). Revisions to the database included changes to various data, including:

- Hydromagnesite solubility
- Borate chemistry
- EDTA chemistry
- Citrate chemistry
- Magnesium-sulfate dissociation constant
- Lead chemistry

Xiong and Domski (2016b) also provided a review of the available actinide aqueous speciation and solubility data in response to EPA Comment 3-C-3 (Edwards 2015c).

EPA began its review of DATA0.FM2 and the supporting documentation and discussed a number of preliminary comments during technical exchange meetings with DOE in Albuquerque

on February 3, 2016 and August 31, 2016 and during a conference call on August 9, 2016. Based on these discussions, EPA determined that a complete review of the supporting information sufficient for accepting DATA0.FM2 or specifying modifications to the database would require a significant amount of time.

In lieu of requesting a revised PABC for the CRA-2014, EPA requested that DOE conduct several sensitivity studies to address some of the significant technical concerns arising from EPA's CRA-2014 review. Because of the issues with DATA0.FM2, these sensitivity studies were performed using the original DATA0.FM1 database. To facilitate completion of the dissolved actinide solubility review for the CRA-2014, EPA and DOE agreed during a technical exchange meeting on September 1, 2016 to use the baseline solubilities calculated for the CRA-2014 PA in a sensitivity study, along with revised +III and +IV actinide solubility uncertainty distributions (Sections 6.6.6 and 14.0).

The following sections summarize EPA's preliminary comments and concerns regarding DATA0.FM2 and its supporting documentation. These observations do not represent the results of a comprehensive review, and additional information will be required before EPA's review can be completed. Consequently, DATA0.FM2 has not been accepted by EPA for use in WIPP PA.

6.6.4.2 Hydromagnesite Solubility

The hydromagnesite solubility used in all WIPP PA calculations through the CRA-2014 PA was based on calorimetric measurements by Robie and Hemingway (1973) using natural hydromagnesite samples (Figure 6-3). These values are compared to other studies including Königsberger et al. (1999), Cheng and Li (2010), Xiong (2015f), and Berninger et al (2014).

Königsberger et al. (1999) reported a lower hydromagnesite solubility than Robie and Hemingway (1973) and stated that these results were consistent with available hydromagnesite solubility measurements. However, little information was provided about the hydromagnesite solubility data cited by Königsberger et al. (1999), including the characteristics of the solid phases, such as grain size or whether the hydromagnesite was synthetic or natural, and no details of the experimental investigations were provided, such as whether solubility was approached from undersaturation or oversaturation.

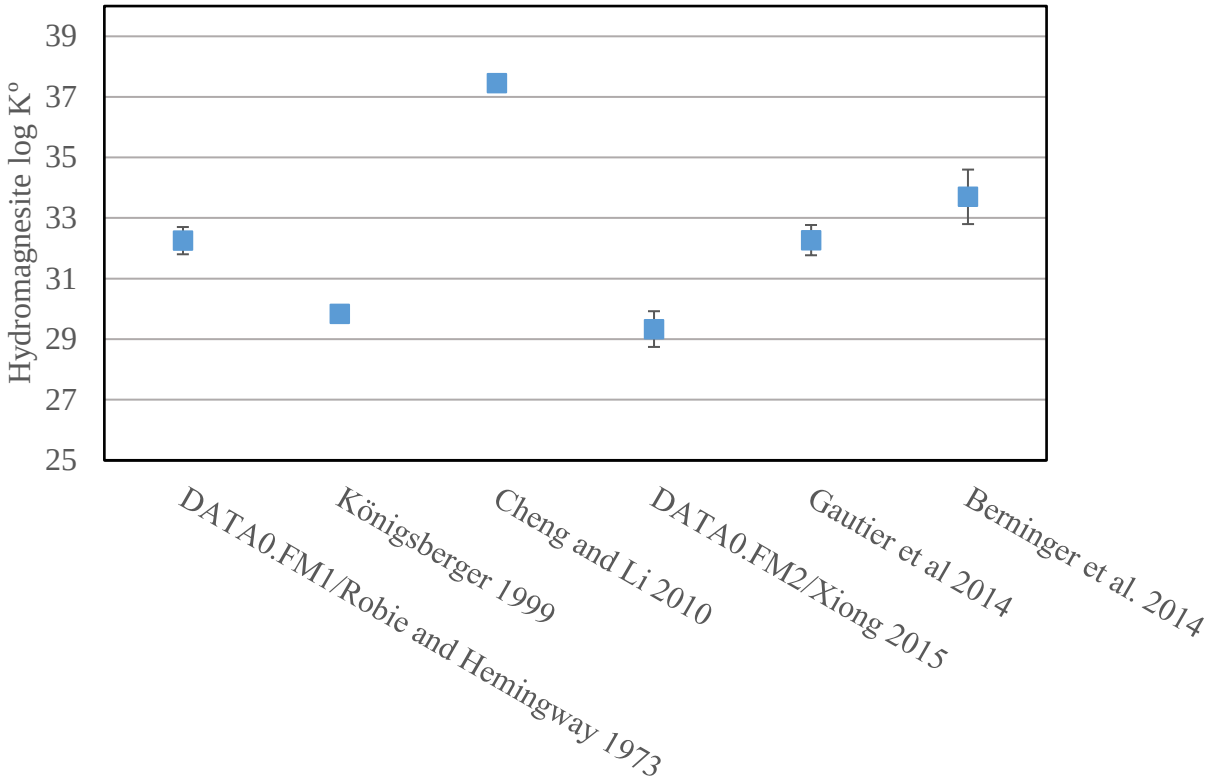

Figure 6-3. Hydromagnesite Solubilities

Cheng and Li (2010) calculated a relatively high hydromagnesite solubility based on experiments with synthetic hydromagnesite conducted from undersaturation from 25ºC to 100ºC (Figure 6-3). As noted by Gautier et al. (2014), the hydromagnesite solubility determined by Cheng and Li (2010) may be unreliable because pH and carbonate concentrations were not monitored during these short (6 hour) experiments.

Xiong (2011a) measured the solubility of two natural hydromagnesite samples and synthetic hydromagnesite from undersaturation in deionized water and in NaCl solutions up to 4.4 molal. The synthetic hydromagnesite solubility determined from these experiments and extrapolated to zero ionic strength with the Pitzer ion activity model (Figure 1, Xiong 2015f) was similar to the solubility reported by Königsberger et al. (1999), but less than the solubilities from Robie and Hemingway (1973) and Cheng and Li (2010). A potential cause of the low solubility calculated from these experiments would be higher CO_2(g) concentrations in the experiments than was assumed in the solubility calculations. Xiong (2011a) did not report carbonate measurements in the experimental solutions, and may have underestimated CO_2 fugacity. Because the experiments were apparently conducted in sealed containers, CO_2 increases from hydromagnesite dissolution could have resulted in an underestimation of how much hydromagnesite dissolved.

Two recently published investigations also indicate that the solubility values reported by Xiong (2011a) and Königsberger et al. (1999) may be too low. Gautier et al. (2014) measured the solubility of natural hydromagnesite at 25ºC and 50ºC. The solubility experiments were

conducted from undersaturation and included measurement of magnesium, pH and alkalinity, with the pH and alkalinity measurements used to directly determine bicarbonate/carbonate concentrations. The solubility determined by Gautier et al. (2014) is consistent with the Robie and Hemingway (1973) solubility from calorimetric data (Figure 6-3), but higher than the solubilities determined by Königsberger et al. (1999) and Xiong (2011a). Xiong (in press) stated that Gautier et al. (2014) did not account for the simultaneous equilibrium of the solutions with brucite. However, Gautier et al. (2014) noted slight supersaturation with respect to brucite in only a few experimental solutions, and X-ray diffraction and scanning electron microscope examination of all solids at the end of the experiments showed that hydromagnesite was the only solid phase present. In addition, because Gautier et al. (2014) directly measured all relevant chemical parameters (magnesium, pH and alkalinity), even if brucite formation had occurred, it would not have affected the calculated hydromagnesite solubility. Consequently, the comment by Xiong (in press) does not raise a significant issue regarding the results of Gautier et al. (2014).

In another recent hydromagnesite solubility study, Berninger et al. (2014) determined the solubility at 22.5ºC of natural, biotic hydromagnesite in experiments conducted from both over- and undersaturation. The natural hydromagnesite was composed of fine-grained crystals (up to ~ 5 µm) in agglomerates ranging up to 50 µm. The solubility values calculated in this study were based on measured magnesium concentrations, pH and alkalinities, with the latter two measurements used to determine directly the bicarbonate/carbonate concentrations. The solubility reported in this investigation is only slightly higher than the solubilities from Gautier et al. (2014) and Robie and Hemingway (1973). This slightly higher solubility may be caused by the fine-grained nature of the hydromagnesite used by Berninger et al. (2014).

Because of the consistency between the reported hydromagnesite solubilities of Robie and Hemingway (1973), Gautier et al. (2014) and Berninger et al. (2014), the original hydromagnesite solubility based on Robie and Hemingway (1973) appears to be the most reliable value. Xiong and Domski (2016b) revised the hydromagnesite solubility based on the synthetic hydromagnesite solubility measurements of Xiong (2011a) and extrapolation to zero ionic strength using the Pitzer model (Xiong 2015f). EPA noted that this solubility appeared to be too low based on the available data from other investigations (Economy 2016). The low hydromagnesite solubility included in DATA0.FM2 would be expected to result in the calculation of unrealistically low, non-conservative +III actinide solubilities because of the effects of pH and CO_2 fugacity on the +III actinides.

6.6.4.3 Borate Data

The CCA and CRA-2004 noted the presence of boric acid [$B(OH)_3$] in WIPP brine. However, in the CRA-2009 (Appendix SOTERM-2009, Table SOTERM-2) and CRA-2014 (Appendix SOTERM-2014, Table SOTERM-4) DOE noted that "boron species will be present in brine as boric acid, hydroxyl polynuclear forms ($B_3O_3(OH)_4^-$), and/or borate forms (e.g., $B_4O_7^{2-}$)." Borkowski et al. (2009) stated that tetraborate is present in WIPP brine and Lucchini (2013) referred to tetraborate in WIPP brines during comparisons of measured and modeled WIPP brine compositions.

Because tetraborate complexation was identified as important for actinide(III) speciation in WIPP brines (Borkowski et al. 2010) and the understanding of WIPP brine boron speciation appeared to have evolved, EPA requested that DOE provide an evaluation of boron speciation in WIPP brines (Comment 3-C-2, Edwards 2015c). In response, DOE provided a speciation diagram indicating that the tetraborate ion [$B_4O_5(OH)_4^{2-}$] and monoborate anion [$B(OH)_4^-$] were most likely to predominate in GWB at WIPP repository pH values (Bryson 2015b). This diagram was developed using borate equilibrium constant data from Anderson et al. (1964), which is applicable to lower ionic strength conditions. Examination of the EQ3/6 output files for GWB and ERDA-6 calculations of actinide solubilities (Table 6-13) indicates that the WIPP model based on Felmy and Weare (1986) (DATA0.FM1 database) predicts that the dominant boron-containing species in WIPP brines will be the monomeric forms, with $B(OH)_4^-$ present in the highest concentration. The polymeric species [$B_4O_5(OH)_4^{2-}$ and $B_3O_3(OH)_4^-$] in the repository brines represent smaller fractions of the total boron, although tetraborate ion was predicted to represent 19.39% of the total boron in GWB.

Table 6-13. Borate Speciation in WIPP Brines Calculated with EQ3/6

Brine	GWB		ERDA-6	
Database	DATA0.FM1	DATA0.FM2	DATA0.FM1	DATA0.FM2
$B(OH)_4^-$ (%)	34.33	6.76	59.48	20.95
$B(OH)_3$(aq) (%)	13.08	2.36	14.74	3.24
$MgB(OH)_4^+$ (%)	24.57	88.01	18.92	67.26
$CaB(OH)_4^+$ (%)	1.23	< 1	2.54	1.20
$NaB(OH)_4$(aq) (%)	--[a]	2.19	--[a]	7.31
$B_4O_5(OH)_4^{2-}$ (%)	19.39	< 1	2.46	< 1
$B_3O_3(OH)_4^-$ (%)	7.40	< 1	1.87	< 1
Total Borate (M)	0.186	0.167	0.062	0.062
Output file name	gwb_1x.6o	gwb_1x.6o	erda6_1xb.6o	erda_1x.6o

a – $NaB(OH)_4$(aq) not included in DATA0.FM1

Since 2009, several studies have examined borate complexation with actinides (Borkowski et al 2010, Hinz et al. 2012, Xiong 2012d, Schott et al. 2014, Hinz et al. 2015). Borkowski et al. (2010) determined the stability constant and Pitzer coefficients for the Nd(III)-tetraborate aqueous species in solutions containing up to 0.16 M total boron (0.04 M $Na_2B_4O_7$). Contrary to the speciation calculated for WIPP brines (Table 6-13), Borkowski et al. (2010) assumed that the boron species in the investigated 1 – 5 M NaCl solutions were present predominantly as tetraborate species [$HB_4O_7^-$ and $B_4O_7^{2-}$]. Borkowski et al. (2010) concluded that tetraborate ion significantly contributes to +III actinide speciation in WIPP brines, competing with carbonate. DOE used the solubility data from Borkowski et al (2010) to calculate the equilibrium constant for $AmHB_4O_7^{2+}$ and its associated Pitzer parameters using speciation consistent with the WIPP model (Xiong 2015e). However, they did not provide documentation of how well the results met the acceptance criteria listed in the applicable analysis plan (Xiong 2014a), including whether the Pitzer parameters were of similar magnitude as those in the peer-reviewed literature for comparable interaction types, a plot of the residuals or a demonstration that the modeled data using the best fit parameters are in close agreement with the experimental data.

Hinz et al. (2012) investigated the solubility of $Nd(OH)_3$(am) in 0.1 M and 5 M NaCl with 0.004 and 0.04 M total boron, and in 0.25 M and 3.5 M $CaCl_2$ solutions with 0.004 and 0.04 M total boron. At these total boron concentrations, which were lower than the maximum concentrations used by Borkowski et al. (2010), Hinz et al. (2012) observed no enhancement in $Nd(OH)_3$(am) solubility, indicating that Nd(III) did not form strong aqueous borate complexes. Time-resolved laser fluorescence spectroscopy (TRLFS) of Cm(III) in NaCl and $CaCl_2$ solutions at pH 8 indicated increasing total boron concentrations from 0.004 to 0.04 M led to increasing Cm(III)-borate complexation. At higher pH (12), there was no TRLFS evidence of Cm(III) complexation by borate in $CaCl_2$ solutions.

New data related to borate complexation of +III actinides has become available since the CRA-2014 data cutoff date of December 31, 2012. Schott et al. (2014) evaluated the speciation of boron and precipitation of Eu(III)-borate solid in solutions containing up to 0.7 M total boron. These studies demonstrated the formation of a weak Eu(III)-borate that was a precursor to formation of a Eu(III)-borate solid phase. Hinz et al. (2015) investigated $Nd(OH)_3$(am) solubility in salt solutions containing up to 0.4 M total boron. Although weak Nd(III)-borate complex formation was observed, no significant increase in Nd(III) solubility was observed. At pcH values of 9 or less in concentrated salt solutions with total boron concentrations of 0.04 M or greater, Nd(III) concentrations were less than observed in boron-free solutions because of the precipitation of a Nd(III)-borate solid phase.

Xiong (2012d) derived thermodynamic properties for Na-$B(OH)_3$-Cl-SO_4 solutions based on experimental solubility measurements of sodium tetraborate [borax, $Na_2B_4O_7{\cdot}10H_2O$(s)] in NaCl (Xiong 2012c, Xiong 2012d) and Na_2SO_4 solutions (Sborgi et al. 1924). In the Felmy and Weare (1986) model used for borate speciation in previous WIPP solubility calculations, the aqueous species $NaB(OH)_4$(aq) was not explicitly considered. Xiong (2012d) included this species in their derivation based on reports of its existence by other researchers, but did not present spectroscopic or other direct evidence of its formation. Xiong (2012d) provided a comparison of sodium tetraborate solubility data calculated using the Felmy and Weare (1986) model (DATA0.FM1) and using the revised speciation and Pitzer parameters that showed that the revised data appeared to provide a better representation of the solubility data. However, additional information related to other acceptance criteria was not provided, including whether the Pitzer parameters were of similar magnitude compared to those in the peer-reviewed literature for comparable interaction types or a plot of the residuals.

In response to EPA's completeness comment regarding adequacy of the EQ3/6 database (Comment 3-C-3, Edwards 2015c), DOE developed a thermodynamic model for the Mg-Ca-Pb-$B(OH)_3$-Cl-SO_4 system (Xiong 2015a). The report describing this effort did not include information related to the acceptance criteria (Xiong 2014a), including whether the Pitzer parameters were of similar magnitude compared to those in the peer-reviewed literature for comparable interaction types, a plot of the residuals or a demonstration that the modeled data using the best fit parameters are in close agreement with the experimental data. Xiong and Domski (2016b) included the $AmHB_4O_7^{2+}$ equilibrium constant developed by Xiong (2015e) in the revised database DATA0.FM2. Xiong and Domski (2016b) also included $AmHB_4O_7^{2+}$-Cl Pitzer binary interaction parameters from Xiong (2015e) in the revised database.

The changes in borate data between DATA0.FM1 and DATA0.FM2 resulted in substantial changes to the borate speciation calculated with EQ3/6 for the actinide solubility calculations (Table 6-13). Using the CRA-2014 PA database (DATA0.FM1), three (ERDA-6) or four (GWB) borate species were present in concentrations that represented more than 10% of the total borate. Actinide solubility calculations with the revised database (DATA0.FM2) resulted in the majority of borate being present as $MgB(OH)_4^+$ in both GWB and ERDA-6 brines and the only other species representing greater than 10% of the total borate was predicted to be $B(OH)_4^-$ in ERDA-6 brine.

DOE also provided a figure from Xiong et al. (2013b) comparing the experimental solubilities of sodium tetraborate obtained in NaCl and Na_2SO_4 (Xiong and Domski 2016b). These results indicate that the revised borate model more closely approximates the sodium tetraborate solubility data than the previous Felmy and Weare (1986) model.

6.6.4.4 EDTA Data

DOE (2014b, Appendix SOTERM-2014, Section 3.8.2) discussed the results of WIPP-specific experiments that were performed to assess the effects of expected concentrations of acetate, citrate, EDTA and oxalate on +III and +IV actinide solubilities. EPA (Edwards 2014, Comment 1-23-12) requested supporting information for the cited organic complexation data, including the experimental approach, materials, analytical methods and solids characterization data. DOE (Franco 2015b) responded with supporting information for the +III actinide analogue data by citing the relevant test plan (Borkowski 2007). In their response, DOE noted that no characterization data were available for the solids in the experiments. The results of these experiments indicated that only EDTA at concentrations from about 1×10^{-5} M to 1×10^{-4} M appeared to significantly increase Nd(III) concentrations (DOE 2014b, Appendix SOTERM-2014, Figure SOTERM-21). These results appear to show that at CRA-2014 PA EDTA concentrations (1.48×10^{-5} M to 7.40×10^{-5} M, Table 6-1), +III actinide solubilities may be increased by EDTA complexation. DOE (Shrader 2016) provided additional information for the cited Th(IV) experiments DOE (2014b, Appendix SOTERM-2014, Section 3.8.2). The results of these preliminary experiments showed no evidence that the tested concentrations of acetate, citrate, EDTA or oxalate would increase repository brine concentrations of +IV actinides.

DOE has updated many of the EDTA Pitzer parameters in DATA0.FM2 using new data obtained. However, EPA has identified significant issues in these updates. DOE calculated Pitzer parameters for the Am(III)-EDTA system in $NaClO_4$ solutions to ionic strengths of 6.6 molal using EDTA acid dissociation constants and stability constants of Am^{3+}, Cm^{3+} and Eu^{3+} with EDTA obtained from P. Thakur at Carlsbad Environmental Monitoring and Research Center (CEMRC) (Xiong 2013b). Thakur et al. (2014) also reported these data. Xiong (2013b) stated that the parameters were derived per Analysis Plan AP-134 (Xiong 2012b), but this analysis plan did not provide any acceptance criteria. Fitting only the data obtained in $NaClO_4$, Xiong (2013b) determined a log β_{101} for $AmEDTA^-$ of 20.55. By simultaneously fitting data in NaCl (Choppin et al. 2001) and the $NaClO_4$ data, Xiong (2013b) determined a log β_{101} for $AmEDTA^-$ of 20.05. Xiong and Domski (2016b) used the 20.55 value obtained using the $NaClO_4$ data in the DATA0.FM2 database but did not provide justification for using the $NaClO_4$ data instead of the combined $NaClO_4$ and NaCl data.

DOE also updated the the Na^+-$AmEDTA^-$ Pitzer binary interaction parameters in DATA0.FM2 using parameter values derived by Xiong (2013b) (Xiong and Domski 2016b). DOE did not explain the reason for changing these Pitzer parameters but not others in the DATA0.FM2 database, but comparison of the parameters in DATA0.FM1 and those derived by Xiong (2013b, Table 3) indicates that the Na^+-$AmEDTA^-$ parameters were the only parameters that differed by more than 10% from the parameters in DATA0.FM1.

DOE derived thermodynamic properties based on the solubility of di-calcium ethylenediaminetetraacetic acid [$Ca_2EDTA(s)$] in $MgCl_2$ solutions, following Analysis Plan AP-154 (Xiong 2013a, Xiong 2015d). Xiong (2015d) obtained the solubility data from Kirkes et al. (2014), which was not included in the supporting documentation provided by DOE and has not yet been reviewed. Xiong (2015d) also updated thermodynamic properties based on the solubility of $Ca_2EDTA(s)$ in NaCl solutions, superseding results reported by Xiong (2012a). Xiong (2015d, Figure 2) provided a comparison of experimental and predicted $Ca_2EDTA(s)$ solubilities as a function of ionic strength in NaCl solutions that demonstrated good agreement. Xiong (2015d) stated that there did not appear to be any published solubility data for $Ca_2EDTA(s)$. However, Hummel et al. (2005, Table VIII-15) cited several solubility studies for Mg- and Ca-EDTA compounds, including solubility studies for $Ca_2EDTA{\cdot}2H_2O(s)$ (Bersin et al. 1957) and for $Ca_2EDTA{\cdot}7H_2O(s)$ (Myachina et al. 1974). Because of the high solubilities of EDTA compounds, Hummel et al. (2005) did not develop a quantitative thermodynamic model or select solubility data for these solids. Because of the high solubilities of the Ca-EDTA and Mg-EDTA solids, solubility limitations on EDTA concentrations in WIPP brines are unlikely unless estimated EDTA inventories in WIPP waste significantly increase.

Xiong and Domski (2016b) incorporated the Na^+- Mg^{2+} - Ca^{2+} - Cl^- - $EDTA^{4-}$ Pitzer interaction parameters, $Ca_2EDTA(s)$ solubility constant and $CaEDTA^{2-}$ stability constant developed by Xiong (2015d) into DATA0.FM2. The $CaEDTA^{2-}$ stability constant increased significantly from the value previously used in WIPP PA, which had been assumed equal to the $MgEDTA^{2-}$ stability constant (Table 6-14). Hummel et al. (2005) estimated higher stability constants for both $CaEDTA^{2-}$ and $MgEDTA^{2-}$ (Table 6-14). The data used by Hummel et al. (2005) to evaluate the $MgEDTA^{2-}$ stability constant included the Choppin et al. (2001) data used by Giambalvo (2002b) and additional data obtained at lower ionic strength. The data used by Hummel et al. (2005) to evaluate the $CaEDTA^{2-}$ stability constant included only data obtained at ~ 0.1 M ionic strength.

Table 6-14. $CaEDTA^{2-}$ and $MgEDTA^{2-}$ Formation Constants

Aqueous Species	Formation Constant	Source	Database
$CaEDTA^{2-}$	10.126	analogy with $MgEDTA^{2-}$	DATA0.FM1
	11.1562	Xiong (2015d)	DATA0.FM2
	12.69	Hummel et al. (2005 Table III-6)	--
$MgEDTA^{2-}$	10.126	Giambalvo (2002b), Choppin et al. (2001)	DATA0.FM1
	10.126	Giambalvo (2002b), Choppin et al. (2001)	DATA0.FM2
	10.9	Hummel et al. (2005 Table III-6)	--
$AmEDTA^-$	18.97	Giambalvo (2002b), Choppin et al. (2001)	DATA0.FM1
	20.55	Xiong (2013b)	DATA0.FM2
	19.67	Hummel et al. (2005 Table III-6)	--

During a EPA/DOE conference call on August 9, 2016 (Economy 2016), EPA noted that when actinide solubilities were calculated in WIPP repository brines using the DATA0.FM2 database, EDTA complexation is not predicted have significant effects on +III actinide concentrations (Domski and Xiong 2015b). EPA noted that this appeared inconsistent with WIPP-specific solubility studies demonstrating that repository-relevant EDTA concentrations increased Nd(III) concentrations (DOE 2014b, Appendix SOTERM-2014, Figure SOTERM-21). DOE responded with a modeling assessment of EDTA-bearing solutions from the experiments illustrated in Figure SOTERM-21 (Patterson 2016b). There are significant differences between the repository brines and the experiments, including lower pcH conditions in the GWB experiments (~8.42) than the pcH conditions anticipated in the WIPP repository (9.59, Domski and Xiong 2015b), absence of carbonate in the experiments and the presence of addtional solid phases in the repository. DOE presented the results of modeling calculations using DATA0.FM2 that demonstrated relatively good agreement between the modeled and experimentally measured Nd(III) concentrations for the EDTA experiments illustrated in Figure SOTERM-21.

6.6.4.5 Citrate Data

DOE (Xiong 2015d) used experimental solubility data for earlandite [$Ca_3[C_3H_5O(COO)_3]_2 \cdot 4H_2O$(s)] obtained in NaCl and $MgCl_2$ solutions and earlandite solubility data obtained in $NaClO_4$ solutions from the literature (Ciavatta et al. 2001) to derive the solubility constant for earlandite, dissociation constant for $CaC_3O_5O(COO)_3^-$ (calcium citrate) and Pitzer interaction parameters for the Na^+- Mg^{2+} - Ca^{2+} - Cl^- - $C_3O_5O(COO)_3^{3-}$ (citrate^{3-}) system. This investigation was carried out according to Analysis Plan AP-154 (Xiong 2013a).

Xiong (2015d) favorably compared the earlandite log K_{sp}^0 calculated from the solubility data (-18.11) to the value (-17.81) reported by Ciavatta et al. (2001) and showed that calculations performed with the revised model differed from the measured solubility data of Ciavatta et al. (2001) by 58% or less. However, Xiong (2015d) did not provide other information related to the acceptance criteria in AP-154, including an evaluation of the magnitudes of the calculated Pitzer parameters compared to literature values for similar interaction types, the differences between the modeled concentrations and those measured in the NaCl and $MgCl_2$ solutions or an assessment of the residuals showing that the selected parameters correspond to a minimum as a function of the parameter values. Xiong (2015d) did not compare the calculated dissociation constant for $CaC_3O_5O(COO)_3^-$ of -4.9730 to to the previous value (-5.2997) in DATA0.FM1 or provide literature data to support this revision.

DOE (Xiong and Domski 2016b) incorporated the earlandite solubility, $CaC_3O_5O(COO)_3^-$ dissociation constant and Na^+- Mg^{2+} - Ca^{2+} - Cl^- - $C_3O_5O(COO)_3^{3-}$ Pitzer parameters in DATA0.FM2. Xiong and Domski (2016b) also incorporated data related to a lead-citrate aqueous species, which is addressed in Section 6.6.4.6.

6.6.4.6 Magnesium-Sulfate Data

Xiong (2015a) determined the dissociation constant for the $MgSO_4$(aq) species as part of an investigation of brucite solubilities in Na_2SO_4 solutions with borate. The calculated dissociation

constant (-2.38) appears to be consistent with the literature data. This ion pair was not included in DATA0.FM1 and was added to DATA0.FM2 (Xiong and Domski 2016b).

6.6.4.7 Lead Data

Xiong and Domski (2016b) added lead data to DATA0.FM2, including solubility data for litharge [PbO(cr)], lead oxalate [PbC_2O_4(cr)], cerussite [$PbCO_3$(cr)] and lead borate [$Pb(BO_2)_2 \cdot H_2O$(s)]. Aqueous dissociation constants were also added to DATA0.FM2 for lead chloride species, lead oxalate species, lead carbonate species, lead hydrolysis species, lead borate species, lead EDTA species, lead citrate species and lead oxalate species. Sandia National Laboratory data sources cited by Xiong and Domski (2016b) included Xiong et al. (2013a), Xiong (2015c), Xiong (2014b), and Xiong (2014c). One publication cited by Xiong and Domski (2016b) as Xiong (2013c) could not be verified because only a title was provided in their reference list, and another listed as Xiong (2014b, ERMS 561917) was superseded by Xiong (2015b). Literature data were cited for lead chloride and lead carbonate aqueous species and interaction parameters (Xiong and Domski 2016b).

Acceptance of the lead aqueous speciation, solubility and Pitzer interaction parameters in DATA0.FM2 would require a detailed review of all supporting information. Because of the large amount of information associated with the addition of lead to DATA0.FM2 and because solubilities calculated with DATA0.FM1 were used in the CRA14_SEN4 sensitivity calculations, these data have not yet been reviewed.

6.6.4.8 Actinide Aqueous Speciation and Solubility Data

Because the actinide aqueous speciation and solubility data had not been modified since the PABC04, EPA requested that DOE carry out and document a review of all available +III and +IV actinide aqueous speciation and solubility data (Comment 3-C-3, Edwards 2015c). EPA (Economy 2016) conveyed additional concerns to DOE regarding whether the current $Am(OH)_3$(s) solubility is too low and thorium speciation (carbonate and silica species) are adequate (Economy 2016). DOE responded with additional information (Patterson 2016b) and a listing of the available Th(IV) and Am(III), Nd(III) and Cm(III) data that included DOE's reasoning for including or excluding these data in development of the Th(IV) and Am(III) aqueous speciation and solid solubility models (Xiong and Domski 2016b). The following summarizes the status of these and some additional comments and issues related to the actinide data in DATA0.FM1 and DATA0.FM2.

6.6.4.9 Thorium Aqueous Speciation and Solubility Data

Patterson (2016b) noted that the log K_s^0 for ThO_2(am) in the DATA0.FM1 and DATA0.FM2 databases is at the lower end of the range established by Rand et al. (2008) and is less than the values reported by Altmaier et al. (2004), Altmaier et al. (2005) and Altmaier et al. (2006). Patterson (2016b) also compares Th(IV) solubilities calculated with the WIPP database to solubilities reported by Wood and Cetiner (2005) for lower pcH experiments in 0.1 M ionic strength $NaNO_3$ in the presence of organic ligands. This study was selected for geochemical modeling because the low pH (~3) and low ionic strength would minimize the effects of the ionic medium and ensure that Th^{4+} is the dominant species. However, these calculations do not address

the fact that under WIPP pcH conditions, both log K_s^0 and the stability constant for $Th(OH)_4(aq)$ are critical for calculating an accurate Th(IV) solubility. DOE states that the calculations presented demonstrate conservatism in the WIPP Th(IV) model because the calculated concentrations exceed measured concentrations. However, because the conditions of the experiments are significantly different than conditions anticipated in the repository, including much lower pH and a $NaNO_3$ medium, for which the WIPP model is not parameterized, this comparison is of questionable utility. A more reliable method for evaluating the relative conservatism of the Th(IV) solubility and aqueous speciation model is provided by the calculation of the Th(IV) solubility uncertainty distribution (Section 6.6.6), which compares measured and calculated Th(IV) solution concentrations for experiments conducted under WIPP-relevant conditions. As described in Section 6.6.6, the uncertainty distribution developed for the CRA14_SEN4 calculations indicates that the model-predicted Th(IV) concentrations agree reasonably well with experimentally measured concentrations.

Altmaier et al. (2004) reported the results of $ThO_2•xH_2O(am)$ solubility experiments in concentrated NaCl and $MgCl_2$ solutions and Altmaier et al. (2008) reported the results of solubility experiments in concentrated $CaCl_2$ solutions. Xiong and Domski (2016b, Appendix A) excluded these data from parameterization of the database because of potential contributions from intrinsic colloids due to the "short" duration of the experiments, which were 20 to 100 days (Altmaier et al. 2004) and 7 to 198 days (Altmaier et al. 2008). However, experiments conducted by Ryan and Rai (1987) and Felmy et al. (1991), the results of which were used to develop the $ThO_2•xH_2O(am)$ and aqueous speciation data currently in the database, were conducted for comparable time periods ranging from 7 to 372 days. In addition, it appears that Altmaier et al. (2004) and Altmaier et al. (2008) adequately removed intrinsic colloids from the sampled solutions through 2 nm filtration or ultracentrifugation. This database will be strengthened if DOE revises the justification for excluding the Altmaier et al. (2004) and Altmaier et al. (2008) from the database development effort or includes the data from these investigations.

Xiong and Domski (2016b, Appendix A) excluded most of the Felmy et al. (1991) data from parameterization of the database because of low ionic strength, and stated that the remainder of the data "alone is not suitable for parameterization." The $ThO_2(am)$ solubility in the DATA0.FM1 and DATA0.FM2 databases was derived from the Felmy et al. (1991) experimental data (Giambalvo 2002c). DOE should clarify whether the statement by Xiong and Domski (2016b) regarding the Felmy et al. (1991) data raises questions about the validity of the $ThO_2(am)$ solubility in the DATA0.FM2 database.

Xiong and Domski (2016b, Appendix A) excluded data from the $ThO_2•xH_2O(am)$ solubility experiments by Neck et al. (2002) from parameterization of the database because of potential contributions from intrinsic colloids due to the "short" duration of the experiments, which ranged from 5 to 204 days. However, experiments conducted by Ryan and Rai (1987) and Felmy et al. (1991), the results of which were used to develop the $ThO_2•xH_2O(am)$ and aqueous speciation data currently in the DATA0.FM1 and DATA0.FM2 databases, were conducted for comparable time periods that ranged from 7 to 372 days. Excluding the Neck et al. (2002) data based on intrinsic colloid formation is also questionable because Neck et al. (2002) performed either 1.4 nm filtration or ultracentrifugation to remove colloids and the solubility results (Neck et al. 2002, Figure 1) are comparable to the results from studies used to develop the Th(IV) model in the DATA0.FM1 and DATA0.FM2 databases (Felmy et al. 1991, Rai et al. 1997 and Östhols et al.

1994). In addition, the $Th(OH)_4(aq)$ stability constant in the DATA0.FM1 and DATA0.FM2 databases is from the investigation by Neck et al. (2002) (Nowak 2005). We would like DOE to explain whether the statement by Xiong and Domski (2016b) about the Neck et al. (2002) experiments raises significant concerns regarding the validity of the $Th(OH)_4(aq)$ stability constant in the DATA0.FM1 and DATA0.FM2 databases.

Rai et al. (1997) performed $ThO_2(am)$ solubility experiments in NaCl and $MgCl_2$ brines. Xiong and Domski (2016b, Appendix A) stated that the data were irrelevant to WIPP and not suitable for parameterization because of the low pcH conditions (about 3.0 to 5.5) of the experiments. However, the ψ_{ijk} and θ_{ij} values in the DATA0.FM1 and DATA0.FM2 databases database for Na^+-Th^{4+}-Cl^- and Mg^{2+}-Th^{4+}-Cl^- were obtained from the Rai et al. (1997) investigation (Giambalvo 2002e). EPA would like DOE to clarify whether the statement by Xiong and Domski (2016b) regarding the Rai et al. (1997) data indicates uncertainty regarding the validity of these parameters in the DATA0.FM1 and DATA0.FM2 databases.

The Th(IV)-carbonate aqueous stability constants and Pitzer parameters in the DATA0.FM1 and DATA0.FM2 databases were obtained from Felmy et al. (1997). Felmy et al. (1997) based their evaluation on the experimental investigations of thorium hydroxide solubility in carbonate solutions by Östhols et al. (1994) and Rai et al. (1995). Additional investigations of thorium hydroxide solubility in carbonate solutions were carried out by Altmaier et al. (2005, 2006). Altmaier et al. (2005) conducted experiments that duplicated the experiments of Östhols et al. (1994) and Rai et al. (1995), with increased attention to possible formation of small intrinsic colloids. A summary of the experimental durations and phase separation methods used in these studies is provided in Table 6-15.

Xiong and Domski (2016b, Appendix A) stated the Altmaier et al. (2005, 2006) experiments could not be used to improve the parameterization of the Th(IV)-carbonate aqueous species because "the experiments elapsed for a relatively short period in comparison with the long-term experiments from Borkowski et al (2012), and therefore the contributions from intrinsic colloids to total Th(IV) concentrations were grossly overestimated according to the results from Borkowski et al. (2012)." This is an inadequate basis for excluding the Altmaier et al. (2005, 2006) data from consideration because appropriate steps were taken by Altmaier et al. (2005, 2006) to remove colloidal material through filtration or ultracentrifugation and because Altmaier et al. (2005, 2006) also demonstrated that the solutions had equilibrated before the end of the experiments. Xiong and Domski (2016b) also provided inadequate justification for eliminating the Altmaier et al. (2005, 2006) data because the current parameterization is based on experiments of similar durations as the Altmaier et al. (2005, 2006) investigations (Östhols et al. 1994 and Rai et al. 1995, Table 6-15), and because it is unknown whether the colloidal effects observed in the complex WIPP brines used by Borkowski et al. (2012) would also be observed in the less-complex brine solutions used by Altmaier et al. (2005, 2006).

Table 6-15. Th(IV)-carbonate Experimental Conditions

Investigation	Experiment Duration	Phase Separation
Östhols et al. (1994)[a]	several months (open system) and a minimum of one month (closed system)	10 nm to 220 nm filtration
Rai et al. (1995)[a]	7 to 55 days	4 nm filtration
Altmaier et al. (2005)	5 to 20 days (open system) and up to 132 days (closed system)	ultracentrifugation or 1.2 nm filtration (demonstrated to be equivalent)
Altmaier et al. (2006)	8 to 14 days	ultracentrifugation or 1.5 nm filtration (demonstrated to be equivalent)

a – data from these investigations were used by Felmy et al. (1997) to derive Th(IV)-carbonate stability constants and Pitzer interaction parameters included in DATA0.FM1 and DATA0.FM2 databases

Xiong and Domski (2016b, page 20) observed that results of investigations conducted by Altmaier et al (2005, 2006) for time periods of two weeks to a few months differed from the results of Borkowski et al. (2012) from experiments conducted for up to four years. However, Borkowski et al. (2012) did not characterize the thorium solids that remained in their experiments after four years of equilibration. It is possible that the initially amorphous ThO_2(s) in those experiments had begun to crystallize, forming less-soluble ThO_2(cr). Such crystallization over time would be consistent with the results of Felmy et al. (1991), who reported the appearance of broad peaks in the XRD patterns that indicated increased crystallinity from solids from 372-day experiments. Consequently, the lower solubilities observed by Borkowski et al. (2012) are an inadequate basis for excluding the experimental results of Altmaier et al. (2005, 2006).

EPA (2010b, Section 6.4.4.1) noted during the CRA-2009 review that the Th(IV)-carbonate speciation in the current database is inconsistent with the Altmaier (2005, 2006) experimental data and stated that DOE should update the speciation for the CRA-2014 PA to be consistent with currently available data. The Th(IV)-carbonate aqueous speciation and Pitzer parameters in the DATA0.FM1 and DATA0.FM2 databases were developed using the results of Östhols et al. (1994) and Rai et al. (1995). The experimental solutions analyzed by Östhols et al. (1994) were either 220 nm or 10 nm filtered (Table 6-15), whereas the solutions analyzed by Altmaier et al. (2005, 2006) were 1.2 nm filtered or subjected to ultracentrifugation that was shown to achieve the same results as filtration. By repeating the open-system experiments of Östhols et al. (1994) and using smaller pore-sized filtration or ultracentrifugation, Altmaier et al. (2005) demonstrated the likely presence of colloids in some of the Östhols et al. (1994) experimental solutions. Consequently, the Östhols et al. (1994) data should not be used to parameterize the Th(IV)-carbonate aqueous species. The solubility data from Rai et al. (1995) also cannot be used, because pcH of the solutions was not reported. Consequently, the Agency recommends DOE use the data provided by Altmaier et al. (2005, 2006) to develop aqueous speciation and Pitzer parameters for the Th(IV)-carbonate species.

Patterson (2016b) compared Th(IV) solubilities measured by Altmaier et al. (2005) in 0.1 M NaOH at 0.01 molal and higher Na_2CO_3 concentrations to solubilities calculated using

DATA0.FM2. However, at this NaOH concentration, the pcH of the solution would be much higher than WIPP conditions, and above the pcH range of 8 to 11.2 for which the WIPP models are parameterized (Brush and Domski 2013c). A more reasonable comparison is provided by the difference values calculated for the PABC09 for high-ionic-strength carbonate solutions (Table 6-9), which shows that the mean and median difference values are slightly positive, indicating that the WIPP model tends to slightly underpredict Th(IV) concentrations in carbonate-bearing solutions.

DOE examined the available thorium-silica complexation data (Rai et al. 2008a) and concluded that there is insufficient data to add the proposed Th-silicate species to the WIPP model (Patterson 2016b). The limitations of this study included relatively low ionic strength (maximum ~0.4 molal) and a lack of data in Na-Mg-Cl solutions.

6.6.4.10 Americium Aqueous Speciation and Solubility Data

DOE provided a comparison of the +III actinide hydrolysis constants included in the WIPP model (DATA0.FM1 and DATA0.FM2), those selected by the NEA review (Guillaumont et al. 2003) and those reported by Neck et al. (2009) and showed that these constants were reasonably consistent (Patterson 2016b). However, there is a range of reported log K_s^0 values for $Am(OH)_3$(s) and $Nd(OH)_3$(s) (Table 6-16). In fact, Figure 1 in Patterson (2016b) shows that the predicted values fall into the lower end of the range of reported solubility data. The low $Am(OH)_3$(s) solubility used in the DATA0.FM1 and DATA0.FM2 databases results in an uncertainty distribution (Section 6.6.6) that demonstrates that the model underpredicts +III actinide solubilities.

Table 6-16. Log K_s^0 Values for $Am(OH)_3$(c), $Am(OH)_3$(am) and $Nd(OH)_3$(am)

Log K_s^0	Solid Phase	Investigation
14.49[a]	$Am(OH)_3$(s)	Könnecke et al. (1997) from Morss and Williams (1994)
15.6 ± 0.6	$Am(OH)_3$(c, aged)	Guillaumont et al. (2003)
16.9 ± 0.6	$Am(OH)_3$(am)	Guillaumont et al. (2003)
16.0 ± 0.4	$Nd(OH)_3$(c, aged)	Neck et al. (2009) from Diakonov et al. (1998)
17.2 ± 0.4	$Nd(OH)_3$(am)	Neck et al. (2009)

a – Solubility in DATA0.FM1 and DATA0.FM2

Xiong and Domski (2016b, Appendix B) cited uncertainty regarding the solid $Nd(OH)_3$(s) used in the Neck et al. (2009) solubility experiments as the reason for excluding the data in a re-parameterization of the EQ3/6 database. However, Neck et al. (2009) performed XRD analysis of the $Nd(OH)_3$(s) before and after the solubility experiments and determined that the solubility-limiting solid did not change during the experiments in chloride media up to 5.0 M NaCl and in 3.5 M $MgCl_2$ and 3.5 M $CaCl_2$. Neck et al. (2009) also noted that the solid phase did not appear to change during the experiments because the solubility remained constant after short and long equilibration periods. The measured $Nd(OH)_3$(s) solubility was found to be consistent with the solubility of $Am(OH)_3$(am), but this was reasonably explained by Neck et al. (2009) as the consequence of the solubility being controlled by less-crystalline surface material made up of smaller particles. The $Am(OH)_3$(s) solubility in DATA0.FM1 and DATA0.FM2 databases is

14.49, based on data obtain in NaCl solutions from Runde and Kim (1994) using solid material that was XRD amorphous. Guillaumont et al. (2003) performed a thorough review of $Am(OH)_3(s)$ solubilities and established solubilities for the amorphous solid equal to 16.9 ± 0.8 and for the crystalline, aged solid equal to 15.6 ± 0.8. Thus, the solubility of the amorphous material in the Runde and Kim (1994) experiments was less than the lower limit established for crystalline, aged $Am(OH)_3(s)$, which will likely lead to an underestimation of the +III actinide solubilities in WIPP brines.

EPA also recommends that DOE use the results of the Neck et al. (2009) investigation to update the WIPP database because this investigation: 1) was carried out using a well-characterized solid phase in high-ionic-strength solutions over a pcH range relevant to WIPP repository brines, 2) is consistent with earlier studies (including the solubility results of Runde and Kim 1994) and Pitzer parameters already included in the database (e.g., Könnecke et al. 1997), and 3) the parameters in this study represent a significant improvement over the existing database parameters because they were developed with data from $MgCl_2$ and $CaCl_2$ solutions as well as data from NaCl solutions.

Giambalvo (2002a, Table 2) cited Könnecke et al. (1997) as the source of an Am^{3+}- Cl^- C^ϕ value of -0.016 kg^2/mol^2. However, the Am^{3+}- Cl^- C^ϕ value in DATA0.FM1 and DATA0.FM2 is instead -0.0166 kg^2/mol^2. DOE should correct this value.

6.6.4.11 DATA0.FM2 Summary and Conclusions

Prior to accepting an updated database for the CRA-2019, EPA would like to see DOE do the following:

- Because of the uncertainties associated with the hydromagnesite solubility measured by Xiong (2011a) and the effects of the hydromagnesite solubility on actinide solubilities, EPA believes the database will be strengthened by including the solubility based on the Robie and Hemingway (1973)
- Acceptance of the borate, lead and $MgSO_4^0$ data added to DATA0.FM2 would require examination of all available data related to speciation, consideration of more recent data (e.g., Hinz et al. 2015) and evaluation of the analysis plan acceptance criteria, including the relative magnitude of the Pitzer parameters and an examination of the plot of the residual as a function of the parameters.
- Acceptance of the revised EDTA and citrate data in DATA0.FM2 would require a comprehensive review of literature data and evaluation of the analysis plan acceptance criteria
- As EPA previously stated during review of the PABC09 (Section 6.5.1), the Agency expects DOE to use the data provided by Altmaier et al. (2005, 2006) to develop aqueous speciation and Pitzer parameters for the Th(IV)-carbonate species
- It would be more appropriate to use the results of the Neck et al. (2009) $Nd(OH)_3(s)$ solubility study to update the WIPP database, which was also previously stated by EPA during review of the PABC09 (Section 6.5.1)

- The appendices attached to Xiong and Domski (2016b) indicate for several parameters that the difference between the documented parameters and those estimated using DATA0.FM2 did not exceed 10% even though for some, such as $\beta^{(0)}$ for Na^+ - $PbEDTA^{2-}$ and Mg^{2+} - $PbEDTA^{2-}$ and C^{ϕ} for Na^+ - $PbCit^-$, the differences exceeded 10%. EPA expects DOE to review these parameter differences and make the appropriate changes
- Xiong and Domski (2016b, Appendix A) excluded high ionic strength data from Felmy et al. (1991), Rai et al. 1997 and Neck et al. (2002) from consideration of the +IV actinide solubilities and aqueous speciation for parameterization of the WIPP EQ3/6 thermodynamic database. Because these data were included in development of the DATA0.FM1 and DATA0.FM2 databases, DOE should clarify whether these statements by Xiong and Domski (2016b) raise significant questions regarding the validity of the +IV solubility and aqueous speciation data in the DATA0.FM1 and DATA0.FM2 databases.

6.6.5 Results of Actinide Solubility Calculations

Brush and Domski (2013b) used EQ3/6 version 8.0a and the DATA0.FM1 database to calculate actinide solubilities with organic ligand concentrations (Table 6-1) calculated for the range of brine volumes that encompass the expected DBR volumes. The results for the minimum brine volume (17,400 m^3) and five times the minimum brine volume (87,000 m^3) are compared in Table 6-17. Five-fold variation in the brine volume and organic ligand concentrations affected Am(III) concentrations because of the predicted complexation of Am(III) by EDTA (Brush and Domski 2013b, Tables 11 and 12) and Np(V) concentrations were affected by variation in the organic ligand concentrations because of its predicted complexation by acetate and oxalate (Brush and Domski 2013b, Tables 9 and 10). Over the ranges of organic ligand concentrations predicted in the WIPP repository brines for the CRA-2014 PA, organic ligands had minimal effects on Th(IV) concentrations, and Th(IV) speciation is dominated by $Th(OH)_4(aq)$ and $Th(OH)_3CO_3^-$ (Brush and Domski 2013b, Tables 7 and 8).

DOE (Domski and Xiong 2015b) used EQ3/6 version 8.0a and the revised database DATA0.FM2 to predict actinide solubilities in WIPP repository brines as a function of brine volume. Predicted Am(III) concentrations were lower than calculated with DATA0.FM1 because of reduced complexation by EDTA, predicted Th(IV) concentrations were slightly lower than calculated with DATA0.FM1 because of lower carbon dioxide fugacities and reduced concentrations of $Th(OH)_3CO_3^-$ and predicted Np(V) concentrations were higher than calculated with DATA0.FM1. Because of unresolved questions regarding DATA0.FM2 (Section 6.6.4), the actinide solubility results calculated with DATA0.FM1 (Brush and Domski 2013b) were used as the baseline actinide solubilities in the sensitivity analysis PA calculations performed for the CRA-2014 (CRA14_SEN4 PA, Section 6.7).

Table 6-17. CRA-2014 PA Actinide Solubility Modeling Results Using 1× and 5× Brine Volumes[a] (Brush and Domski 2013b).

Brine	GWB		ERDA-6	
	1× Brine Volume	5× Brine Volume	1× Brine Volume	5× Brine Volume
pH (standard units)	8.82	8.82	8.99	9.02
pcH	9.54	9.54	9.69	9.72
Ionic Strength	6.44	6.41	5.99	5.94
Carbon dioxide fugacity (atm)	3.14×10^{-6}	3.14×10^{-6}	3.14×10^{-6}	3.14×10^{-6}
Sodium (M)	4.77	4.78	5.30	5.33
Potassium (M)	0.550	0.549	0.0960	0.0960
Magnesium (M)	0.330	0.313	0.136	0.111
Calcium (M)	0.0111	0.0113	0.0116	0.0119
Chloride (M)	5.36	5.39	5.24	5.26
Sulfate (M)	0.216	0.205	0.182	0.171
Total Carbon (M)	3.79×10^{-4}	3.80×10^{-4}	4.55×10^{-4}	4.75×10^{-4}
Boron (M)	0.186	0.186	0.0623	0.0624
Bromine (M)	0.0313	0.0313	0.0109	0.0109
Acetate (M)	0.0230	4.61×10^{-3}	0.0230	4.61×10^{-3}
Citrate (M)	2.33×10^{-3}	4.65×10^{-4}	2.33×10^{-3}	4.65×10^{-4}
EDTA (M)	7.40×10^{-5}	1.48×10^{-5}	7.40×10^{-5}	1.48×10^{-5}
Oxalate (M)	0.0118	2.36×10^{-3}	0.0118	2.36×10^{-3}
Am(III) (M)	2.59×10^{-6}	6.47×10^{-7}	1.48×10^{-6}	3.92×10^{-7}
Th(IV) (M)	6.05×10^{-8}	6.07×10^{-8}	7.02×10^{-8}	7.20×10^{-8}
Np(V) (M)	2.77×10^{-7}	1.82×10^{-7}	8.76×10^{-7}	6.44×10^{-7}
U(VI) (M)[b]	0.001	0.001	0.001	0.001
Solid Phases	Anhydrite, halite, brucite, hydromagnesite, phase 5, ThO_2(am), $KNpO_2CO_3$(s), $Am(OH)_3$(s), whewellite		Anhydrite, halite, brucite, hydromagnesite, ThO_2(am), $KNpO_2CO_3$(s), $Am(OH)_3$(s), whewellite, glauberite	
Output File Name	gwb_1x.6o	gwb_5x.6o	erda_1xb.6o	erda_5xb.6o

a – Calculations performed using EQ3/6 code and DATA0.FM1 database.

b – DOE did not develop a solubility model for the +VI actinides. Consequently, a fixed concentration was assumed for U(VI), which is the only +VI actinide predicted to be present in the WIPP repository in significant concentrations

6.6.6 Actinide Solubility Uncertainties

Brush and Domski (2013c) described the development of the uncertainty distributions for the CRA-2014 PA actinide solubilities. Am(III), Nd(III), Cm(III) and Th(IV) solubility studies were evaluated for calculating actinide solubility uncertainty distributions for Am(III) and Th(IV). A solubility uncertainty distribution was not developed for Np(V) because this uncertainty is not sampled for WIPP PA due to neptunium's insignificant effects on long-term WIPP performance. An uncertainty distribution also was not developed for the U(VI) solubility because a WIPP solubility model has not been developed for U(VI) and DOE instead uses a constant, upper-limit U(VI) concentration of 1×10^{-3} M for WIPP PA.

Brush and Domski (2013c) used criteria developed by Xiong et al. (2009a), to determine whether data from available solubility studies should be included in the uncertainty analysis. The data cutoff date in criterion G1 was modified to include data published through October 31, 2011. Brush and Domski (2013c) also included results from Borkowski et al. (2012) and Borkowski (2012b) because they were directed to do so by their management.

Brush and Domski (2013b) included as an additional criterion:

> G11. Include only results from experimental studies carried out under conditions at or close to those predicted for WIPP disposal rooms. Specifically, include only results from experiments in which: (1) I ≥ 3 molal or M, (2) pcH = 8.0 – 11.2, and (3) total inorganic carbon (TIC) = 0 – 0.014 M.

Criterion G11 extends Criterion S1 from Xiong et al. (2009a), which applied minimum ionic strength limits to the +IV actinide solubility data, to the +III actinide solubility data and adds pcH and TIC limits for both the +III and +IV data.

Brush and Domski (2013b) used three additional criteria during their data selection process that they linked to Criterion G9:

> A1: Include only results from GWB brine experiments with pcH ≤ 7.4 and include only results from ERDA-6 brine experiments with pcH ≤ 8.1 because Borkowski et al. (2009) determined that significant Nd(III) complexation by borate can occur at higher pcH in WIPP brines.
>
> A2: Include only +III actinide solubility results from concentrated $CaCl_2$ brine experiments with pcH < 10. This pcH limit is included because Neck et al. (2009) found that Cm(III) forms significant $Ca_x[Cm(OH)_y]^{2x+3-y}$ aqueous species at pcH > 10. Significant concentrations of these species are unlikely to form in WIPP repository brines because of the low calcium concentrations maintained by anhydrite precipitation.
>
> A3: Include only Th(IV) actinide solubility results from concentrated $CaCl_2$ brine experiments with pcH < 10. This limit is included because Brendebach et al. (2007) and Altmaier et al. (2008) found that significant concentrations of the $Ca_4[Th(OH)_8]^{4+}$ form in concentrated $CaCl_2$ solutions at pcH > 10. Significant concentrations of this species are unlikely to form in WIPP repository brines because of the low calcium concentrations maintained by anhydrite precipitation.

Criterion G1 establishes the range of publication dates for the peer-reviewed literature and reports considered for the Am(III) and Th(IV) solubility uncertainty distributions. EPA (2010b) noted during review of the CRA-2009 PABC that establishing January 1, 1990 as the starting date for a literature search may be practical, but using an arbitrarily selected date to remove previously identified solubility data (Silva 1982) from the uncertainty distribution evaluation is unjustified (Section 6.5.5.2).

Criteria G2 through G10 and S1 were previously used for the CRA-2009 PABC and EPA (2010b), for the most part, accepted these criteria. However, EPA did not accept exclusion of +III actinide solubility data in WIPP brines above pcH 7.4 (GWB) and above pcH 8.1 (ERDA-6) during review of the CRA-2009 PABC (Section 6.5.5.2). EPA reiterated their disagreement in Comment 3-C-4 (Edwards 2015c), noting that application of Criterion G9 was only appropriate for species that are not present in WIPP brines. Accepting that the WIPP thermodynamic database cannot be used to model higher-pcH brines containing borate would be an admission that the database cannot be used to adequately model WIPP repository brines, which contain 0.0623 M (ERDA-6) to 0.186 M (GWB) borate and are predicted to have pcH values of 9.5 to 9.7 (Table 6-17). The +III actinide solubilities obtained in higher-pcH experiments with borate-containing brine should be included in the actinide solubility uncertainty calculations to account for possible underestimation of +III actinide solubilities due to the lack of Am(III)-borate species in the WIPP thermodynamic database. All +III actinide solubility data in WIPP brines with pcH 8.0 – 11.2 that meet the other criteria should be included in the uncertainty evaluation (Edwards 2015c, Comment 3-C-4). Accordingly, Criterion A1 should be omitted from the data selection process and Criterion G9 should be revised as described in Section 6.7.1.

Criterion G11 specifies that only experiments conducted under ionic strength, pcH and TIC conditions similar to WIPP repository brines should be included in the calculation of the actinide solubility uncertainty distributions. Limiting the selected solubility studies to those with conditions similar to anticipated WIPP repository brine conditions is likely to provide a more reasonable assessment of the actinide solubility uncertainty distributions. For example, during review of the CRA-2009 PABC, EPA noted that some measured +III actinide solubilities at relatively low pcH values were systematically less than the corresponding calculated solubilities; including the lower-pcH data with these consistent differences between measured and predicted solubilities would tend to underestimate the mean +III actinide solubility uncertainty.

The Criterion G11 pcH and ionic strength limitations appear reasonable and do not systematically exclude specific categories of data. However, because TIC was limited to 0 – 0.014 M, no Th(IV) solubilities measured with any carbonate in solution were included in the calculation of the CRA-2014 PA Th(IV) solubility uncertainty distribution (Brush and Domski 2013c). In addition, only a single solubility measurement in a solution containing carbonate from Rao et al. (1999) was included in the Am(III) solubility uncertainty distribution calculation because of the limits on pcH for solubility measurements in WIPP brines (Criterion A1). Although TIC will be constrained to low concentrations by reaction with the MgO backfill, carbonate and bicarbonate are predicted to be present in WIPP brines at concentrations ranging from 3.79×10^{-4} M to 4.75×10^{-4} M (Table 6-17). At these TIC concentrations, CRA-2014 PA calculations predicted 25 – 34% of total aqueous Th(IV) will be present in the form of $Th(OH)_3CO_3^-$. During review of the PABC09, EPA noted that Th(IV) solubilities measured in 4 M NaCl solutions with TIC of 0.02 M (Altmaier et al. 2006) were consistently higher than

predicted by WIPP geochemical modeling calculations (Section 6.5.5.1). Excluding the Altmaier et al. (2006) data excludes all available, high-ionic-strength Th(IV) solubility data obtained with nonzero TIC concentrations. Consequently, the upper limit on TIC in Criterion G11 for both the +III and +IV actinide solubility uncertainty determination should be revised upward to 0.02 M.

Criteria A2 and A3 are adequately supported based on the currently available data showing that the $Ca_x[Cm(OH)_y]^{2x+3-y}$ and $Ca_4(Th(OH)_8)^{4+}$ species are unlikely to form in WIPP repository brines because of relatively low calcium concentrations (Altmaier et al. 2008, Neck et al. 2009). Criterion S1 is redundant, because Criterion G11 addresses both the +III and +IV actinides. The revised criteria based on the current review of Brush and Domski (2013c) are summarized in Section 6.7.1.

6.6.6.1 +IV Actinide Solubility Uncertainty Distribution

Brush and Domski (2013c) identified 64 solubility measurements for calculation of the Th(IV) uncertainty distribution:

- 40 values from Borkowski et al. (2012) and Borkowski (2012b)
- 18 values from Felmy et al. (1991)
- 6 values from Altmaier et al. (2004)

Selection of the solubilities measured by Borkowski et al. (2012b) is contrary to Criterion G7, because the solid phases in the experiments were not characterized. As a result, the Borkowski et al. (2012b) data should have been excluded from the evaluation. The samples from Felmy et al. (1991) met the selection criteria and were appropriately included in the uncertainty evaluation. The six measurements from solubility experiments with amorphous hydrated thorium oxyhydroxide reported by Altmaier et al. (2004, Figure 2) were unfiltered and uncentrifuged samples. Including these samples is inconsistent with Criterion G5 because no phase separation was performed and the solutions undoubtedly contained Th(IV) colloids. Table 6-8 compares the results of the CRA-2014 uncertainty distribution to the 2009-CRA distribution. The positive mean and median values suggest a tendency for the CRA-2014 +IV actinide solubility model to predict Th(IV) solubilities less than the measured solubilities.

6.6.6.2 +III Actinide Solubility Uncertainty Distribution

Brush and Domski (2013c) used 172 solubility measurements to determine the Am(III) solubility uncertainty distribution:

- 109 values from Borkowski et al. (2009), Borkowski et al. (2010) and Borkowski (2012a)
- 56 values from Neck et al. (2009)
- 6 values from Runde and Kim (1994)
- 1 value from Rao et al. (1999)

The solubility measurements from Neck et al. (2009), Runde and Kim (1994) and Rao et al. (1999) met the selection criteria and were appropriately included in the Am(III) solubility uncertainty distribution calculations.

The majority of the solubility measurements used to calculate the Am(III) solubility uncertainty distribution were from Borkowski et al. (2009). As noted during review of the PABC09, inclusion of the Nd(III) solubility data from Borkowski et al. (2009) in the uncertainty analysis is inconsistent with Criterion G7 because only indirect means were used to characterize the solid phases and modeling calculations during the PABC09 review predicted different solid phases than those indirectly determined under some conditions (Section 6.4.4.5). Including the Borkowski et al. (2009) data in the uncertainty evaluation significantly decreases the mean concentration of the +III actinides used in PA and would lead to non-conservative predicted +III actinide concentrations. EPA stated during the CRA-2014 PA review that DOE must recalculate the Am(III) uncertainty distribution and exclude the Borkowski et al. (2009) data (Edwards 2015c, Comment 3-C-5). DOE acknowledged that the Borkowski et al. (2009) data does not meet Criterion G7 and that its large number of solubility measurements may have inordinately affected the uncertainty distribution (Shrader 2016). Table 6-8 compares the results of the uncertainty distribution in comparison to the 2009-CRA uncertainty distribution. The negative mean and median values suggests a tendency towards predicting Am(III) solubilities that are higher than measured values.

6.7 CRA14_SEN4 PA DISSOLVED ACTINIDE SOURCE TERM

EPA requested that DOE perform a limited sensitivity study of the CRA-2014 PA (Werner 2016). For this PA (CRA14_SEN4 PA), EPA requested DOE use the baseline actinide solubilities calculated for the CRA-2014 PA with the DATA0.FM1 database (Table 6-17) with Am(III) and Th(IV) solubility uncertainty distributions developed using data identified by EPA (Peake 2016b). EPA also requested that DOE use a GLOBAL:PBRINE[17] distribution provided by EPA (EPA 2017), a modified lower bound for the sampled TAUFAIL[18] distribution for the 50% degraded waste, a corrected version of the DRSPALL code[19] and a corrected representative length of the furthest northern set of panel closures (Werner 2016).

6.7.1 Revised Selection Criteria for Am(III) and Th(IV) Actinide Solubility Uncertainty Distributions

The selection criteria Brush and Domski (2013c) developed were revised to accommodate the later date of the CRA14_SEN4 PA (Criterion G1), to address the presence of borate in WIPP brines (revision of Criterion G9 and deletion of Criterion A1) and to increase the TIC concentration limit for included solubility data (Criterion G11). Criterion S1 was eliminated as redundant, because Criterion G11 addresses both the +III and +IV actinides. Criterion G7 was edited to remove an obsolete reference to the FMT database, because the FMT code and database have been replaced by the EQ3/6 code and database.

The revised criteria used to evaluate and select solubility data for inclusion in the Am(III) and Th(IV) actinide solubility distribution calculations for the CRA14_SEN4 PA are:

[17] Parameter representing the probability that a drilling intrusion into the excavated region of the repository encounters a region of pressurized brine below the repository

[18] Effective shear strength for erosion of waste

[19] The DRSPALL code is used to calculate spallings releases

G1: (revised): Include only results from experimental studies published by December 31, 2012.

G2: Include results from papers published in peer-reviewed journals and from unpublished reports (e.g., officially released reports from government laboratories such as Los Alamos National Laboratory, Lawrence Livermore National Laboratory, Pacific Northwest National Laboratory, etc.).

G3: Include only results from solubility studies. Exclude other studies that do not provide solubilities (e.g., studies of corrosion, leaching, sorption, or transport).

G4: Include only results from studies in which water was the solvent. Exclude studies in which other solvents were used (e.g., solids, molten metal or salts, or organic liquids).

G5: Include only results obtained from studies at pressures at or close to atmospheric, at temperatures at or close to those expected in the WIPP (i.e., 20-30°C), and with posttest phase-separation methods similar to those used for the WIPP, because these were the conditions and methods used to parameterize the Th(IV) and Am(III) speciation and solubility models for WIPP compliance-related PA calculations.

G6: Include only results from studies of Th(IV), Nd(III), Am(III), and Cm(III) because these elements were used to parameterize the WIPP Th(IV) and Am(III) solubility models. Exclude studies of U(IV), Np(IV), Pu(IV) and Pu(III) because there could be systematic differences between the solubilities of these elements and those of their oxidation-state analogs used to parameterize the models and because the difficulties inherent in maintaining these elements in these oxidation states could introduce experimental artifacts in the results obtained with these elements.

G7: (revised): Include only results from studies with a characterized solubility-controlling solid for which solubility data is in the WIPP Th(IV) or Am(III) model (currently the DATA0.FM1 database), and in which the quantity of solid initially present was sufficient to prevent complete dissolution of this solid during the experiments.

G8: Include only results from studies with aqueous solutions of known composition. Exclude studies performed with groundwaters, sedimentary pore waters, and soil solutions that may contain unknown quantities of species that can be complexants or adsorbents (e.g., humic acids or other dissolved organic compounds, microbial colloids, or pseudocolloids).

G9: (revised): Include results from studies with dissolved elements or species that are present in WIPP brines. Exclude studies with dissolved elements or species that are absent in WIPP repository brines and for which our models do not include association/dissociation constants or Pitzer parameters.

G10: Include only results from studies for which the investigators provided a complete description of their experiments and the original solubilities. Exclude literature reviews and summaries, and studies in which the authors only provided average dissolved

concentrations or solubility products, thus necessitating back calculation of the solubilities.

G11: (revised). Include only results from experimental studies carried out under conditions at or close to those predicted for WIPP disposal rooms. Specifically, include only results from experiments in which: (1) I ≥ 3 molal or M, (2) pcH = 8.0 – 11.2, and (3) total inorganic carbon (TIC) = 0 – 0.02 M.

A2: Include only +III actinide solubility results from concentrated $CaCl_2$ brine experiments with pcH < 10. This pcH limit is included because Neck et al. (2009) found that Cm(III) forms significant $Ca_x[Cm(OH)_y]^{2x+3-y}$ aqueous species at pcH > 10. Significant concentrations of these species are unlikely to form in WIPP repository brines because of the low calcium concentrations maintained by anhydrite precipitation.

A3: Include only Th(IV) actinide solubility results from concentrated $CaCl_2$ brine experiments with pcH < 10. This limit is included because Brendebach et al. (2007) and Altmaier et al. (2008) found that significant concentrations of the $Ca_4[Th(OH)_8]^{4+}$ form in concentrated $CaCl_2$ solutions at pcH > 10. Significant concentrations of this species are unlikely to form in WIPP repository brines because of the low calcium concentrations maintained by anhydrite precipitation.

6.7.2 Th(IV) Uncertainty Data Selection

The following discussion provides an explanation of data included by EPA in the CRA14_SEN4 PA calculation of the Th(IV) solubility uncertainty distribution (Table 6-18) and compares the selected data to the CRA-2014 PA calculation data set (Brush and Domski 2013c). Brush and Domski (2013c) included 18 samples from amorphous ThO_2(s) experiments in 3 M NaCl from Felmy et al. (1991) that met their criteria (Section 6.6.6.1). These samples met the revised criteria (Section 6.7.1) and were included in the Th(IV) solubility uncertainty distribution calculation.

Brush and Domski (2013c) included six unfiltered and uncentrifuged samples from solubility experiments with amorphous hydrated thorium oxyhydroxide reported by Altmaier et al. (2004). Including these samples is inconsistent with Criterion G5 because phase separation was not performed and these solutions undoubtedly contained Th(IV) colloids. Colloidal Th(IV) was removed by ultracentrifugation in five samples each from experiments carried out in 5 M NaCl and 2.5 M $MgCl_2$ (Altmaier et al. 2004); these samples were included in the Th(IV) uncertainty distribution calculation. However, ultracentrifugation was insufficient to remove Th(IV) colloids from experiments carried out in 4.5 M $MgCl_2$. Altmaier et al. (2004) reported summary Th(IV) solubility data in 4.5 M $MgCl_2$ at pcH 8.9 based on 2 nm (10 kD) filtration, but did not report the primary data. Consequently, EPA excluded the 4.5 M $MgCl_2$ data based on Criterion G10.

Altmaier et al. (2006) investigated the solubility of amorphous $Th(OH)_4$(s) or $ThO_2 \cdot xH_2O$(s) in $NaHCO_3$-Na_2CO_3-NaCl solutions and reported twelve solubilities with TIC equal to 0.02 M and ionic strength of 4.0 M. Brush and Domski (2013c) excluded these data because the $Th(OH)_y(CO_3)_z^{4-y-z}$ complexes found to be important by Altmaier et al. (2006) are not in the

WIPP Th(IV) model. Based on the revised Criteria G9 and G11, EPA included these solubilities in the calculation of the Th(IV) solubility uncertainty distribution.

Altmaier et al. (2008) reported four solubility results for amorphous $ThO_2 \cdot xH_2O(s)$ at pcH less than 10 in 5.26 M $CaCl_2$. Brush and Domski (2013c) excluded the results based on the use of ultracentrifugation for phase separation. However, Altmaier et al. (2008) performed both ultracentrifugation and ultrafiltration and reported no difference between the two phase-separation methods. EPA therefore included these four solubilities at pcH less than 10 in 5.26 M $CaCl_2$.

Brush and Domski (2013c) included Th(IV) solid solubility data from Borkowski et al. (2012) and Borkowski (2012b) in their determination of the Th(IV) solubility uncertainty distribution. These data comprised 40 of the 64 samples used by Brush and Domski (2013c) for the Th(IV) uncertainty distribution (Section 6.6.6.1). However, as they noted, the solid phases were not characterized in the Borkowski et al. (2012b) experiments and these samples were excluded by EPA based on Criterion G7.

Exclusion of the Borkowski et al. (2012b) experimental data results in fewer samples in the data set for calculating the CRA14_SEN4 PA Th(IV) solubility uncertainty distribution than was used for the CRA-2014 PA (Table 6-18). However, the updated CRA14_SEN4 PA data set: 1) is less reliant on a single investigation, 2) includes only samples with post-test phase separation by filtration or ultracentrifugation and 3) includes some samples from solubility experiments carried out with low carbonate concentrations in the experimental solution.

Table 6-18. Th(IV) Uncertainty Distribution Data Evaluation

Solubility Study	CRA-2014 PA	CRA14_SEN4 PA
Felmy et al. (1991)	18 samples in 3 M NaCl, $8.0 \leq$ pcH ≤ 11.2	18 samples in 3 M NaCl, $8.0 \leq$ pcH ≤ 11.2
Altmaier et al. (2004)	six uncentrifuged samples, two each in 5 M NaCl, 2.5 M $MgCl_2$ and 4.5 M $MgCl_2$	10 ultracentrifuged samples, five in 5 M NaCl and five in 2.5 M $MgCl_2$
Altmaier et al. (2006)	no samples	12 samples in 4 M NaCl with 0.02 M TIC
Altmaier et al. (2008)	no samples	4 samples in 5.26 M $CaCl_2$ with pcH < 10
Borkowski et al. (2012), Borkowski (2012b)	40	no samples
Total Samples	64[20]	44

[20] DOE (2014b) stated in the caption of Figure SOTERM-31 that 45 measured and predicted solubilities were compared for Th(IV); however, the histogram in Figure SOTERM-31 contains 64 values, which is consistent with the number of measured and predicted solubilities reported by Brush and Domski (2013c).

6.7.3 Am(III) Uncertainty Data Selection

Brush and Domski (2013c) summarized the results of DOE's screening of available Am(III), Nd(III) and Cm(III) solubility data for calculation of the CRA-2014 PA Am(III) solubility uncertainty distribution. EPA reached the same conclusions as DOE for many of the excluded studies based on the revised criteria (Section 6.7.1). The following discussion provides an explanation of data included in the CRA14_SEN4 PA calculation of the Am(III) solubility uncertainty distribution and compares the selected data to the data selected by Brush and Domski (2013c) in the CRA-2014 PA.

Brush and Domski (2013b) excluded solubility data from Silva (1982) because of its pre-1990 publication date. Although its publication date is not a valid reason for its exclusion, the Silva (1982) $Am(OH)_3(s)$ and $Nd(OH)_3(s)$ solubility results were obtained in low ionic strength solutions (0.1 M $NaClO_4$) and EPA appropriately excluded these data based on Criterion G11 (Section 6.7.1).

Brush and Domski (2013c) excluded the Khalili et al. (1994) amorphous $Nd(OH)_3 \cdot xH_2O(s)$ solubility results obtained in WIPP G-Seep brine at pcH 8.4 because of possible Nd(III)-borate complexation at this pcH. Based on the revised Criterion G9 (Section 6.7.1), these data were included in the CRA14_SEN4 calculation of the Am(III) solubility uncertainty distribution (Table 6-19).

Table 6-19. Am(III) Uncertainty Distribution Data Evaluation

Solubility Study	CRA-2014 PA	CRA14_SEN4 PA
Khalili et al. (1994)	no samples	26 samples in G-Seep brine at pcH 8.4
Runde and Kim (1994)	six samples in carbonate-free 5 M NaCl	11 samples in carbonate-free 5 M NaCl
Rao et al. (1999)	one sample in ERDA-6 brine	15 samples in ERDA-6 brine from pcH 8.05 to 9.55
Borkowski et al. (2009), Borkowski (2010)	100 samples in 5 M NaCl, six samples in ERDA-6	no samples
Neck et al. (2009)	eight samples in 5 M NaCl, eight samples in 1 M $MgCl_2$, eight samples in 3 M $MgCl_2$, nine samples in 1 M $CaCl_2$, and 23 samples in 3 M $CaCl_2$	eight samples in 5 M NaCl; eight samples in 1 M $MgCl_2$, eight samples in 3 M $MgCl_2$, nine samples in 1 M $CaCl_2$, and 23 samples in 3 M $CaCl_2$
Borkowski et al. (2010), Borkowski (2012a)	three samples in 3 – 5 M NaCl with $Na_2B_4O_7$	no samples
Total Samples	172	108

Brush and Domski (2013c) included six samples from Runde and Kim (1994) experiments with $Am(OH)_3(s)$ in 5 M NaCl. EPA's examination of Runde and Kim (1994, Figure 5.17) shows that there were 11 samples from the 5 M NaCl experiments within the appropriate pcH range (8 –

11.2) and included these data. Brush and Domski (2013b) excluded data Runde and Kim (1994) reported for experiments conducted at P_{CO2} of 0.01 atm because the reported solid phase [$Am_2(CO_3)_3(s)$] is not in the WIPP database. Because of the high TIC concentrations in these experiments and the absence of $Am_2(CO_3)_3(s)$ in the WIPP database, EPA also excluded these data from the CRA14_SEN4 PA calculations.

Brush and Domski (2013c) included one sample from $NaNd(CO_3)_2 \cdot xH_2O(c)$ solubility experiments from Rao et al. (1999), with all other samples excluded because of high TIC (Criterion G11) or because the pcH in the G-Seep brine (similar to GWB) or ERDA-6 brine exceeded the estimated pcH limit established to eliminate possible borate complexation of Am(III) (Criterion A1). Using the revised criteria (Section 6.7.1), 15 samples from solubility experiments in ERDA-6 brine carried out with $P_{CO2} = 10^{-3.5}$ atm had TIC concentrations less than or equal to 0.02 M, and these samples were included in the calculation of the CRA14_SEN4 PA Am(III) solubility uncertainty distribution.

Brush and Domski (2013c) included 106 samples from Nd(III) experiments in 5 M NaCl, GWB and ERDA-6 brines (Borkowski et al. 2009, Borkowski 2010) and three samples from Nd(III) solubility experiments in 3 – 5 M NaCl solutions with sodium tetraborate. EPA excluded these samples from the Am(III) solubility uncertainty calculation because the post-test solid phases were not characterized (Criterion G7).

Brush and Domski (2013c) selected a total of 56 samples from the $Nd(OH)_3(c)$ solubility experiments from Neck et al. (2009) in concentrated NaCl, $MgCl_2$ and $CaCl_2$ solutions. These solubility data meet the revised criteria (Section 1.2) and EPA included them in the Am(III) solubility uncertainty distribution calculation.

Hinz et al. (2012) reported the results of amorphous $Nd(OH)_3(s)$ solubility experiments in 5 M NaCl and 3.5 M $CaCl_2$ solutions with up to 0.04 M borate. This study was published after the October 31, 2011 cut-off date Brush and Domski (2013c) established and before the December 31, 2012 cut-off date established for the CRA14_SEN4 PA. Hinz et al. (2012) stated that the solid phase was amorphous $Nd(OH)_3(s)$ and reported the results of post-test phase characterization. However, because of the preliminary nature of this investigation, which was reported in conference proceedings, these data were not included in the CRA_SEN414 PA Am(III) solubility uncertainty calculation.

Exclusion of the Borkowski et al. (2009, 2010) data resulted in a smaller number of solubilities in the data set for the CRA14_SEN4 PA calculation of the Am(III) solubility uncertainty than the number used for the CRA-2014 PA (Table 6-19). However, the revised data set is less reliant on a single study and includes a subset of data performed with borate and/or low TIC concentrations in the experimental solutions.

6.7.4 CRA14_SEN4 Th(IV) Solubility Uncertainty Results

Xiong and Domski (2016a) reported the results of the Th(IV) solubility uncertainty distribution calculations for the CRA14_SEN4 PA. Table 6-8 compares the statistical properties of this distribution to previous WIPP PAs. The mean and median values calculated for the Th(IV) solubility uncertainty distribution are close to zero, indicating that there is no general tendency

toward under- or over-prediction of the measured Th(IV) solubility measurements. The effects of the Th(IV) CRA14_SEN4 PA solubility uncertainty distribution on total mobilized +IV actinide concentrations are discussed in Section 8.0.

The statistics associated with Th(IV) solubility data from the individual investigations are summarized in Table 6-20. The agreement between the modeled solubilities and solubilities measured by Felmy et al. (1991) is expected, because Giambalvo (2002c) included these data in the derivation of the thorium solubility and speciation data in DATA0.FM1. Measured and modeled Th(IV) solubilities are also in good agreement for the four samples obtained from solubility experiments in concentrated $CaCl_2$ solutions below pH 10 (Altmaier et al. 2008). The geochemical model appears to consistently predict Th(IV) concentrations that exceeded measured concentrations in experiments in concentrated NaCl and $MgCl_2$ (Altmaier et al. 2004). This consistent difference may be related to the higher ionic strengths in the Altmaier et al. (2004) experiments or to more effective removal of nanoscale colloids by ultracentrifugation used by Altmaier et al. (2004) than the 1.8 nm filtration used by Felmy et al. (1991). The Th(IV) solubilities measured by Altmaier et al. (2006) in concentrated NaCl solutions with 0.02 M TIC are consistently higher than predicted using the geochemical model. This result indicates that the reevaluation of the thorium-carbonate speciation is recommended.

Table 6-20. Comparison of Th(IV) Difference Value Statistics Calculated for the CRA14_SEN4 PA and Individual Investigations

Data	Mean	Median	Standard Deviation	Maximum	Minimum	Number
Felmy et al. (1991)	-0.12	-0.21	0.53	0.75	-0.80	18
Altmaier et al. (2004)	-0.93	-0.80	0.51	-0.40	-2.01	10
Altmaier et al. (2006)	0.97	0.84	0.23	1.43	0.73	12
Altmaier et al. (2008)	-0.17	-0.26	0.37	0.39	-0.56	4
CRA14_SEN4	-0.11	-0.09	0.82	1.43	-2.01	44

6.7.5 CRA14_SEN4 Am(III) Solubility Uncertainty Results

Xiong and Domski (2016a) described the results of the Am(III) solubility uncertainty distribution calculations for the CRA14_SEN4 PA. Table 6-8 compares the statistical properties of this distribution to previous WIPP PAs. The mean and median of the Am(III) difference values are positive, indicating that the model generally predicts Am(III) concentrations that are lower than the measured solubilities. The effects of the Am(III) CRA14_SEN4 PA solubility uncertainty distribution on total mobilized +III actinide concentrations are discussed in Section 8.0.

The difference value statistic for the Runde et al. (1994) $Am(OH)_3(s)$ solubility data shows that the model tends to predict slightly higher solubilities than the concentrations measured in the experiments (Table 6-21). This result is consistent with the evaluation Giambalvo (2002a) carried out during selection of the DATA0.FM1 Am(III) parameters.

The Khalili et al. (1994) solubility experiments were carried out at pcH 8.4 in G-Seep brine, a Salado brine formulation with 0.144 M borate (Brush 1990) that is similar to GWB. Brush and Domski (2013c) used their Criterion A1 to screen out the Khalili et al. (1994) data because of

postulated complexation of +III actinides at pcH values greater than 7.4. However, the near-zero mean and median difference values for the Khalili et al. (1994) data shows that the model-predicted Am(III) solubilities at this pcH are in excellent agreement with the measured concentrations.

Criterion G11 from Brush and Domski (2013c) resulted in exclusion of all but one of the Rao et al. (1999) solubility measurements from experiments conducted in ERDA-6 brine, because TIC concentrations exceeded the limit of 0.014 M. Revising the TIC concentration upper limit to 0.02 M resulted in the inclusion of 15 solubility measurements from Rao et al. (1999). Even with the higher upper limit for TIC concentrations and the inclusion of samples with pcH values in excess of the Criterion A1 upper limit of 8.1 for ERDA-6 brine, the mean and median difference values for the Rao et al. (1999) data are close to zero. This small difference value for the Rao et al. (1999) solubility data indicates that borate complexation at pcH greater than 8.1 (Criterion A1) does not cause increased difference values.

Table 6-21. Comparison of Am(III) Difference Value Statistics Calculated for the CRA14_SEN4 PA and Individual Investigations

Data	Mean	Median	Standard Deviation	Maximum	Minimum	Number
Runde et al. (1994)	-0.45	-0.44	0.41	0.22	-1.14	11
Khalili et al. (1994)	-0.04	-0.04	0.16	0.42	-0.27	26
Rao et al. (1999)	-0.24	-0.20	0.29	0.16	-0.81	15
Neck et al. (2009)	1.11	1.22	0.87	2.97	-0.69	56
CRA14_SEN4	0.48	0.07	0.93	2.97	-1.14	108

Neck et al. (2009) measured higher $Nd(OH)_3(s)$ solubilities than previous investigations (Table 6-16). This higher solubility and resulting positive difference values are likely related to the amorphous nature of the solubility-controlling material in the experiments. Consequently, including the Neck et al. (2009) data in the difference value calculations accounts for the possible persistence of amorphous +III actinide hydroxide solids in the repository.

6.8 ACTINIDE SOURCE TERM SUMMARY AND CONCLUSIONS

Dissolved actinide source term concentrations are calculated using the Dissolved Actinide Source Term and Chemical Conditions conceptual models. These source term concentrations and the associated uncertainties influence dissolved and colloidal actinide concentrations (Section 7.0) in WIPP brines. Actinide concentrations in WIPP brines affect potential releases from the repository through DBR and through the Culebra. EPA has reviewed the CRA-2014 calculations of the dissolved actinide source term and concludes:

- Calculations of the CRA-2014 PA dissolved actinide source term concentrations were carried out with no revisions to the Dissolved Source Term or Chemical Conditions conceptual model
- WIPP inventory concentrations of curium and neptunium are low and are insignificant to repository releases through DBR or through the Culebra

- The cement inventory will not significantly affect brine pH because of the presence of sufficient magnesium in brine and Salado minerals
- Comparison of modeling calculations with measured brine compositions during titration to higher pcH indicate additional data are required to improve the modeling of magnesium and borate concentrations in WIPP brines at pcH 9.5 and greater
- DOE calculated organic ligand concentrations as a function of the brine volume and used these concentrations to calculate baseline actinide solubilities. This approach accounts for possible dilution of the organic ligands in larger brine volumes and is adequately justified. This change in calculation of the actinide solubilities mainly affects the dissolved concentrations of +III actinides
- U(VI) concentrations in WIPP brines continue to be fixed at 1.0×10^{-3} M and no evidence has been presented that would justify changing this concentration
- The EQ3/6 geochemical modeling code has replaced the FMT code for solubility calculations, and DOE converted the FMT database for use with the EQ3/6 code. DOE added the solubility data for phase 5, a Mg-chloride-hydroxide-hydrate solid phase that forms in Salado brines to create the database DATA0.FM1, which was used for the CRA-2014 PA actinide solubility calculations
- During the CRA-2009 review, EPA expected DOE to update the +III actinide solubility data in the WIPP thermodynamic database to account for the results of Neck et al. (2009) and to update the Th(IV)-carbonate speciation in the database to account for data from Altmaier et al. (2005, 2006). DOE did not update the EQ3/6 thermodynamic database to account for these data showing the thermodynamic database continues to be deficient
- In response to EPA comments regarding recent data for borate aqueous speciation, hydromagnesite solubility and EDTA aqueous speciation, DOE created an updated datablase (DATA0.FM2) that included changes to these data as well as changes to citrate, magnesium-sulfate, and lead aqueous speciation and solubility data. EPA's preliminary review indicates more work will need to be performed on this database prior to the Agency's acceptance. Additionally, EPA's acceptance of this new database will require a thorough review of the data.
- The relatively low hydromagnesite solubility in the revised DATA0.FM2 database is inconsistent with literature data. EPA would like this value revised back to the Robie and Hemingway (1973) solubility used in previous WIPP actinide solubility calculations
- EPA found inconsistencies in DOE's selection of +III and +IV actinide solubility data used to calculate the CRA-2014 PA actinide solubility uncertainty distributions. EPA developed a defensible set of criteria for selecting data for the actinide solubility uncertainty distribution calculations and used these criteria to identify appropriate +III and +IV actinide solubility data for these calculations. Recalculating the +III and +IV actinide solubility data using the revised data set had significant effects on the uncertainty distributions and would increase mean and median +III actinide solubilities and decrease mean and median +IV actinide solubilities relative to the concentrations used in the CRA-2014 PA.

7.0 COLLOIDAL ACTINIDE SOURCE TERM

The Colloidal Actinide Source Term conceptual model was peer reviewed prior to the CCA PA and PAVT and found to be adequate, if somewhat conservative (Wilson et al. 1996a). This conceptual model and its implementation were unchanged for the CCA PAVT, PABC04 and PABC09. The colloidal actinide source term was unchanged from the CCA PA until the CRA-2014 PA.

Four types of colloids can form in the WIPP repository and influence the Actinide Source Term:

- Microbial colloids
- Humic colloids
- Intrinsic colloids
- Mineral fragment colloids

DOE described these four types of colloids in the CCA (DOE 1996, Appendix SOTERM, Section 6.1.2). Microbial colloids may act as substrates for actinide sorption, or they may intracellularly bioaccumulate actinides. Humic substances are relatively small organic compounds (less than 100,000 atomic mass units) and are often powerful substrates for uptake of metal cations. Intrinsic colloids are hydrophilic actinide macromolecules that may in some cases mature into larger hydrophobic mineral fragment colloids. Mineral fragment colloids are hydrophobic, hard-sphere amorphous or crystalline solids. Mineral fragment colloids may act as substrates for actinide sorption, or may consist of precipitated or coprecipitated actinide solids.

The concentrations of mineral fragment colloids and actinide intrinsic colloids used in WIPP PA are constant values (Table 7-1) and are represented by the parameters CONCMIN and CONCINT, respectively. Actinide concentrations associated with humic substances are calculated by multiplying the dissolved actinide concentration by a proportionality constant (parameters PHUMSIM for Salado brine and PHUMCIM for Castile brine), with the total humic colloid actinide concentration limited by a maximum value (parameter CAPHUM, Table 7-2). Actinide concentrations associated with microbial colloids are also based on proportionality constants (parameter PROPMIC), with assigned upper limits on the actinide concentrations associated with microbial colloids (parameter CAPMIC, Table 7-3).

7.1 MINERAL FRAGMENT COLLOIDS

DOE (1996) did not explicitly state a size range for mineral fragment colloids, but did assume a diameter range of 1 nm to 1 μm during particle surface area calculations used to derive the mineral fragment concentrations used in PA (DOE 1996, Appendix SOTERM, Section 6.3.1.2). Mineral fragment colloid parameters(CONCMIN) have not changed since the original CCA.

The concentrations of actinides associated with mineral fragment colloids, also called pseudocolloids, were determined for the CCA PA from experiments that measured their kinetic stability in WIPP-relevant brines and estimates of adsorption site densities. These experiments were carried out using a variety of minerals or materials (Papenguth 1996). The actinide concentrations from mineral fragment colloids developed for the CCA PA have been used in all WIPP PAs (Table 7-1). At the time the experiments were designed, MgO backfill was not

included in the repository design, so formation of mineral fragment colloids from MgO and its reaction products was not investigated. A triangular distribution spanning one order of magnitude about the geometric mean was developed for mineral fragment colloid concentrations, but this distribution was not sampled for PA. Instead, the maximum parameter values were used (DOE 1996, Appendix SOTERM, Section 6.3.1.2).

Table 7-1. Actinide Concentrations Associated with Mineral Fragment and Intrinsic Colloids

	Mineral Fragment Colloids (M) (Parameter CONCMIN)	**Intrinsic Colloids (M) (Parameter CONCINT)**	
Actinide	CCA PAVT, PABC04, PABC09, CRA-2014 PA and CRA14_SEN4	CCA PAVT, PABC04 and PABC09	CRA-2014 PA and CRA14_SEN4
Th(IV)	2.6×10^{-8}	0.0	2×10^{-8}
U(IV)	2.6×10^{-8}	0.0	2×10^{-8}
U(VI)	2.6×10^{-8}	0.0	3×10^{-8}
Np(IV)	2.6×10^{-8}	0.0	2×10^{-8}
Np(V)	2.6×10^{-8}	0.0	Not determined
Pu(III)	2.6×10^{-8}	0.0	2×10^{-8}
Pu(IV)	2.6×10^{-8}	1.0×10^{-9}	2×10^{-8}
Am(III)	2.6×10^{-8}	0.0	4×10^{-9}

Source: DOE 1996, Appendix SOTERM, Table SOTERM-14 and DOE 2014b, Table SOTERM-21

Table 7-2. Proportionality Constants and Maximum Concentrations for Humic Colloids Used in All WIPP PAs

Actinide	**Proportionality Constant Humic Colloids in Salado Brine[a] (Parameter PHUMSIM)**	**Proportionality Constant Humic Colloids in Castile Brine[b] (Parameter PHUMCIM)**	**Maximum Sorbed on Humics (M) (Parameter CAPHUM)**
Th(IV)	6.3	6.3	1.1×10^{-5}
U(IV)	6.3	6.3	1.1×10^{-5}
U(VI)	0.12	0.51	1.1×10^{-5}
Np(IV)	6.3	6.3	1.1×10^{-5}
Np(V)	9.1×10^{-4}	7.4×10^{-3}	1.1×10^{-5}
Pu(III)	0.19[d]	1.1[d]	1.1×10^{-5}
Pu(IV)	6.3	6.3	1.1×10^{-5}
Am(III)	0.19[d]	1.1[d]	1.1×10^{-5}

a – Units of moles colloidal actinide per mole dissolved actinide
b – Units of moles colloidal actinide per mole dissolved actinide
c – Units of moles total mobile actinide per liter
d – For Salado brine, the maximum value in the distribution is used for PA; for Castile brine, a cumulative distribution from 0.065 to 1.60 with a mean value of 1.1 and a median of 1.37 is sampled for PA
e – Not applicable
Source: DOE 2014b, Appendix SOTERM-2014, Table SOTERM-21

Table 7-3. Proportionality Constants and Maximum Concentrations for Microbial Colloids

	Proportionality Constant Microbes[a] (Parameter PROPMIC)		Maximum Sorbed by Microbes[c] (CAPMIC)	
	CCA PAVT, PABC04 and PABC09	CRA-2014 PA and CRA14_SEN4	CCA PAVT, PABC04 and PABC09	CRA-2014 PA and CRA14_SEN4
Th(IV)	3.1	1.76	0.0019	2.3×10^{-6}
U(IV)	0.0021	1.76	0.0021	2.3×10^{-6}
U(VI)	0.0021	1.76	0.0023	2.3×10^{-6}
Np(IV)	12.0	1.76	0.0027	2.3×10^{-6}
Np(V)	12.0	1.76	0.0027	2.3×10^{-6}
Pu(III)	0.3	1.76	6.8×10^{-5}	2.3×10^{-6}
Pu(IV)	0.3	1.76	6.8×10^{-5}	2.3×10^{-6}
Am(III)	3.6	0.32	NA[e]	3.1×10^{-8}

a – Units of moles colloidal actinide per mole dissolved actinide
b – Units of moles colloidal actinide per mole dissolved actinide
c – Units of moles total mobile actinide per liter
d – For Salado brine, the maximum value in the distribution is used for PA; for Castile brine, a cumulative distribution from 0.065 to 1.60 with a mean value of 1.1 and a median of 1.37 is sampled for PA
e – Not applicable
Source: DOE 1996, Appendix SOTERM, Table SOTERM-14 and DOE 2014b, Appendix SOTERM-2014, Table SOTERM-21

EPA (2010b) found that the potential formation of mineral fragment colloids by MgO and its hydration and carbonation products under WIPP-relevant conditions had not been adequately evaluated and recommended that DOE investigate the possible formation of mineral fragment colloids by minerals in the MgO backfill. For example, Altmaier et al. (2004) found that mineral fragment colloids formed in $MgCl_2$ solutions with ionic strengths from 2.5 to 4.5 M may mobilize thorium in brines suggesting actinides can form colloids with Mg. During review of the CRA-2009, EPA (2010b) determined that the colloids reported by Altmaier et al. (2004) are unlikely to form in the repository because the korshunovskite solid observed in the experiments does not form in WIPP brines.

DOE (Xiong and Kim 2011) described an investigative approach for determining the possible formation of mineral fragment colloids from MgO under WIPP repository conditions. Experiments were planned in GWB or simplified GWB, because a Mg-chloride-hydroxide-hydrate solid (phase 5) has been observed to precipitate from GWB but not from ERDA-6. Samples from long-term MgO hydration and carbonation experiments performed in GWB (Deng et al. 2009) were to be analyzed by filtration from 220 nm to 10 nm. The filtrates would be analyzed for Mg to determine if Mg-bearing colloids were present. Additional experiments were planned in 1.0 M and 1.65 M $MgCl_2$ with Martin Marrietta MgO and 0 – 1.0 M NaCl to assess the role of Na^+ on the stabilization of phase 5. DOE did not report the results of these experiments. DOE (Reed et al. 2013) considered the magnesium colloid effects reported by Altmaier et al. (2004) and stated that they were likely transient. However, Altmaier has reiterated that there was strong evidence that Th(IV) or perhaps Th(IV) colloid was strongly sorbed on the

korshunovskite solid phase (Sassani 2013). Although formation of the Mg colloids observed by Altmaier et al. (2004) remains unlikely because of differences in the brines and Mg chloride-hydroxide-hydrate solid phases between their experiments and WIPP brines, whether MgO reaction products in WIPP brines might form mineral fragment colloids capable of sorbing actinides remains unresolved. It would be appropriate for DOE to address this issue by performing experiments with WIPP brines and MgO.

DOE (Reed et al. 2013) reported the results of long-term experiments of Pu(VI) reduction in WIPP brine by iron coupons or magnetite. Reed et al. (2013) defined dissolved plutonium as the concentration passing through a 2.5 nm filter, intrinsic colloid plutonium as the concentration between 2.5 nm and 10 nm, and mineral colloid plutonium as greater than 10 nm material. After approximately six years of reaction, filtration of the brines showed that in pcH 9.1 – 9.5 ERDA-6 brine, the mineral-colloid Pu concentration ranged from 8.6×10^{-9} M to 2.3×10^{-8} M. Because this concentration range was bounded by the 2.6×10^{-8} M concentration originally established for the CCA PAVT (Table 7-1), the value of CONCMIN remained unchanged for the CRA-2014 PA.

The current value of parameter CONCMIN remains consistent with the available data. However, EPA believes DOE will strengthen this parameter by addressing uncertainty regarding possible formation of mineral fragment colloids from MgO under WIPP repository conditions .

7.2 INTRINSIC COLLOIDS

The concentrations of intrinsic Pu(IV) colloids were determined for the CCA PAVT based on the results of experimental investigations carried out with Pu(IV) (DOE 1996 Appendix SOTERM Section 6.3.2.3, Papenguth and Behl 1996). Intrinsic Pu(IV) colloids were detected in NaCl brines at pcH values of approximately 4 and 7, but at pcH values of approximately 8 and higher, intrinsic Pu(IV) colloid concentrations in the experiments were below the analytical detection limit of 10^{-9} M (DOE 1996, Appendix SOTERM Section 6.3.2.3). Because the expected pcH of the repository was approximately 9.3, the concentration of intrinsic Pu(IV) colloids used in the CCA PAVT was set equal to the analytical detection limit (Table 7-1). A literature review did not provide evidence of the formation of other actinide intrinsic colloids, so the concentrations of thorium, uranium, neptunium, Pu(III) and americium intrinsic colloids were set equal to zero (DOE 1996, Appendix SOTERM, Section 6.3.2.4).

DOE has updated the intrinsic colloid concentrations (parameter CONCINT) using data from recent investigations. EPA has identified issues with the pcH ranges considered by DOE. Because of the narrow pcH ranges DOE used to develop the CONCINT parameters, many of the parameter values used in the CRA-2014 PA do not represent upper limiting values. The investigations used to develop CONCINT parameter values for Th(IV), Nd(III) (an analogue for Am(III)), Pu(III), and U(VI) are considered below.

Reed et al. (2013) examined the results of sequential filtration of samples from Nd(III), Pu(III), Th(IV) and U(VI) solubility experiments carried out in WIPP brines. Using filtration data with a size range of 2 nm to 10 nm for intrinsic colloids and a pcH range from 9 to 10, Reed et al. (2013) established revised intrinsic colloid concentrations that were used in the CRA-2014 PA and CRA14_SEN4 PA (Table 7-1). EPA noted that these concentrations did not appear to be

bounding and requested that DOE demonstrate that these parameters were upper limiting values based on the available data (Edwards 2015c, Comment 3-C-9, Economy 2016).

Recent investigations have identified the formation of intrinsic Th(IV) colloids in dilute solutions and in brines. Neck et al. (2002) found that intrinsic Th(IV) colloids were present at low ionic strength based on ultracentrifugation of sampled solutions. Neck et al. (2002) determined that previous investigations of amorphous Th(IV) hydrous oxide solubility had established higher log K_{sp}^0 values because of incomplete separation of these colloids from solution. Bitea et al. (2003) investigated the formation and stability of Th(IV) colloids in 0.5 M NaCl and found that these colloids remained stable over the course of 400 days without exhibiting agglomeration or precipitation. Results reported by Altmaier et al. (2004) indicated that intrinsic Th(IV) colloids can form and remain stable at high ionic strength, with total mobilized Th(IV) concentrations (dissolved plus intrinsic colloids) of approximately $10^{-6.3}$ M. EPA (2010b) reviewed the literature data, found the evidence of Th(IV) intrinsic colloids to be credible and recommended that DOE revise future calculations of Th(IV) intrinsic colloid concentrations.

Reed et al. (2013) selected Th(IV) intrinsic colloid concentration data by limiting the pcH range from 9 to 10. Limiting the pcH to this very narrow range resulted in only two data sets (duplicates from the same experiment) for Th(IV) and may be unjustified given the low pcH dependence of Th(IV) solubilities in this pcH range (Economy 2016). Three experiments with two duplicate samples each were within ± 1 pcH unit of expected repository brine pcH conditions (Reed et al. 2013, Figure 4-6, samples G8C2-1, UG9C2-2 and E10C3-1). The filtration results from these three experiments demonstrated a wide range of intrinsic colloid concentrations. However, the dissolved thorium concentrations (3 kDa, approximately 2.5 nm) in the E10C3-1 samples were fairly high (approximately 7×10^{-7} M) compared to ThO_2(am) solubilities in WIPP brine, which are on the order of 7×10^{-8} M (Table 6-17). Consequently, experiment E10C3-1 was likely too far from equilibrium to be used to determine the intrinsic colloid concentration. The dissolved Th(IV) concentration in G8C2-1 and the predicted Th(IV) solubility were similar, so this experiment may have been close to equilibrium. The intrinsic Th(IV) colloid concentrations in the duplicate samples from G8C2-1 were approximately 3×10^{-6} M (Borkowski 2012b), which is greater than both the 2×10^{-8} M intrinsic Th(IV) colloid concentration used in the CRA-2014 PA and the dissolved Th(IV) concentrations calculated in WIPP brines (6×10^{-8} M to 7×10^{-8} M, Table 6-19), indicating that including the G8C2-1 concentrations in the intrinsic Th(IV) colloid concentration evaluation could significantly affect total mobilized Th(IV). Although the pcH of UG9C2-2 was close to pcH values expected in the WIPP repository, the Th(IV) intrinsic colloid concentrations measured in G8C2-1 were consistent with the concentrations measured in 0.5 M and 5 M NaCl by Altmaier et al. (2004). Because of the low dependence of thorium solubility on pcH in the range anticipated in the WIPP brines and because significantly higher Th(IV) intrinsic colloid concentrations were measured within a pcH range of 8.5 – 10.5, EPA recommends DOE include data obtained within this pcH range in the calculation of intrinsic Th(IV) colloid concentrations.

The Am(III) intrinsic colloid concentration was calculated to be 2×10^{-9} M based on a single Nd(III) measurement in ERDA-6 brine at pcH 9.1, where 33% of the total Nd(III) in solution was present as intrinsic colloids (Reed et al. 2013). At slightly lower pcH values (8.53 and 8.55) in GWB, dissolved concentrations were significantly higher with widely differing percentages of intrinsic colloids (30% and 77%). Because of the much higher solubilities in the lower pcH

samples, the use of only the higher pcH sample (9.1) by Reed et al. (2013) is reasonable. The Nd(III) filtration data in Figure 4-2 of Reed et al. (2013) do not appear to be documented by the cited reference (Borkowski et al. 2009) because of differing pcH and filter sizes based on a comparison with Figure 4-2 of Borkowski et al. (2009). In addition, identification of colloids in the Nd(III) experiments appears to contradict the statement by Borkowski et al. (2009, page 23): "All the neodymium concentrations determined in filtered samples and unfiltered samples (with one exception) were in good agreement and within experimental error. This indicates that colloids or a fine particle suspension were not formed during the solubility experiments."

For Pu(III) in ERDA-6 with a pcH range from 9.1 to 9.5, the intrinsic colloid concentrations ranged from 9.3×10^{-10} to 7.4×10^{-9} M. Although Reed et al. (2013, Attachment 2, page 96) stated that the highest concentration for each actinide or analogue species would be selected as the recommended values for intrinsic colloids, Reed et al. (2013) selected an average value of 4×10^{-9} M for Pu(III) intrinsic colloids. Substituting the highest measured intrinsic colloid concentration of 7.4×10^{-9} M would provide an upper-bound value, but would have little effect on total mobilized +III actinide concentrations because the dissolved concentrations are much higher (Table 6-17). The plutonium 0.45 μm, 0.22 μm, 20 nm and 10 nm filtration data in Figures 4-3 and 4-4 of Reed et al. (2013) do not appear to be documented by the cited reference (Reed et al. 2010), which reported only 20 nm filtration.

U(VI) sequential filtration results from experiments carried out in CO_2-free ERDA-6 brines, with final pcH values of 9.3 and 9.8 had low intrinsic colloid concentrations (~ 0 M and 6×10^{-8} M). Reed et al. (2013) used an average of 3×10^{-8} M, but even the higher 6×10^{-8} M concentration is insignificant compared to the dissolved U(VI) concentration of 1×10^{-3} M assumed for PA.

Roselle (2013) provided a summary of the recommended intrinsic colloid enhancement parameters based on the results of Reed et al. (2013, Table 1). The U(IV) intrinsic colloid concentration (2×10^{-8} M) used in the CRA-2014 PA was lower than the 3×10^{-8} M concentration recommended by Roselle (2013), but is consistent with the recommended Th(IV) intrinsic colloid concentration.

7.3 HUMIC COLLOIDS

Actinide concentrations associated with humic substances are based on proportionality constants (Table 7-2). Proportionality constants determined for Th(IV) were extended to U(IV), Np(IV), and Pu(IV), and proportionality constants developed for Am(III) were extended to Pu(III). Proportionality constants for Np(V) and U(VI) were based on data for these oxidation states (DOE 1996, Appendix SOTERM, Table SOTERM-12). The proportionality constants were calculated from experimentally determined humic substance solubilities in brines at various concentrations of Ca^{2+} and Mg^{2+}; data on site-binding capacities measured for the WIPP research program and literature values; actinide complexation factors for Am(III), Th(IV), Np(V) and U(VI) binding on humic substances; and stability constants for Ca^{2+} and Mg^{2+} binding to humic substances. The maximum value used in PA (CAPHUM, Table 7-2) represents the theoretical maximum concentration of actinides that can be bound by a humic substance, assuming a solubility limit of 2 mg/L, the highest site-binding capacity for fulvic acids of 5.56 meq OH^-/g and the limiting case of a monovalent actinide species (DOE 1996, Appendix SOTERM, Section 6.3.3.2).

Wall and Mathews (2005) evaluated the solubility of humic acids in GWB and ERDA-6 brines and the effects of MgO on the quantities of humic acids in WIPP brines. Wall and Mathews (2005) found that GWB and ERDA-6 brine promoted coagulation of the humic acid, although complete humic acid removal was not observed. Humic acids were completely removed from the brines in the presence of either reagent-grade MgO or Premier MgO, which was the backfill material being emplaced in WIPP at the time of the experiments (Section 4.3.1).

No new data were included in the CRA-2014 PA regarding humic colloids. The parameters used to estimate humic colloid contributions to total mobile actinide concentrations have remained unchanged since the CCA PA (Table 7-2).

7.4 MICROBIAL COLLOIDS

Actinide concentrations associated with microbial colloids in WIPP PA are based on proportionality constants (Table 7-3). For microbial colloids, the CCA PA proportionality constants were developed for each element. Experimental data on the mobile concentrations of microbes and bioaccumulation and toxicity experiments were used to develop the proportionality constants (Papenguth 1996; DOE 1996, Appendix SOTERM Section 6.3.4) using a bacterium isolated from WIPP environs (*Halomonas* sp. WIPP-1A) and an uncharacterized mixed culture which presumably contained largely archaea (BAB). Upper limits for the concentrations of actinides for microbial colloids were established based on the concentration at which no growth was observed (Table 7-3). Because the high radiation levels of Am(III) prevented increasing concentrations until toxicity effects were observed, no maximum concentration value was determined for Am(III). Because of limited data, distributions were not developed for the proportionality constants or the maximum concentrations for microbial colloids and single values were used in PA.

These parameters have been updated for the CRA-2014 based on new experiments on pure cultures of a representative bacterium and a representative archaeon, both isolated from WIPP. While these experiments provide new data and new parameters to include for +4 and +3 actinides, EPA finds many issues with the experiments and the assumptions, some of which are major changes to the previous conceptual models. These experiments are summarized below.

Reed et al. (2013) summarized experiments investigating the biosorption of Nd(III) and Th(IV) on representative halophilic bacteria (*Chromohalobacter* sp) and archaea (*Halobacterium noricense*). *Chromohalobacter* sp was isolated from area groundwater and *Halobacterium noricense* was isolated from incubations of halite in generic media and brine. Four WIPP simulated brines (Lucchini et al. 2013) were used in biosorption experiments conducted at pcH 8.5, 9.0, 9.5 and 9.7 and at 90% saturation to prevent precipitation of solids from the brine during the experiments. The Nd(III) stock solution concentration was 4×10^{-8} M, which is less than the expected solubility of Nd(III) solids under the experimental conditions. The Th(IV) stock solution was prepared by adding 1×10^{-4} M Th(IV) to each pcH-specific brine, which after equilibration was filtered with a 100 kDa (~ 20 nm) filter. These stock solutions had initial concentrations ranging from 1×10^{-6} to 1×10^{-7} M that decreased with increasing pcH. Metal-EDTA stock solutions were similarly prepared using an excess of EDTA equal to or greater than a factor of 2 times the Nd(III) and Th(IV) concentrations. Nd(III) stock solutions were 0.22 µm filtered and Th(IV) stock solutions were 20 nm filtered immediately prior to the experiments.

The biosorption experiments were carried out for two hours. At the end of the experiments, the solutions were ~ 20 nm filtered to remove microorganisms and the supernatants were analyzed. Abiotic control experiments were conducted to account for all other possible causes of Nd(III) and Th(IV) losses from the solutions.

Reed et al. (2013) noted significant biosorption of Nd(III) both in the absence and presence of EDTA. Significant biosorption was not anticipated in the presence of EDTA, because Reed et al. (2013) had expected EDTA complexation of Nd(III) to out-compete biosorption. Reed et al. (2013) attributed these results to precipitation of Nd(III) as colloidal or solid Nd(III), even though the solubility of Nd(III) in WIPP brine should have been higher than the initial 4×10^{-8} M (Table 6-17). Evaluation of biosorption test results as a function of biomass showed that hydrolysis/precipitation could account for about 35% of the Nd(III) removed from solution at pcH 9.4 without EDTA and about 12% of the Nd(III) removed from solution at pcH 8.9 in the presence of EDTA. Geochemical modeling of the brines used in the experiments showed that the initial EDTA-free brines were oversaturated with respect to Nd(III) solid and that as much as 20% of the Nd(III) was not complexed by EDTA.

Reed et al. (2013) observed significant precipitation of Th(IV) in the controls at the highest pcH values. The biosorption results showed that metastable Th(IV)-EDTA complexes formed. Plots of biosorption as a function of biomass for the archaea extrapolated to near zero at zero biomass. However, extrapolation to zero biosorption at zero biomass loading was not observed for the bacteria. Based on the observation of precipitation in the Th(IV) stock solution at high pcH and the biomass loading data, Reed et al. (2013) determined that greater reliance should be placed on the EDTA-free data, on lower pcH data and on the archaea data.

Reed et al. (2013) generated oxidation-state specific recommendations for PROPMIC parameters for archaea and for bacteria for Th(IV), U(IV) and Pu(IV) and for Am(III) and Pu(III) based on their experimental results. A PROPMIC parameter was proposed for Np(V) based on the results of Ams et al. (2013) using *Chromohalobacter* sp in 2 M and 4 M $NaClO_4$ solutions. PROPMIC parameters were also developed on an element-by-element basis, assuming the highest PROPMIC values developed for the different oxidation states of each element. For example, the oxidation-state-specific PROPMIC parameters proposed for Pu(III) were less than the proposed Pu(IV) parameters, so the Pu(IV) parameters were recommended for both plutonium oxidation states.

Reed et al. (2013) recommended revision of the CAPMIC parameters to correspond with a biomass of 10^9 cell/ml, multiplied by the moles of actinide per cell reported by Francis (1998) and measured values from Reed et al. (2013). This approach differs from the approach taken for the CCA, which used the actinide concentration at which microbial growth was no longer observed. The revised approach resulted in significantly lower CAPMIC parameter values than were developed for the CCA PA (Table 7-3). Reed et al. (2013, Section 5.2) based the maximum 10^9 cells on the number of haloarchea in optimal growth media rather than all microbes (bacteria and haloarchea) and the absence of growth. This represents a change in the conceptual model, which is acknowledged by Reed et al. (2013) because this change is explicitly addressed as a changed assumption (Assumption 1, Reed et al. 2013, Section 5.2). Because the WIPP PA model only allows for a single set of microbial colloid parameters, Roselle et al. (2013) selected the

higher PROPMIC and CAPMIC parameter values Reed et al. (2013) developed. The number selected was from the bacterium as this had a higher sorption than the archaeon.

EPA noted (Economy 2016) that Reed et al. (2013) used results from microbial adsorption tests conducted for two hours, which is much shorter than the 11- to 21-day experiments used for previous WIPP microbial adsorption tests (Papenguth 1996; DOE 1996, Appendix SOTERM-2014). EPA requested evidence that the two-hour period was sufficient to achieve steady state conditions. Patterson (2016b) responded that the tests were designed only to evaluate biosorption, and not intracellular accumulation or biomineralization (surface-catalyzed precipitation) on the cell surface. This represents a significant departure from the original microbial colloid conceptual model. In the tests, the sorption kinetics were determined to typically take less than 90 minutes to reach steady state, so DOE expected the two-hour period for the experiments to be adequate. Patterson (2016b) stated that longer-term data were obtained over periods of days to weeks, with no significant change in the absence of precipitation. However, the Nd(III) data provided in the response (Patterson 20a6b, Figure 1) show an apparent upward trend between 3 and 20 hours. In the response, this slight increase is noted but the small changes are said to be within the uncertainty of the data. The information provided does not demonstrate steady state, because it is possible that experiments conducted over days or weeks could have shown increases that exceed the data uncertainties.

EPA (Economy 2016) noted that the Th(IV) solutions used in the biosorption tests were passed through 20 nm filters both before the tests were conducted and at the end of the tests (Reed et al. 2013). However, intrinsic colloids less than 10 nm have been reported for thorium (Reed et al. 2013) so these solutions may have contained intrinsic colloids. The presence of intrinsic colloids in the test solutions would result in dissolved concentrations that were less than the total concentrations. PROPMIC is calculated from the ratio of sorbed and dissolved concentrations:

$$PROPMIC = \frac{[Actinide\ or\ Analog\ Sorbed]}{[Dissolved\ Actinide\ or\ Analog]} \quad \textbf{(36)}$$

Overestimating the dissolved concentration would result in an underestimated value for PROPMIC. In response, DOE (Patterson 2016b) addressed two possible cases: one in the absence of colloids and one in the presence of colloids in the test solutions. Because significant concentrations of colloids are likely to be present in the solutions, only the second case appears to be applicable. DOE stated in their response that the effects of colloids depends on whether colloids are sorbed: if colloids are not sorbed, then biosorption is underestimated, and if colloids are preferentially sorbed, biosorption is overestimated. DOE stated that experimental data have shown that colloids are preferentially sorbed and seem to facilitate biomineralization on the cell surface, but DOE did not provide any supporting data in its response. In addition, DOE stated that Th(IV) colloids are "always present at WIPP-relevant pH and we were not able to isolate true dissolved species sorption given our experimental limitations." Although DOE explained the use of 20-nm filtration to remove microbes at the end of the tests, DOE did not explain why additional 2-nm filtration was not performed to remove intrinsic colloids both before and after the sorption tests were conducted.

Uncertainties have been introduced into the calculation of the revised PROPMIC parameters (Table 7-3) because of the short experiment durations and the possible effects of intrinsic colloids on the biosorption results. Although the CRA-2014 PA PROPMIC parameters increased for U(IV), U(VI), Pu(III) and Pu(IV), these parameters decreased for Th(IV), Np(IV), Np(V) and Am(III). Because of a change to the conceptual model, the CAPMIC concentrations decreased for all elements (Table 7-3). For the +IV actinides in Salado and Castile brines, CAPMIC (2.3×10^{-6} M) would not limit the microbial colloids for the baseline solubility plus mean uncertainty. However, for Pu(III) and Am(III), CAPMIC is low compared to the baseline dissolved concentration and would likely affect the actinide concentrations associated with microbial colloids (Section 8.0).

DOE has changed the conceptual model assumptions for calculating CAPMIC, microbial cultures present, and bioaccumulation/biomineralization. In addition, EPA disagrees with many of the experimental parameters chosen and as a result believe the CRA-2014 microbial colloid parameter updates are not adequately justified for implementation. EPA expects this model to continue to be updated for the CRA-2019. Until then, EPA will accept the higher CAPMIC values originally developed for the CCA PA. DOE has stated that they continue to study actinide biosorption, intracellular accumulation and biomineralization (Patterson 2016b). Because these studies are incomplete and the effects of intracellular accumulation and biomineralization may not have been assessed in the more recent tests, EPA will also continue to accept the higher PROPMIC parameter (either from the CCA PA or Reed et al. 2013) until the issues cited in this review are resolved.

7.5 COLLOIDS SUMMARY AND CONCLUSIONS

DOE (2014b) provided the first update to the colloids parameters since the CCA PA. During review of the colloid parameters, it was noted:

- Humic colloid parameters remained unchanged
- Parameter values reflecting mineral fragment colloids (CONCMIN) remain unchanged, which is consistent with the available data
- Whether mineral fragment colloids might form during reaction of MgO in WIPP brines and transport actinides remains unresolved and formation of these mineral fragment colloids should be experimentally investigated
- The revised intrinsic colloid parameter (CONCINT) for Th(IV) should reflect upper bounding values for samples collected within the pcH range of 8.5 – 10.5
- The Pu(III) and Am(III) intrinsic colloid parameters do not appear to be documented by the references cited by Reed et al. (2013) and the Pu(III) intrinsic colloid parameter does not appear to be an upper, bounding value
- DOE changed the upper bounds for the microbially associated actinides (CAPMIC) for the CRA-2014 PA based on a revised conceptual model assumption regarding the upper limit on microbially associated actinides. Previous PAs assumed that the maximum concentration is the concentration at which no growth was observed, but DOE changed this upper limit to the concentration calculated from an assumed maximum cell

concentration multiplied by the moles of actinides per cell. These departures from the original conceptual model suggest the revised microbial colloidal conceptual model and revised parameters have not been adequately justified. Consequently, it would be appropriate for DOE to continue to evaluate the model and parameters for the CRA-2019 and continue using the original CAPMIC values until this evaluation is complete

- Because of the short reaction times in tests reported by DOE, the current microbial proportionality constants (PROPMIC) likely reflect only biosorption and not bioaccumulation or biomineralization. This represents a conceptual model change because previous WIPP PAs included biosorption, bioaccumulation and biomineralization. DOE has stated that further research into the biosorption, bioaccumulation and biomineralization processes is planned, and these investigations should include longer reaction times to substantiate steady state conditions and that the effects of bioaccumulation and biomineralization have been addressed
- Uncertainty has been introduced into the biosorption data developed by DOE because of the possible inclusion of intrinsic colloids in the experimental solutions which may or may not have sorbed; EPA expects DOE to use 2 nm filtration to remove intrinsic colloids from their post-test solutions in future experiments to establish the dissolved concentration for calculating PROPMIC parameter values.

8.0 TOTAL MOBILIZED ACTINIDE CALCULATIONS FOR PA

The total mobilized actinides in WIPP brines is defined for PA as the sum of the dissolved actinide concentrations and the colloidal actinide concentrations. The information required to calculate the dissolved and colloidal actinide concentrations for each PA realization includes:

- Whether the scenario uses the Salado or Castile end-member brine composition (DOE 2014b, Appendix SOTERM-2014, Table SOTERM-22)
- The baseline dissolved concentrations of +III, +IV, +V, and +VI actinides in the brine (Table 6-17)
- Sampled uncertainty values for the +III and +IV actinide solubilities (Section 6.6.6)[21]
- Whether actinides with multiple possible oxidation states are present in their relatively reduced [U(IV), Np(IV) and Pu(III)] or relatively oxidized [U(VI), Np(V) and Pu(IV)] oxidation states
- The constant concentrations of intrinsic and mineral-fragment colloids (Table 7-1)
- The proportionality constants and maximum concentrations of humic and microbial colloid actinides (Tables 7-2 and 7-3); of these parameters, only the proportionality constant for the +III actinide humic colloids in ERDA-6 brine is sampled for PA; all other proportionality constants and the maximum concentrations are fixed values
- The total inventory of the actinide

8.1 CRA-2014 PA TOTAL MOBILIZED ACTINIDE RESULTS

DOE (2014b, Appendix SOTERM-2014, Section SOTERM-5.0) provided a discussion of the PA calculations of the actinide source term and example calculations of actinide solubility and colloidal actinides. Table SOTERM-23 (DOE 2014b, Appendix SOTERM-2014) summarized dissolved and colloidal actinide concentrations calculated using median parameter values for the CCA PAVT, PABC04, PABC09 and CRA-2014 PA.

Baseline dissolved actinide concentrations calculated using EQ3/6, the mean uncertainty parameters and the mean colloidal actinide parameters for the CRA-2014 PA are summarized in Table 8-1. Because the constant concentrations of mineral fragment colloids and intrinsic colloids are relatively small, contributions to the total mobile actinide concentrationss are low from these types of colloids for all actinide oxidation states for calculations using the mean CRA-2014 PA parameter values (Table 8-1). In GWB brine, total mobilized Am(III) is dominated by dissolved species, with the next largest contribution from humic colloids. For total mobilized Am(III) concentrations in ERDA-6 brine, higher concentrations are associated with humic colloids because of a higher proportionality constant for Am(III) humic colloids in Castile brine, with the next largest contribution from dissolved species. For both GWB and ERDA-6

[21] Neptunium, which is the only actinide predicted in repository brines in the +V state, does not have a significant effect on PA because of its low concentration in the inventory (see Section 9.0). An upper-limit concentration is used for U(VI), which is the only+VI actinide predicted in WIPP brines.

brine, Am(III) concentrations associated with microbial colloids are low because they are limited by the maximum concentration. For Pu(III) in both GWB and ERDA-6 brine, the largest contributions to total mobilized concentrations are from microbial colloids, with significant additional contributions from dissolved species and humic colloids.

For +IV actinides in both GWB and ERDA-6 brine, humic colloids are the most significant contributors to the total mobilized concentrations (Table 8-1). Microbial colloids are the second-most important contributors, with dissolved species constituting only 11% of the total mobilized concentrations. Total mobilized Np(V) is dominated by microbial colloids and total mobilized U(VI) is dominated by dissolved species.

The overall mean CCDF for DBR was lower for the CRA-2014 PA than for the PABC09 (DOE 2014b Appendix PA-2014, Figure PA-78). This decrease was likely caused by the lower sampled range for the probability of a drilling intrusion encountering pressurized brine (GLOBAL:PBRINE) for the CRA-2014 PA. The lower mean DBR CCDF for the CRA-2014 PA may also be related to lower total mobilized actinide concentrations in the CRA-2014 PA. Evidence supporting the effects of total mobilized actinide concentrations on DBR includes the observation that the sampled parameter SOLMOD3:SOLVAR (the solubility uncertainty for the +III oxidation state) accounted for a significant fraction of the uncertainty in DBRs (Kirchner 2013). In addition, the median total mobilized Pu(III) and Am(III) concentrations in Castile brine in the CRA-2014 PA were only 18% and 5% of their respective values in the PABC09 (DOE 2014b, Appendix SOTERM, Table SOTERM-23). There is no evidence that the +IV actinides significantly affected DBRs, because the median total mobilized +IV concentrations increased between the PABC09 and CRA-2014 PA while the overall mean CCDF for DBR decreased.

The total mobilized Am(III) concentrations in the CRA-2014 PA for both GWB and ERDA-6 brine were lower than the PABC09 concentration because: 1) the mean solubilities were reduced because of a more negative mean SOLMOD3:SOLVAR value; 2) the humic colloid concentration was lower because it is proportional to the mean solubility; and 3) the microbial colloidal Am(III) concentration was reduced by the smaller actinide solubility, a smaller proportionality constant and smaller maximum concentration. The largest difference for Am(III) was observed for the microbial colloid concentration, which decreased by more than two orders of magnitude from the PABC09 to the CRA-2014 PA. The overall decreases in the total mobilized Am(III) concentrations for both GWB and ERDA-6 brine were nearly an order of magnitude between the PABC09 and CRA-2014 PA (Tables 8-1 and 8-2).

The changes in total mobilized Pu(III) concentrations from the PABC09 to the CRA-2014 PA differed for the two WIPP brines. The total mobilized Pu(III) concentration in GWB brine for the CRA-2014 PA decreased relative to the PABC09 by only about 10% because lower dissolved Pu(III) and humic colloid Pu(III) concentrations were partially offset by a higher microbial colloid Pu(III) concentration. On the other hand, the total mobilized Pu(III) concentration in ERDA-6 brine for the CRA-2014 PA was less than half of the PABC09 concentration because of a lower mean Pu(III) solubility and humic colloid concentration.

8.2 CRA14_SEN4 PA TOTAL MOBILIZED ACTINIDE RESULTS

The total mobilized actinides for the CRA14_SEN4 PA are summarized in Table 8-3. The total mobilized actinide concentrations for the CRA14_SEN4 PA differed from the concentrations for the CRA-2014 PA because of the revised solubility uncertainty distributions used for the +III and +IV actinides (Xiong and Domski 2016a). The revised solubility uncertainty distributions increased the mean +III actinide solubilities and decreased the mean +IV actinide solubilities used in the CRA14_SEN4 PA. Because the humic colloid and microbial colloid concentrations are proportional to the dissolved actinide solubilities, the humic colloid, microbial colloid and total colloidal concentrations also changed relative to the CRA-2014 PA.

8.3 SENSITIVITY OF TOTAL MOBILIZED ACTINIDE CONCENTRATIONS TO PARAMETER CHANGES

The changes to microbial colloid proportionality constants and maximum microbial colloid concentrations for Am(III) and Pu(III) for the CRA-2014 PA and CRA14_SEN4 significantly affected total mobilized Am(III) and Pu(III) concentrations relative to the PABC09. For the PABC09, using the CCA PA microbial colloid parameters resulted in total mobilized Am(III) concentrations composed of 75% (GWB) and 63% (ERDA-6) microbial colloids. In contrast, the Am(III) concentrations associated with microbial colloids for the CRA-2014 PA were 4% of the total mobilized concentration in both GWB and ERDA-6 brine, whereas for the CRA14_SEN4 PA, the Am(III) concentrations associated with microbial colloids were 0.3% of the total mobilized concentration. Microbial colloids accounted for 20% (GWB) and 12% (ERDA-6) of the total mobilized Pu(III) in the PABC09, 58% (GWB) and 44% (ERDA-6) of the total mobilized Pu(III) in the CRA-2014 PA and 20% (GWB) and 19% (ERDA-6) of the total mobilized Pu(III) in the CRA14_SEN4 PA.

The total mobilized actinide concentrations for Castile brines in the PABC09, CRA-2014 PA and CRA14_SEN4 PA are compared in Table 8-4. For Am(III) and Pu(III), which are the actinide oxidation states most likely to affect releases, the highest total mobilized concentrations were observed in the CRA14_SEN4 PA. The total mobilized Am(III) concentration in the CRA14_SEN4 would have been even higher (1.09×10^{-5} M) if the Am(III) maximum microbial colloid concentration had not been changed from its previously unlimited value to 3.1×10^{-8} M (Table 7-3). The total mobilized Pu(III) concentration for the CRA14_SEN4 PA increased by nearly an order of magnitude over the concentrations predicted for the PABC09 or CRA-2014 PA. The total mobilized Pu(III) concentration would have been even higher (1.75×10^{-5} M), but was limited by the downward revision of the maximum microbial colloid concentration from 6.8×10^{-5} M to 2.3×10^{-6} M (Table 7-3).

Because the baseline solubility of Pu(III) is higher than the Pu(IV) baseline solubility in WIPP PA and humic and microbial colloid concentrations are proportional to aqueous solubilities, it would be reasonable to expect that mean and median total mobilized Pu(III) concentrations will be greater than mean and median total mobilized Pu(IV) concentrations. For the PABC09 and CRA14_SEN4 PA, total mobilized Pu(III) concentrations were significantly higher than total mobilized Pu(IV) concentrations (Table 8-4). However, for the CRA-2014 PA both mean and median total mobilized Pu(IV) concentrations exceeded the mean and median total mobilized Pu(III) concentrations (Table 8-4; DOE 2014b Appendix SOTERM-2014, Table SOTERM-23).

For the CRA-2014 PA, the mean Pu(III) dissolved concentration was only slightly higher than the mean Pu(IV) dissolved concentration because of the negative mean Pu(III) solubility uncertainty parameter and the positive mean Pu(IV) solubility uncertainty parameter. The total mobilized Pu(IV) concentration was also increased relative to Pu(III) by the higher mean humic colloid concentration for Pu(IV) (Table 8-1).

Table 8-1. CRA-2014 PA Mean Dissolved and Colloidal Actinides

Radionuclide and Oxidation State	Brine	Baseline Dissolved Concentration (M)	Mean SOLVAR (Brush and Domski 2013c)	Mean Solubility (M)	Mineral Fragment Colloids (M)	Intrinsic Colloids (M)	Humic Colloids (M)	Microbial Colloids (M)	Total Colloidal (M)	Total Mobilized (M)
Am(III)	GWB	2.59×10^{-6}	-0.678	5.44×10^{-7} (77%)	2.60×10^{-8}	4.00×10^{-9}	1.03×10^{-7}	3.10×10^{-8} [d]	1.64×10^{-7} (23%)	7.08×10^{-7}
Pu(III)	GWB	2.59×10^{-6}	-0.678	5.44×10^{-7} (33%)	2.60×10^{-8}	2.00×10^{-8}	1.03×10^{-7}	9.57×10^{-7}	1.11×10^{-6} (67%)	1.65×10^{-6}
Th(IV)	GWB	6.05×10^{-8}	0.673	2.85×10^{-7} (11%)	2.60×10^{-8}	2.00×10^{-8}	1.80×10^{-6}	5.01×10^{-7}	2.34×10^{-6} (89%)	2.63×10^{-6}
U(IV)	GWB	6.05×10^{-8}	0.673	2.85×10^{-7} (11%)	2.60×10^{-8}	2.00×10^{-8}	1.80×10^{-6}	5.01×10^{-7}	2.34×10^{-6} (89%)	2.63×10^{-6}
Np(IV)	GWB	6.05×10^{-8}	0.673	2.85×10^{-7} (11%)	2.60×10^{-8}	2.00×10^{-8}	1.80×10^{-6}	5.01×10^{-7}	2.34×10^{-6} (89%)	2.63×10^{-6}
Pu(IV)	GWB	6.05×10^{-8}	0.673	2.85×10^{-7} (11%)	2.60×10^{-8}	2.00×10^{-8}	1.80×10^{-6}	5.01×10^{-7}	2.34×10^{-6} (89%)	2.63×10^{-6}
Np(V)	GWB	2.77×10^{-7}	--[a]	2.77×10^{-7} (35%)	2.60×10^{-8}	--[b]	2.52×10^{-10}	4.88×10^{-7}	5.14×10^{-7} (65%)	7.91×10^{-7}
U(VI)	GWB	1.00×10^{-3}	--[a]	1.00×10^{-3} (99%)	2.60×10^{-8}	3.00×10^{-8}	1.10×10^{-5} [c]	2.30×10^{-6} [d]	1.34×10^{-5} (1%)	1.01×10^{-3}
Am(III)	ERDA-6	1.48×10^{-6}	-0.678	3.11×10^{-7} (44%)	2.60×10^{-8}	4.00×10^{-9}	3.42×10^{-7}	3.10×10^{-8} [d]	4.03×10^{-7} (56%)	7.13×10^{-7}
Pu(III)	ERDA-6	1.48×10^{-6}	-0.678	3.11×10^{-7} (25%)	2.60×10^{-8}	2.00×10^{-8}	3.42×10^{-7}	5.47×10^{-7}	9.34×10^{-7} (75%)	1.25×10^{-6}
Th(IV)	ERDA-6	7.02×10^{-8}	0.673	3.31×10^{-7} (11%)	2.60×10^{-8}	2.00×10^{-8}	2.08×10^{-6}	5.82×10^{-7}	2.71×10^{-6} (89%)	3.04×10^{-6}
U(IV)	ERDA-6	7.02×10^{-8}	0.673	3.31×10^{-7} (11%)	2.60×10^{-8}	2.00×10^{-8}	2.08×10^{-6}	5.82×10^{-7}	2.71×10^{-6} (89%)	3.04×10^{-6}
Np(IV)	ERDA-6	7.02×10^{-8}	0.673	3.31×10^{-7} (11%)	2.60×10^{-8}	2.00×10^{-8}	2.08×10^{-6}	5.82×10^{-7}	2.71×10^{-6} (89%)	3.04×10^{-6}
Pu(IV)	ERDA-6	7.02×10^{-8}	0.673	3.31×10^{-7} (11%)	2.60×10^{-8}	2.00×10^{-8}	2.08×10^{-6}	5.82×10^{-7}	2.71×10^{-6} (89%)	3.04×10^{-6}
Np(V)	ERDA-6	8.76×10^{-7}	--[a]	8.76×10^{-7} (36%)	2.60×10^{-8}	--[b]	6.48×10^{-9}	1.54×10^{-5}	1.57×10^{-6} (64%)	2.45×10^{-6}
U(VI)	ERDA-6	1.00×10^{-3}	--[a]	1.00×10^{-3} (99%)	2.60×10^{-8}	3.00×10^{-8}	1.10×10^{-5} [c]	2.30×10^{-6} [d]	1.34×10^{-5} (1%)	1.01×10^{-3}

a – Np(V) and U(VI) solubility uncertainty parameters are not sampled for PA
b – Np(V) intrinsic colloids are not included in the PA calculations
c – CAPHUM value
d – CAPMIC value

Table 8-2. PABC09 Mean Dissolved and Colloidal Actinides

Radionuclide and Oxidation State	Brine	Baseline Dissolved Concentration (M)	Mean SOLVAR (Xiong et al. 2009a)	Mean Solubility (M)	Mineral Fragment Colloids (M)	Intrinsic Colloids (M)	Humic Colloids (M)	Microbial Colloids (M)	Total Colloidal (M)	Total Mobilized (M)
Am(III)	GWB	1.66×10^{-6}	-0.142	1.20×10^{-6} (21%)	2.60×10^{-8}	0.00	2.27×10^{-7}	4.31×10^{-6}	4.56×10^{-6} (79%)	5.76×10^{-6}
Pu(III)	GWB	1.66×10^{-6}	-0.142	1.20×10^{-6} (66%)	2.60×10^{-8}	0.00	2.27×10^{-7}	3.59×10^{-7}	6.13×10^{-7} (34%)	1.81×10^{-6}
Th(IV)	GWB	5.63×10^{-8}	-0.346	2.54×10^{-8} (9%)	2.60×10^{-8}	0.00	1.60×10^{-7}	7.87×10^{-8}	2.65×10^{-7} (91%)	2.90×10^{-7}
U(IV)	GWB	5.63×10^{-8}	-0.346	2.54×10^{-8} (12%)	2.60×10^{-8}	0.00	1.60×10^{-7}	5.33×10^{-11}	1.86×10^{-7} (88%)	2.11×10^{-7}
Np(IV)	GWB	5.63×10^{-8}	-0.346	2.54×10^{-8} (5%)	2.60×10^{-8}	0.00	1.60×10^{-7}	3.05×10^{-7}	4.90×10^{-7} (95%)	5.16×10^{-7}
Pu(IV)	GWB	5.63×10^{-8}	-0.346	2.54×10^{-8} (12%)	2.60×10^{-8}	1.00×10^{-9}	1.60×10^{-7}	7.61×10^{-9}	1.95×10^{-7} (88%)	2.20×10^{-7}
Np(V)	GWB	3.90×10^{-7}	--[a]	3.90×10^{-7} (8%)	2.60×10^{-8}	0.00	3.55×10^{-10}	4.68×10^{-6}	4.71×10^{-6} (92%)	5.10×10^{-6}
U(VI)	GWB	1.00×10^{-3}	--[a]	1.00×10^{-3} (99%)	2.60×10^{-8}	0.00	1.10×10^{-5}	2.10×10^{-6}	1.31×10^{-5} (1%)	1.01×10^{-3}
Am(III)	ERDA-6	1.51×10^{-6}	-0.142	1.09×10^{-6} (17%)	2.60×10^{-8}	0.00	1.20×10^{-6}	3.92×10^{-6}	5.14×10^{-6} (83%)	6.23×10^{-6}
Pu(III)	ERDA-6	1.51×10^{-6}	-0.142	1.09×10^{-6} (41%)	2.60×10^{-8}	0.00	1.20×10^{-6}	3.27×10^{-7}	1.55×10^{-6} (59%)	2.64×10^{-6}
Th(IV)	ERDA-6	6.98×10^{-8}	-0.346	3.15×10^{-8} (9%)	2.60×10^{-8}	0.00	1.98×10^{-7}	9.75×10^{-8}	3.22×10^{-7} (91%)	3.53×10^{-7}
U(IV)	ERDA-6	6.98×10^{-8}	-0.346	3.15×10^{-8} (12%)	2.60×10^{-8}	0.00	1.98×10^{-7}	6.61×10^{-11}	2.24×10^{-7} (88%)	2.56×10^{-7}
Np(IV)	ERDA-6	6.98×10^{-8}	-0.346	3.15×10^{-8} (5%)	2.60×10^{-8}	0.00	1.98×10^{-7}	3.78×10^{-7}	6.02×10^{-7} (95%)	6.33×10^{-7}
Pu(IV)	ERDA-6	6.98×10^{-8}	-0.346	3.15×10^{-8} (12%)	2.60×10^{-8}	1.00×10^{-9}	1.98×10^{-7}	9.44×10^{-9}	2.35×10^{-7} (88%)	2.66×10^{-7}
Np(V)	ERDA-6	8.75×10^{-7}	--[a]	8.75×10^{-7} (8%)	2.60×10^{-8}	0.00	6.48×10^{-9}	1.05×10^{-5}	1.05×10^{-5} (92%)	1.14×10^{-5}
U(VI)	ERDA-6	1.00×10^{-3}	--[a]	1.00×10^{-3} (99%)	2.60×10^{-8}	0.00	1.10×10^{-5}	2.10×10^{-6}	1.31×10^{-5} (1%)	1.01×10^{-3}

a – Np(V) and uranium (VI) solubility uncertainty parameters are not sampled for PA

Table 8-3. CRA14_SEN4 PA Mean Dissolved and Colloidal Actinides

Radionuclide and Oxidation State	Brine	Baseline Dissolved Concentration (M)	Mean SOLVAR (Xiong and Domski 2016a)	Mean Solubility (M)	Mineral Fragment Colloids (M)	Intrinsic Colloids (M)	Humic Colloids (M)	Microbial Colloids (M)	Total Colloidal (M)	Total Mobilized (M)
Am(III)	GWB	2.59×10^{-6}	0.484	7.89×10^{-6} (83%)	2.60×10^{-8}	4.00×10^{-9}	1.50×10^{-6}	3.10×10^{-8} [d]	1.56×10^{-6} (23%)	9.45×10^{-6}
Pu(III)	GWB	2.59×10^{-6}	0.484	7.89×10^{-6} (34%)	2.60×10^{-8}	2.00×10^{-8}	1.50×10^{-6}	2.30×10^{-6} [d]	3.83×10^{-6} (33%)	1.17×10^{-5}
Th(IV)	GWB	6.05×10^{-8}	-0.011	5.90×10^{-8} (10%)	2.60×10^{-8}	2.00×10^{-8}	3.72×10^{-7}	1.04×10^{-7}	5.21×10^{-7} (90%)	5.80×10^{-7}
U(IV)	GWB	6.05×10^{-8}	-0.011	5.90×10^{-8} (10%)	2.60×10^{-8}	2.00×10^{-8}	3.72×10^{-7}	1.04×10^{-7}	5.21×10^{-7} (90%)	5.80×10^{-7}
Np(IV)	GWB	6.05×10^{-8}	-0.011	5.90×10^{-8} (10%)	2.60×10^{-8}	2.00×10^{-8}	3.72×10^{-7}	1.04×10^{-7}	5.21×10^{-7} (90%)	5.80×10^{-7}
Pu(IV)	GWB	6.05×10^{-8}	-0.011	5.90×10^{-8} (10%)	2.60×10^{-8}	2.00×10^{-8}	3.72×10^{-7}	1.04×10^{-7}	5.21×10^{-7} (90%)	5.80×10^{-7}
Np(V)	GWB	2.77×10^{-7}	--[a]	2.77×10^{-7} (35%)	2.60×10^{-8}	--[b]	2.52×10^{-10}	4.88×10^{-7}	5.14×10^{-7} (65%)	7.91×10^{-7}
U(VI)	GWB	1.00×10^{-3}	--[a]	1.00×10^{-3} (99%)	2.60×10^{-8}	3.00×10^{-8}	1.10×10^{-5} [c]	2.30×10^{-6} [d]	1.34×10^{-5} (1%)	1.01×10^{-3}
Am(III)	ERDA-6	1.48×10^{-6}	0.484	4.51×10^{-6} (26%)	2.60×10^{-8}	4.00×10^{-9}	4.96×10^{-6}	3.10×10^{-8} [d]	5.02×10^{-6} (53%)	9.53×10^{-6}
Pu(III)	ERDA-6	1.48×10^{-6}	0.484	4.51×10^{-6} (10%)	2.60×10^{-8}	2.00×10^{-8}	4.96×10^{-6}	2.30×10^{-6} [d]	7.29×10^{-6} (62%)	1.18×10^{-5}
Th(IV)	ERDA-6	7.02×10^{-8}	-0.011	6.84×10^{-8} (10%)	2.60×10^{-8}	2.00×10^{-8}	4.31×10^{-7}	1.20×10^{-7}	5.98×10^{-7} (90%)	6.66×10^{-7}
U(IV)	ERDA-6	7.02×10^{-8}	-0.011	6.84×10^{-8} (10%)	2.60×10^{-8}	2.00×10^{-8}	4.31×10^{-7}	1.20×10^{-7}	5.98×10^{-7} (90%)	6.66×10^{-7}
Np(IV)	ERDA-6	7.02×10^{-8}	-0.011	6.84×10^{-8} (10%)	2.60×10^{-8}	2.00×10^{-8}	4.31×10^{-7}	1.20×10^{-7}	5.98×10^{-7} (90%)	6.66×10^{-7}
Pu(IV)	ERDA-6	7.02×10^{-8}	-0.011	6.84×10^{-8} (10%)	2.60×10^{-8}	2.00×10^{-8}	4.31×10^{-7}	1.20×10^{-7}	5.98×10^{-7} (90%)	6.66×10^{-7}
Np(V)	ERDA-6	8.76×10^{-7}	--[a]	8.76×10^{-7} (36%)	2.60×10^{-8}	--[b]	6.48×10^{-9}	1.54×10^{-5}	1.57×10^{-6} (64%)	2.45×10^{-6}
U(VI)	ERDA-6	1.00×10^{-3}	--[a]	1.00×10^{-3} (99%)	2.60×10^{-8}	3.00×10^{-8}	1.10×10^{-5} [c]	2.30×10^{-6} [d]	1.34×10^{-5} (1%)	1.01×10^{-3}

a – Np(V) and U(VI) solubility uncertainty parameters are not sampled for PA
b – Np(V) intrinsic colloids are not included in the PA calculations
c – CAPHUM value
d – CAPMIC value

Table 8-4. Mean Total Mobilized Concentrations in Castile Brine for the PABC09, CRA-2014 PA and CRA14_SEN4 PA

Radionuclide and Oxidation State	PABC09 (M)	CRA-2014 PA (M)	CRA14_SEN4 PA (M)
Am(III)	6.23×10^{-6}	7.13×10^{-7}	9.53×10^{-6}
Pu(III)	2.64×10^{-6}	1.25×10^{-6}	1.18×10^{-5}
Th(IV)	3.53×10^{-7}	3.04×10^{-6}	6.66×10^{-7}
U(IV)	2.56×10^{-7}	3.04×10^{-6}	6.66×10^{-7}
Np(IV)	6.33×10^{-7}	3.04×10^{-6}	6.66×10^{-7}
Pu(IV)	2.66×10^{-7}	3.04×10^{-6}	6.66×10^{-7}
Np(V)	1.14×10^{-5}	2.45×10^{-6}	2.45×10^{-6}
U(VI)	1.01×10^{-3}	1.01×10^{-3}	1.01×10^{-3}

Consideration of the effects of parameter changes on total mobilized actinide concentrations for the PABC09, CRA-2014 PA and CRA14_SEN4 PA has demonstrated that:

- Mineral fragment and intrinsic colloids contribute relatively little to total mobilized actinide concentrations using the mean parameters from these PAs
- For both GWB and ERDA-6 brine, mean Am(III) total mobilized concentrations are significantly decreased relative to PABC09 concentrations by the smaller PROPMIC and CAPMIC parameters used in the CRA-2014 PA and CRA14_SEN4 PA
- For both GWB and ERDA-6 brine, mean Am(III) and Pu(III) total mobilized concentrations for the CRA-2014 PA are significantly decreased relative to PABC09 and CRA14_SEN4 PA concentrations by the negative mean SOLMOD3:SOLVAR parameter
- Because of the negative SOLMOD3:SOLVAR parameter and positive SOLMOD4:SOLVAR parameter used in the CRA-2014 PA and different PROPHUM parameters for Pu(III) and Pu(IV), mean and median total mobilized Pu(IV) concentrations are higher than the mean and median total mobilized Pu(III) concentrations, even though the baseline Pu(III) solubilities in GWB and ERDA-6 were significantly greater than the baseline Pu(IV) solubilities

These results demonstrate the importance of the PROPMIC and CAPMIC parameters developed by DOE for the CRA-2014 PA (Section 7.4) and the importance of consistently applying a defensible set of criteria for selection solubility data for calculating the SOLMOD3:SOLVAR and SOLMOD4:SOLVAR parameters (Sections 6.6.6 and 6.7).

9.0 ACTINIDES INCLUDED IN PERFORMANCE ASSESSMENT CALCULATIONS

Total mobilized actinide concentrations are important only for calculating DBRs and releases by transport through the Culebra to the WIPP boundary. The primary release mechanism at high probability—cuttings and cavings—is independent of the extent of total actinide mobilization in brine. Spallings, which is not currently predicted to be an important release mechanism, are also not affected by actinides mobilized in brine.

Although actinide solubilities and colloidal actinide concentrations are calculated for thorium, uranium, neptunium, plutonium, americium and curium, not all elements and isotopes contribute significantly to DBR or releases through the Culebra and Salado. DOE has noted that inclusion of all radionuclides in the WIPP inventory in the PA calculations would be both computationally complex and prohibitively time consuming. Consequently, the number of radionuclides directly included in PA was reduced using an algorithm developed for the CCA (DOE 2014b, Appendix PA-2014, Section PA-4.3.2 and Figure PA-17). Isotopes identified for calculations of CRA-2014 PA DBR releases included 23 radioisotopes of plutonium, americium, uranium, thorium, neptunium, curium, cesium and strontium (Kicker and Zeitler 2013). These isotopes represent 99.96% of the potential releases, in EPA units[22], of the CRA-2014 PA inventory at the time of repository closure (Kicker and Zeitler 2013).

Ten plutonium, americium, uranium and thorium isotopes were identified for calculations of releases by transport through the Culebra and Salado (Kicker and Zeitler 2013). DOE reduced the number of isotopes identified for the transport release calculations based on total inventories, removing radionuclides with inventories that total less than one EPA unit. DOE further omitted ^{137}Cs and ^{90}Sr because their short half lives cause their concentrations to drop below one EPA unit within 150 years. ^{241}Pu was added to the list of modeled isotopes because it is a parent isotope for ^{241}Am and has a significant inventory at the start of the calculation. ^{229}Th and ^{233}U were included because they have potential releases close to one EPA unit and were included in previous PA calculations. The isotopes ^{14}C, ^{243}Cm, ^{59}Ni and ^{63}Ni were excluded because their contributions to the overall potential release are negligible. The remaining ten isotopes were ^{241}Am, ^{238}Pu, ^{239}Pu, ^{240}Pu, ^{241}Pu, ^{242}Pu, ^{233}U, ^{234}U, ^{229}Th and ^{230}Th. This list of isotopes accounts for 97.83%, in EPA units, of the potential releases at the time of repository closure in the CRA-2014 PA inventory (Kicker and Zeitler 2013).

The inventories of the ten isotopes identified for calculating releases by transport through the Culebra and Salado were combined into a smaller number of “lumped” inventory parameters based on the reasonable assumption that radionuclides of the same element will transport at the same rate. Therefore, the inventories of the uranium isotopes; ^{239}Pu, ^{240}Pu and ^{242}Pu; and thorium isotopes were combined into the lumped inventory parameters U234L, PU239L and TH230L,

[22] The activity in “EPA Units” for a radionuclide is the initial source term activity (in Ci) of that radionuclide divided by the product of the waste unit factor (WUF) and the release limit (in Ci/unit of waste) for the same radionuclide (Kicker and Herrick 2013). The WUF, also referred to as the "unit of waste," is defined as the number of millions of curies of alpha-emitting TRU radionuclides with half-lives longer than 20 years destined for disposal in the WIPP repository (DOE 1996).

respectively. ^{238}Pu was not included in the PU239L parameter because of its short half life. As a final step, the inventory of ^{241}Pu was combined with the ^{241}Am inventory to create the inventory for AM241L in the transport calculations (Kicker and Zeitler 2013). Depending on the half-lives of the isotopes, combining the inventories based on curies or on moles will result in differing combined activities. The lumped parameters were combined using an approach that maximized their combined activities (Kicker and Zeitler 2013).

10.0 CULEBRA DOLOMITE DISTRIBUTION COEFFICIENTS

Radionuclides may reach the Culebra member of the Rustler Formation via brine flow through a borehole that intersects the repository (DOE 2014b, Appendix PA-2014, Section 6.8.3). Radionuclides introduced into the Culebra may be transported through natural groundwater flow to the accessible environment (DOE 2004, Section 6.4.6.2). Predictions of radionuclide transport and release through the Culebra are affected by sorption onto minerals along this potential pathway. Accordingly, DOE developed distribution coefficients (K_ds) to express a linear relationship between sorbed and aqueous concentrations of the radionuclides (DOE 2004, Section 6.4.6.2.1).

10.1 DISTRIBUTION COEFFICIENTS USED IN THE CCA PA AND PAVT

The distribution coefficients used in the CCA PA and PAVT were developed using data from experiments carried out at Los Alamos National Laboratory (LANL) and SNL:

- Sorption studies carried out with 'dolomite-rich Culebra rock' by Triay and coworkers
- Sorption studies performed using pure dolomite from Norway and synthetic NaCl solutions by Brady and coworkers
- Transport studies using intact core samples of Culebra rock by Lucero and coworkers

Brush (1996) compiled and evaluated sorption data from these sources , and the selected K_d values were used in the CCA PA and CCA PAVT (Table 10-1). Brush and Storz (1996) subsequently updated these values because of slight errors in the calculated K_d values. The differences between the K_d values Brush (1996) and by Brush and Storz (1996) reported resulted from corrections of errors in the mass of dolomite used to calculate K_d values in the sorption studies by Brady and coworkers and corrections of errors in the density of brine Triay and coworkers used to calculate K_d values in the experiments (Brush and Storz 1996). The revised values from Brush and Storz (1996) were not available in time for inclusion in the CCA PA or PAVT. However, Brush and Storz (1996) stated that the relatively small changes in the K_d values were unlikely to significantly impact PA results.

Brush (1996) and Brush and Storz (1996) provided K_d values for actinide elements for both deep (Castile and Salado) brines and Culebra brines. For conservatism, only the ranges of K_ds for the brine having the smaller mean value were used in PA. A uniform distribution was used for all K_d ranges in the CCA PA (Brush 1996; Brush and Storz 1996). Sorption experiments were conducted in the presence of organic ligands, but DOE did not revise the ranges of K_ds to include the potential effects of organic ligands because they assumed that metals present in the waste (such as iron and nickel) would compete with actinides for the organic ligands and would limit the effects of ligands on actinide sorption (Brush 1996, Brush and Storz 1996).

Table 10-1. Comparison of Matrix K_d Values for the CCA PA and PAVT With Matrix K_d Values for the CRA-2004 PA, PABC04, CRA-2009 PA and PABC09

K_d Range [m^3/kg]	CCA PA and PAVT (Brush 1996)	CRA-2004 PA, PABC04 and CRA-2009 PA (Brush and Storz 1996)	High Concentration Organics (Brush and Storz 1996)[a]	PABC09 and CRA-2014 PA (Clayton 2009)[b]
Am(III)	0.02–0.5	0.02–0.4	0.00505–0.00740	0.005–0.4
Pu(III)	0.02–0.5	0.02–0.4	--	0.005–0.4
Th(IV)	0.9–20	0.7–10	0.000467–0.00469	0.0005–10
U(IV)	0.9–20	0.7–10	--	0.0005–10
Np(IV)	0.9–20	0.7–10	--	0.0005–10
Pu(IV)	0.9–20	0.7–10	--	0.0005–10
Np(V)	0.001–0.2	0.001–0.2	0.00–0.00249	0.00003–0.2
U(VI)	0.00003–0.03	0.00003–0.02	0.00–0.0101	0.00003–0.02

a – SPC brine (Salado) with 0.0489 M acetate, 0.003417 M citrate, 1.1×10^{-5} M EDTA, and 0.00288 M lactate; H-17 brine (Culebra) and ERDA-6 brine (Castile) with 0.0195 M acetate, 0.00340 M citrate, 1.46×10^{-5} M EDTA, and 0.00076 M lactate

b – Log-uniform distribution

EPA (1998c) evaluated the ranges and distributions of K_d values used in the CCA PA. EPA accepted the ranges used in the CCA, but disagreed with the uniform distribution for these ranges. EPA instead specified a log-uniform distribution for the K_d ranges for use in the PAVT.

10.2 DISTRIBUTION COEFFICIENTS USED IN THE CRA-2004 PA, PABC04 AND CRA-2009 PA

Hansen and Leigh (2003) provided a reconciliation of parameter values between the CCA (PAVT) and the CRA-2004 PA. Hansen and Leigh (2003) documented that there were no changes in the ranges of K_d values for U(VI), U(IV), Pu(III), Pu(IV), Th(IV), and Am(III) between the CCA PA and the PAVT. Hansen and Leigh (2003) noted the two errors in the procedures used to calculate the matrix K_ds that were identified by Brush and Storz (1996), and reiterated the conclusion of Brush and Storz (1996) that these errors would have minimal effects on the CCA PA and the PAVT results.

The CRA-2004 PA, PABC04 and CRA-2009 PA used the revised K_d ranges from Brush and Storz (1996) (Table 10-1). During the review of the CRA-2004 PA and PABC04, EPA (2006c) evaluated the K_d ranges and log-uniform distribution of the data. The key references EPA (2006c) used in their evaluation of the matrix K_d values were Brush (1996), Brush and Storz (1996), Wall (2001) and Hansen and Leigh (2003).

In discussing the parameter baseline, including K_ds, Wall (2001) appeared to use the EPA (1998d) conclusions to address key technical issues, such as the use of brines with lower pH than expected in the repository and the effect of organic ligands. EPA (1998d) agreed that the effect of organic ligands on actinide sorption could be ruled out because sufficient concentrations of non-actinide cations would be available to complex with these ligands. However, aqueous speciation data and modeling calculations available from the CRA-2004 (EPA 2006c, Section 8.0) indicated that solubilities of the +III and +V actinides could be affected by organic ligands.

Consequently, EPA (2006c) re-examined the K_d values measured in brines with organic ligands (Brush and Storz 1996).

The reported values for low and intermediate organic ligand concentrations were judged to be the most applicable to WIPP repository conditions. The ranges of K_d values reported for Am(III) and U(VI) in the presence of organic ligands were found to be consistent with the ranges of K_d values used in the CRA-2004 PA and PABC04. However, values on the order of approximately 4 ml/g were observed for Th(IV) in the presence of organic ligands, whereas the range of values used in the CRA-2004 PA and PABC04 was 700 to 10,000 ml/g. This lower K_d for Th(IV) appeared to be inconsistent with the results of geochemical modeling because Th(IV) does not appear to be significantly complexed by organic ligands (EPA 2006c, Section 8.5). EPA (2006c) concluded that this inconsistency may have been the result of higher CO_2 fugacities and lower pH in the experiments than are expected in the WIPP repository.

The data regarding the potential effects of organic ligands on actinide sorption were previously considered by EPA (1998b). At that time, EPA concluded that the results of the speciation calculations, K_d values reported in the literature and expected increased adsorption under alkaline conditions indicated that the K_d ranges exclusive of the organic ligands were sufficiently representative of actinide solid/liquid partitioning for modeling actinide transport in the Culebra.

Comparison of the K_d ranges used in the CCA PA and PAVT with the ranges used in the CRA-2004 PA, PABC04 and CRA-2009 PA, indicated that the differences were small (Table 10-1). Furthermore, the revised K_d ranges are more conservative because the lower K_d values should result in less sorption. EPA (2006c) determined that the revised K_d ranges used in the CRA-2004 PA and PABC04 were acceptable, because no new experimental sorption data were available, the changes to the K_d ranges were minor and conservative and these changes had been previously reviewed and found acceptable by EPA (1998b).

10.3 DISTRIBUTION COEFFICIENTS USED IN THE PABC09 AND CRA-2014 PA

The CRA-2009 PA used the same ranges of K_d values and distributions as the CRA-2004 PA and PABC04 (DOE 2009, Appendix PA-2009, Section PA-2.1.4.7). However, higher ligand concentrations were predicted for the PABC09 than for previous PAs (Table 6-1). EPA (2010b) found that the predicted acetate and citrate concentrations for the PABC09 were similar to concentrations in the high-ligand-concentration experiments Brush and Storz (1996) reported, and the predicted EDTA concentration exceeded the concentrations reported for the high-ligand-concentration experiments.

The range of K_d values measured for Np(V) in the presence of high concentrations of organic ligands is compared to the range of K_d values Brush and Storz (1996) established in Table 10-1. Although the measured K_d values for Np(V) in the presence of high concentrations of organic ligands falls at the lower end of the K_d range used in PA, the effects on PA of lower K_d values for Np(V) are likely insignificant because of the relatively small amount of neptunium in the WIPP inventory. The range of K_d values measured for U(VI) with high concentrations of organic ligands is reasonably similar to the range selected for PA by Brush and Storz (1996). Consequently, EPA (2010b) concluded that the effects of organic ligands on the transport of Np(V) or U(VI) through the Culebra are not likely to be significant for PA.

For both Am(III) and Th(IV), however, EPA (2010b) observed that the K_d ranges measured in experiments with high concentrations of organic ligands were significantly lower than the K_d ranges used in the CCA PAVT, PABC04 and CRA-2009 PA calculations. Because of the importance of Am(III), Pu(III) and Pu(IV) to total releases from the repository, smaller K_d values for the +III and +IV oxidation state have the potential to significantly affect PA results. For that reason, EPA requested additional information from DOE regarding the possible effects of increased ligand concentrations and lower K_d values on +III and +IV actinide releases by transport through the Culebra (Comment 3-C-25, Cotsworth 2009c).

DOE re-evaluated the range of K_d values used to assess retardation of actinides during transport through the Culebra (Moody 2010b). There was no evidence that the upper bound should be changed. Consequently, the upper bounds for the K_d ranges were maintained, but the lower bounds were reduced to account for the possibility of higher organic ligand concentrations.

Clayton (2009) provided details regarding the changes in the K_d ranges. The lower limit for the U(VI) K_d range was not modified, because this value was already effectively equal to zero. Although neptunium is not currently included in the Culebra transport calculations, DOE updated its K_d range to maintain consistency. Because the K_d ranges sampled for PA are assumed to have a log-uniform distribution, assumption of a lower K_d limit of zero is not valid. Consequently, the lower limit of the U(VI) K_d was also assumed for the lower limit for the Np(V) K_d (Table 10-1). The K_d ranges used in the PABC09 are summarized in Table 10-1. The revised lower-bound values for the K_ds used in the PABC09 are consistent with the lower limits of the ranges observed in the experiments with high concentrations of organic ligands. Consequently, EPA (2010b) found that the K_d ranges were appropriately conservative for use in the PABC09.

The K_d ranges sampled for the PABC09 were also used for the CRA-2014 PA (DOE 2014b, Appendix PA, Table PA-1). During review of the CRA-2014, EPA requested that DOE assess the possible effects on the K_d ranges of changed organic ligand concentrations since the PABC09 (Edwards 2014, Comment 1-23-1) and DOE responded with an assessment of the organic ligand inventory changes (Franco 2015b). The acetate, citrate and EDTA concentrations calculated for the CRA-2014 PA were consistent with the concentrations used for the PABC09 (Table 6-1). Oxalate concentrations for all brine volumes were higher in the CRA-2014 PA than in the PABC09. However, because aqueous speciation calculations indicate that oxalate is likely to precipitate as the Ca-oxalate solid whewellite and is unlikely to affect actinide speciation in WIPP brines (Brush and Domski 2013b), oxalate is not expected to significantly affect sorption in the Culebra. Additionally, the lower bounds of the sampled K_d ranges are quite low (Table 10-1), which would maximize Culebra transport.

Organic kitty litter was mistakenly used as an absorbent for nitrate salts for Waste Stream LA-MIN02-V.001 (NMED 2014) and 349 drums of this waste were placed in Panels 6 and 7 (Wallace 2014) which lead to the radionuclide release. EPA requested that DOE assess the potential effects of the organic kitty litter added to the LANL waste on the Culebra K_ds (Edwards 2014, Comment 1-23-1). In their response to this comment (Franco 2015b), DOE deferred the Culebra K_d portion to their response to Comment 1-C-1 (Franco 2015c). DOE noted that the possible 41,000 lbs of kitty litter in the LANL waste cellulosic kitty litter makes up less than 0.4% of the currently expected total amount of cellulose and 0.1% of the total CPR based on a

scaled full repository volume (Franco 2015c). DOE identified microbial degradation of the kitty litter and changes to the repository chemical conditions through CO_2 production as the process likely to affect Culebra K_ds. DOE stated that the excess MgO emplaced in the repository would adequately control CO_2 generation by microbial degradation of cellulosic kitty litter and prevent any effects on Culebra K_ds, which is reasonable. DOE also cited an earlier assessment of the effects of increased CPR on repository performance (Dunagan et al. 2005). However, this study was performed before parameters such as microbial degradation rates and probabilities were changed (Tables 3-9 and 3-10) and other PA changes have been made such as an updated water balance. Consequently, it is not clear that this older PA sensitivity analysis still applies. DOE did not directly address the potential effects of organics or surfactants that might be leached from the kitty litter, but only a small amount of waste included the kitty litter sorbent, which includes four waste streams placed in 507 drums (Shrader 2015). The small volume of waste likely precludes any significant effects on Culebra K_ds.

No additional Culebra sorption data have been developed since the PABC09. Because the concentrations of acetate, citrate and EDTA in WIPP repository brines are consistent with the high-organic-ligand concentrations used in the Brush and Storz (1996) experiments, the K_d ranges sampled for the CRA-2014 PA continue to be appropriate.

10.4 CULEBRA DOLOMITE DISTRIBUTION COEFFICIENTS CONCLUSIONS

- Radionuclides may reach the Culebra, the most transmissive member of the Rustler Formation. This could happen through brine flow up a borehole and will be affected by sorption onto the minerals along this pathway.
- Sorption data were collected from experiments using Culebra dolomite. The K_d values remain the same as those used in the PABC09 and reflect updated data on the effects of higher concentrations of organic ligands on actinide sorption.
- The K_d values likely provide a conservative assessment of actinide transport and continue to remain appropriate.

11.0 EFFECTS OF HETEROGENEOUS WASTE LOADING

All solubility calculations carried out for WIPP PA assume that waste would be homogeneously loaded in the repository. At the time of the CCA, no information was available regarding the potential patterns of waste loading that might occur, and this assumption was appropriate. However, EPA noted during their review of the CRA-2004 PA that Panel 1 waste loading information indicated that the assumption of homogeneity was incorrect. Because shipments of waste placed in Panel 1 included an intensive campaign of waste shipments from the Rocky Flats site, 54% of the waste in Panel 1 was from that site (Leigh 2003).

EPA (2006c) evaluated the potential effects of waste heterogeneity on the results of PA. This evaluation included the potential effects on actinide solubility calculations and the MgO EF calculations. As described in Section 4.7.1, DOE has accounted for the potential effects of heterogeneous waste loading on the MgO EF by implementing an approved emplacement plan that ensures the required minimum EF is maintained. Kouba (2013) provided an analysis showing that the EF value in each panel exceeds the required minimum value of 1.2.

The Environmental Evaluation Group (EEG) questioned whether the assumption of homogeneous chemical conditions in the repository is appropriate (Oversby 2000). As an alternative to the approach used by DOE, EEG recommended calculating releases that would occur if a small number of waste drums containing relatively high concentrations of actinides and organic ligands are intersected by a borehole. This waste could be leached by drilling fluid, and if this borehole then reached an underlying brine pocket, EEG maintained that an unacceptable release of actinides could result. EEG recommended that DOE assess repository performance by calculating the range of actinide concentrations that could be released under this scenario, and multiplying by the probability of the scenario. This approach was considered on several occasions (EPA 1998a, TEA 2000, TEA 2001). EPA observed that WIPP PAs are based on a probabilistic approach, rather than the calculation of solubilities associated with a worst-case scenario as suggested by EEG, and this probabilistic approach had been peer-reviewed and found acceptable. EPA also found that the effects of waste heterogeneity on PA were adequately addressed by the uncertainties assigned to the actinide solubilities (EPA 1998a, TEA 2000, TEA 2001).

During review of the CRA-2004 PA, EPA requested additional information from DOE regarding the potential effects of heterogeneous waste loading on the assumption of homogeneous chemical conditions throughout the entire repository (Cotsworth 2004a, Comment G-12). DOE responded with an assessment of the potential effects of higher amounts of plutonium in Panel 1 than would be expected, based on homogeneous emplacement throughout a 10-panel repository (Detwiler 2004c). DOE stated that the only likely effect of this higher-than-expected loading of plutonium in Panel 1 would be increased radiolysis that could cause plutonium to speciate as plutonium(V) or plutonium(VI), instead of the reduced oxidation states predicted for the repository (see Section 5.0). However, because of microbial consumption of CPR and the amounts of metallic iron in the repository, including the large amounts of stainless steel in the pipe overpacks in Panel 1, DOE stated that reducing conditions and lower plutonium oxidation states would still be maintained in Panel 1.

Heterogeneous waste loading is unlikely to affect actinide solubilities if a relatively high proportion of the actinide inventory is present in a single panel, because of the assumption of chemical equilibrium with respect to the solubilities of actinide solid phases. However, the placement of waste with a high proportion of the organic ligand inventory in a panel could affect actinide solubilities. DOE has accounted for this possibility in the actinide solubility calculations by assuming the entire organic ligand inventory is dissolved in the amount of brine released from the repository (Brush and Domski 2013a). This approach ensures that the effects of heterogeneous waste placement are adequately accounted for in the actinide solubility calculations, provided that the inventory of organic ligands is bounded.

Use of shielded containers for disposal of RH waste will increase the lead inventory in panels filled after EPA's approval was received (Edwards 2011, 2013). Evaluation of the lead inventory increase associated with placement of candidate RH waste streams indicates that the repository-average lead inventory could increase to 17% of the mass of iron-based waste and packaging materials (Section 3.2). Because the excess lead will only be placed in panels filled after the approval of RH shielded containers, the lead inventory in those panels may be higher than 17%. Consequently, it would be appropriate to include bounding calculations for the CRA-2019 to evaluate possible increased lead inventory based on candidate waste forms that could be placed in shielded containers (Section 3.2). The principal effects of lead on PA are likely to be caused by gas generation through anoxic corrosion. Because the increased amount of lead and increased lead surface area will depend on the amounts of RH waste emplaced in shielded containers, the magnitude of the effects of increased lead on gas generation and repository performance cannot be quantitatively addressed at this time. However, it is reasonable to assume that the sampled uncertainty of the anoxic corrosion gas generation rates (Section 3.1.2) adequately bounds the effects of anoxic corrosion of the possible increase in the lead inventory. Consequently, the effects of heterogeneous placement of lead in the repository is unlikely to have major effects on PA.

The panel closures are expected to have extremely low permeabilities (Camphouse et al. 2012) and will effectively limit the contact of brine between panels. The effects of heterogeneous CPR inventory and iron inventory placement leading to variable gas generation between panels have been considered and found to be unlikely to significantly affect PA (TEA 2004). In addition, the heterogeneous distribution of organic ligands is conservatively bounded by assuming the entire inventory is dissolved in the mobilized brine volume. Consequently, the available information indicates that the effects of heterogeneous waste loading have been adequately addressed in PA.

In summary:

- The effects of heterogenous waste loading are unlikely to significantly affect actinide solubilities because of the assumption of chemical equilibrium between actinide solid phases.
- DOE accounts for organic ligands by dissolving the entire inventory in the minimum amount of brine needed for a release from the repository.
- Even though lead inventories may increase, uncertainty in gas generation rates likely bounds the effects of this increase. Consequently, lead is unlikely to have major effects on PA based on current information. By performing a bounding calculation for CRA-2019, DOE can deomonstrate this.

- Although panel closures will likely have extremely low permeabilities effectively limiting brine contact between panels, heterogeneous CPR and iron inventory, as well as gas generation, are unlikely to significantly affect PA and have been adequately been addressed.

12.0 EFFECTS OF CHEMICAL PROCESSES ON REPOSITORY WATER BALANCE

Chemical processes that may affect the quantity of water in the repository include microbial degradation of CPR, MgO hydration to form brucite or hydromagnesite, dehydration of hydromagnesite to form magnesite and anoxic corrosion of iron-based metal or other metals. For the CCA PAVT, PABC04 and PABC09, brine consumption from anoxic corrosion of iron-based metal was the only chemical process included in the repository water balance. SC&A (2008b) performed a qualitative evaluation of the possible effects of various chemical processes on brine generation and consumption, and concluded that the potential importance of CPR degradation, MgO hydration and carbonation and FeS precipitation on the water balance in the repository warranted additional evaluation.

EPA observed during their review of the CRA-2009 (DOE 2009) that the potential effects of processes other than anoxic corrosion on the repository water balance had not been addressed (Cotsworth 2009a, Comment 1-C-5). Consequently, EPA requested additional information from DOE regarding whether production of water by CPR degradation and consumption of water by brucite hydration and hydromagnesite persistence might significantly affect predicted repository performance. DOE acknowledged the potential for water consumption or production with reactions involving magnesium-based minerals and microbial degradation of CPR (Moody 2009a). DOE concluded that although it would be appropriate to include all water balance considerations in future PA calculations, the uncertainties associated with water balance changes caused by brucite hydration, hydromagnesite persistence in the repository and production of water by CPR degradation precluded adding these processes to the repository water balance calculations at that time. EPA (2010b) agreed that this conclusion was reasonable, but recommended DOE continue evaluating the effects of chemical processes on the repository water balance for the CRA-2014.

For the CRA-2014 PA, DOE (2014b) modified the repository water balance to include multiple chemical processes. In addition to the flow of water in and out of the repository, the chemical processes in the revised water balance included major brine production and consumption reactions (DOE 2014b, Appendix PA, Section PA-4.2.5). The reactions included in the water balance are: brine consumption by anoxic corrosion of iron-based metals, brine production by sulfidation of iron-based metals, brine production by microbial degradation of CPR materials, brine consumption by MgO hydration and brine production by hydromagnesite conversion to magnesite. Camphouse (2013b) summarized the reactions included in the water balance and Clayton (2013) provided justification for the implementation and stoichiometric coefficients for the water balance.

12.1 ANOXIC CORROSION AND SULFIDATION OF IRON-BASED METALS

Anoxic corrosion consumes water, which has been accounted for in PAs preceeding the CRA-2014. Brine consumption through anoxic corrosion occurs via the reaction:

$$Fe(s) + 2\ H_2O(l) \rightarrow Fe(OH)_2(s) + H_2(g) \quad \textbf{(37)}$$

Reaction (37) results in the consumption of two moles of water for each mole of iron consumed (Clayton 2013). The rates of this anoxic corrosion reaction in humid and inundated conditions are based on sampled parameters (Section 3.1.2).

The CRA-2014 PA assumes that H_2S created by CPR degradation [reaction (11)] preferentially reacts with iron hydroxide versus metallic iron (CRA-2014 Appendix MASS, Section MASS-6.3). These sulfidation reactions are shown in reactions 6 and:

$$Fe(s) + H_2S(g) \rightarrow FeS(s) + H_2(g) \quad \textbf{(38)}$$

The assumption that H_2S preferentially reacts with $Fe(OH)_2(s)$ [reaction (6)] increases brine production and decreases gas production compared to the assumption that all or some of the H_2S reacts with metallic iron [reaction (38)]. EPA requested supporting data for this water-balance assumption from DOE and an evaluation of the potential magnitude of its effects on the water balance (Edwards 2015b, Comment 2-C-3). In response, DOE (Bryson 2015a) cited the results of WIPP project-specific iron sulfidation experiments Telander and Westerman performed (1993, 1997). These test results showed that FeS(s) and not $Fe(OH)_2(s)$ formed during reaction of H_2S with steel in the presence of Brine A, which provides reasonable justification for assuming H_2S will preferentially react with any $Fe(OH)_2(s)$ present in the repository.

DOE also assumed for the CRA-2014 PA water balance that all H_2S produced by CPR degradation will instantanously and completely react with the iron in steel to produce FeS(s) (Clayton 2013). EPA requested information justifying this assumption (Edwards 2015a, Comment 4-C-5; Economy 2016), noting that it appears to contradict evidence of steel passivation by H_2S Telander and Westerman (1997) reported (Section 3.1.2). DOE agreed to remove reactions (6) and (38) from calculations of the water balance and gas production in PA by setting the stoichiometric coefficients to zero for Appendix PA equations PA.89 and PA.90 (DOE 2014b). Removing reaction (6) from PA calculations will increase the amount of gas in the repository and decrease the amount of brine. The effects of the change to the stoichiometric coefficients for the steel sulfidation reactions are addressed in Section 13.0 as part of the assessment of the CRA14_SEN4 PA.

12.2 LEAD CORROSION

EPA requested additional information related to effects of the increased lead inventory from the use of shielded RH waste containers on gas generation and the water balance (Edwards 2015c, Comment 3-C-7). DOE's response to this comment (Bryson 2015b) is discussed in detail as part of the gas generation evaluation (Section 3.2). As previously noted for gas generation, the potential mass of lead compared to iron using the candidate waste streams identified by Crawford and Taggart (2007) indicates that lead corrosion may have a small effect on water balance. Because WIPP-specific lead corrosion rate data are available (Roselle 2013), EPA believes additional work is necessary to consider the effects of lead corrosion on water balance in the CRA-2019 PA calculations if bounding calculations using candidate waste forms indicate significant masses of lead will be present in the repository.

12.3 MICROBIAL DEGRADATION OF CPR

The CPR microbial degradation reactions [reactions (10) and (11), Section 3.3.1) and rate parameters used to calculate gas generation for the CRA-2014 PA (Table 3-9) were used to calculate the production of water by CPR degradation (Camphouse 2013b). Because the moles of water produced differs for reaction (10) (denitrification) and reaction 11 (sulfate reduction), the average stoichiometry model (Wang and Brush 1996) is used to calculate the production of gas and water by CPR degradation:

$$[C_6H_{10}O_5]/6 + \text{microbes} \rightarrow y\ H_2(g) + z\ H_2O + \text{unknowns} \quad \textbf{(39)}$$

Clayton (2013) describes the calculation of y and z in equation (39) using the maximum amount of CPR that can be degraded within 10,000 years in a particular vector and the potential amounts of CPR that can be degraded by denitrification [reaction (10)] and sulfate reduction [reaction (11)]. This approach adequately incorporates the effects of CPR degradation on water balance.

12.4 BACKFILL REACTIONS

The MgO backfill reactions included in the water balance were: 1) MgO hydration to form brucite [reaction (14)], which consumes water; 2) the carbonation of brucite to form hydromagnesite [reaction (17)], which does not consume or produce water; and 3) conversion of hydromagnesite to magnesite [reaction (20)], which produces water (Camphouse 2013b). Clayton (2013) also included reaction of MgO directly to magnesite when brucite is not available:

$$MgO(s) + CO_2(g) \rightarrow MgCO_3(s) \quad \textbf{(40)}$$

12.4.1 MgO Hydration Rate

The parameters used to represent the rate of MgO hydration to brucite (reaction 14, Section 4.1.1) were WAS_AREA:BRUCITEC in ERDA-6 brine, WAS_AREA:BRUCITES in GWB brine and WAS_AREA:BRUCITEH under humid conditions. Clayton (2013) developed these parameters using MgO hydration rates and associated uncertainties for each brine type developed by Nowak and Clayton (2007). EPA requested that DOE provide a copy of the Excel file used to calculate the MgO hydration rates (Edwards 2015b, Comment 2-C-7) and DOE provided this file (2-C-7 data spreadsheet.xlsx, Franco 2015a).

EPA noted that the MgO hydration rate data were based on experiments conducted with Premier MgO, whereas MgO in the repository has been provided by three vendors, with a relatively small amount from National Magnesia Chemicals and larger amounts from Premier Chemicals and Martin Marietta Magnesia Specialties (Edwards 2015b, Comment 2-C-6). Wall (2005) performed preliminary tests with the Martin Marietta MgO and concluded that it reacted to form brucite faster than Premier MgO, which indicates that using hydration rates obtained only with Premier MgO would underestimate the MgO hydration rate and overestimate the amount of brine in the repository. EPA requested that DOE provide the inundated and humid hydration rates for

MgO from the three vendors, the potential effects of the various hydration rates on repository performance and the amounts of National Magnesia Chemicals, Premier MgO and Martin Marietta MgO that will be present in the WIPP repository at the time of closure, and assumptions regarding the future source(s) of MgO.

In their response, DOE reported that the percentages of the different MgO sources emplaced in WIPP were 0.4% National Magnesia Chemicals, 30.1% Premier Chemicals and 69.5% Martin Marietta (Franco 2015c). Because of the relatively small amount of National Magnesia Chemicals MgO, DOE has not characterized its hydration rate and the effects of its hydration rate on the repository water balance are likely to be minimal. However, Martin Marietta MgO represents a large fraction of the MgO currently emplaced in the repository and the proportion of this material is likely to become more significant over time because Martin Marietta is the current MgO supplier. DOE acknowledged that the hydration rate of Martin Marietta MgO is higher than Premier MgO (Franco 2015c). Deng et al. (2009) reported some results of Martin Marietta MgO hydration experiments, but Franco (2015c) stated that these experiments had not been completed. Franco (2015c) asserted that using the slower hydration rates for Premier MgO was a conservative assumption, but did not provide evidence to substantiate this claim. Franco (2015c) also stated that releases did not appear to be sensitive to the MgO hydration rates based on sensitivity analyses of the sampled PA parameters (Kirchner 2013).

During an EPA/DOE technical exchange meeting in February 2016, EPA requested that DOE provide additional information on the status of the Martin Marietta MgO hydration experiments. DOE later stated that the Martin Marietta hydration rate data had "not been processed into the form that is usable for PA" (Shrader 2016). However, DOE committed to combining the Martin Marietta MgO hydration rate data with the Premier MgO hydration rate data for use in future PAs.

12.4.2 MgO and Brucite Carbonation Rates

The reaction rates for the MgO and brucite carbonation reactions are defined by the sampled CPR degradation rate because the available CO_2 is produced by CPR degradation. The Gas Generation conceptual model includes the assumption that essentially all CO_2 is rapidly consumed by reaction with the MgO backfill (SCA 2008b). DOE assumed for the CRA-2014 PA that CO_2 preferentially reacts with brucite instead of unreacted MgO via the carbonation (see reaction 17).

For the stoichiometric coefficients used in PA, this reaction was normalized by Clayton (2013) to the moles of CO_2:

$$1.25\ Mg(OH)_2(s) + CO_2 \rightarrow 0.25\ Mg_5(CO_3)_4(OH)_2{\bullet}4H_2O(s) \quad \textbf{(41)}$$

EPA observed that assuming CO_2 preferentially reacts with brucite instead of with MgO:

$$1.25\ MgO(s) + CO_2 + 1.25\ H_2O \rightarrow 0.25\ Mg_5(CO_3)_4(OH)_2{\bullet}4H_2O(s) \quad \textbf{(42)}$$

increases brine in the repository because more brine is consumed by reaction (42) than by reaction (41). EPA requested that DOE provide supporting data for this assumption and an evaluation of the potential magnitude of the effects of this assumption on the water balance (Edwards 2015b, Comment 2-C-3). In response, DOE cited WIPP-specific experiments carried out to evaluate MgO hydration and carbonation (Xiong and Snider 2003, Xiong and Lord 2008). The cited experiments appear to substantiate the assumption that brucite to hydromagnesite is the reasonably expected pathway for carbonation. The DOE response noted the differences in the results of the CRA14-BV and CRA14-0 PA calculations, which only differed in the implementation of updated iron corrosion rates that reduced the rate of brine consumption and implementation of the revised water balance calculations. DOE stated that the overall impact of the changes in iron corrosion rates and water balance calculations were small.

Clayton (2013) stated that "In the event that CO_2 generation is occurring, but brucite is not available in BRAGFLO simulations, MgO will be converted directly to magnesite:" EPA has repeatedly reviewed the potential for magnesite formation in the WIPP repository directly from MgO and determined that magnesite formation directly from MgO will not occur under WIPP conditions and the formation of hydromagnesite should be assumed instead of magnesite (EPA 1998d, SCA 2008, EPA 2010b). EPA stated that correctly including the formation of hydromagnesite [reaction (42)] instead of magnesite [reaction (40)] would decrease the amount of water in the repository and asked that DOE assess the effects on the water balance of incorrectly assuming the formation of magnesite instead of hydromagnesite (Edwards 2015c, Comment 3-C-6). In response, DOE stated that this assumption remained in the BRAGFLO code to be compatible with previous versions and to reduce potential numerical instabilities (Bryson 2015b). DOE also stated that the direct conversion of MgO to magnesite occurred only in the first 20 years when CO_2 has been generated but no brine is yet available. DOE calculated that the potential decrease in water is a maximum of 0.081 m^3, which is insignificant to the overall water balance.

12.4.3 Hydromagnesite Conversion Rate

DOE (Clayton 2013) formulated the conversion reaction from hydromagnesite to magnesite for inclusion in the BRAGFLO calculations as:

$$Mg_5(CO_3)_4(OH)_2{\bullet}4H_2O(s) \rightarrow 4\ MgCO_3(s) + Mg(OH)_2(s) + 4\ H_2O \qquad \textbf{(43)}$$

Clayton (2013) calculated the range for the hydromagnesite conversion rate used in the CRA-2014 PA from reaction times of 100 years to 10,000 years based on a general statement by EPA (1998d) that hydromagnesite would undergo slow conversion to magnesite over hundreds to thousands of years (Table 12-1). This represents a selective reading of EPA (1998d), because EPA (1998d) also noted that "deposits of hydromagnesite are found in some evaporite basins dated as late Quaternary in age (<23.7 million years) (Stamatakis, 1995), indicating that the hydromagnesite has persisted in a metastable state for a long period with only partial conversion to magnesite and other magnesium carbonates." DOE also ignored a more recent EPA review regarding hydromagnesite metastability (SCA 2008a). SCA (2008a) reviewed the available experimental and natural analogue data and found that "a slow rate of hydromagnesite to magnesite conversion in WIPP could result in the persistence of hydromagnesite throughout

much, if not all, of the 10,000-year regulatory period." SCA (2008a) concluded that hydromagnesite conversion is best represented by a range of zero conversion (only hydromagnesite remains after 10,000 years) to complete conversion (only magnesite remains after 10,000 years), with a uniform distribution across this range.

Table 12-1. Hydromagnesite Conversion Rates (WAS_AREA:HYMAGCON)

Minimum Rate (mol kg^{-1} sec^{-1})	Maximum Rate (mol kg^{-1} sec^{-1})	Reaction Time (years)	Source
6.8×10^{-12}	6.8×10^{-10}	100 – 10,000	Clayton (2013)
0	$< 6.8 \times 10^{-10}$	> 100 - infinite	Peake (2016a)
5.7×10^{-11}	3.7×10^{-9}	18 – 1,180	Shrader (2016)
0	3.4×10^{-10}	200 - infinite	This evaluation

EPA noted that the minimum reaction time (maximum reaction rate) for the hydromagnesite conversion reaction was uncertain and requested that DOE provide additional justification for the selection of the hydromagnesite reaction rate limits used in the CRA-2014 PA (Edwards 2015b, Comment 2-C-4; Peake 2016a, Addendum to Comment 2-C-4(a)). EPA recommended a minimum reaction rate of 0 mol kg^{-1} sec^{-1} (Table 12-1) to include the possibility of no hydromagnesite conversion to magnesite during the 10,000-year repository performance period (Peake 2016a). EPA also requested that DOE re-evaluate the maximum reaction rate (consistent with a minimum reaction time of greater than 100 years) that is consistent with the available data (Peake 2016a).

DOE provided a revised reaction rate range (Table 12-1) based on an evaluation of the reaction rate data in Zhang et al. (2000) that corresponds to even shorter reaction times of 18 to 1,180 years (Shrader 2016). The rate calculation assumed order of magnitude uncertainties around the induction periods extrapolated to 25ºC by Zhang et al. (2000), resulting in DOE's prediction of induction periods ranging from 3.3 to 33 years for ERDA-6 brine and 33 to 364 years for GWB brine. These induction period ranges were used with the mean reaction rates and calculated standard deviations from Zhang et al. (2000) to calculate a range of rates for hydromagnesite to magnesite conversion. Using 3.3 years as the minimum induction period at 25ºC in ERDA-6 brine is indefensible because conversion of hydromagnesite to magnesite at 25ºC in laboratory experiments has not been reported. In the absence of any experimental evidence over this reasonably achievable time frame for laboratory experiments, this lower limit is unjustified.

EPA has previously reviewed the Zhang et al. (2000) study and extrapolation of its rate data to low temperature and concluded the extrapolation had many issues, including uncertainties regarding the form of the rate equation, unknown effects of hydromagnesite chemical and physical properties on the induction period, uncertainties in determining the rates during the induction period and questions regarding whether the activation energy would remain constant at lower temperatures. DOE did not consider more recent data, such as investigations showing that citrate, which is present in WIPP repository brines (Table 6-1), can inhibit magnesite growth (Gautier 2012, Gautier et al. 2016), or that higher pH can slow magnesite precipitation (Saldi et al. 2012). DOE's evaluation results are not supported by the available geologic record, which was reviewed by SCA (2008a). Although it is true that magnesite may form under low-temperature hypersaline conditions with high Mg/Ca ratios (SCA 2008a), DOE has not

demonstrated that such conditions will exist in the repository. Consequently, DOE's evaluation of the hydromagnesite to magnesite conversion rate (Shrader 2016) is inadequate.

Because of the lack of experimental evidence that hydromagnesite converts to magnesite at 25ºC and uncertainties associated with extrapolating higher temperature data to lower temperature, it is possible that no hydromagnesite will convert to magnesite during the 10,000-year repository performance period. Accordingly, the minimum reaction rate for hydromagnesite conversion must be 0 mol kg^{-1} sec^{-1}. The Zhang et al. (2000) experiments in saturated NaCl solution are less applicable to WIPP than the GWB experiments because of the possible effects of other WIPP brine constituents on the hydromagnesite conversion rate. The rate data from Zhang et al. (2000) is expressed as an induction period plus a reaction half time. Using the 25ºC extrapolation of the induction period of 273 years and 10 times the reaction half-time of 73 years for essentially complete reaction yields a reaction time of 1,000 years. However, given the uncertainty in the extrapolations, using a smaller reaction time of 200 years would provide a reasonably bounding estimate that is consistent with the "hundreds" of years mentioned by EPA (1998d) and accepted by Clayton (2013) (Table 12-1). The effect of a lower rate range compared to the range used in the CRA-2014 would be less brine production in the repository.

12.5 EFFECTS OF WATER BALANCE ASSUMPTIONS ON PA

The following issues have been identified in DOE's implementation of the water balance for the CRA-2014 PA:

- DOE developed revised ranges of humid and inundated steel corrosion rates that are higher than the ranges used in the CRA-2014 PA by including data collected at low CO_2 concentrations (Section 3.1.2) and EPA has revised the inundated rate upward to account for the effects of higher repository pressure. These higher corrosion rate ranges are more appropriate for the CRA-2019 PA, which would increase gas pressure and decrease brine volumes in the repository
- DOE's assumption that all H_2S created by CPR degradation will react instanteously and completely with iron-based metals in the waste and waste containers was not adequately supported (Section 3.1.2). EPA wants to see the stoichiometric coefficients for these reactions set to zero, which will increase gas pressure and decrease brine volumes in the repository
- The MgO hydration rates were based on data from Premier MgO, which is present in smaller quantities than Martin Marietta MgO and also hydrates more slowly than Martin Marietta MgO. It would be appropriate for DOE to develop hydration rates using Martin Marietta MgO and use these rates with Premier MgO hydration rates in the CRA-2019 PA (Section 12.4.1). Including the Martin Marietta MgO hydration rate data is likely to decrease brine volumes in the repository.
- The hydromagnesite conversion rate used in the CRA-2014 PA was inadequately justified. EPA recommends the lower rate range identified in Section 12.4.3 to be included in the CRA-2019 PA, which will decrease brine in the repository.

EPA requested that DOE assess the likely cumulative effects of water balance assumptions on PA (Edwards 2015b, Comment 2-C-5). DOE's response indicated that the effects of the updated

water balance and steel corrosion rates implemented for the CRA-2014 PA should be relatively small (Bryson 2015). This assessment was justified by comparing the total normalized releases calculated for the CRA14-BV PA to total normalized releases for the CRA-2014 PA. The total normalized releases for the two PAs differed only slightly because the CRA-2014 PA included implementation of the revised iron corrosion rates, which would increase brine and reduce gas in the repository compared to the previous rates (Section 3.1.2) and implementation of the revised water balance.

Incorporation of chemical processes in addition to anoxic corrosion in the water balance represents a significant step toward a more realistic and defensible water balance calculations for WIPP PA. The available information indicates that the issues identified by EPA with the CRA-2014 PA water balance are likely to have reasonably minor effects on PA. DOE stated that the overall impacts of the water balance assumptions on the normalized releases from the repository are likely to be small because DBRs would be dominated by the large amount of brine entering the repository from a pressurized brine pocket in the Castile (Bryson 2015, Response to Comment 2-C-3). Nevertheless, the interactions of brine with repository contents can be influenced by the brine saturation, including iron corrosion rates and CPR degradation, which can affect gas pressures. Because increased gas pressures have the potential to affect repository releases, EPA will expect DOE to revise the water balance in the CRA-2019 PA to incorporate the changes listed above.

13.0 SENSITIVITY STUDY

At EPA's request, DOE performed an additional PA (CRA14_SEN4) to assess the effects of a limited number of parameter changes on repository releases. Chemistry parameter changes included revised uncertainty distributions for the +III (SOLMOD3:SOLVAR) and +IV actinide solubility uncertainties (SOLMOD3:SOLVAR) based on EPA-selected experimental data (Section 6.7) and changes to the stoichiometric parameters for reaction of H_2S with Fe(s) and $Fe(OH)_2$(s) to correspond with zero reaction rates (Section 12.1). Other changes included in the CRA14_SEN4 PA were the use of an EPA-developed distribution for the probability of encountering pressurized brine during a drilling intrusion (GLOBAL:PBRINE, EPA 2017), use of a reduced lower bound for the distribution of the effective shear strength for erosion of waste (BOREHOLE:TAUFAIL), use of a new version of the DRSPALL code to calculate spallings releases and use of the correct representative length of the northernmost set of panel closures. Changes to the +III and +IV actinide solubility uncertainties increased the ranges of dissolved and total mobilized Am(III) and Pu(III) concentrations and reduced the ranges of dissolved and total mobilized Th(IV), U(IV), Np(IV) and Pu(IV) concentrations in the CRA14_SEN4 PA relative to the CRA-2014 PA (Section 8.0). Comparison of the mean total mobilized actinide concentrations in Castile brine (Table 8-4) shows that the mean Am(III) and Pu(III) concentrations were increased by an order of magnitude in the CRA14_SEN4 PA compared to the CRA-2014 PA. Removing sulfidation from the gas generation and water balance models in the WIPP PA resulted in more gas with higher pressure and less brine with lower saturations in the repository in the CRA14_SEN4 PA calculations than in the CRA-2014 PA calculations (Section 12.1).

13.1 EFFECTS OF CRA14_SEN4 PA PARAMETER CHANGES ON RELEASES

Cuttings and cavings releases are important to PA because these releases dominate total releases at high probabilities. The combined changes made for the CRA14_SEN4 PA resulted in minimal increases in cuttings and cavings releases because of the change to the BOREHOLE:TAUFAIL distribution lower bound (Zeitler and Day 2016).

Spallings releases were affected by the changes related to the iron sulfidation reactions and changes to the GLOBAL:PBRINE distribution. Removing the effects of the iron sulfidation reactions in the CRA14_SEN4 PA resulted in slightly higher gas pressures and decreased saturations in the waste areas, and the revised, higher GLOBAL:PBRINE distribution increased the number of intrusions into pressurized brine below the repository and increased pressures in the repository. The increased pressures caused by the removal of the iron sulfidation reactions and the increased probability of drilling into pressurized brine resulted in increased spallings releases (Zeitler and Day 2016). Spallings releases, however, have minimal effects on total releases in both the CRA-2014 PA and CRA14_SEN4 PA.

Releases through the Culebra can be affected by the volume of brine reaching the Culebra and the actinide concentrations in the brine. The brine volumes flowing up the borehole to the Culebra decreased slightly in the CRA14_SEN4 PA relative to the CRA-2014 PA, which Zeitler and Day (2016) attributed to the removal of iron sulfidation and modification of the northernmost panel closure (Zeitler and Day 2016). The effects of the changed actinide solubility uncertainty distributions were to increase the +III actinide total mobilized concentrations and

decrease the +IV actinide total mobilized concentrations, which would be expected to increase Culebra releases because of the higher baseline solubilities of the +III actinides. The increased pressures caused by the revised, higher GLOBAL:PBRINE distributions would tend to increase releases to the Culebra. The combined effects of all changes to the CRA14_SEN4 PA were to generally increase Culebra releases, with a slight decrease in Culebra releases at the lowest probabilities (Zeitler and Day 2016). Releases through the Culebra do not significantly affect total releases.

Removal of the iron sulfidation reactions, the increased GLOBAL:PBRINE distribution, and the changes to the distributions for the +III and +IV actinide solubility uncertainties affected DBR in the CRA14_SEN4 PA. The combined effects of these changes increased DBR at all probabilities (Zeitler and Day 2016). The increase in DBR from the increased SOLMOD3:SOLVAR uncertainty distribution is consistent with regression analysis results for both the CRA-2014 PA and CRA14_SEN4 PA that showed that this parameter is a significant contributor to the uncertainty in total releases. The parameter GLOBAL:PBRINE is a significant contributor to total releases for the CRA14_SEN4 PA as a result of the increased distribution range for this parameter in the CRA14_SEN4 PA.

Total releases calculated for the CRA14_SEN4 PA were minimally changed at high probabilities, because the high-probability releases are dominated by cuttings and cavings. Higher total releases were calculated for the CRA14_SEN4 PA at low probabilities than for the CRA-2014 PA because DBR is the most important cause of releases at low probability. The mean DBR CCDF increased significantly from the CRA-2014 PA to the CRA14_SEN4 PA (Zeitler and Day 2016, Figure 4-4). Because both the GLOBAL:PBRINE distribution and total mobilized +III actinide concentrations increased from the CRA-2014 PA and CRA14_SEN4 PA, the relative importance of these two changes cannot be distinguished.

13.2 POSSIBLE EFFECTS OF ADDITIONAL CHEMISTRY PARAMETER CHANGES

Chemistry-related issues identified by EPA during the CRA-2014 PA completeness review that were not addressed in the CRA14_SEN4 PA included:

- Underestimates of humid and inundated steel corrosion rates,
- Possible increase in gas generation rates due to lead corrosion
- Underestimation of the MgO hydration rate
- Overestimation of the hydromagnesite conversion rate
- Increased probability of the Pu(III) oxidation state

The combined effects of addressing the first four issues would be to reduce brine saturation and to increase gas pressures. Because of the relatively small effects of implementing the revised water balance and steel corrosion rates on releases noted when comparing CRA14-BV and CRA-2014 PA results (Zeitler 2013), it is reasonable to assume that the effects on PA of the steel corrosion rates, lead corrosion, MgO hydration rate, water consumption by brucite carbonation and hydromagnesite conversion rates would be relatively minor. The effects of changes in water saturation would be expected to be relatively unimportant because the amount of water

introduced by a borehole intrusion into pressurized brine would likely overwhelm the brine already present in the repository. Higher gas pressures would be expected to increase spallings and possibly other release mechanisms, but it is reasonable to believe that these effects would be overwhelmed by the pressure increases caused by an intruding borehole into pressurized brine.

The effects of a higher likelihood of the Pu(III) oxidation state because of reductive dissolution of Pu(IV) solid (Section 5.3.2.6) were not considered in the CRA14_SEN4 PA. Because of the higher total mobilized Pu(III) concentrations compared to Pu(IV) total mobilized concentrations in the CRA14_SEN4 PA (Table 8-3) and the regression analysis results showing the sensitivity of releases to the +III actinide concentrations through the SOLMOD3:SOLVAR (Zeitler and Sarathi 2017), an increased probability of the Pu(III) oxidation state would be expected to increase DBR releases and consequently to increase total releases at low probabilities. Because of the importance of an increased probability of the Pu(III) oxidation state to repository releases, EPA expects an independent technical review of likely Pu oxidation states to be performed prior to the CRA-2019 PA.

13.3 SENSITIVITY CALCULATIONS CONCLUSIONS

EPA requested DOE to perform an additional PA, the CRA14_SEN4, to assess the sensitivity of releases to a limited number of physical and chemical parameter changes:

- EPA-specified actinide uncertainty distributions that increased total mobilized +III actinides and reduced total mobilized +IV actinides
- Iron sulfidation rate parameters equal to zero, simulating iron passivation by H_2S
- An EPA-developed distribution for the probability of encountering pressurized brine during a drilling intrusion
- A reduced lower bound for the distribution for the effective shear strength of waste for erosion

The combined changes affected CRA14_SEN4 PA releases compared to the CRA-2014 PA:

- The combined changes resulted in minimal changes to cuttings and cavings releases
- Spallings releases were slightly increased due to slightly higher gas pressures from the removal of sulfidation reactions
- Releases through the Culebra were generally increased, with a slight decrease in releases at the lowest probabilities
- Direct brine releases were increased at all probabilities
- Total releases calculated minimally changed at high probabilities where total releases are dominated by cuttings and cavings, but were increased at low probabilities where releases are dominated by DBR

14.0 SUMMARY AND CONCLUSIONS

This technical support document summarizes EPA's review of chemistry-related CRA-2014 PA issues, with the conclusions outlined below. DOE updated many of the chemistry-related PA parameters and EPA has identified issues with a number of these changes. The results of this review, including the CRA14_SEN4 PA sensitivity analysis, show that predicted repository releases will remain within regulatory limits. However, EPA's review indicated many of the chemistry related parmaters that DOE's adopted in the 2014-CRA PA were not aligned with the available experimental data. Consequently, EPA would like to see DOE address those specific issues identified by EPA in this technical report for the CRA-2019 PA to minimize uncertainties associated with the PA results and to increase its defensibility.

The conceptual model and implementation of gas generation from anoxic corrosion of iron-based metals used for the CRA-2014 PA are supported by the available data. Iron corrosion rates for the CRA-2014 PA were lower than previous WIPP PAs based on new project-specific investigations of humid and inundated iron corrosion rates. EPA would like the sampled distributions for the humid and inundated rates to be modified for the CRA-2019 PA to account for the presence of low CO_2 concentrations in the WIPP repository and the inundated corrosion rate also increased to account for the effects of high repository pressures. For the CRA-2014 PA, DOE assumed that all H_2S generated by CPR degradation would instantaneously react with iron metal and $Fe(OH)_2$. This assumption is inconsistent with project-specific data that show H_2S may passivate iron. Because the reaction of H_2S with $Fe(OH)_2$ can result in lower gas pressures and reduce spallings releases and DBRs, EPA would also like these iron sulfidation reactions eliminated from the CRA-2019 PA by setting the appropriate stoichiometric coefficients to zero.

Metals and alloys other than iron-based materials in the WIPP waste or packaging materials, such as aluminum and lead, may generate gas through anoxic corrosion. Inventories of these metals for the CRA-2014 PA were insignificant relative to iron-based metals and alloys, so aluminum and lead corrosion were not included in the CRA-2014 PA gas generation calculations. However, future lead inventories are likely to significantly increase compared to the CRA-2014 PA inventory because of the recent approval of shielded containers for RH waste disposal. Bounding calculations based on the volumes of waste streams that are candidates for disposal in shielded containers would be appropriate to assess the possible significance of gas generation from lead corrosion, which will provide a more defensible calculation of potential WIPP gas generation rates.

The microbial gas generation rates used for the CRA-2014 PA are suitable for modeling gas generation rates from degradation of cellulosic materials, but may overestimate gas generation rates from the degradation of plastics and rubber. DOE accounted for uncertainties regarding the rates of plastic and rubber degradation in the WIPP repository environment by assuming plastic and rubber degradation occurs in only 25% of the realizations. Based on the available data, the current approach for modeling microbial gas generation rates is appropriate for PA.

The assumption that radiolytic processes will not significantly influence overall rates of gas generation has remained unchanged since the CCA PA. However, lower microbial gas generation rates used in the PABC04, PABC09 and CRA-2014 PA may invalidate this assumption. DOE has perfomed $H_2(g)$ monitoring in WIPP Panels 3 and 4 and concluded that

radiolytic $H_2(g)$ generation is occurring. Future PAs will be strengthened if DOE assesses the possible significance of radiolytic gas generation relative to the rates of gas generation by microbial degradation and anoxic corrosion for the CRA-2019 PA.

The available data indicate that the MgO backfill will adequately control brine pH and CO_2 fugacities, and thereby limit actinide solubilities in WIPP brines under inundated conditions. Because of uncertainties in the rate at which hydromagnesite will convert to magnesite in the repository environment, PA calculations of actinide solubilities assume that the brucite-hydromagnesite reaction will buffer CO_2 fugacity at low levels consistent with relatively low actinide solubilities under inundated conditions. Calculation of the amount of emplaced MgO appropriately accounts for the uncertainties associated with the rate of hydromagnesite conversion to magnesite and the chemical composition of the MgO. The current MgO emplacement plan ensures that a sufficient quantity of MgO is emplaced in each room of the repository. The MgO reactivity testing procedure and test results provided by DOE demonstrate that the current backfill material contains a sufficient percentage of reactive periclase plus lime to control chemical conditions in the repository, and that the current testing procedure would detect any MgO shipments with inadequate reactive material percentages.

Assumptions related to actinide oxidation states in the WIPP repository have remained unchanged since they were developed and peer reviewed for the CCA. It is assumed for PA that Th(IV), Am(III), and Cm(III) are the only oxidation states of these actinides that will be present in the WIPP repository. It is also assumed that neptunium may be present in the +IV or +V oxidation states and uranium may be present in the +IV or +VI oxidation states. Because reducing conditions will be established in the repository shortly after closure, the peer-reviewed oxidation state assumptions for neptunium and uranium remain appropriate, although conservative.

For all WIPP PAs, DOE has assumed equal probabilities that aqueous and solid-phase plutonium will be present in either the +III or +IV oxidation states. EPA's interpretation of data that have become available since the CRA-2009 is that the data demonstrate a high likelihood that plutonium concentrations in WIPP brines will be controlled by the solubility of Pu(III) solids in equilibrium with Pu(III) aqueous species or by the solubility of Pu(IV) solids in equilibrium with Pu(III) aqueous species, also referred to as reductive dissolution. Reductive dissolution of Pu(IV) solids in equilibrium with Pu(III) aqueous species results in higher dissolved plutonium concentrations than would occur if Pu(IV) solids are in equilibrium with Pu(IV) aqueous species.

Dissolved Pu(III) and total mobilized Pu(III) used in the more oxidizing realizations may have beensignificantly underestimated in the CRA-2014 PA. This underestimation in turn likely caused an underestimation of total mobilized plutonium concentrations in DBRs for the CRA14_SEN4 and a consequent underestimation of total releases at low probabilities. Because plutonium oxidation state will significantly influence total mobilized plutonium in PA, EPA would like to see an independent technical review of the likely plutonium oxidation states in the repository setting as soon as possible, with an update incorporated into PA calculations.

DOE included the solubility for phase 5 in the EQ3/6 database (DATA0.FM1) used to calculate actinide solubilities for the CRA-2014 PA, because this solid has been shown to form in GWB brines. DOE (2014b, Appendix SOTERM-2014) provided a qualitative review of actinide

solubility and speciation data relevant to WIPP brines that have become available since the PABC04. However, DOE did not revise the actinide aqueous speciation or solubility data in DATA0.FM1. Consideration of all new geochemical data and other relevant data is required for each CRA [40 CFR 194.15(a)]. Because DOE did not quantitatively re-evaluate the data in the DATA0.FM1 database, there is uncertainty regarding the possible effects of the new data on the CRA-2014 PA predictions of the +III and +IV actinide solubilities.

In response to EPA comments during the CRA-2014 completeness review, DOE revised the EQ3/6 database used in the CRA-2014 PA actinide solubility calculations and produced DATA0.FM2. The revised database included revisions to the hydromagnesite solubility, addition of borate aqueous and solid species, revisions to EDTA aqueous and solid species, revisions to citrate aqueous and solid species, addition of the $MgSO_4$(aq) aqueous species and addition of lead aqueous and solid species. EPA performed a preliminary review of the revised database and concluded that the hydromagnesite solubility previously used for WIPP PA is much more preferable for inclusion in the CRA-2019 because of uncertainties associated with the experiments used to determine the revised hydromagnesite solubility. EPA acceptance of the new borate, lead data and $MgSO_4$(aq) data added to the database and the revised EDTA and citrate data will require review of more recent data and analysis of the revised data with respect to appropriate acceptance criteria. In addition, EPA has determined that aqueous speciation and Pitzer parameters for the Th(IV)-carbonate species from Altmaier et al. (2005, 2006) and thermodynamic and Pitzer parameters from Neck et al. (2009) for Am(III) aqueous species and solids phases would be appropriate revisions to the EQ3/6 database. Both sets of thermodynamic data are more consistent with existing actinide solubility results from the literature than the data currently in DATA0.FM1. EPA encourages DOE to update the geochemical database for the next CRAwith the latest data and to provide the Agency with proper justifications for the updates.

DOE has not developed an aqueous speciation and solubility model for U(VI) and continues to use a fixed concentration of 1.0×10^{-3} M for the dissolved concentration. DOE has reported the results of U(VI) solubility measurements in carbonate-free WIPP brines. Because of the likely importance of carbonate complexation on the solubility of U(VI), these results cannot be used to determine likely U(VI) concentrations under anticipated WIPP repository conditions. Thus, continued use of a fixed concentration is appropriate.

Inconsistencies were identified in DOE's selection of +III and +IV actinide solubility data that were used to develop the CRA-2014 PA solubility uncertainty distributions. EPA re-evaluated the selection criteria and the +III and +IV actinide solubility data selection process and specified the solubility data used to develop revised +III and +IV actinide solubility uncertainty distributions. The revised +III actinide solubility uncertainty distribution had a higher mean and median than the distribution used for the CRA-2014 PA, and the revised +IV actinide solubility uncertainty distribution had a lower mean and median than the distribution used for the CRA-2014 PA. Because of the importance of +III actinides for DBR and consequently for total releases from the repository at low probabilities, results of the CRA14_SEN4 PA show that these changed actinide solubility uncertainty distributions result in higher repository releases at low probabilities.

Additional mineral-fragment colloid data from experiments with Pu(VI) in the presence of iron metal and magnetite in WIPP brines indicated that the current parameters are adequately bounding of the data. However, DOE has not investigated the potential formation of pseudocolloids from MgO hydration and carbonation products under WIPP conditions. Because colloids capable of transporting actinides have been demonstrated to form from reaction of MgO in brines under some conditions, this omission introduces some uncertainty into the colloidal actinide source term model. To minimize this uncertainty, we recommend DOE evaluate the potential formation of mineral-fragment colloids from MgO hydration and carbonation under WIPP-relevant conditions before the CRA-2019 PA.

Intrinsic colloid concentrations used in the CRA-2014 PA were revised based on new WIPP-specific data. The Th(IV) intrinsic colloid data were developed using experimental data from an extremely narrow pcH range of 9 – 10. EPA expects DOE to revise the Th(IV) intrinsic colloid parameter to reflect upper bounding values for data collected from experiments within the pcH range of 8.5 – 10.5. The Pu(III) intrinsic colloid parameter does not appear to be an upper, bounding value and should also be revised to be consistent with a reasonable upper bound.

DOE revised the microbial colloid parameters for the CRA-2014 PA based on newly collected data. DOE changed the maximum concentrations for the microbially associated actinides based on a revised conceptual model assumption regarding the upper limit on microbially associated actinides. Whereas for previous WIPP PAs it was assumed the maximum microbial colloids concentration would be the concentration at which no growth was observed, DOE revised this upper limit to be the concentration calculated from an assumed maximum cell concentration multiplied by the moles of actinides per cell. This change alters the conceptual model and has significant effects on total mobilized actinides.

Because of the short reaction times in tests reported by DOE, the CRA-2014 PA microbial proportionality constants likely include only biosorption and not bioaccumulation or biomineralization. Omission of bioaccumulation and biomineralization represents a conceptual model change because previous WIPP PAs included biosorption, bioaccumulation and biomineralization. DOE has stated that further research into the biosorption, bioaccumulation and biomineralization processes is planned, and EPA would like these investigations to include longer reaction times to substantiate steady state conditions and to include the possible effects of bioaccumulation and biomineralization. Uncertainty has been introduced into the biosorption data DOE developed because of the possible inclusion of intrinsic colloids in the experimental solutions which may or may not have sorbed; EPA recommends that DOE use 2 nm filtration to remove intrinsic colloids from their post-test solutions in future experiments to establish the dissolved concentration for calculating microbial colloid proportionality constant parameter values.

Based on EPA's assessment of DOE's microbial colloid conceptual model changes and microbial colloid experiments, EPA will reject the CRA-2014 PA microbial colloid parameters for the CRA-2019 PA. We encourage DOE to continue their investigation of microbial colloid parameters and expect any updates for the CRA-2019 PA to be consistent with the peer-reviewed conceptual model assumptions.

The results of the mobile actinide source term calculations indicate that for the case using mean values of the CRA-2014 PA parameters, total mobile Am(III) concentrations consist mainly of dissolved Am(III) and Am(III) associated with humic colloids, with microbial colloid Am(III) limited by the maximum concentration. Total mobile Pu concentrations calculated using mean parameter values for the CRA-2014 PA were dominated by dissolved Pu(III) and Pu(III) associated with humic and microbial colloids and by humic and microbial colloids for Pu(IV). Using the mean CRA-2014 PA parameter values, the total mobilized Pu(IV) concentrations for both GWB and ERDA-6 brine exceed the total mobilized Pu(III) concentrations. Higher total mobilized Pu(IV) than Pu(III) concentrations are the result of the negative mean value for the +III solubility uncertainty distribution, and demonstrates the importance of developing a defensible actinide solubility data set for determining this distribution for the CRA-2019 PA. The revised maximum microbial colloid parameter for Am(III) also significantly affects total mobilized Am(III) concentrations, and we expect DOE to resolve the issues surrounding the maximum actinide concentrations associated with microbial colloids as soon as possible and ideally for the CRA-2019 PA.

The total mobilized actinide concentrations calculations using CRA14_SEN4 PA mean parameters differed from the CRA-2014 PA calculations only in the +III and +IV actinide solubility uncertainty parameters. Using the CRA14_SEN4 PA mean parameters, microbially associated Am(III) and Pu(III) concentrations were limited by the maximum concentration established for the CRA-2014 PA. This result illustrates the importance of the issues identified with the revised parameters for the maximum microbially associated actinide concentrations. Because of changes made to the +III and +IV actinide solubility uncertainty distributions for the CRA14_SEN4 PA, the mean total mobilized Pu(III) concentrations in GWB and ERDA-6 brines exceed the mean total mobilized Pu(IV) concentrations, which is consistent with previous WIPP PAs, such as the PABC09.

Distribution coefficients used to model actinide transport through the Culebra for the CRA-2014 PA are consistent with the estimated organic ligand concentrations based on the CRA-2014 PA inventory for these compounds. These K_d values are likely to provide a conservative assessment of actinide transport through the Culebra.

The potential effects of heterogeneous waste loading are unlikely to significantly affect actinide solubilities, except in the case where a large proportion of the organic ligands in the inventory are placed in a single panel. DOE has accounted for this possibility in the actinide solubility calculations by assuming that the entire organic ligand inventory is dissolved in the minimum amount of brine necessary for a release from the repository. Provided that the inventory of organic ligands is adequately bounded, this approach ensures that the effects of heterogeneous waste placement are adequately accounted for in the actinide solubility calculations.

The only chemical process included in the water balance calculations for the CCA PAVT, PABC04 and PABC09 was the consumption of water by anoxic corrosion. DOE modified the water balance for the CRA-2014 PA to also include water production by microbial degradation of CPR, water consumption by the MgO hydration reaction and water produced by conversion of hydromagnesite to magnesite. Incorporation of these chemical processes in addition to anoxic corrosion in the water balance represents a significant improvement in the water balance calculations for WIPP PA. However, EPA has found several outstanding issues to be addressed

for CRA-2019 including: using the revised ranges of humid and inundated steel corrosion rates that are higher than the ranges used in the CRA-2014 PA, removing the steel sulfidation reactions from the water balance by setting the relevant stoichiometric parameters to zero, revising the MgO hydration rates to account for the higher rates of hydration of Martin Marietta MgO and modifying the hydromagnesite conversion rate to a lower range of values.

DOE performed an additional PA (CRA14_SEN4 PA) to assess the effects of a limited number of parameter changes on repository releases. The chemistry-related parameter changes relative to the CRA-2014 PA for this sensitivity analysis were revised uncertainty distributions for the +III and +IV actinide solubilities and changes to the stoichiometric parameters for reaction of H_2S with Fe(s) and $Fe(OH)_2$(s) to correspond with zero reaction rates. The use of an EPA-developed distribution for the probability of encountering pressurized brine during a drilling intrusion, use of a reduced lower bound for the distribution of the effective shear strength for erosion, use of a new version of the DRSPALL code and use of the correct representative length of the northernmost set of panel closures were also included in the CRA14_SEN4 PA. Total releases calculated for the CRA14_SEN4 PA relative to the CRA-2014 PA were minimally changed at high probabilities, because the high-probability releases are dominated by cuttings and cavings. Higher total releases were calculated for the CRA14_SEN4 PA at low probabilities than for the CRA-2014 PA because DBR is the most important cause of releases at low probability and the mean DBR CCDF increased significantly from the CRA-2014 PA to the CRA14_SEN4 PA. Because both the distribution for the probability of encountering pressurized brine during a drilling intrusion and the sampled range of total mobilized +III actinide concentrations increased from the CRA-2014 PA and CRA14_SEN4 PA, the relative importance of these two changes to DBR cannot be distinguished.

The following is a summary of the issues related to chemical processes EPA would like to see DOE address prior to the CRA-2019:

- Use the revised, higher humid and inundated anoxic corrosion rate ranges identified by EPA that account for the effects of CO_2 and high pressure
- Confirm that the steel surface area per unit disposal volume is representative of WIPP waste using updated inventory data, the sheet metal surrogate and 55-gallon drum surrogate assumptions and updated waste emplacement data
- Develop a reasonable upper-bound estimate for the lead inventory and lead surface area per unit disposal volume for the CRA-2019 PA that adequately accounts for the increased lead associated with shielded containers; if the upper-bound lead inventory is significant relative to iron-based metals and alloys, we recommend that DOE use available project-specific lead corrosion data to assess the effects of lead corrosion on gas generation and brine consumption in the WIPP repository
- Use the available radiolytic H_2(g) generation data from monitoring of sealed WIPP panels to evaluate whether radiolytic gas generation rate is significant relative to the rates of gas generation by microbial degradation and anoxic corrosion
- Remove the assumption that all H_2S(g) generated by CPR degradation will instantaneously react with Fe(s) and $Fe(OH)_2$(s) from the gas generation rate calculations by revising the relevant stoichiometric coefficients

- Perform an independent technical review of likely plutonium oxidation states in solids and aqueous species in the repository and update the model as soon as possible using recommendations from this review
- Use the solubility of hydromagnesite established by Robie and Hemingway (1973) in the EQ3/6 database
- Review the results of investigations published after the CRA-2014 cutoff date related to complexation of +III actinides by borate species and precipitation of borate solid phases, and if appropriate, revise the EQ3/6 thermodynamic database to incorporate the data
- Use the data provided by Altmaier et al. (2005, 2006) to develop revised aqueous speciation and Pitzer parameters for the Th(IV)-carbonate aqueous species and incorporate the results in the EQ3/6 database
- Use the results of the Neck et al. (2009) $Nd(OH)_3(s)$ solubility study to update the solubility of $Am(OH)_3(s)$ in the EQ3/6 database
- Provide supporting information for the revised data in the EQ3/6 database DATA0.FM2 to demonstrate agreement with acceptance criteria; EPA needs this supporting information in advance of the CRA-2019 to enable EPA review and acceptance before its use to calculate dissolved actinide concentrations for the CRA-2019 PA
- Modify the criteria to select solubility data for the +III and +IV actinide solubility uncertainty distributions
- Experimentally evaluate formation of mineral fragment colloids from MgO hydration and carbonation products and their effects on total mobilized actinides
- Revise the Th(IV) intrinsic colloid parameter to be consistent with upper bounding values for samples collected within the pcH range of 8.5 – 10.5
- Provide documentation for the data used to determine the Pu(III) and Am(III) intrinsic colloid parameters and develop a Pu(III) intrinsic colloid parameter that is an upper bounding value
- Incorporate the effects of bioaccumulation and biomineralization in addition to biosorption in the development of revised microbial colloid parameters; until the effects of bioaccumulation and biomineralization have been included in the revised parameters, we will accept the higher proportionality constants (either from the CCA PA or CRA-2014 PA) for the CRA-2019 PA
- Use the higher CAPMIC parameters developed for the CCA based on the conceptual model assumption that these parameters represent the concentrations at which no growth occurs
- Use 2 nm filtration to remove intrinsic colloids from post-test solutions in future microbial colloid experiments to establish the dissolved concentration for calculating proportionality constants for microbial colloids
- Develop MgO hydration rates that adequately account for the more rapid hydration rates of Martin Marietta MgO relative to Premier MgO for use in the CRA-2019 PA water balance

- Use the lower rate range established by EPA for the hydromagnesite conversion rate for the CRA-2019 PA water balance

15.0 REFERENCES

AlMahamid, I., K.A. Becraft, N.L. Hakem, R.C. Gatti and H. Nitsche. 1996. Stability of various plutonium valence states in the presence of NTA and EDTA. *Radiochimica Acta* 74:129-134.

Altmaier, M., and H. Geckeis. 2011. Plutonium and actinide chemistry in saline solutions. *Plutonium Futures, Actinide Research Quarterly* 2:29-32.

Altmaier, M., V. Metz, V. Neck, R. Müller, and T. Fanghänel. 2003. Solid-liquid equilibria of $Mg(OH)_2$(cr) and $Mg_2(OH)_3Cl•4H_2O$(cr) in the system Mg-Na-H-OH-Cl-H_2O at 25°C. *Geochimica et Cosmochimica Acta* 67:3595-3601.

Altmaier, M., V. Neck and T. Fanghänel. 2004. Solubility and colloid formation of Th(IV) in concentrated NaCl and $MgCl_2$ solution. *Radiochimica Acta* 92:537-543.

Altmaier, M., V. Neck, R. Müller and T. Fanghänel. 2005. Solubility of $ThO_2•xH_2O$ in carbonate solution and the formation of ternary Th(IV) hydroxide-carbonate complexes. *Radiochimica Acta* 93:83-92.

Altmaier, M., V. Neck, M.A. Denecke, R. Yin and T. Fanghänel. 2006. Solubility of $ThO_2•xH_2O$ and the formation of ternary Th(IV) hydroxide-carbonate complexes in $NaHCO_3$-Na_2CO_3 solutions containing 0-4 M NaCl. *Radiochimica Acta* 94:495-500.

Altmaier, M., V. Neck and T. Fanghänel. 2008. Solubility of Zr(IV), Th(IV) and Pu(IV) hydrous oxides in $CaCl_2$ solutions and the formation of ternary Ca-M(IV)-OH complexes. *Radiochimica Acta* 96:541-550.

Altmaier, M., V. Neck, J. Lützenkirchen and T. Fanghänel. 2009. Solubility of plutonium in $MgCl_2$ and $CaCl_2$ solutions in contact with metallic iron. *Radiochimica Acta* 97:187-192.

Ams, D.A., J.S. Swanson, J.E.S. Szymanowski, J.B. Fein, M. Richmann and D.T. Reed. 2013. The effect of high ionic stgrength on neptunium (V) adsorption to a halophilic bacterium. *Geochimica et Cosmochimica Acta* 110:45-57.

André, C., and G.R. Choppin. 2000. Reduction of Pu(V) by Humic Acid. *Radiochimica Acta* 88:613-616.

ANL (Argonne National Laboratory). 1997. *Actinide Stability/Solubility Studies in Support of the Waste Isolation Pilot Plant*. Chemical Technology Division Annual Technical Report 1997. ANL-98/13, pp. 50-52.

Babb, S.C. 1996. *NONLIN, Ver. 2.00 User's Manual.* Sandia National Laboratories, Albuquerque, New Mexico, January 31, ERMS 230740.

Banaszak, J.E., S.M. Webb, B.E. Rittmann, J.-F. Gaillard, and D.T. Reed. 1999. Fate of Neptunium in Anaerobic, Methanogenic Microcosm. *Scientific Basis for Nuclear Waste Management XXII* 556:1141–1149.

Banik, N. 2006. *Speciation of Tetravalent Plutonium in Contact with Humic Substances and Kaolinite Under Environmental Conditions.* PhD thesis, Johannes Gutenberg-University Mainz.

Bellot-Gurlet, L., D. Neff, S. Réguer, J. Monnier, M. Saheb, and P. Dillmann. 2009. Raman studies of corrosion layers formed on archaeological irons in various media. *Journal of Nano Research* 8:147-156.

Berninger, U.-N., G. Jordan, J. Schott and E.H. Oelkers. 2014. The experimental determination of hydromagnesite precipitation rates at 22.5 – 75ºC. *Mineralogical Magazine* 78:1405-1416.

Bersin, T., A. Müller and H. Schwarz. 1957. Zur pharmakologischen Wirkung einiger anorganish-organischer Komplexverbindungen. *Archives of Biochemistry and Biophysics* 69:507-513.

Bitea, C., R. Müller, V. Neck, C. Walther and J.I. Kim. 2003. Study of the generation and stability of thorium(IV) colloids by LIBD combined with ultrafiltration. *Colloids and Surfaces A: Physicochem. Eng. Aspects* 217:63-70.

Bolton, H., D. Rai, and L Xun. 2006. Biotransformation of Pu-EDTA: implications to Pu immobilization. *DOE-BER Environmental Remediation Sciences Project #1010283*. Richland, WA.

Borkowski, M. 2007. *Effect of Acetate, Citrate, EDTA, Oxalate and Borate Ions on Neodymium Solubility in WIPP Brine.* Test Plan LCO-ACP-07, Revision 0, Los Alamos National Laboratory, Carlsbad Operations.

Borkowski, M. 2010. *Numerical Values for Graphs Presented in the Report LCO-ACP-08, Rev. 0 Entitled: "Actinide (III) Solubility in WIPP Brine: Data Summary and Recommendations."* LANL-CO ACRSP ACP-1002-05-17-01, Los Alamos National Laboratory, Carlsbad, New Mexico.

Borkowski, M. 2012a. *Numerical Values for Graphs Presented in Report LCO-ACP-08, Rev. 0, Entitled Actinide(III) Solubility in WIPP Brine: Data Summary and Recommendations.* LA-UR-10-00898; LANL-CO ACRSP ACP-1002-05-17-01. Los Alamos National Laboratory, Carlsbad, New Mexico.

Borkowski, M. 2012b. *Numerical Values for Graphs Presented in Report LCO-ACP-08, Rev. 0, Entitled Solubility of An(IV) in WIPP Brine: Thorium Analog Studies in WIPP Simulated Brine, and for Graphs Published in Borkowski, M., et al. Radiochimica Acta 98 (9-11), 577-582 (2010).* LA-UR- 12-26640; LANL-CO ACRSP ACP-01/2012, Rev. 0. Los Alamos National Laboratory, Carlsbad, New Mexico.

Borkowski, M, and M. Richmann. 2009. *Comparison of Recent Thorium Thermodynamic Data with Those Used in the WIPP FMT_050405.CHEMDAT Database.* LANL-CO ACRSP ACP-0911-01-03-01, Los Alamos National Laboratory, Carlsbad, New Mexico, November 3, 2009.

Borkowski, M., J.F. Lucchini, M.K. Richmann, and D.T. Reed. 2009. *Actinide (III) Solubility in WIPP Brine: Data Summary and Recommendations*. LCO-ACP-08. LANL\ACRSP Report. Los

Alamos National Laboratory, Los Alamos, New Mexico. Cited by DOE (2009) as Borkowski et al. (2008).

Borkowski, M, M. Richmann, D.T. Reed and Y. Xiong. 2010. Complexation of Nd(III) with tetraborate ion and its effect on actinide(III) solubility in WIPP brine. *Radiochimica Acta* 98:577-582.

Borkowski, M, M. Richmann, and J.F. Lucchini. 2012. *Solubility of An(IV) in WIPP Brine: Thorium Analog Studies in WIPP Simulated Brine.* LA-UR 12-24417. Los Alamos National Laboratory, Carlsbad, New Mexico.

Boukhalfa, H., S. Reilly, W. Smith, and M. Neu. 2003. Stability and redox behavior of plutonium-EDTA and Mixed Pu(IV)-EDTA-L (L= Hydroxide, Carbonate, Citrate) Complexes. *AIP Conference Proceedings* 673:238.

Boukhalfa, H., S. Reilly, W. Smith, and M. Neu. 2004. EDTA and mixed-ligand complexes of tetravalent and trivalent plutonium. *Inorganic Chemistry* 43:5816-5823.

Boukhalfa, H., G.A. Icopini, S.D. Reilly, and M.P. Neu. 2007. Plutonium(IV) retention by the metal-reducing bacteria *Geobacter metallireducens* GS15 and *Shewanella oneidensis* MR1. *Applied and Environmental Microbiology* 73:5897-5903.

Brendebach, B., M. Altmaier, J. Rothe, V. Neck and M.A. Denecke. 2007. EXAFS study of aqueous Zr^{IV} and Th^{IV} complexes in alkaline $CaCl_2$ solutions: $Ca_3[Zr(OH)_6]^{4+}$ and $Ca_4[Th(OH)_8]^{4+}$. *Inorganic Chemistry* 46:6804-6810.

Brooks, S.C., J.K. Fredrickson, S.L. Carroll, D.W. Kennedy, J.M. Zachara, A.E. Plymale, S.D. Kelly, K.M. Kemner, and S. Fendorf. 2003. Inhibition of bacterial U(VI) reduction by calcium. *Environmental Science and Technology* 37:1850-1858.

Brush, L.H. 1990. *Test Plan for Laboratory and Modeling Studies of Repository and Radionuclide Chemistry for the Waste Isolation Pilot Plant*. SAND90-0266. Sandia National Laboratories, Albuquerque, New Mexico.

Brush, L.H. 1995. *Systems Prioritization Method - Iteration 2 Baseline Position Paper: Gas Generation in the Waste Isolation Pilot Plant*. Unpublished report, Sandia National Laboratories, Albuquerque, New Mexico, March 17, 1995, ERMS 228740.

Brush, L.H. 1996. *Ranges and Probability Distributions of K_ds for Dissolved Pu, Am, U, Th and Np in the Culebra for the PA calculations to Support the WIPP CCA*. Memorandum to M.S. Tierney, Sandia National Laboratories, Albuquerque, New Mexico, June 10, 1996, ERMS 238801.

Brush, L.H. 2004. *Implications of New (Post-CCA) Information for the Probability of Significant Microbial Activity in the WIPP*. Sandia National Laboratories Carlsbad Programs Group, Carlsbad, New Mexico, July 28, 2004, ERMS 536205.

Brush, L.H. 2005. *Results of Calculations of Actinide Solubilities for the WIPP Performance Assessment Baseline Calculations*. Analysis Report, Sandia National Laboratories, Carlsbad, New Mexico, ERMS 539800.

Brush, L.H., and P.S. Domski. 2013a. *Calculation of Organic Ligand Concentrations for the WIPP CRA-2014 PA.* Sandia National Laboratories, Carlsbad, New Mexico, ERMS 559005.

Brush, L.H., and P.S. Domski. 2013b. *Prediction of Baseline Actinide Solubilities for the WIPP CRA-2014 PA.* Sandia National Laboratories, Carlsbad, New Mexico, ERMS 559138.

Brush, L.H., and P.S. Domski. 2013c. *Uncertainty Analysis of Actinide Solubilities for the WIPP CRA-2014 PA, Rev. 1. Supersedes ERMS 559278.* Sandia National Laboratories, Carlsbad, New Mexico, ERMS 559712.

Brush, L.H. and L.J. Storz. 1996. *Revised Ranges and Probability Distributions of K_ds for Dissolved Pu, Am, U, Th and Np in the Culebra for the PA calculations to Support the WIPP CCA*. Memorandum to M.S. Tierney, Sandia National Laboratories, Albuquerque, New Mexico, July 24, 1996, ERMS 241561.

Brush, L.H., and Y. Xiong. 2003a. *Calculation of Actinide Solubilities for the WIPP Compliance Recertification Application*. Sandia National Laboratories Carlsbad Programs Group, Carlsbad, New Mexico, May 8, 2003, ERMS 529131.

Brush, L.H., and Y. Xiong. 2003b. *Calculation of Actinide Solubilities for the WIPP Compliance Recertification Application, Analysis Plan AP 098, Rev 1*. Sandia National Laboratories, Carlsbad, New Mexico, ERMS 527714.

Brush, L.H., and Y. Xiong. 2003c. *Calculation of Organic Ligand Concentrations for the WIPP Compliance Recertification Application*. Sandia National Laboratories, Carlsbad, New Mexico, ERMS 527567.

Brush, L.H., and Y. Xiong. 2003d. *Calculation of Organic Ligand Concentrations for the WIPP Compliance Recertification Application and for Evaluating Assumptions of Homogeneity in WIPP PA.* Sandia National Laboratories, Carlsbad, New Mexico, ERMS 531488.

Brush, L.H., and Y. Xiong. 2004. *Sensitivities of the Solubilities of +III, +IV, and +V Actinides to the Concentrations of Organic Ligands in WIPP Brines. R*ev. *0*, Sandia National Laboratories, Carlsbad, New Mexico, December 15, 2004, ERMS 538203.

Brush, L.H., and Y. Xiong. 2005a. *Calculation of Actinide Solubilities for the WIPP Performance-Assessment Baseline Calculations. Analysis Plan AP-120, Rev. 0*. Sandia National Laboratories, Carlsbad, New Mexico, ERMS 539255.

Brush, L.H., and Y. Xiong. 2005b. *Calculation of Organic-Ligand Concentrations for the WIPP Performance-Assessment Baseline Calculations*. Sandia National Laboratories, Carlsbad, New Mexico, ERMS 539635.

Brush, L.H. and Y. Xiong. 2009. *Calculation of Organic-Ligand Concentrations for the WIPP CRA-2009 PABC*. Sandia National Laboratories, Carlsbad, New Mexico, ERMS 551481.

Brush, L.H., J. Garner, and E. Vugrin. 2005. *PA Implementation of Uncertainties Associated with Calculated Actinide Solubilities*. Memorandum to Dave Kessel, Sandia National Laboratories, Carlsbad, New Mexico, February 2, 2005, ERMS 538537.

Brush, L.H., Y. Xiong, J.W. Garner, A. Ismail, and G.T. Roselle. 2006. *Consumption of Carbon Dioxide by Precipitation of Carbonate Minerals Resulting from Dissolution of Sulfate Minerals in the Salado Formation in Response to Microbial Sulfate Reduction in the WIPP*. Sandia National Laboratories, Carlsbad, New Mexico, ERMS 544785.

Brush, L.H., Y. Xiong, J.W. Garner, T.B. Kirchner and J.J. Long. 2008. *Sensitivity of the Long-Term Performance of the WIPP to EDTA*. Sandia National Laboratories, Carlsbad, New Mexico, ERMS 548398.

Brush, L.H., Y. Xiong, and J.J. Long. 2009. *Results of the Calculations of Actinide Solubilities for the WIPP CRA-2009 PABC*. Sandia National Laboratories, Carlsbad, New Mexico, ERMS 552201.

Brush, L.H., P.S. Domski and Y.-L. Xiong. 2011. *Predictions of the Compositions of Standard WIPP Brines as a Function of pcH for Laboratory Studies of the Speciation and Solubilities of Actinides.* Sandia National Laboratories, Carlsbad, New Mexico, ERMS 555727.

Bryan, C.R., and A.C. Snider. 2001a. *MgO Hydration and Carbonation at SNL/Carlsbad, Sandia National Laboratories Technical Baseline Reports, WBS 1.3.5.4, Repository Investigations, Milestone RI010, January 31, 2001*. Sandia National Laboratories, Carlsbad, New Mexico, ERMS 516749, pp. 66 to 83.

Bryan, C.R., and A.C. Snider. 2001b. MgO Experimental Work Conducted at SNL/CB: Continuing Investigations with Premier Chemicals MgO, *Sandia National Laboratories Technical Baseline Reports, WBS 1.3.5.4, Repository Investigations, Milestone RI020, July 31, 2001*.

Bryson, D. 2015. *Letter to Mr. Jonathan D. Edwards, Director, Radiation Protection Division (Subject: Response to the U.S. Environmental Protection Agency Letters Dated February 27, 2015 and June 5, 2015 Regarding the 2014 Compliance Recertification Application)*. September 25, 2015. Carlsbad Field Office, Carlsbad, NM.

Bryson, D.C. 2015a. *Response to the U.S. Environmental Protection Agency Letters Dated February 27, 2015 and June 5, 2015 Regarding the 2014 Compliance Recertification Application.* Letter to J.D. Edwards, U.S. Environmental Protection Agency, July 15, 2015.

Bryson, D.C. 2015b. *Response to the U.S. Environmental Protection Agency Letters Dated February 27, 2015 and June 5, 2015 Regarding the 2014 Compliance Recertification Application.* Letter to J.D. Edwards, U.S. Environmental Protection Agency, September 25, 2015.

Camphouse, R.C. 2013a. *Analysis Pacakage for Salado Flow Modeling Done in the 2014 Compliance Recertification Application Performance Assessment (CRA-2014 PA).* Sandia National Laboratories, Carlsbad, New Mexico.

Camphouse, R.C. 2013b. *Analysis Plan for the 2014 WIPP Compliance Recertification Application Performance Assessment.* AP-164, Sandia National Laboratories, Carlsbad, New Mexico.

Camphouse, R.C., M. Gross, C.G. Herrick, D.C. Kicker and B. Thompson. 2012. *Recommendations and Justifications of Parameter Values for the Run-of-Mine Salt Panel Closure System Design Modeled in the PCS-2012 PA.* Sandia National Laboratories, Carlsbad, New Mexico, ERMS 557396.

Cheng, W. and Z. Li. 2010. Controlled supersaturation precipitation of hydromagnesite for the $MgCl_2 – Na_2CO_3$ system at elevated temperatures: chemical modeling and experiment. *Industrial & Engineering Chemistry Research* 49:1964-1974.

Choppin, G.R. 1991. Redox Speciation of Plutonium in Natural Waters. *Journal of Radioanalytical and Nuclear Chemistry Articles*, 147:109-116.

Choppin, G.R., A.H. Bond, M. Borkowski, M. Bronikowski, J.-F. Chen, S. Lis, J. Mizera, O.S. Pokrovsky, N.A. Wall, Y.X. Xia, and R.C. Moore. 2001. *Waste Isolation Pilot Plant Actinide Source Term Test Program: Solubility Studies and Development of Modeling Parameters*. Sandia National Laboratories, Albuquerque, New Mexico, April 2001, SAND99-0943.

Ciavatta, L., G. De Tommaso and M. Iuliano. 2001. The solubility of calcium citrate in sodium perchlorate solutions. *Journal of Analytical Letters* 34:1053-1062.

Clark, D.L., and C.D. Tait. 1996. *Monthly Reports Under SNL Contract AP2274*. Sandia WIPP Central File A:WBS 1.1.10.1.1. WPO 31106.

Clayton, D. 2008. *Update to the Calculation of the Minimum Brine Volume for a Direct Brine Release.* Memorandum to L. Brush, Sandia National Laboratories, Carlsbad, New Mexico, April 2, 2008.

Clayton, D. 2009. *Update to the K_d Values for the PABC-2009. S*andia National Laboratories, Carlsbad, New Mexico, ERMS 552395.

Clayton, D. 2010. *Update to the Actinide(III) Solubility Uncertainty Distribution.* Sandia National Laboratories, Carlsbad, New Mexico, ERMS 553405.

Clayton, D.J. 2013. *Justification of Chemistry Parameters for Use in BRAGFLO for AP-164, Rev. 1.* Sandia National Laboratories, Carlsbad, New Mexico, ERMS 559466.

Clayton, D. and M. Nemer. 2006. *Normalized Moles of Castile Sulfate Entering the Repository and Fraction of MgO Lost Due to Brine Flow Out of the Repository.* Memorandum to E.D. Vugrin, Sandia National Laboratories, Carlsbad, New Mexico, October 9, 2006.

Cotsworth, E. 2004a. *CRA Completeness Comments - 3rd set - August 2004*. U.S. Environmental Protection Agency Office of Radiation and Indoor Air, Washington DC, letter (with enclosure) to R. Paul Detwiler, U.S. Department of Energy Carlsbad Field Office, September 2, 2004.

Cotsworth, E. 2004b. *First Set of CRA Comments (with enclosure).* U.S. Environmental Protection Agency Office of Radiation and Indoor Air, Washington DC, letter to R. Paul Detwiler, U.S. Department of Energy Carlsbad Field Office, May 20, 2004.

Cotsworth, E. 2005. *EPA Letter on Conducting the Performance Assessment Baseline Change (PABC) Verification Test.* Environmental Protection Agency Office of Radiation and Indoor Air, Washington DC., letter (with enclosure) to Inés Triay, U.S. Department of Energy, Carlsbad Field Office. March 4, 2005, ERMS 538858. Docket A-98-49, Item II-B3-80.

Cotsworth, E. 2009a. *CRA-2009 First (1) Completeness Letter.* U.S. Environmental Protection Agency Office of Radiation and Indoor Air, letter to D. Moody, U.S. Department of Energy Carlsbad Field Office, May 21, 2009.

Cotsworth, E. 2009b. *CRA-2009 Second Completeness Letter.* U.S. Environmental Protection Agency Office of Radiation and Indoor Air, letter to D. Moody, U.S. Department of Energy Carlsbad Field Office, July 16, 2009.

Cotsworth, E. 2009c. *CRA-2009 Third Completeness Letter*. U.S. Environmental Protection Agency Office of Radiation and Indoor Air, letter to D. Moody, U.S. Department of Energy Carlsbad Field Office, October 19, 2009.

Crawford, B.A., and C.D. Leigh. 2003. *Estimate of Complexing Agents in TRU Waste for the Compliance Recertification Application*. Los Alamos National Laboratory, Carlsbad, New Mexico, ERMS 531107.

Crawford, B.A. and D.P Taggart. 2007. *Analysis of RH TRU Wastes for Containment in Lead Shielded Containers.* Los Alamos National Laboratory, Carlsbad, New Mexico, INV-SAR-08.

Crawford, B., D. Guerin, S. Lott, B. McInroy, J. McTaggart, and G. Van Soest. 2009. *Performance Assessment Inventory Report – 2008.* INV-PA-08, Revision 0, Los Alamos National Laboratory Carlsbad Operations, LA-UR-09-02260, April 23, 2009.

Dardenne, K., A. Seibert, M.A. Denecke and C.M. Marquardt. 2009. Plutonium(III,IV,VI) speciation in Gorleben groundwater using XAFS. *Radiochimica Acta* 97:91-97.

Day, B. 2015. *Review of the Technical Basis for REFCON:ASDRUM, DRROOM, and VROOM Performance Assessment Analysis Parameters with Comparison to the Currently Emplaced Steel Surface Area per Unit Volume in the WIPP Repository.* Sandia National Laboratories, Carlsbad, New Mexico. ERMS 564670.

Deng, H., S. Johnsen, Y. Xiong, G.T. Roselle, and M. Nemer. 2006. *Analysis of Martin Marietta MagChem® 10 WTS-60 MgO.* Sandia National Laboratories, Carlsbad, New Mexico. ERMS 544712.

Deng, H., M.B. Nemer, and Y. Xiong. 2007. *Experimental Study of MgO Reaction Pathways and Kinetics (Rev. 1, January 10)*. TP 06-03, Sandia National Laboratories, Carlsbad, New Mexico, ERMS 545182.

Deng, H., Y. Xiong, M. Nemer, and S. Johnsen. 2009. *Experimental Work Conducted on MgO Long-Term Hydration, 2008 Milestone Report. S*andia National Laboratories, Carlsbad, New Mexico, ERMS 551421.

Detwiler, R.P. 2004a. *MgO Emplacement.* U.S. Department of Energy Carlsbad Field Office, letter to Elizabeth Cotsworth, U.S. Environmental Protection Agency Office of Radiation and Indoor Air, Washington DC, October 20, 2004.

Detwiler, R.P. 2004b. *Partial Response to Environmental Protection Agency (EPA) May 20, 2004 Letter on CRA, Enclosure 1.* U.S. Department of Energy Carlsbad Field Office, Letter to Elizabeth Cotsworth, U.S. Environmental Protection Agency Office of Radiation and Indoor Air, Washington, DC, August 16, 2004.

Detwiler, R.P. 2004c. *Partial Response to Environmental Protection Agency (EPA) September 2, 2004, Letter on Compliance Recertification Application.* U.S. Department of Energy Carlsbad Field Office, Letter to Elizabeth Cotsworth, U.S. Environmental Protection Agency Office of Radiation and Indoor Air, Washington, DC, December 23, 2004.

Detwiler, R.P. 2004d. *Response to EPA May 20, 2004, Letter on CRA.* U.S. Department of Energy Carlsbad Field Office, letter to Elizabeth Cotsworth, U.S. Environmental Protection Agency Office of Radiation and Indoor Air, Washington, DC, September 29, 2004.

Díaz Arocas, P., and B. Grambow. 1998. Solid-Liquid Phase Equilibria of U(VI) in NaCl Solutions. *Geochimica et Cosmochimica Acta* 62:245-263.

Ding, M., J.L. Conca, C. den Auwer, R.I. Gabitov, N.J. Hess, P. Paviet-Hartmann, P.D. Palmer, V. LoPresti, and S.D. Conradson. 2006. Chemical speciation of heterogeneously reduced Pu in synthetic brines. *Radiochimica Acta* 94:249-259.

Dodge, C.J., A.J. Francis, J.B. Gillow, G.P. Halada, C. Eng, and C.R. Clayton. 2002. Association of uranium with iron oxides typically formed on corroding steel surfaces. *Environmental Science and Technology* 36:3504–3511.

DOE (U.S. Department of Energy) 1996. *Title 40 CFR Part 191 Compliance Certification Application for the Waste Isolation Pilot Plant*, DOE/CAO-1996-2184, October 1996, Carlsbad Field Office, Carlsbad, New Mexico.

DOE (U.S. Department of Energy) 2004. *Title 40 CFR 191 Parts B and C Compliance Recertification Application*. U.S. Department of Energy Carlsbad Field Office, March 2004.

DOE (U.S. Department of Energy) 2009. *Title 40 CFR 191 Parts B and C Compliance Recertification Application*. U.S. Department of Energy Carlsbad Field Office, March 2009.

DOE (Department of Energy). 2012. *Annual Transuranic Waste Inventory Report – 2012. Revision 0.* U.S. Department of Energy, Carlsbad Field Office, DOE/CBFO-94-1012.

DOE (Department of Energy). 2014a. *Annual Transuranic Waste Inventory Report – 2014. Revision 0.* U.S. Department of Energy, Carlsbad Field Office, DOE/TRU-14-3425.

DOE (U.S. Department of Energy) 2014b. *Title 40 CFR 191 Parts B and C Compliance Recertification Application*. U.S. Department of Energy Carlsbad Field Office, March 2014.

Domski, P.S., and Y. Xiong. 2015a. *Analysis Plan for the Compilation and Testing of Selected Parameters from AP-134, Revision 3, AP-154, Revision 2 and AP-155, Revision 3 for Incorporation in a New QA EQ3/6 Thermodynamic Database.* Sandia National Laboratories, Carlsbad, New Mexico, ERMS 564585

Domski, P.S., and Y. Xiong. 2015b. *Prediction of Baseline Actinide Solubilities with an Updated EQ3/6 Thermodynamic Database (DATA0.FM2) in Response to EPA Completeness Comment 3-C-3 For CRA 2014.* Sandia National Laboratories, Carlsbad, New Mexico, ERMS 565032.

Du, A., B. Boonchayaanant, W.-M. Wu, S. Fendorf, J. Bargar and C.S. Criddle. 2011. Reduction of uranium(V) by soluble iron(II) conforms with thermodynamic predictions. *Environmental Science and Technology* 45:4718-4725.

Dunagan, S., C. Hansen and W. Zelinski. 2005. *Effect of Increasing Cellulosics, Plastics and Rubbers on WIPP Performance Assessment, Revision 1.* Sandia National Laboratories, Carlsbad, New Mexico, ERMS 538445.

Economy, K. 2016. *High Order Chemistry Discussion Points.* U.S. Environmental Protection Agency, Email to R. Patterson, U.S. Department of Energy, July 28, 2016.

Edwards, J.D. 2011. U.S. Environmental Protection Agency, Office of Air and Radiation, to E. Ziemianski, U.S. Department of Energy, Carlsbad Field Office, August 8, 2011.

Edwards, J.D. 2013. U.S. Environmental Protection Agency, Office of Air and Radiation, to J. Franco, U.S. Department of Energy, Carlsbad Field Office, September 3, 2013.

Edwards, J.D. 2014. *First Set of EPA Completeness Comments for CRA 2014.* U.S. Environmental Protection Agency, Letter to J.R. Franco, U.S. DOE Carlsbad Field Office, December 17, 2014.

Edwards, J.D. 2015a. *Fourth Set of EPA Completeness Questions.* U.S. Environmental Protection Agency, Letter to J.R. Franco, U.S. DOE Carlsbad Field Office, July 30, 2015.

Edwards, J.D. 2015b. *Second Set of EPA Completeness Questions.* U.S. Environmental Protection Agency, Letter to J.R. Franco, U.S. DOE Carlsbad Field Office, February 27, 2015.

Edwards, J.D. 2015c. *Third Set of EPA Completeness Questions.* U.S. Environmental Protection Agency, Letter to J.R. Franco, U.S. DOE Carlsbad Field Office, June 5, 2015.

Ekberg, C., Y. Albinsson, M.J. Comarmond and P.L. Brown. 2000. Studies on the complexation behavior of thorium(IV). 1. Hydrolysis equilibria. *Journal of Solution Chemistry* 29:63-86.

Emmerich, M., A. Bhansali, T. Lösekann-Behrens, C. Schröder, A. Kappler and S. Behrens. 2012. Abundance, distribution, and activity of Fe(II)-oxidizing and Fe(III)-reducing microorganisms in hypersaline sediments of Lake Kasin, Southern Russia. *Applied and Environmental Microbiology* 78:4386–4399.

EPA (Environmental Protection Agency) 1997a. *Compliance Application Review Documents for the Criteria for the Certification and Recertification of the Waste Isolation Pilot Plant's Compliance with the 40 CFR Part 191 Disposal Regulations: Final Certification Decision. CARD 23: Models and Computer Codes.* U.S. Environmental Protection Agency Office of Radiation and Indoor Air. Washington, DC. Docket A-93-02 Item V-B-2.

EPA (Environmental Protection Agency) 1997b. *Compliance Application Review Documents for the Criteria for the Certification and Recertification of the Waste Isolation Pilot Plant's Compliance with the 40 CFR Part 191 Disposal Regulations: Final Certification Decision CARD 24: Waste Characterization.* U.S. Environmental Protection Agency Office of Radiation and Indoor Air. Washington, DC. Docket A-93-02 Item V-B-2.

EPA (U.S. Environmental Protection Agency) 1997c. *Compliance Application Review Documents for the Criteria for the Certification and Recertification of the Waste Isolation Pilot Plant's Compliance with the 40 CFR Part 191 Disposal Regulations: Final Certification Decision. CARD 44: Engineered Barrier*. EPA Air Docket A-93-02-V-B-2. U.S. Environmental Protection Agency Office of Radiation and Indoor Air. Washington, DC.

EPA (U.S. Environmental Protection Agency) 1998a. *Final WIPP Certification Decision Response to Comments, Criteria for the Certification of the Waste Isolation Pilot Plant's Compliance with 40 CFR Part 191 Disposal Regulations: Certification Decision*. Office of Radiation and Indoor Air, Washington DC. Docket No. A-93-02 Item V-C-1.

EPA (U.S. Environmental Protection Agency) 1998b. *Technical Support Document for Section 194.14: Assessment of K_ds used in the CCA*. U.S. Environmental Protection Agency Office of Radiation and Indoor Air, Washington DC. Docket A-93-02 Item V-B-4.

EPA (U.S. Environmental Protection Agency) 1998c. *Technical Support Document for Section 194.23: Parameter Justification Report.* Environmental Protection Agency Office of Radiation and Indoor Air, Washington, DC. Docket A-93-02 Item V-B-14.

EPA (U.S. Environmental Protection Agency) 1998d. *Technical Support Document for Section 194.24: EPA's Evaluation of DOE's Actinide Source Term.* Environmental Protection Agency Office of Radiation and Indoor Air, Washington, DC. Docket A-93-02 Item V-B-17.

EPA (U.S. Environmental Protection Agency) 2001a. *Approval of Elimination of Minisacks*. Environmental Protection Agency Office of Radiation and Indoor Air, Washington, DC. Docket A-98-49, II-B-3, Item 15.

Environmental Protection Agency (EPA) 2001b. *MgO Minisack Review*. U.S. Environmental Protection Agency Office of Radiation and Indoor Air, Washington, DC. ERMS 519362 (US EPA 2001a, enclosure).

EPA (U.S. Environmental Protection Agency) 2006a. *Criteria for the Certification and Recertification of the Waste Isolation Pilot Plant's Compliance With the Disposal Regulations: Recertification Decision*. *Federal Register* 71:18010-18021, April 10.

EPA (Environmental Protection Agency) 2006b. *Technical Support Document for Section 194.23: Review of the 2004 Compliance Recertification Performance Assessment Baseline Calculation*. Office of Radiation and Indoor Air, Docket No. A-98-49, Item II-B1-3, March 2006.

EPA (U.S. Environmental Protection Agency) 2006c. *Technical Support Document for Section 194.24: Evaluation of the Compliance Recertification Actinide Source Term and Culebra Dolomite Distribution Coefficient Values*. Office of Radiation and Indoor Air, Docket No. A-98-49, Item II-B1-16, March 2006.

EPA (U.S. Environmental Protection Agency) 2006d. *Technical Support Document for Section 194.24: Review of the Baseline Inventory Used in the Compliance Recertification Application and the Performance Assessment Baseline Calculation.* Office of Radiation and Indoor Air, Docket No. A-98-49, Item II-B1-9, March 2006.

EPA (U.S. Environmental Protection Agency) 2010a. *Criteria for the Certification and Recertification of the Waste Isolation Pilot Plant's Compliance With the Disposal Regulations: Recertification Decision*. *Federal Register* 75:70584-70595, November 18.

EPA (U.S. Environmental Protection Agency) 2010b. *Technical Support Document for Section 194.24: Evaluation of the Compliance Recertification Actinide Source Term, Backfill Efficacy and Culebra Dolomite Distribution Coefficient Values (Revision 1)*. Office of Radiation and Indoor Air, Docket No. A-98-49, Item II-B1-25, November 2010.

EPA (U.S. Environmental Protection Agency) 2017. *Probability of Encountering Castile Brine beneath the WIPP Waste Panels Using the TDEM Block Method*. Docket ///. U.S. Environmental Protection Agency. Washington, DC.

Felicione, F.S., K.P. Carney, and C.C. Dwight. 2001. Results from the Gas Generation Experiments at Argonne National Laboratory-West. *Sandia National Laboratories Technical Baseline Reports, WBS 1.3.5.4, Repository Investigations Milestone R1020, July 31, 2001*. Sandia National Laboratories, Carlsbad, New Mexico, ERMS 518970, pp. 2-1 to 2-5.

Felmy, A.R., and J.H. Weare. 1986. The prediction of borate mineral equilibria in natural waters: application to Searles Lake, California. *Geochimica et Cosmochimica Acta* 0:2771-2783.

Felmy, A.R., D. Rai, J.A. Schramke, and J.L. Ryan. 1989. The solubility of plutonium hydroxide in dilute solutions and in high-ionic-strength chloride brines. *Radiochimica Acta* 48:29-35.

Felmy, A.R., D. Rai and M.J. Mason. 1991. The solubility of hydrous thorium(IV) oxide in chloride media: development of an aqueous ion-interaction model. *Radiochimica Acta*55:177-185.

Felmy, A.R., D. Rai, M.S. Sterner, M.J. Mason, N.J. Hess and S.D. Conradson. 1997. Thermodynamic models for highly charged aqueous species: solubility of Th(1V) hydrous oxide in concentrated $NaHCO_3$ and Na_2CO_3 solutions. *Journal of Solution Chemistry* 26:233-248.

Felmy, A.R., D.A. Moore, K.M. Rosso, O. Qafoku, D. Rai, E.C. Buck and E.S. Ilton. 2011. Heterogeneous reduction of PuO_2 with Fe(II): importance of the Fe(III) reaction product. *Environmental Science and Technology* 45:3952-3958.

Felmy, A.R., D.A. Moore, C.I. Pearce, S.D. Conradson, O. Qafoku, E.C. Buck, K.M. Rosso and E.S. Ilton. 2012. Controls on soluble Pu concentrations in PuO_2/magnetite suspensions. *Environmental Science and Technology* 46:11610-11617.

Fiedor, J.N., W.D. Bostick, R.J. Jarabek, and J. Farrell. 1998. Understanding the mechanism of uranium removal from groundwater by zero-valent iron using X-ray photoelectron spectroscopy. *Environmental Science and Technology* 32:1466-1473.

Fox, B. 2008. *Parameter Summary Report for the CRA-2009.* Rev. 0, Sandia National Laboratories, Carlsbad, New Mexico, ERMS 549747.

Francis, A.J. 1998. Biotransformation of Uranium and Other Actinides in Radioactive Wastes. Journal of Alloys and Compounds, vol. 271–273: 78–84.

Francis, A.J., and C.J. Dodge. 2008. Bioreduction of uranium(VI) complexed with citric acid by *clostridia* affects its structure and solubility. *Environmental Science and Technology* 42:8277-8282.

Francis, A.J., and J.B. Gillow. 1994. *Effects of Microbial Processes on Gas Generation Under Expected Waste Isolation Pilot Plant Repository Conditions. Progress Report through 1992.* Sandia National Laboratories, Albuquerque, New Mexico, SAND93-7036, WPO 26555.

Francis, A.J., and J.B. Gillow. 2000. *Progress Report: Microbial Gas Generation Program*. Unpublished memorandum to Y. Wang, January 6, 2000. Brookhaven National Laboratory, Upton, New York, ERMS 509352.

Francis A.J., J.B. Gillow, and M.R. Giles. 1997. *Microbial Gas Generation Under Expected Waste Isolation Pilot Plant Repository Conditions*. Sandia National Laboratories, Albuquerque, New Mexico, SAND96-2582.

Francis, A.J., C.J. Dodge, J.B. Gillow, and H.W. Papenguth. 2000. Biotransformation of uranium compounds in high ionic strength brine by a halophilic bacterium under denitrifying conditions. *Environmental Science and Technology* 34:2311-2317.

Francis, A.J., C.J. Dodge and T. Ohnuki. 2007. Microbial transformations of plutonium. *Journal of Nuclear and Radiochemical Sciences* 8:121-126.

Franco, J.R. 2012. *Planned Change Notice for Placement of Magnesium Oxide Supersacks.* U.S. Department of Energy Letter to A. Perrin, U.S. Environmental Protection Agency, February 14, 2012.

Franco, J.R. 2015a. *Response to Environmental Protection Agency Letters Dated December 17, 2014 and February 27, 2015 Regarding the 2014 Compliance Recertification Application.* U.S. Department of Energy Letter to J.D. Edwards, U.S. Environmental Protection Agency, April 8, 2015.

Franco, J.R. 2015b. *Response to Environmental Protection Agency Letter Dated December 17, 2014 Regarding the 2014 Compliance Recertification Application.* U.S. Department of Energy Letter to J.D. Edwards, U.S. Environmental Protection Agency, March 18, 2015.

Franco, J.R. 2015c. *Response to Environmental Protection Agency Letters Dated December 17, 2014 and February 27, 2015 Regarding the 2014 Compliance Recertification Application.* U.S. Department of Energy Letter to J.D. Edwards, U.S. Environmental Protection Agency, May 29, 2015.

Frederickson, J.K., J.M. Zachara, D.W. Kennedy, M.C. Duff, Y.A. Gorby, S.-M. W. Li, and K. Krupka. 2000. Reduction of U(VI) in goethite (α-FeOOH) suspensions by a dissimilatory metal-reducing bacterium. *Geochimica et Cosmochimica Acta* 64:3085-3098.

Gallegos, T.J., C.C. Fuller, S.M. Webb and W. Betterton. 2013. Uranium(VI) interactions with mackinawite in the presence and absence of bicarbonate and oxygen. *Environmental Science and Technology* 47:7357-7364.

Gautier, Q. 2012. *Cinétiques de Précipitation de Minéraux Carbonatés Magnésiens, Influence de Ligands Organiques, et Conséquences pour la Séquestration Minérale du CO_2.* PhD thesis, University of Paris – Est.

Gautier, Q., P. Bénézeth, V. Mavromatis and J. Schott. 2014. Hydromagnesite solubility product and growth kinetics in aqueous solution from 25 to 75ºC. *Geochimica et Cosmochimica Acta* 138:1-20.

Gautier, Q., P. Bénézeth and J. Schott. 2016. Magnesite growth inhibition by organic ligands: an experimental study at 100, 120 and 146ºC. *Geochimica et Cosmochimica Acta* 181:101-125.

Giambalvo, E.R. 2002a. *Recommended Parameter Values for Modeling An(III) Solubility in WIPP Brines*. Memorandum to L.H. Brush, July 25, 2002, ERMS 522982.

Giambalvo, E.R. 2002b. *Recommended Parameter Values for Modeling Organic Ligands in WIPP Brines*. Memorandum to L.H. Brush, July 25, 2002, ERMS 522981.

Giambalvo, E.R. 2002c. *Recommended Parameter Values for Modeling An(IV) Solubility in WIPP Brines*. Memorandum to L.H. Brush, July 26, 2002, ERMS 522986.

Giambalvo, E.R. 2002d. *Recommended Parameter Values for Modeling An(V) Solubility in WIPP Brines*. Memorandum to L.H. Brush, July 26, 2002, ERMS 522990.

Giambalvo, E.R. 2002e. *Recommended μ^0/RT Values for Modeling the Solubility of Oxalate Solids in WIPP Brines.* Memorandum to L.H. Brush, July 31, 2002, ERMS 523057.

Giambalvo, E.R. 2003. *Release of FMT Database FMT_021120.CHEMDAT*. Memorandum to L.H. Brush, March 10, 2003, ERMS 526372.

Gillow, J.B., and A.J. Francis. 2001a. Re-evaluation of Microbial Gas Generation Under Expected Waste Isolation Pilot Plant Conditions: Data Summary Report, January 24, 2001, *Sandia National Laboratories Technical Baseline Reports, WBS 1.3.5.4, Repository Investigations Milestone RI010, January 31, 2001.* Sandia National Laboratories, Carlsbad, New Mexico, ERMS 516749, pp. 19–46.

Gillow, J.B., and A.J. Francis. 2001b. Re-evaluation of Microbial Gas Generation Under Expected Waste Isolation Pilot Plant Conditions: Data Summary and Progress Report (February 1 - July 13, 2001), *Sandia National Laboratories Technical Baseline Reports, WBS 1.3.5.4, Repository Investigations Milestone R1020, July 31, 2001.* Sandia National Laboratories. Carlsbad, New Mexico, ERMS 518970, pp. 3-1 to 3-21.

Gillow J.B., and A.J. Francis. 2002a. Re-evaluation of Microbial Gas Generation Under Expected Waste Isolation Pilot Plant Conditions: Data Summary and Progress Report (July 14, 2001 - January 31, 2002), January 22, 2002. *Sandia National Laboratories Technical Baseline Reports, WBS 1.3.5.3, Compliance Monitoring; WBS 1.3.5.4, Repository Investigations, Milestone RI110, January 31, 2002.* Sandia National Laboratories, Carlsbad, New Mexico, ERMS 520467, pp. 2.1-1 to 2.1-26.

Gillow, J.B., and A.J. Francis. 2002b. Re-evaluation of Microbial Gas Generation Under Expected Waste Isolation Pilot Plant Conditions: Data Summary and Progress Report (February 1–July 15, 2002), January 18, 2002. *Sandia National Laboratories Technical Baseline Reports, WBS 1.3.5.3, Compliance Monitoring; WBS 1.3.5.4, Repository Investigations, Milestone RI130, July 31, 2002.* Sandia National Laboratories, Carlsbad, New Mexico, ERMS 523189, pp. 3.1-1 to 3.1-A10.

Gillow, J., and A.J. Francis. 2003. *Microbial Gas Generation Under Expected Waste Isolation Pilot Plant Repository Conditions.* Final Report, Revision 0, October 6 Draft, ERMS 532877.

Gitlin, B.C. 2006. U.S. Environmental Protection Agency, Office of Air and Radiation, Washington, DC. Letter to D.C. Moody, U.S. Department of Energy, Carlsbad Field Office, Carlsbad, New Mexico. April 28, 2006.

Grambow, B., E. Smailos, H. Geckeis, R. Müller, and H. Hentschel. 1996. Sorption and Reduction of Uranium(VI) on Iron Corrosion Products under Reducing Saline Conditions. *Radiochimica Acta* 74:149 154.

Gu, B., L. Liang, M.J. Dickey, X. Yin, and S. Dai. 1998. Reductive precipitation of uranium (VI) by zero-valent iron. *Environmental Science and Technology* 32:3366–3373.

Guillaumont, R., T. Fanghänel, V. Neck, J. Fuger, D.A. Palmer, I. Grenthe and M.H. Rand. 2003. *Update on the Chemical Thermodynamics of Uranium, Neptunium, Plutonium, Americium*

and Technetium. OECD Nuclear Energy Agency Data Bank, Eds., OECD Publications, Issy-les-Moulineaux, France. Hansen, C.W., L.H. Brush, M.B. Gross, F.D. Hansen, B. Thompson, J.S. Stein, and B-Y Park 2003a. *Effects of Supercompacted Waste and Heterogeneous Waste Emplacement on Repository Performance, Rev. 0*. Sandia National Laboratories Carlsbad Programs Group, Carlsbad, New Mexico, October 7, 2003.

Hansen, C. and C. Leigh. 2003. *A Reconciliation of the CCA and PAVT Parameter Baselines*. Revision 3, Sandia National Laboratories, Carlsbad, New Mexico, April 11, 2003, ERMS 528582.

Hansen, C.W., L.H. Brush, M.B. Gross, F.D. Hansen, B-Y Park, J.S. Stein, and B. Thompson 2003b. *Effects of Supercompacted Waste and Heterogeneous Waste Emplacement on Repository Performance, Rev. 1*. Sandia National Laboratories Carlsbad Programs Group, Carlsbad, New Mexico, October 17, 2003, ERMS 532475.

Haschke, J.M., T.H. Allen, and L.A. Morales. 2000. Reaction of Plutonium Dioxide with Water: Formation and Properties of PuO_{2+x}. *Science* 287:285-287.

Hinz, K., M. Altmaier, T. Rabung, M. Richmann, M. Borkowski, D. Reed, and H. Geckeis. 2012. Solubility and speciation of Cm(III) and Nd(III) in borate rich NaCl and $CaCl_2$ solutions. *Proceedings of the International Workshop ABC – Salt (II) and HiTAC 2011.* M. Altmaier, C. Bube, B. Kienzler, V. Metz and D.T. Reed, eds. Karlsruhe Institute of Technology Scientific Publishing.

Hinz, K., M. Altmaier, X. Gaona, T. Rabung, D. Schild, M. Richmann, D. Reed, E. Alekseev and H. Geckeis. 2015. Interaction of Nd(III) and Cm(III) with borate in dilute to concentrated alkaline NaCl, $MgCl_2$ and $CaCl_2$ solutions: solubility and TRLFS studies. *New Journal of Chemistry* 39:849-859.

Hobart, D.E., and R.C. Moore. 1996. *Analysis of Uranium (VI) Solubility Data for WIPP Performance Assessment WBS 1.1.10.1.1.* Sandia National Laboratories, May 28, 1996, ERMS 239856.

Hua, B., J. Xu, J. Terry, and B. Deng. 2006. Kinetics of uranium(VI) reduction by hydrogen sulfide in anoxic aqueous systems. *Environmental Science and Technology* 40:4666-4671.

Hummel, W., G. Anderegg, L. Rao, I. Puigdomènech and O. Tochiyama. 2005. *Chemical Thermodynamics of COmpunds and Complexes of U, Np, Pu, Am, Tc, Se, Ni and Zr with Selected Organic Ligands.* OECD Nuclear Energy Agency Data Bank, Eds., OECD Publications, Issy-les-Moulineaux, France.

Hyun, S.P., J.A. Davis, K. Sun and K.F. Hayes. 2012. Uranium(VI) reduction by iron(II) monosulfide mackinawite. *Environmental Science and Technology* 46:3369-3376.

Icopini, G.A., J. Boukhalfa, and M.P. Neu. 2007. Biological reduction of Np(V) and Np(V) citrate by metal-reducing bacteria. *Environmental Science and Technology* 41:2764–69.

Icopini, G.A., J.G. Lack, L.E. Hersman, M.P. Neu and H. Boukhalfa. 2009. Plutonium(V/VI) reduction by the metal-reducing bacteria *Geobacter metallireducens* GS-15 and *Shewanella oneidensis* MR-1. *Applied and Environmental Microbiology* 75:3641-3647.

Ikeda, A., M. Ueda and S. Mukai. 1983. CO_2 corrosion behavior and mechanism of carbon steel and alloy steel. *Corrosion '83, Anaheim, CA, April 18-22, 1983.* National Association of Corrosion Engineers, Houston, TX.

Ismail, A.E., J. Deng. J.-H. Jang and T.J. Wolery. 2009. *Verification of FMT Database and Conversion to EQ3/6 Format.* Sandia National Laboratories, Carlsbad, New Mexico, ERMS 550689.

Kanney, J.F., A.C. Snider, T.W. Thompson, and L.H. Brush. 2004. *Effect of Naturally Occurring Sulfate on the MgO Safety Factor in the Presence of Supercompacted Waste and Heterogeneous Waste Emplacement.* Sandia National Laboratories Carlsbad Programs Group, Carlsbad, New Mexico, March 5, 2004.

Kanney, J.F. and E.D. Vugrin, 2006. *Updated Analysis of Characteristic Time and Length Scales for Mixing Processes in the WIPP Repository to Reflect the CRA-2004 PABC Technical Baseline and the Impact of Supercompacted Mixed Waste and Heterogeneous Waste Emplacement.* Memorandum to D.S. Kessel, Sandia National Laboratories, Carlsbad, New Mexico, August 31, 2006.

Kelly, T.E. 2010. *Fourth WIPP Completeness Letter*. U.S. Environmental Protection Agency, Letter to D. Moody, U.S. Department of Energy, February 22, 2010.

Khalili, F.K., V. Symeopoulos, J.F. Chen and G.R. Choppin. 1994. Solubility of Nd in brine. *Radiochimica Acta* 66/67:51-54.

Kicker, D.C, and C.G. Herrick. 2013. *Parameter Summary Report for the Compliance Recertification Application, Rev. 0*. Sandia National Laboratories, ERMS 560298.

Kicker, D.C. and T. Zeitler. 2013. *Radionuclide Inventory Screening Analysis for the Compliance Recertification Application Performance Assessment (CRA-2014 PA).* Sandia National Laboratories, Carlsbad, New Mexico, ERMS 559257.

Kirchner, T. 2008. *Generation of the LHS Samples for the AP-137 Revision 0 (CRA09) PA Calculations.* Sandia National Laboratories, Carlsbad, New Mexico, ERMS 547971.

Kirchner, T. 2013. *Sensitivity of the CRA-2014 Performance Assessment Releases to Parameters.* Sandia National Laboratories, Carlsbad, New Mexico, ERMS 560043.

Kirchner, T., and E. Vugrin, 2006. *Uncertainty in Cellulose, Plastic, and Rubber Measurements for the Waste Isolation Pilot Plant Inventory*. Sandia National Laboratories, Carlsbad, New Mexico. ERMS 543848.

Kirsch, R., D. Fellhauer, M. Altmaier, V. Neck, A. Rossberg, L. Charlet and A.C. Scheinost. 2010. Reaction of Pu(III) and Pu(V) with magnetite and mackinawite: a XANES/EXAFS investigation. *Goldschmidt Conference Abstracts* 2010:A520.

Kirsch, R., D. Fellhauer, M. Altmaier, V. Neck, A. Rossberg, T. Fanghänel, L. Charlet and A.C. Scheinost. 2011. Oxidation state and local structure of plutonium reacted with magnetite, mackinawite and chukanovite. *Environmental Science and Technology* 45:7267-7274.

Königsberger, E., L.-C. Königsberger, and H. Gamsjäger. 1999. Low-temperature thermodynamic model for the system Na_2CO_3 – $MgCO_3$ – $CaCO_3$ – H_2O. *Geochimica et Cosmochimica Acta* 19/20:3105-3119.

Könnecke, T., T. Fanghänel and J.I. Kim. 1997. Thermodynamics of trivalent actinides in concentratated electrolyte solutions: modelling the chloride complexation of Cm(III). *Radiochimica Acta* 76:131-135.

Kouba, S. 2013. *Re: MgO Emplacement Factor as of December 31, 2012; Attachment: CBFO_Emplacement_Statistics-12-31-2012.txt.* Nuclear Waste Partnership LLC, Email to L. Brush, Sandia National Laboratories October 8, 2013.

Krumhansl, J.L., Kelly, J.W., Papenguth, H.W., and R.V. Bynum. 1997. *MgO Acceptance Criteria*. Unpublished memorandum to E.J. Nowak, December 10, 1997. Sandia National Laboratories, Albuquerque, New Mexico, ERMS 248997.

Lambert, S.J. 1992. Geochemistry of the Waste Isolation Pilot Plant (WIPP) site, southeastern New Mexico, USA. *Applied Geochemistry* 7:513-531.

Larson, K.W. 1996. *Brine-Waste Contact Volume for Scoping Analysis of Organic Ligand Concentration*. Unpublished memorandum to R.V. Bynum, Sandia National Laboratories, Albuquerque, New Mexico, March 13, 1996, ERMS 236044.

Latta, D.E., C.A. Gorski, M.I Boyanov, E. J. O'Loughlin, K.M. Kemner, and M.M. Scherer. 2012. Influence of magnetite stoichiometry on U^{VI} reduction. *Environmental Science and Technology* 46:778-786.

Leigh, C. 2003. *Estimate of Cellulosics, Plastics, and Rubbers in a Single Panel in the WIPP Repository in Support of AP-107, Supersedes ERMS 530959*. Unpublished Analysis Report. Sandia National Laboratories, Carlsbad, New Mexico, ERMS 531324.

Leigh, C.D. 2005. *Organic Ligand Masses TRU Waste Streams from TWBID Revision 2.1 Version 3.13 Data Version D4.15, Revision 1*. Memorandum to L.H. Brush, Sandia National Laboratories, April 18, 2005, ERMS 539550.

Leigh, C., J. Kanney, L. Brush, J. Garner, R. Kirkes, T. Lowry, M. Nemer, J. Stein, E. Vugrin, S. Wagner, and T. Kirchner. 2005a. *2004 Compliance Recertification Application Performance Assessment Baseline Calculation*. Sandia National Laboratories, Carlsbad, New Mexico, ERMS 541521.

Leigh, C.D., J.R. Trone and B. Fox. 2005b. *TRU Waste Inventory for the 2004 Compliance Recertification Application Performance Assessment Baseline Calculation*. Sandia National Laboratories, Carlsbad, New Mexico. ERMS 541118.

Lin, M.R., P. Paviet-Hartmann, Y. Xu, and W.H. Runde. 1998. Uranyl Compounds in NaCl Solutions: Structure, Solubility and Thermodynamics. *American Chemical Society, Division of Environmental Chemistry, Preprints of Extended Abstracts.* 216th ACS National Meeting, Boston Massachusetts, August 23-27, 38:208.

Lovley, D.R., and E.J.P. Phillips. 1992. Reduction of uranium by *desulfovibrio desulfuricans*. A*pplied and Environmental Microbiology* 58:850-856.

Lucchini, J.F., H. Khaing, M. Borkowski, M.K. Richmann, and D.T. Reed. 2010. *Actinide (VI) Solubility in Carbonate-free WIPP Brine: Data Summary and Recommendations.* LCO-ACP-10, LANL\ACRSP Report. Los Alamos National Laboratory, Los Alamos, New Mexico. Cited in the text of DOE (2009) as Lucchini et al. 2009 and as Lucchini et al. 2008 in the reference list.

Lucchini, J.F., M. Borkowski, H. Khaing, M.K. Richmann, J.S. Swanson, K. Simmons and D.T. Reed. 2013. *WIPP Actinide-Relevant Brine Chemistry.* Los Alamos National Laboratory, Carlsbad, New Mexico, LA-UR 13-20620.

Marcinowski, F. 2004. U.S. Environmental Protection Agency Office of Radiation and Indoor Air, Washington DC, letter to R. Paul Detwiler, U.S. Department of Energy Carlsbad Field Office, March 26, 2004.

Marquardt, C.M., A. Seibert, R. Artinger, M.A. Denecke, B. Kuczewski, D. Schild and T. Fanghänel. 2004. The redox behavior of plutonium in humic rich groundwater. *Radiochimica Acta* 92:617-623.

Marquardt, C.M., N.L. Banik, N Shcherbina and H. Geckeis. 2008. Redox behavior of plutonium and neptunium in aqueous solution containing humic substances or hydroquinone. *NRC7 – Seventh International Conference on Nuclear and Radiochemistry.* Hungary, August 24 – 28, 2008.

Meinrath, D., and J.I. Kim. 1991. Solubility products of different Am(III) and Nd(III) carbonates. *European Journal of Solid State and Inorganic Chemistry* 28:383-388.

Meinrath, D., and H. Takeishi. 1993. Solid-liquid equilibria of Nd^{3+} in carbonate solutions. *Journal of Alloys and Compounds* 194:93-99.

Meyer, M., R. Burgat, S. Faure, B. Batifol, J-C Hubinois, H. Chollet, and R. Guilard. 2007. Thermodynamic studies of actinide complexes. 1. A reappraisal of the solution equilibria between plutonium(IV) and EDTAH4 in nitric media. *Comptes Rendus Chimie* 10:929-947.

MFG. 2000. *Evaluation of the Reported Presence of Oxidized Plutonium in the STTP Experiments and in Plutonium Oxide Solid.* Prepared for the U.S. Environmental Protection Agency Office of Radiation and Indoor Air by MFG Inc., Boulder, Colorado, in association with TechLaw Inc., Lakewood, Colorado and Monitor Scientific, Denver, Colorado.

Moody, D.C. 2006. U.S. Department of Energy, Carlsbad Field Office, Letter to E.A. Cotsworth, U.S. Environmental Protection Agency, requesting a reduction in the MgO EF from 1.67 to 1.2. April 10, 2006. ERMS 543262.

Moody, D.C. 2007. *Transmittal of Planned Change Request for Shielded Containers.* U.S. Department of Energy, Carlsbad Field Office, Letter to to J. Reyes, US. Environmental Protection Agency, November 15, 2007.

Moody, D.C. 2009a. *Response to Environmental Protection Agency Letter dated May 21, 2009 Regarding Compliance Recertification Application*. U.S. Department of Energy, Carlsbad Field Office, Letter to E. Cotsworth, Office of Radiation and Indoor Air, Environmental Protection Agency, August 24, 2009.

Moody, D.C. 2009b. *Response to Environmental Protection Agency May 21, 2009 and July 16, 2009 Letters on the 2009 Compliance Recertification Application*. U.S. Department of Energy, Carlsbad Field Office, Letter to E. Cotsworth, Office of Radiation and Indoor Air, Environmental Protection Agency, November 25, 2009.

Moody, D.C. 2010a. *Response to Environmental Protection Agency January 25, 2010 Email Regarding the Follow-Up Questions from the May 21, 2009 Letter on the 2009 Compliance Recertification Application*. U.S. Department of Energy, Carlsbad Field Office, Letter to M. Flynn, Office of Radiation and Indoor Air, Environmental Protection Agency, February 19, 2010.

Moody, D.C. 2010b. Response *to Environmental Protection Agency October 19, 2009 Letter on the 2009 Compliance Recertification Application*. U.S. Department of Energy, Carlsbad Field Office, Letter to E. Cotsworth, Office of Radiation and Indoor Air, Environmental Protection Agency, February 19, 2010.

Morss, L.R. and C.W. Williams. 1994. Synthesis of crystalline americium hydroxide, $Am(OH)_3$ and determination of its enthalpy of formation; estimation of the solubility-product constants of actinide(III) hydroxides. *Radiochimica Acta* 66-67:89-94.

Myachina, L.I., V.A. Logvinenko, and N.N. Knyazeva. 1974. Binuclear complexes of EDTA. 1. The synthesis of binuclear ethylenediaminetetraacetates of alkine-earth and transition metals (in Russian). *Izv. Sib. Otd. Akad. Nauk SSR, Ser. Khim. Nauk* 6:77-82.

Neck, V., R. Müller, M. Bouby, M. Altmaier, J. Rothe, M.A. Denecke, and J.I. Kim. 2002. Solubility of Amorphous Th(IV) Hydroxide-Application of LIBD to Determine the Solubility Product and EXAFS for Aqueous Speciation. *Radiochimica Acta* 90:485-494.

Neck, V., M. Altmaier and T. Fanghänel. 2007. Solubility of plutonium hydroxides/hydrous oxides under reducing conditions and in the presence of oxygen. *Comptes Rendus Chimie* 10:959-977.

Neck, V., M. Altmaier, T. Rabung, J. Lützenkirchen and T. Fanghänel. 2009. Thermodynamics of trivalent actinides and neodymium in NaCl, $MgCl_2$, and $CaCl_2$ solutions: solubility, hydrolysis, and ternary Ca-M(III)-OH complexes. *Pure and Applied Chemistry* 81:1555-1568.

Neff, D., P. Dillman, L. Bellot-Gurlet and G. Beranger. 2005. Corrosion of iron archaeological artefacts in soil: characterization of the corrosion system. *Corrosion Science* 47:515-535.

Neiss, J., B.D. Stewart, P.S. Nico, and S. Fendorf. 2007. Speciation-dependent microbial reduction of uranium within iron-coated sands. *Environmental Science and Technology* 41:7343-7348.

Nelson, R.A. 2011. Radiolytic hydrogen generation and methanogenesis in WIPP: an empirical point of view. *WM2011 Symposium*, February 27 – March 3, 2011, Phoenix, Arizona.

Nemer, M. 2005. *Updated Value of WAS_AREA:PROBDEG*. Sandia National Laboratories, Carlsbad, New Mexico. Memorandum to D.S. Kessel, April 20, 2005, ERMS 539441.

Nemer, M. 2008. *Procedure for Testing for the Periclase + Lime Content in Martin Marietta MgO Rev. 1*. Sandia National Laboratories, Carlsbad, New Mexico, November 17, 2008, ERMS 550455.

Nemer, M. 2009. *Adequacy of MgO Reactivity Test (EPA Re-Certification Question 1-C-2) and Interpreting MgO Reactivity Test Results Above 96 Mol %.* Sandia National Laboratories, Carlsbad, New Mexico, ERMS 551892.

Nemer, M. and D. Clayton. 2008. *Analysis Package for Salado Flow Modeling: 2009 Compliance Recertification Application Calculation.* Sandia National Laboratories, Carlsbad, New Mexico, ERMS 548607.

Nemer, M., and J. Stein. 2005. *Analysis Package for BRAGFLO: 2004 Compliance Recertification Application Performance Assessment Baseline Calculation*. Sandia National Laboratories, Carlsbad, New Mexico, ERMS 540527.

Nemer, M., J. Stein, and W. Zelinski. 2005. *Analysis Report for BRAGFLO Preliminary Modeling Results With New Gas Generation Rates Based Upon Recent Experimental Results*. Analysis Report, Sandia National Laboratories, Carlsbad, New Mexico, ERMS 539437.

Nemer, M., Y. Xiong, A.E. Ismail, and J. Jang. 2011. Solubility of $Fe_2(OH)_3Cl$ (pure-iron end-member of hibbingite) in NaCl and Na_2SO_4 brines. *Chemical Geology* 280:26-32.

Nešić S., H. Fang, W. Sun and J. K.-L. Lee. 2008. A new updated model of CO_2/H_2S Corrosion in multiphase flow. Paper Number 08538, *NACE International Corrosion 2008 Conference & Expo*.

NMED (New Mexico Environment Department). 2014. May 20, 2014 Administrative Order. https://www.env.nm.gov/NMED/Issues/WIPP_docs/NMED_051214%20WIPP%20Administrative%20Order.pdf

Novak, C.F., 1996. *Preliminary Inorganic Model for Thorium Solubility in WIPP Brines, in Database File HMW_3Th5_960119.CHEMDAT*. Memo to E.J. Nowak, 19 January 1996, Sandia National Laboratories, Albuquerque, New Mexico. WPO #30930

Novak, C.F. and R.C. Moore. 1996. *Estimates of Dissolved Concentrations for +III, +IV, +V, and +VI Actinides in a Salado and a Castile Brine under Anticipated Repository Conditions*. Memo to M.D. Siegel, March 28, 1996, Sandia National Laboratories, Albuquerque, New Mexico, CCA Ref. No. 479.

Nowak, E.J. 2005. *Recommended Change in the FMT Thermodynamic Data Base.* Memorandum to L.H. Brush, April 1, Sandia National Laboratories, Carlsbad, New Mexico, ERMS 539227.

Nowak, E.J., and D.J. Clayton. 2007. *Analysis of MgO Hydration Laboratory Results and Calculation of Extent of Hydration and Resulting Water Uptake Versus Time Under Postulated WIPP Conditions.* Sandia National Laboratories, Carlsbad, New Mexico, ERMS 546769.

Ohnuki, T., T. Yoshida, T. Ozaki, N. Kozai, F. Sakamoto, T. Nankawa, Y. Suzuki and A.J. Francis. 2007. Chemical speciation and association of plutonium with bacteria, kaolinite clay, and their mixture. *Environmental Science and Technology* 41:3134-3139.

O'Loughlin, E.J., S.D. Kelly, R.E. Cook, R. Csencsits, and K.M. Kemner. 2003. Reduction of uranium(VI) by mixed iron(II)/iron(III) hydroxide (green rust): formation of UO_2 nanoparticles. *Environmental Science and Technology* 37:721–727.

Ősthols, E., J. Bruno, and I. Grenthe. 1994. On the influence of carbonate on mineral dissolution. III. The solubility of microcrystalline ThO_2 in CO_2H_2O media. *Geochimica et Cosmochimica Acta* 58:613-623.

Oversby, V.M. 2000. *Plutonium Chemistry Under Conditions Relevant for WIPP Performance Assessment. E*EG-77, Prepared for the Environmental Evaluation Group by VMO Konsult, September 2000.

Palmer, C.E. 1996. Private communication to R. Van Bynum (SAIC/SNL) from C. Palmer (LLNL), dated February 27, 1996, reported by Hobart and Moore (1996).

Papenguth, H.W. 1996. *Parameter Record Package for Colloidal Actinide Source Term Parameters.* Memorandum to C.T. Stockman, Sandia National Laboratories, Albuquerque, New Mexico, May 7, 1996, ERMS 235850.

Papenguth, H.W. and Y.K. Behl. 1996. *Test Plan for Evaluation of Colloid-Facilitated Actinide Transport at the Waste Isolation Pilot Plant.* TP 96-01, Sandia National Laboratories, Albuquerque, New Mexico.

Patterson, R. 2016a. *Pu Oxidation State Implementation.* U.S. Department of Energy Email to T. Peake and K. Economy, U.S. Environmental Protection Agency, September 8, 2016.

Patterson, R. 2016b. *Response to the U.S. Environmental Protection Agency Email Dated July 28, 2016 Regarding Chemistry Questions on the 2014 Compliance Recertification Application.* U.S. Department of Energy, Letter to T. Peake, U.S. Environmental Protection Agency, October 6, 2016.

Peake, T. 2012. *Magnesium Oxide Supersack Size Reduction and Alternative Emplacement Plan.* U.S. Environmental Protection Agency, email to R. Patterson, U.S. Department of Energy, July 13, 2012.

Peake, T. 2016a. *Addendum to Comment 2-C-4(a).* U.S. Environmental Protection Agency Letter to R. Patterson, U.S. Department of Energy Carlsbad Field Office, February 26, 2016.

Peake, T. 2016b. *Changes to Actinide References Used in the Calculation of Actinide Solubility Uncertainty.* U.S. Environmental Protection Agency, email to S. Dunagan, U.S. Department of Energy, Carlsbad, New Mexico, September 30, 2016.

Plymale, A.E., V.L. Bailey, J.K. Fredrickson, S.M. Heald, L. Shi, Z. Wang, C.T. Resch, D.A. Moore and H. Bolton. 2012. Biotic and abiotic reduction and solubilization of $Pu(IV)O_2•xH_2O(am)$ as affected by anthraquinone-2,6-disulfonate (AQDS) and ethylenediaminetetraacetate (EDTA). *Environmental Science and Technology* 46:2132-2140.

Rabung, T., M. Altmaier, V. Neck and T. Fanghänel. 2008. A TRLFS study of Cm(III) hydroxide complexes in alkaline $CaCl_2$ solutions. *Radiochimica Acta* 96:551-560.

Rai, D., and J.L. Ryan. 1985. Neptunium(IV) hydrous oxide solubility under reducing and carbonate conditions. *Inorganic Chemistry* 24: 247–251.

Rai, D., A.R. Felmy, D.A. Moore and M.J. Mason. 1995. The solubility of Th(IV) and U(IV) hydrous oxides in concentrated $NaHCO_3$ and Na_2CO_3 aqueous solutions. *Scientific Basis for Nuclear Waste Management XVIII.* Kyoto, Japan, pp. 1143–1150.

Rai, D., A.R. Felmy, S.M. Sterner, D.A. Moore, M.J. Mason and Novak. 1997. The solubility of Th(IV) and U(IV) hydrous oxides in concentrated NaCl and $MgCl_2$ solutions. *Radiochimica Acta* 79:239-247.

Rai, D., Y.A. Gorby, J.K. Frederickson, D.A. Moore and M. Yui. 2002. Reductive dissolution of $PuO_2(am)$: the effect of Fe(II) and hydroquinone. *Journal of Solution Chemistry* 31:433-453.

Rai, D., M. Yui, D. Moore, G. Lumetta, K.M. Rosso, Y. Xia, A. Felmy and F.N. Skomurski. 2008a. Thermodynamic model for $ThO_2(am)$ solubility in alkaline silica solutions. *Journal of Solution Chemistry* 37:1725-1746.

Rai, D., D. Moore, K. Rosso, A. Felmy, and H. Bolton. 2008b. Environmental mobility of Pu(IV) in the presence of EDTA: myth or reality? *Journal of Solution Chemistry* 37:957-986.

Rai, D., D. Moore, A. Felmy, K. Rosso, and H. Bolton. 2010. $PuPO_4$(cr, hyd.) solubility product and Pu^{3+} complexes with phosphate and EDTA. *Journal of Solution Chemistry* 39:778-807.

Rand, M., J. Fuger, I. Grenthe, V. Neck, and D. Rai. 2008. *Chemical Thermodynamics of Thorium.* OECD Nuclear Energy Agency Data Bank, Eds., OECD Publications, Issy-les-Moulineaux, France.

Rao, L.F., D. Rai and A.R. Felmy. 1996a. Solubility of $Nd(OH)_3(c)$ in 0.1 M NaCl aqueous solution at 25°C and 90°C. *Radiochimica Acta* 72:151-155.

Rao, L.F., D. Rai A.R. Felmy, R.W. Fulton and C.F. Novak. 1996b. Solubility of $NaNd(CO_3)_3 \cdot 6H_2O(c)$ in concentrated Na_2CO_3 and $NaHCO_3$ solutions at 25°C and 90°C. *Radiochimica Acta* 75:141-147.

Rao, L., D. Rai, A.R. Felmy and C.F. Novak. 1999. Solubility of $NaNd(CO_3)_3 \cdot 6H_2O(c)$ in mixed electrolyte (Na-Cl-CO_3-HCO_3) and synthetic brine solutions. In *Actinide Speciation in High Ionic Strength Media: Experimental and Modeling Approaches to Predicting Actinide Speciation and Migration in the Subsurface.* Proceedings of an American Chemical Society Symposium on Experimental and Modeling Studies of Actinide Speciation in Non-Ideal Systems. Held August 26-28, 1996 in Orlando, Florida. Eds. D.T. Reed, S.B. Clark and L. Rao. Kluwer Academic/Plenum Publishers, pp. 153-169.

Reed, D.R., M. Borkowski, J. Swanson, M. Richmann, H. Khaing, J.F. Lucchini and David Ams. 2011. Redox-controlling processes for multivalent metals and actinides in the WIPP. in *Redox Phenomena Controlling Systems*, M. Altmaier, B. Kienzler, L. Duro, M. Grivé, and V. Montoya (eds.) 3rd Annual Workshop Proceedings, 7th EC Recosy Cooperative Project, Karlsruhe Institute for Technology, March 2011.

Reed, D.T. and D.R. Wygmans. 1997. *Actinide Stability/Solubility in Simulated WIPP Brines*. Interim Report 3/21/97, Actinide Speciation and Chemistry Group, Chemical Technology Group, Argonne National Laboratory, Argonne, Illinois. WPO 44625.

Reed, D. T., D. G. Wygmans, and M. K. Richmann. 1996. *Stability of Pu(VI), Np(VI), and U(VI) in Simulated WIPP Brine*. Argonne National Laboratory Interim Report.

Reed, D.T., D.R. Wygmans, S.B. Aase, and J.E. Banaszak. 1997. *Reduction of Np(VI) and Pu(VI) by Organic Chelating Agents*. Sandia National Laboratories, SAND97-2845C.

Reed, D.T., D.G. Wygmans, S.B. Aase and J.E. Banaszak. 1998. Reduction of Np(VI) and Pu(VI) by organic chelating agents. *Radiochimica Acta* 82:109-114.

Reed, D.T., J.F. Lucchini, S.B. Aase and A.J. Kropf. 2006. Reduction of plutonium(VI) in brine under subsurface conditions. *Radiochimica Acta* 94:591-597.

Reed, D.T., S.E. Pepper, M.K. Richmann, G. Smith, R. Deo, and B.E. Rittmann. 2007. Subsurface bio-mediated reduction of higher-valent uranium and plutonium. *Journal of Alloys and Compounds* 444/445:376–382.

Reed, D.T., J.F. Lucchini, M. Borkowski, and M.K. Richmann. 2010. *Reduction of Higher-Valent Plutonium by Iron under Waste Isolation Pilot Plant (WIPP)-Relevant Conditions: Data Summary and Recommendations*. LCO-ACP-09, Rev. 0, LANL\ACRSP Report, Los Alamos National Laboratory, Los Alamos, New Mexico. Cited by DOE (2009), DOE (2014b) and Shrader (2015) as Reed et al. (2009).

Reed, D.T., J.S. Swanson, J.F. Lucchini and M.K. Richmann. 2013. *Intrinsic, Mineral and Microbial Colloid Enhancement Parameters for the WIPP Actinide Source Term.* LCO-ACP-18, Revision 0, Los Alamos National Laboratory, Carlsbad, New Mexico.

Regenspurg, S., D. Schild, T. Schäfer, F. Huber and M. Malmström. 2009. Removal of uranium(VI) from the aqueous phase by iron(II) minerals in the presence of bicarbonate. *Applied Geochemistry* 24:1617-1625.

Réguer, S., P. Dillman and F. Mirambet. 2007. Buried iron archaeological artefacts: Corrosion mechanisms related to the presence of Cl-containing phases. *Corrosion Science* 49:2726-2744.

Rémazeilles, C., D. Neff, F. Kergourlay, E. Foy, E. Conforto, S. Réguer, P. Refait and P. Dillmann. 2009. Mechanisms of long-term anaerobic corrosion of iron archaeological artefacts in seawater. *Corrosion Science* 51:2932-2041.

Renshaw, J.C., N. Law, A. Geissler, F.R. Livens and J.R. Lloyd. 2009. Impact of the Fe(III)-reducing bacteria *Geobacter sulfurreducens* and *Shewanella oneidensis* on the speciation of plutonium. *Biogeochemistry* 94:191-196.

Reyes, J. 2008. U.S. Environmental Protection Agency, Office of Air and Radiation, Washington DC, letter to D. Moody, U.S. Department of Energy Carlsbad Field Office, February 11, 2009.

Rittmann, B.E., J.E. Banaszak, and D.T. Reed. 2002. Reduction of Np(V) and precipitation of Np(IV) by an anaerobic microbial consortium. *Biodegradation* 13:329–342.

Robie, R.A. and B.S. Hemingway. 1973. The enthalpies of formation of nesquehonite, $MgCO_3 \cdot 3H_2O$, and hydromagnesite, $5MgO \cdot 4CO_2 \cdot 5H_2O$. *Journal of Research of the U.S. Geological Survey* 1:543-547.

Roselle, G.T. 2009. *Iron and Lead Corrosion in WIPP-Relevant Conditions: Six Month Results.* Sandia National Laboratories, Carlsbad, New Mexico, ERMS 546084.

Roselle, G.T. 2010. *Iron and Lead Corrosion in WIPP-Relevant Conditions: 12 Month Results.* Sandia National Laboratories, Carlsbad, New Mexico, ERMS 554383.

Roselle, G.T. 2011a. *Iron and Lead Corrosion in WIPP-Relevant Conditions: 18 Month Results.* Sandia National Laboratories, Carlsbad, New Mexico, ERMS 554715.

Roselle, G.T. 2011b. *Iron and Lead Corrosion in WIPP-Relevant Conditions: 24 Month Results.* Sandia National Laboratories, Carlsbad, New Mexico, ERMS 555246.

Roselle, G.T. 2013. *Determination of Corrosion Rates from Iron/Lead Corrosion Experiments to be Used for Gas Generation Calculations, Revision 1.* Analysis Report, Sandia National Laboratories, Carlsbad, New Mexico, ERMS 559077.

Rothe, J., M.A. Denecke, V. Neck, R. Müller, and J.I. Kim. 2002. XAFS investigation of the structure of aqueous thorium(IV) species, colloids and solid thorium(IV) oxide/hydroxide. *Inorganic Chemistry* 41:249-258.

RSI (Institute for Regulatory Science). 2006. *Application of Magnesium Oxide as an Engineered Barrier at Waste Isolation Pilot Plant, Report of the Expert Panel*. RSI-06-01.

Runde, W., and J.I. Kim. 1994. *Untersuchungen der Übertragbarkeit von Labordaten Natürliche Verhältnisse: Chemisches Verhalten von Drei- und Fünfwertigem Americium in Salinen NaCl-Lösungen (Study of the Extrapolability of Laboratory Data to Natural Conditions: Chemical Behavior of Trivalent and Pentavalent Americium in Saline NaCl Solutions).* RCM-01094, Institute for Radiochemistry, Technical University of Munich, Munich, Federal Republic of German, ERMS 241862.

Rusin, P.A., Quintana, L., Brainard, J.R., Strietelmeir, B.A., Trait, C.D., Ekberg, S.A., Palmer, P.D., Newton, T.W., Clark, D.L.: 1994. Solubilization of plutonium hydrous oxide by iron-reducing bacteria. *Environmental Science and Technology* 28:1686–1690.

Ryan J.L. and D. Rai. 1987. Thorium(IV) hydrous oxide solubility. *Inorganic Chemistry* 26:4140-4142.

Saheb, M., D. Neff, P. Dillmann, H. Matthiesen, E. Foy and L. Bellot-Gurlet. 2009. Multisecular corrosion behaviour of low carbon steel in anoxic soils: characterization of corrosion system on archaeological artefacts. *Materials and Corrosion* 60:99-105.

Saldi, G.D., J. Schott, O.S. Pokrovsky, Q. Gautier and E.H. Oelkers. 2012. An experimental study of magnesite precipitation rates at neutral to alkaline conditions and 100 – 200ºC as a function of pH, aqueous solution composition and chemical affinity. *Geochimica et Cosmochimica Acta* 83:93-109.

Sassani, D. 2013. *Our Discussion on Intrinsic Th Colloids and Mg-Cl-OH Colloids.* Sandia National Laboratories, Albuquerque, New Mexico, Email to G.T. Roselle, Sandia National Laboratories, Carlsbad, New Mexico, May 30, 2013.

Sborgi, U., E. Bovalini and L. Cappellini. 1924. Per lo stuio della doppia decompasizione $(NH_4)_2 + Na_2SO_4 \leftrightarrow Na_2B_4O_7 + (NH_4)_2SO_4$ in soluzione acqusa. Parte III. Sistema ternario $Na_2B_4O_7$, Na_2SO_4, H_2O. *Gazzetta chimica Italiana* 54:298-322.

SC&A (S. Cohen & Associates). 2000. *Implications Regarding the Efficacy of MgO Backfill Based on Preliminary Results of STTP Liter-Scale Experiment L-28.* Prepared for U.S. Environmental Protection Agency Office of Radiation and Indoor Air, September 4, 2000.

SC&A (S. Cohen & Associates). 2006. *Preliminary Review of the Degradation of Cellulosic, Plastic and Rubber Materials in the Waste isolation Pilot Plant, and Possible Effects on Magnesium Oxide Safety Factor.* Prepared for the U.S. Environmental Protection Agency Office of Radiation and Indoor Air, August 21.

SC&A (S. Cohen & Associates). 2008a. *Review of MgO-Related Uncertainties in the Waste Isolation Pilot Plant.* Prepared for the U.S. Environmental Protection Agency Office of Radiation and Indoor Air, January 24.

SC&A (S. Cohen & Associates). 2008b. *Verification of the Waste Isolation Pilot Plant Chemistry Conceptual Models.* Prepared for the U.S. Environmental Protection Agency Office of Radiation and Indoor Air, September 19.

SC&A (S. Cohen and Associates). 2011. *EQ3/6 Computer Code Evaluation*. Prepared for U.S. Environmental Protection Agency Office of Radiation and Indoor Air. Draft March 2011.

Schmitt, G. 1983. CO_2 corrosion of steels – An attempt to range parameters and their effects. *Advances in CO_2 Corrosion in the Oil and Gas Industry, Proceedings of the Corrosion/83 Symposium, Anaheim, CA, April 18-19.* Ed. R.H. Hausler, National Association of Corrosion Engineers, Houston, Texas.

Schott, J., J. Kretzchmar, M. Acker, S. Eidner, M.U. Kumke, B. Drobot, A. Barkleit, S. Taut, V. Brendler and T. Stumpf. 2014. Formation of a Eu(III) borate solid species from a weak Eu(III) borate complex in aqueous solution. *Dalton Transactions* 43:11516-11528.

Schreiber, J. 1991. *Analyst CalculationL Schreiber, 7/26/91, Updated Waste Storage Volumes.* Sandia National Laboratories, Carlsbad, New Mexico, ERMS 237713.

Schuessler, W., B. Kienzler, S. Wilhelm, V. Neck, and J.I. Kim. 2001. Modeling of Near Field Actinide Concentrations in Radioactive Waste Repositories in Salt Formations: Effect of Buffer Materials. *Materials Research Society Symposium Proceedings* 663:791-798.

Shrader, T. 2015. *Response to the U.S. Environmental Protection Agency Letters Dated June 5, 2015 and July 30, 2015 Regarding the 2014 Compliance Recertification Application.* U.S. Department of Energy Letter to J.D. Edwards, U.S. Environmental Protection Agency, December 8, 2015.

Shrader, T. 2016. *Response to the U.S. Environmental Protection Agency Letters Dated June 5, 2015, July 30, 2015 and February 26, 2016 Regarding the 2014 Compliance Recertification Application.* U.S. Department of Energy Letter to J.D. Edwards, U.S. Environmental Protection Agency, May 25, 2016.Silva , R.J. 1982. *The Solubilities of Crystalline Neodymium and Americium Trihydroxides.* LBL-15055. Lawrence Berkeley National Laboratory, Berkeley, California.

Simpkins, L.A. 2011. *Influence of Natural Organic Matter on Plutonium Sorption to Gibbsite.* Masters thesis, Clemson University.
Slater, S.A., D.B. Chamberlain, S.A. Base, B.D. Babcock, C. Conner, J. Sedlet, and G.F. Vandegrift. 1997. Optimization of Magnetite Carrier Precipitation Process for Plutonium Waste Reduction. *Separation Science and Technology* 32:127 147.

Singer, D.M., S.M. Chatman, E.S. Ilton, K.M. Rosso, J.F. Banfield, and G.A. Waychunas. 2012a. Identification of simultqaneous U(VI) sorption complexes and U(IV) nanoprecipitates on the magnetite (III) suface. *Environmental Science and Technology* 46:3811-3820.

Singer, D.M., S.M. Chatman, E.S. Ilton, K.M. Rosso, J.F. Banfield and G.A. Waychunas. 2012b. U(VI) sorption and reduction kinetics on the magnetite (111) surface. *Environmental Science and Technology* 46:3821-3830.

Snider, A.C. 2001. MgO Hydration Experiments Conducted at SNL/ABQ. *Sandia National Laboratories Technical Baseline Reports, WBS 1.3.5.4, Repository Investigations, Milestone RI020, July 31, 2001*. Sandia National Laboratories, Carlsbad, New Mexico. ERMS 518970, pp. 4-1 to 4-3.

Snider, A.C. 2002. MgO Studies: Experimental Work Conducted at SNL/Carlsbad. Efficacy of Premier Chemicals MgO as an Engineered Barrier, *Sandia National Laboratories Technical Baseline Reports, WBS 1.3.5.3, Compliance Monitoring; WBS 1.3.5.4, Repository Investigations, Milestone RI110, January 31, 2002.* Sandia National Laboratories, Carlsbad, New Mexico. ERMS 520467, pp. 3.1-1 to 3.1-18.

Snider, A.C. 2003a. Hydration of Magnesium Oxide in the Waste Isolation Pilot Plant, *Sandia National Laboratories Technical Baseline Reports, WBS 1.3.5.3, Compliance Monitoring; WBS 1.3.5.4, Repository Investigations, Milestone RI 03-210, January 31, 2003.* Sandia National Laboratories, Carlsbad, New Mexico, ERMS 526049, pp. 4.2-1 to 4.2-6.

Snider, A.C. 2003b. *Verification of the Definition of Generic Weep Brine and the Development of a Recipe for this Brine*. Unpublished Analysis Report, Sandia National Laboratories, Carlsbad, New Mexico, April 8, 2003, ERMS 527505.

Snider, A.C., and Y. L. Xiong. 2002. Carbonation of Magnesium Oxide, *Sandia National Laboratories Technical Baseline Reports, WBS 1.3.5.3, Compliance Monitoring; WBS 1.3.5.4, Repository Investigations, Milestone RI130, July 31, 2002.* Sandia National Laboratories, Carlsbad, New Mexico, ERMS 523189, pp. 4.1-1 to 4.1-28.

SNL (Sandia National Laboratories). 1997. *Chemical Conditions Model: Results of the MgO Backfill Efficacy Investigation.* Prepared for the U.S. Department of Energy, Carlsbad Area Office, April 23, 1997. Docket No. A-93-02, II-A-39.

Stamatakis, M.G. 1995. Occurrence and genesis of huntite-hyudromagnesite assemblages, Kozani, Greece – important new white filters and extenders. *Applied Earth Science, Transactions* 104:B157-B210.

Stein, C.S. 1985. *Mineralogy in the Waste Isolation Pilot Plant (WIPP) Facility Stratigraphic Horizon*. SAND-85-0321, Sandia National Laboratories, Albuquerque, New Mexico, September 1985.

Stein, J. 2005. Estimate *of Volume of Brine in Repository That Leads to a Brine Release*. Memorandum to L.H. Brush, April 13, Sandia National Laboratories, Carlsbad, New Mexico, ERMS 539372.

Stein, J., and M. Nemer. 2005. *Analysis Plan for Updating the Microbial Degradation Rates for Performance Assessment*. AP-116, Sandia National Laboratories, Carlsbad, New Mexico, ERMS 538596.

Stein, J.S., and W.P. Zelinski. 2004. *Effect of Increased Iron Surface Area from Supercompacted AMWTP Waste on Long-Term Repository Conditions as Modeled in Performance Assessment of the WIPP*. Sandia National Laboratories Carlsbad Programs Group, Carlsbad, New Mexico.

Storz, L. 1996. *Estimate of the Amount of $Ca(OH)_2$ Contained in the Portland Cement Fraction of the Waste for Disposal in the WIPP*. Memorandum to Y. Wang, Sandia National Laboratories, Albuquerque, New Mexico, ERMS 240351, June 24, 1996.

Suzuki, Y., S.D. Kelly, K.M. Kemner, and J.F. Banfield. 2003. Microbial populations stimulated for hexavalent uranium reduction in uranium mine sediment. *Applied and Environmental Microbiology* 69:1337-1346.

Swanson, J.S. 2013. *Microbial Characterization of Halite and Groundwater Samples from the WIPP*. Los Alamos National Laboratory LA-UR-13-26280.

TEA (Trinity Engineering Associates). 2000. *Review of Comments and Issues Raised by the Environmental Evaluation Group in Report EEG-77 - "Plutonium Chemistry Under Conditions Relevant for WIPP Performance Assessment,"* Prepared for the U.S. Environmental Protection Agency Office of Radiation and Indoor Air, November 30, 2000.

TEA (Trinity Engineering Associates). 2001. *Actinide Solubility Technical Exchange Meeting Report, Albuquerque, New Mexico, May 24, 2001*. Prepared for the U.S. Environmental Protection Agency Office of Radiation and Indoor Air, June 8, 2001.

TEA (Trinity Engineering Associates) 2004. *Review of Effects of Supercompacted Waste and Heterogeneous Waste Emplacement on WIPP Repository Performance. Final Report*. Prepared for U.S. Environmental Protection Agency, Office of Radiation and Indoor Air, Washington, DC, March 17, 2004.

Telander, M.R., and R.E. Westerman. 1993. *Hydrogen Generation by Metal Corrosion in Simulated Waste Isolation Pilot Plant Environments: Progress Report for the Period November 1989 through December 1992*. SAND92-7347, Sandia National Laboratories, Albuquerque, New Mexico, ERMS 223456.

Telander, M.R., and R.E. Westerman. 1997. *Hydrogen Generation by Metal Corrosion in Simulated Waste Isolation Pilot Plant Environments.* SAND96-2538, Prepared for Sandia National Laboratories, Albuquerque, New Mexico by Pacific Northwest National Laboratory, Richland, Washington.

Thakur, P., P. Pathak, and R. Choppin. 2009. Complexation thermodynamics and the formation of the binary and the ternary complexes of tetravalent plutonium with carboxylate and aminocarboxylate ligands in aqueous solution of high ionic strength. *Inorganica Chimica Acta* 362:179-184.

Thakur, P., Y. Xiong, M. Borkowski and G.R. Choppin. 2014. Improved thermodynamic model for interaction of EDTA with trivalent actinides and lanthanide to ionic strength of 6.60 m. *Geochimica et Cosmochimica Acta* 133:299-312.

Triay I.R. 2002. December 10, 2002 Letter to Frank Marcinowski related to AMWTF planned change request.

Triay, I.R. 2005. *Partial Response to Environmental Protection Agency (EPA) September 2, 2004, Letter on Compliance Recertification Application.* U.S. Department of Energy Carlsbad Field Office, letter to Elizabeth Cotsworth, U.S. Environmental Protection Agency Office of Radiation and Indoor Air, Washington, DC, January 19, 2005.

Vance, R.E., R.W. Mathewes, and J.J. Clague. 1992. 7000-year record of lake-level change on the northern Great Plains: a high-resolution proxy of past climate. *Geology* 20:879-882.

Van Soest, G.D. 2012. *Performance Assessment Inventory Report – 2012*. Los Alamos National Laboratory Carlsbad Operations INV-PA-12, Revision 0, LA-UR-12-26643.

Villareal, R. 1996. *Test Plan for the Actinide Source-Term Waste Test Program (STTP*). MST5-TP-TST1-013/1, Sandia National Laboratories, July 16, 1996.

Villareal, R., J.M. Bergquist, and S.L. Leonard. 2001. *The Actinide Source Term Waste Test Program (STTP) Final Report*, Volume I. Los Alamos National Laboratory, LA UR 01 6822.

Vugrin, E.D., M.B. Nemer, and S. Wagner, 2006. *Uncertainties Affecting MgO Effectiveness and Calculation of the MgO Effective Excess Factor*. Revision 0, Sandia National Laboratories, Carlsbad, New Mexico.

Vugrin, E.D., M.B. Nemer, and S. Wagner, 2007. *Uncertainties Affecting MgO Effectiveness and Calculation of the MgO Effective Excess Factor*. Revision 1, Sandia National Laboratories, Carlsbad, New Mexico. ERMS 546377.

Wall, D. 2001. *Technical Baseline Migration Parameter Report*. Sandia National Laboratories Document, Revision 0, September 28, 2001. Sandia National Laboratories, Carlsbad, New Mexico.

Wall, N.A., 2005. *Preliminary Results for the Evaluation of Potential New MgO*. Sandia National Laboratories, Carlsbad, New Mexico. ERMS 538514.

Wall, N.A. and S.A. Mathews. 2005. Sustainability of humic acids in the presence of magnesium oxide. *Applied Geochemistry* 20:1704-1713.

Wallace, T.C. 2014. Understanding the "What" and the "Why" of February 14, 2014. Los Alamos National Laboratory, LA-UR-14-27201.

Wang, Y. and LH. Brush. 1996. *Estimates of Gas-Generation Parameters for the Long-Term WIPP Performance Assessment*. Unpublished memorandum to M.S. Tierney, Sandia National Laboratories, Albuquerque, New Mexico, January 26, 1996, WPO 31943.

Wang, Y., L.H. Brush. H. Gao, and J.S. Stein. 2003. Re-evaluation of Microbial Gas Generation Rates for Long-Term WIPP Performance Assessment. *Sandia National Laboratories Technical Baseline Reports, WBS 1.3.5.3, Compliance Monitoring; WBS 1.3.5.4, Repository Investigations, Milestone RI 03-210, January 31, 2003*. Sandia National Laboratories, Carlsbad, New Mexico, pp. 3.1-1 to 3.1-12.

Weiner, R.F. 1996. *Oxidation State Distribution in the WIPP*. Presentation at Technical Exchange Meeting on June 27, 1996, Sandia National Laboratory, Albuquerque, New Mexico.

Werner, J.R. 2016. U.S. Environmental Protection Agency. Letter to S. Dunagan, U.S. Department of Energy, Carlsbad New Mexico, November 4, 2016.

Wilson, C., D. Porter, J. Gibbons, E. Oswald, G. Sjoblom, and F. Caporuscio. 1996a. *Conceptual Models Peer Review Report*, Prepared for the U.S. Department of Energy, Carlsbad, New Mexico, July 1996, Docket No. A-93-02 Item II-G-1.

Wilson, C., D. Porter, J. Gibbons, E. Oswald, G. Sjoblom, and F. Caporuscio. 1996b. *Conceptual Models Supplementary Peer Review Report*, Prepared for the U.S. Department of Energy, Carlsbad, New Mexico, December 1996, Docket No. A-93-02 Item II-G-12.

Wilson, C., D. Porter, J. Gibbons, E. Oswald, G. Sjoblom, and F. Caporuscio. 1997a. *Conceptual Models Second Supplementary Peer Review Report*, Prepared for the U.S. Department of Energy, Carlsbad, New Mexico, January 1997, Docket No. A-93-02 Item II-G-21.

Wilson, C., D. Porter, J. Gibbons, E. Oswald, G. Sjoblom, and F. Caporuscio. 1997b. *Conceptual Models Third Supplementary Peer Review Report*, Prepared for the U.S. Department of Energy, Carlsbad, New Mexico, April 1997, Docket No. A-93-02 Item II-G-22.

Wilson, D.L., M.L. Baker, B.R. Hart, J.E. Marra, J.M. Schwantes, and P.E. Shoemaker. 2015. *Waste Isolation Pilot Plant Technical Assessment Team Report.* U.S. Department of Energy, SRNL-RP-2014-01198.

Wolery, T.J., Y.-L. Xiong and J.J. Long. 2010. *Verification and Validation Plan/Validation Document for EQ3/6 Version 8.0a for Actinide Chemistry, Document Version 8.10.* Sandia National Laboratories, Carlsbad, New Mexico, ERMS 550239.

Wood, S.A. and Z.S. Cetiner. 2005. Experimental measurements of the solubility of ThO_2 in $NaNO_3$ solutions: Hydrolysis of Th(IV) and complexation by organic ligands. *Geochimica et Cosmochimica Acta Supplement* 69:A430.

WTS (Washington TRU Solutions LLC). 2003. *Specification for Prepackaged MgO Backfill.* Unpublished Specification, D-0101, Rev. 5. Washington TRU Solutions LLC, Carlsbad, New Mexico.

WTS (Washington TRU Solutions) 2005. *Specifications for Prepackaged Backfill*. Waste Isolation Pilot Plant Procedure D-0101, Revision 7, May 2005.

WTS (Washington TRU Solutions) 2009a. *Engineering Change Order (ECO) 12137.* January 2009.

WTS (Washington TRU Solutions) 2009b. *Specifications for Prepackaged MgO Backfill*. Waste Isolation Pilot Plant Procedure D-0101, Revision 8, February 2009.

Xia, Y., L. Rao, A.R. Felmy, and D. Rai. 2001. Determining the Distribution of Pu, Np, and U Oxidation States in Dilute NaCl and Synthetic Brine Solutions. *Journal of Radioanalytical and Nuclear Chemistry* 250:27-37.

Xiong, Y.-L. 2004. *A Correction of the Molecular Weight of Oxalate in FMT_021120.CHEMDAT and Incorporation of Calcium Oxalate Monohydrate (Whewellite) Into CHEMDAT With Its Recommended Dimensionless Standard Chemical Potential (μ^0/RT) Value*. Memorandum to L.H. Brush, June 8, 2004, Sandia National Laboratories, Carlsbad, New Mexico, ERMS 535813.

Xiong, Y. 2009. *Release of FMT_090720.CHEMDAT.* E-mail to Jennifer Long, July 22, 2009, Sandia National Laboratories, Carlsbad, New Mexico, ERMS 539304.

Xiong, Y.L. 2011a. Experimental determination of solubility constant of hydromagnesite (5424) in NaCl solutions up to 4.4 m at room temperature. *Chemical Geology* 284:262-269.

Xiong, Y. 2011b. *Release of EQ3/6 Database DATA0.FM1*. Email to J.J. Long, Sandia National Laboratories, Carlsbad, New Mexico, March 9, 2011.

Xiong, Y. 2012a. *Experimental Determination of Solubility Constant of Di-Calcium Ethylenediaminetetraacetic acid (Ca_2EDTA), $Ca_2C_{10}H_{12}N_2O_8(s)$, in the NaCl-$H_2O$ System.* Sandia National Laboratories, Carlsbad, New Mexico, ERMS 558669.

Xiong, Y. 2012b. *Analysis Plan AP-134, Revision 3, Analysis Plan for Derivation of Pitzer Parameters in Support of Experimental Work at LANL-CO.* Sandia National Laboratories, Carlsbad, New Mexico, ERMS 557474.

Xiong, Y. 2012c. *Second Milestone Report on Test Plan TP 10-01 "Experimental Study of Thermodynamic Parameters of Borate in WIPP Relevant Brines at Sandia National Laboratories Carlsbad Facility."* Sandia National Laboratories, Carlsbad, New Mexico, ERMS 557333.

Xiong, Y. 2012d. *Thermodynamic Model for the Na-$B(OH)_3$-Cl-SO_4 System, Revision 1, Superseding ERMS 558111*. Sandia National Laboratories, Carlsbad, New Mexico, ERMS 558566.

Xiong, Y.L. 2013a. *AP-154, Revision 2, Analysis Plan for Derivation of Thermodynamic Properties Including Pitzer Parameters for Solubility Studies of Iron, Lead and EDTA.* Sandia National Laboratories, Carlsbad, New Mexico, ERMS 561114.

Xiong, Y.L. 2013b. *Calculations of Thermodynamic Parameters in EDTA System for Experimental Data from Carlsbad Environmental Monitoring and Research Center.* Sandia National Laboratories, Carlsbad, New Mexico, ERMS 560761.

Xiong, Y.L. 2014a. *AP-155, Revision 3, Analysis Plan for Derivation of Thermodynamic Properties Including Pitzer Parameters for Solubility Studies of Borate.* Sandia National Laboratories, Carlsbad, New Mexico, ERMS 562807.

Xiong, Y. 2014b. *Experimental and Thermodynamic Modeling of $PbCit^-$ Interactions in NaCl and $MgCl_2$ Solutions.* Sandia National Laboratories, Carlsbad, New Mexico, ERMS 562836.

Xiong, Y. 2014c. *Experimental and Thermodynamic Modeling of $PbEDTA^{2-}$ Interactions in NaCl and $MgCl_2$ Solutions.* Sandia National Laboratories, Carlsbad, New Mexico, ERMS 562877.

Xiong, Y. 2015a. *Derivation of Thermodynamic Parameters in Borate Systems for Experimental Data Under TP10-01.* Sandia National Laboratories, Carlsbad, New Mexico, ERMS 564800.

Xiong, Y. 2015b. *Experimental and Thermodynamic Modeling Solubility of Cerussite, $PbCO_3$(cr), in the Carbonate System to High Ionic Strengths, Revision 1, Supersedes ERMS 561917.* Sandia National Laboratories, Carlsbad, New Mexico, ERMS 564929.

Xiong, Y. 2015c. Experimental determination of lead carbonate solubility at high ionic strengths: a Pitzer model description. *Monatshefte für Chemie* 146:1433-1443.

Xiong, Y. 2015d. *Experimental Determination of Solubilities of Lead Oxalate (PbC_2O_4), Di-calcium ethylenediamenetetraacetic acid (Ca_2EDTA(s)) in $MgCl_2$-H_2O System, and Earlandite ($Ca_3[C_3H_5O(COO)_3]_2 \cdot 4H_2O$) in NaCl-$H_2O$ and $MgCl_2$-H_2O Systems, and Their Respective Pitzer Interaction Parameters, Revision 1, Supersedes ERMS 564844.* Sandia National Laboratories, Carlsbad, New Mexico, ERMS 564948.

Xiong, Y. 2015e. *Modeling Equilibrium Constant for $AmHB_4O_7^2$, by reevaluation of the Nd(III) data for $NdHB_4O_7^{2+}$, and its associated Pitzer parameters to be consistent with the WIPP thermodynamic model.* Sandia National Laboratories, Carlsbad, New Mexico, ERMS 564857.

Xiong, Y. 2015f. *Recalculation of Solubility Constants of Synthetic Hydromagnesite(5424) Using the Pitzer Model.* Sandia National Laboratories, Carlsbad, New Mexico, ERMS 564356.

Xiong, Y.L. in press. Comment on "Hydromagnesite solubility product and growth kinetics in aqueous solution from 25 to 75ºC" by Gautier, Q., Bénézeth, P., Mavormatis, V., and Schott, J. *Geochemica et Cosmochimica Acta* available online December, 2016.

Xiong, Y., and P.S. Domski. 2016a. *Uncertainty Analysis of Actinide Solubilities for CRA 2014 Sensitivity Investigation Number 4 (CRA 2014_SEN4).* Sandia National Laboratories, Carlsbad, New Mexico, ERMS 567306.

Xiong, Y., and P.S. Domski. 2016b. *Updating the WIPP Thermodynamic Database, Revision 1, Supersedes ERMS 565730.* Sandia National Laboratories, Carlsbad, New Mexico, ERMS 566047.

Xiong, Y., and S. Kim. 2011. *Experimental Investigation of Absence or Presence of Colloids of Magnesium Chloride Hydroxide Hydate (Phase 5) in the WIPP Generic Weep Brine (GWB) Under the WIPP Relevant Conditions at Sandia Nation Laboratories Carlsbad Facility.* Task 1.4.2.2, Rev. 0. Sandia National Laboratories, Carlsbad, New Mexico.

Xiong, Y. and A.S. Lord. 2008. Experimental investigations of the reation path in the MgO-CO_2-H_2O system in solutions with various ionic strengths, and their applications to nuclear waste isolation. *Applied Geochemistry* 23:1634-1659.

Xiong, Y., and A.C. Snider. 2003. *Carbonation Rates of the Magnesium Oxide Hydration Product Brucite in Various Solutions. Sandia National Laboratories Technical Baseline Reports, WBS 1.3.5.4, Repository Investigations, Milestone RI 03-210, January 31, 2003.* Sandia National Laboratories, Carlsbad, New Mexico, ERMS 526049, pp. 4.3-1 to 4.3-11.

Xiong, Y.-L., L.H. Brush, J.W. Garner, and J.J. Long. 2010b. *Responses to Three EPA Comments Pertaining to Comparisons of Measured and Predicted Dissolved and Colloidal Th(IV) and Am(III) Concentrations, Revision 1*. Supersedes ERMS 553409. Analysis report, May 19, 2010. ERMS 553595. Carlsbad, NM: Sandia National Laboratories.

Xiong, Y., E.J. Nowak, and L.H. Brush. 2004. *Updated Uncertainty Analysis of Actinide Solubilities for the Response to EPA Comment C-23-16.* Sandia National Laboratories, Carlsbad, New Mexico, ERMS 538219.

Xiong, Y., E.J. Nowak, and L.H. Brush. 2005. *Updated Uncertainty Analysis of Actinide Solubilities for the Response to EPA Comment C-23-16, Rev. 1 (Supersedes ERMS 538219).* Sandia National Laboratories, Carlsbad, New Mexico, ERMS 539595.

Xiong, Y. L.H., Brush, A. Ismail, and J.J. Long. 2009a. *Uncertainty Analysis of Actinide Solubilities for the WIPP CRA-2009 PABC.* Sandia National Laboratories, Carlsbad, New Mexico, ERMS 552500.

Xiong, Y., H. Deng, M.B. Nemer and S. Johnsen. 2009b. *Thermodynamic Data for Phase 5 ($Mg_3Cl(OH)_5$•$4H_2O$) Determined from Solubility Experiments.* Memorandum to L.H. Brush, May 8, 2009, Sandia National Laboratories, Carlsbad, New Mexico, ERMS 551706.

Xiong, Y., H. Deng, M. Nemer and S. Johnsen. 2010a. Experimental determination of the solubility constant for magnesium chloride hydroxide hydrate ($Mg_3Cl(OH)_5$•$4H_2O$, Phase 5) at room temperature, and its Importance to nuclear waste isolation in geological repositories in salt formations. *Geochimica et Cosmochimica Acta* 74:4605-4611.Xiong, Y., L.H. Brush, J. W. Garner and J.J. Long. 2010b. *Response to Three EPA Comments Pertaining to Comparisons of Measured and Predicted Dissolved and Colloidal Th(IV) and Am(III) Concentrations.* Revision 1. (Supersedes ERMS 553409.) Sandia National Laboratories, Carlsbad, New Mexico, ERMS 553595.

Xiong, Y., L. Kirkes, T. Westfall and R. Roselle. 2013a. Experimental determination of solubilities of lead oxalate (PbC_2O_4(cr)) in a NaCl medium to high ionic strengths, and the importance of lead oxalate in low temperature environments. *Chemical Geology* 342:128-137.

Xiong, Y., L. Kirkes and T. Westfall. 2013b. Experimental determination of solubilities of sodium tetraborate (borax) in NaCl and a thermodynamic model for the Na-$B(OH)_3$-Cl-SO_4 system to high-ionic-strengths at 25ºC. *American Mineralogist* 98:2030-2036.

Yamazaki, H., B. Lagerman, V. Symeopoulos, and G.R. Choppin. 1992. Solubility of Uranyl in Brine. *Proceedings of the Third International High Level Radioactive Waste Management Conference,* Las Vegas, Nevada, American Nuclear Society, La Grange Park, and American Society of Engineers, New York, pp. 1607–1611.

Zeitler, T.R. 2013. *Analysis Package for CCDFGF: 2014 Compliance Recertification Application Performance Assessment (CRA-2014 PA).* Sandia National Laboratories, Carlsbad New Mexico, ERMS 560074.

Zeitler, T.R. and B. Day. 2016. *CRA14_SEN4 Sensitivity Study Revision 1.* Sandia National Laboratories, Carlsbad, New Mexico, ERMS 567505.

Zeitler, T.R. and C. Hansen. 2015a. *Cumulative Distribution for STEEL:CORRMCO2*. Sandia National Laboratories, ERMS 565005.

Zeitler, T. R. and C. Hansen. 2015b. *Cumulative Distribution for STEEL:HUMMCORR*. Sandia National Laboratories, ERMS 565009.

Zeitler, T.R. and R. Sarathi. 2017. *Comparison of STEPWISE Regressiona Analysis Results for CRA14_SEN4 and CRA-2014 Analyses.* Sandia National Laboratories, ERMS 567718.

Zhang, P.C., H.L. Anderson, J.W. Kelly, J.L. Krumhansl and H. W. Papenguth. 2000. *Kinetics and Mechanisms of Formation of Magnesite from Hydromagnesite in Brine.* Sandia National Laboratories, Carlsbad, New Mexico, SAND99-1946J.

Zhang, P., J. Hardesty, and H. Papenguth. 2001. *MgO Hydration Experiments Conducted at SNL-ABQ. Sandia National Laboratories Technical Baseline Reports, WBS 1.3.5.4, Compliance Monitoring; WBS 1.3.5.4, Repository Investigations, Milestone RI010, January 31, 2001.* Sandia National Laboratories, Carlsbad, New Mexico, ERMS 516749, pp. 55-65.